

Alma Mater Studiorum – Università di Bologna

DOTTORATO DI RICERCA IN

SCIENZE BIOTECNOLOGICHE, BIOCOMPUTAZIONALI,
FARMACEUTICHE E FARMACOLOGICHE

Ciclo XXXIII

Settore Concorsuale: 03/D1

Settore Scientifico Disciplinare: CHIM/08

DESIGN AND SYNTHESIS OF RAD51-BRCA2 DISRUPTORS THAT
TRIGGER SYNTHETIC LETHALITY IN PANCREATIC CANCER IN
COMBINATION WITH OLAPARIB

Presentata da: Greta Bagnolini

Coordinatore Dottorato

Prof.ssa Maria Laura Bolognesi

Supervisore

Prof.ssa Marinella Roberti

Co-Supervisore

Prof. Andrea Cavalli

Esame finale anno 2021

Contents

Abstract	3
1. Introduction	4
1.1 Tumor heterogeneity	4
1.2 Combination cancer therapy	7
1.3 Synthetic lethality	9
1.4 Synthetic lethality as strategy for drug combination	12
1.4.1 Computational approaches to synthetic lethal drug combinations	15
1.5 DNA double strand breaks (DSBs) repair pathways	17
1.5.1 Homologous recombination (HR) pathway	18
1.5.1.1 BRCA2 protein: structure and functional domains	21
1.5.1.2 RAD51 protein: structure and functional domains	22
1.6 RAD51-BRCA2 protein-protein interaction (PPI)	23
1.6.1 BRCA2 as principal RAD51 mediator in HR	23
1.6.2 RAD51-BRC4 interaction	25
1.7 Targeting DNA repair machinery	27
1.7.1 PARP inhibitors	27
1.7.2 Inhibitors of HR proteins	30
1.7.2.1 RAD51 inhibitors	30
1.7.2.2 RAD52 inhibitors	35
1.7.2.3 RAD54 inhibitors	36
2. Motivations, aims and hit identification strategies	38
3. Part I: STRUCTURE-BASED DESIGN APPROACH TO THE IDENTIFICATION OF RAD51-BRCA2 PPI DISRUPTORS	42
3.1 Hit identification and optimization targeting Zone II	49
3.2 Chemistry	52
3.3 SAR studies and biological evaluation	63
3.4 Conclusions	72
4. Part II: DISCOVERY OF RAD51-BRCA2 PPI DISRUPTORS VIA TARGET DIRECTED DYNAMIC COMBINATORIAL CHEMISTRY	73
4.1 Introduction to dynamic combinatorial chemistry	73
4.2 Application of tdDCC on RAD51	81

4.2.1 Protein stability assessment	83
4.2.2 tdDCC-1	84
4.2.3 Biochemical evaluation and results.....	88
4.2.4 tdDCC-2	89
4.2.5 tdDCC-3	92
4.3 Conclusions.....	95
5. Concluding remarks and future perspectives.....	96
6. Experimental section	98
6.1 Experimental section: Part I.....	98
6.1.1 Material and methods	98
6.1.2 General procedure for synthesis of final 1,2,4-triazoles (5–10).....	99
6.1.3 Synthesis of intermediates 13, 14, 16	102
6.1.4 General procedure for synthesis of chloroacetamides (17a–d).....	103
6.2.1 General Procedure A for the synthesis of acroyl intermediates (91b–113b, 133, 139)	105
6.2.2 General Procedure B for synthesis of pyrazoline intermediates (91c–113c, 134, 140)	105
6.2.3 General procedures C ₁ for final dihydroquinolone pyrazolines (19, 28–44, 62–66)...	105
6.2.4 General procedures C ₂ for final dihydroquinolone pyrazolines (22, 45–47).....	106
6.2.5 General procedures C ₃ for final dihydroquinolone pyrazolines (20, 21, 23, 48–61, 67, 68).....	106
6.2.6 Synthesis of 3-acetyl-4-phenylquinolin-2(1 <i>H</i>)-one intermediates (71a–72a)	158
6.2.7 Synthesis of aldehydes 79, 83– 90	159
6.3 Experimental section: Part II	164
6.3.1 General Procedures for tdDCC experiments	165
6.3.2 tdDCC experiments	167
6.3.3 <i>N</i> -acylhydrazone synthesis and characterization	169
Appendix.....	177
Abbreviations and acronyms	181
References	185
<i>Acknowledgements</i>	201

Abstract

My PhD research project has been finalized to the discovery of potential RAD51-BRCA2 protein-protein interaction (PPI) disruptors, able to trigger synthetic lethality (SL) in pancreatic cancer in combination with PARP inhibitor Olaparib. SL has been validated clinically, as anticancer therapeutic strategy, through the efficacy of Olaparib in BRCA2-defective cancers. In this context, we proposed to trigger a fully small-molecule-induced SL, combining RAD51-BRCA2 PPI disruptor with Olaparib to target pancreatic cancer. RAD51-BRCA2 PPI is essential in homologous recombination (HR) for DNA repair and it is mediated by two critical “hotspots” on RAD51 surface, Zone I and Zone II, suitable sites to design small molecule disruptors.

This thesis reports the application of two distinct hit identification strategies to identify potential RAD51-BRCA2 PPI disruptors.

In the first part of this project, an approach of structure-based design was applied, which exploited Virtual Screening (VS) campaign as hit identification strategy, followed by chemical modifications and SAR studies. Two VS, targeting separately Zone I and Zone II, led to the discovery of two classes of potential RAD51-BRCA2 PPI disruptors. In particular, VS targeting Zone II identified the dihydroquinolone pyrazoline **19** as hit compound. The optimization of a general synthetic strategy gave access to a series of analogs for SAR investigation, leading to compound **47** with the desired biological profile. Indeed, **47** inhibited RAD51-BRCA2 PPI, reduced cell HR and triggered cell death in combination with Olaparib in BxPC-3 cells, fully reproducing the paradigm of SL.

The second part of this thesis was devoted to a second hit identification strategy. During the six-month placement at HIPS in Prof. A. K. H. Hirsch’s group, I applied a technique of target directed dynamic combinatorial chemistry (tdDCC) on RAD51. This approach allowed the identification of *N*-acylhydrazone-based compounds, which proved to inhibit RAD51-BRCA2 PPI at micromolar range in the preliminary biochemical assay.

1. Introduction

1.1 Tumor heterogeneity

Cancer is defined as a broad group of diseases and represent the second leading cause of death in the world, accounting for an estimated 9.6 million deaths, or one in six deaths, in 2018 (Figure 1).¹ Despite the extraordinary research efforts and funding employed over the past several decades, successful eradication and cure of advanced disease is still elusive.² In parallel, our knowledge of cancer biology and genetics has significantly improved, leading to the translation of cancer genomics to cancer therapeutic needs.² Addressing cancer cellular complexity and dynamics is meant as promising approach to develop successful cancer therapies.

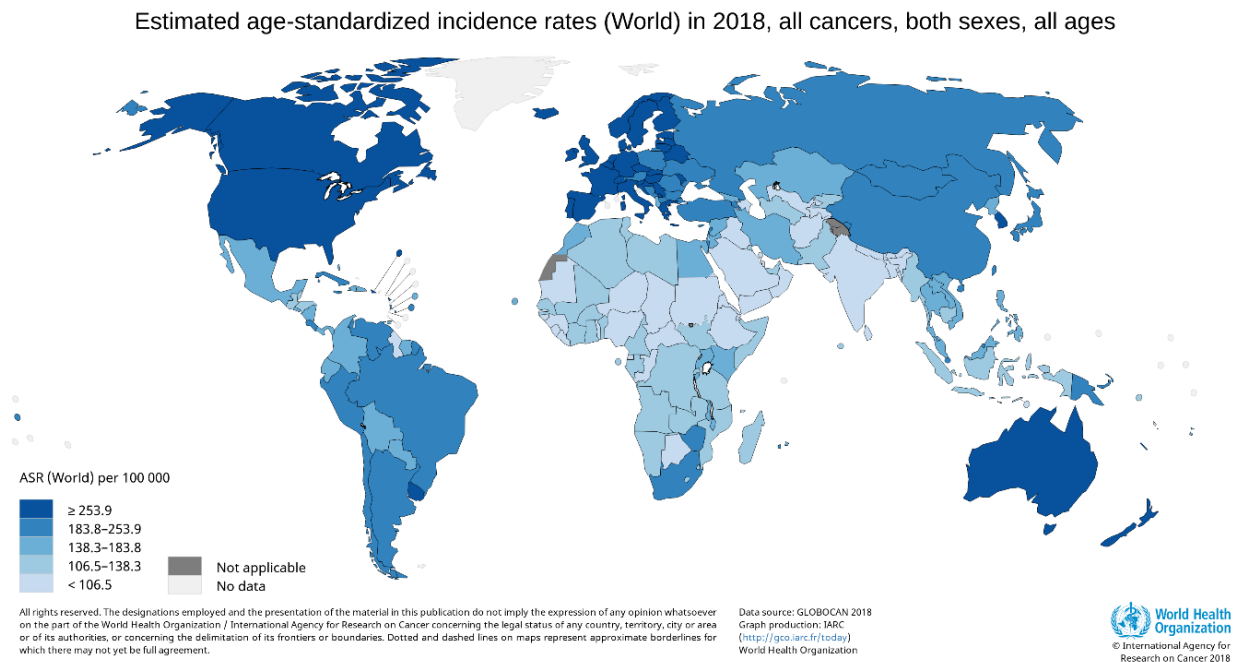


Figure 1. Estimated age-standardized incidence rates (World) in 2018, all cancers, both sexes, all ages¹.

Since the German biologist Theodor Boveri firstly proposed that pathogenesis of cancer could be driven by a “specific and abnormal chromosome constitution”,³ genomic instability has been recognized as a huge feature of most cancers.⁴ In fact, tumours are associated with deep alterations in their genome at multiple levels, including alterations in chromosome number and structure, a phenotype termed *chromosomal instability*.^{4,5} The number of mutations found in any cancer can vary up to hundreds of thousands. ² Tumours accumulate somatic aberrations as

result of the interplay of *driver* and *passenger* mutations.² Gene mutations, which directly or indirectly confers a selective growth advantage to the cell in which they occur, are considered *driver*, accounting for the real leading cause of oncogenesis.^{6,7} A tumor can contain *driver* gene mutations, affecting genes involved mainly in cell proliferation, DNA damage response (DDR), and cell cycle regulation. These mutations can alter cellular behavior, drive the disease progression and influence how the tumor will respond to therapy.⁴ Cancer *driver* mutations are often classified into *gain-of-function* and *loss-of-function* mutations. *Gain-of-function* mutations lead to protein overexpression or pathway hyper activation, including genes such as RAS⁸ and MYC,⁹ which mediate signal transduction, cellular proliferation, growth, and metabolism. Whereas *loss-of-function* mutations lead to inactive proteins or impaired pathways, and involve genes such as BRCA1/2,¹⁰ TP53,¹¹ RB1,¹² which mediate DNA damage repair, cell cycle control, and ultimately apoptosis. Alongside key *driver* mutations, a typical tumor may contain many thousands of *passenger* mutations, which do not contribute directly to the disease, but are more context-dependent,⁴ triggered by the exposure to environmental factors or defects in the molecular mechanisms that maintain genome integrity, such as DNA repair processes.

Accumulating studies suggest that type and distribution of mutations, whether *drivers* or *passengers*, are significantly heterogeneous among cancer cells within a single tumor, and this evidence accounts for an intratumour heterogeneity.¹³ Thus, the presence of subclonal mutations that exist only in a subset of neoplastic cells within a tumor, generates the onset of sub-clonal populations.⁷ Indeed, despite it is well recognized that cancers are associated with genomic alterations, what is less commonly appreciated is that these changes occur heterogeneously within a single tumour, giving raise to genetically distinct cellular subpopulations.^{5,14}

In 1976 Peter Nowell firstly described cancer as a model of evolutionary process,¹⁵ where somatic cell mutations and selective pressure contribute to drive the selection of sub-clonal lines. In this model, cancer is defined as a dynamic disease where cancer heterogeneity represents a substrate for the clonal evolution.¹⁶ The combination of genomic instability, which contributes by providing a rich pool of genetic mutations, and the selective pressure, ensured by factors in the tumour microenvironment and reversible changes in cell properties, results in the positive selection of subclonal cell lines, which drive tumour progression and invasiveness (Figure 2).^{13,16} Noteworthy, among cellular sub-populations, cancer stem cells (CSCs) have been identified as cellular drivers of sub-clonal expansion and promoter of intratumour heterogeneity, due to their extensive self-renewal and replicative potential.^{2,17}

Intratumour heterogeneity has been linked to different responsiveness to chemotherapeutics, and to the onset of mechanisms of intrinsic and acquired drug resistance.¹⁴ Indeed, based on their genotypic and phenotypic profiles, distinct sub-clonal populations can depend differently on targeted pathways, and respond heterogeneously to targeted monotherapies (intrinsic resistance). On the other hand, they can become resistant after drug treatment, with drug acting as an external selective pressure, which drives the positive selection of drug resistant tumour subpopulations, contributing to cancer relapse and progression.^{14,18} All these evidences suggest that intratumour heterogeneity cancers hamper significantly the effectiveness of available anticancer therapy. The overcome of such features has been one of the first rationale proposed for combination cancer therapy.

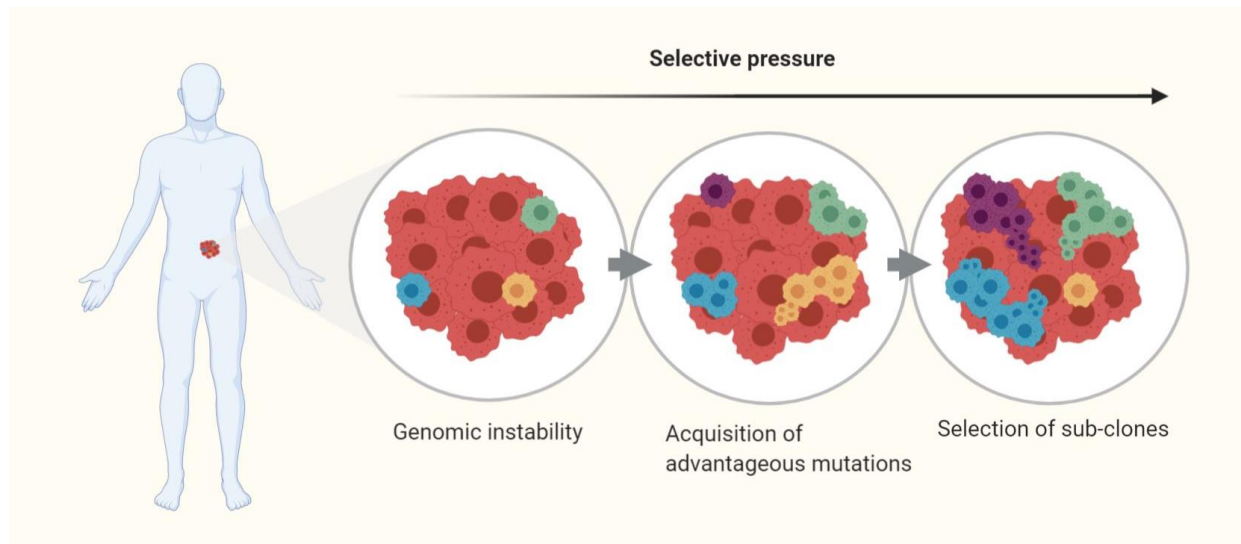


Figure 2. Intratumour heterogeneity promoted by genomic instability and selective pressure.

1.2 Combination cancer therapy

Targeted therapy is an approach where therapeutics are rationally designed to target specific molecular alterations in the tumour.¹⁹ This approach has been put in contrast to the outdated cytotoxic chemotherapy, based on non-selective drugs, which kill cancer and normal cells undergoing high proliferation rate, and exhibit severe side effects. To be effective, targeted therapies need to be directed at the founding clonal mutations shared by all cells in the cancer. For cancers, which are strictly dependent on a single *driver* mutation, single-agent treatment is potentially curative.¹⁹ However, the intratumour heterogeneity, combined with the ability to adapt to external stimuli, can prevent the effectiveness of targeted monotherapy, also facilitating drug resistance.^{14,19} Definitively, cancer mutational complexity underscores the need for combined treatment approaches to target different sub-clonal populations, and exploit robustness and redundancy of cellular pathways overlaps, which guarantee cell sustain and survival.¹⁴

The combination treatments with two or more therapeutics, which specifically target cancer inducing or cell sustaining pathways, is a cornerstone of cancer therapy and has provided significant advantages.²⁰ First, multiple drug combinations could enable to target multiple pathways, often dysregulated in cancer cells, leading to an increased chance of disease control. Next, multiple drug combinations could target the heterogeneous nature of tumors, including CSCs sub-population.^{20,21} In some cases, this results into increased efficacy, reduced dose required for each agents, shortened time of treatment, decreased risk of toxicity and side effects and slowed down development of drug resistance.^{20,22} Indeed, since cancer cells are frequently not able to adapt simultaneously to multiple therapeutic agents, combination therapy can minimize the risk of acquired resistance and attenuate the likelihood of relapse, if compared to monotherapy, which can foster cancer cells to recruit alternative salvage pathways.²⁰

Targeted combination therapies are currently designed based on molecular reasoning about the functions of targets.²³ In general we can distinguish between drug-independence and drug-interaction combinations. In the case of independent-drug combination, two or more cellular functions, which do not necessarily overlap, are selectively impaired, in order to increase the chance to treat different oncological patients, bearing a similar type of cancer.²³ Whereas, in the case of a drug-interaction combination, the benefit stems from the possibility to target the crosstalk between different pathways among sub-clonal cancer cells, addressing the intratumour heterogeneity.²³ Drug-interaction combinations offer the possibility to target the emerging activation of compensatory or bypassing pathways, which ultimately promote drug

resistance.²⁴ In this context, the combined effect of two drugs can be classified in synergistic, additive, or antagonistic, correlated to whether it is greater than, equal to, or less than the sum of the drugs individual effects. Based on Loewe's additivity model and Greco's response surface model,²⁵ the Equation 1 leads to the quantification of the effect of combination of drug A and B:

$$D_{A,i} = S_{A,i} d_A + S_{B,i} d_B R + \alpha S_{A,i} S_{B,i} \frac{d_A d_B}{ED_{50,B}}$$

D = equivalent dose;

$D_{X,i}$ = dose of drug X effectively sensed by each subpopulation;

ED_{50} = effective dose in 50% of population;

$S_{X,i}$ = dose sensitivity % of drug X in subpopulation;

d_X = drug X dose

α = interaction parameter

Equation 1. Greco's response surface model

The interaction parameter α spots the magnitude of synergy ($\alpha > 0$), additivity ($\alpha = 0$), or antagonism ($\alpha < 0$) (Figure 3).

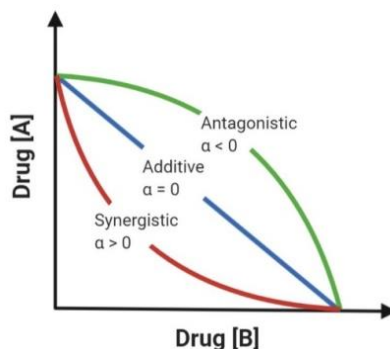


Figure 3. Isobologram for additive, synergistic, and antagonistic two-drug combinations, based on Greco's model.²⁶

As synergism by definition has the greatest potency relative to the sum of the total dose, much interest has been focused on finding potent synergistic combinations.²⁶ Thus, the research has been directed to synergic combination therapies, which exhibit enhanced therapeutic efficacy at lower doses.^{23,27} Among the available combination strategies, the synthetic lethality concept has been emerging as promising framework for the development of synergic anticancer drug combinations.

1.3 Synthetic lethality

Synthetic lethality (SL) concept was originally derived from genetic studies on gene-gene interactions in model organisms, such as fruit flies^{28,29} and yeasts,³⁰⁻³² and it is based on the interaction of two genes, which both contribute to processes, essential for cell viability.^{33,34} According to this genetic principle, two genes are “synthetic lethal” if the mutation of either gene alone is compatible with cell viability, but the simultaneous mutation of both genes induces cell death (Figure 4).³⁴ Indeed, in case of either gene mutation, the non-mutated gene can buffer the loss of the mutated one and *vice-versa*, whereas if both genes are impaired, the buffering effect is lost and cell death is triggered.³⁴ The concept of SL can be extended to the proteins encoded by synthetic lethal genes and, in turn, to the cellular pathways mediated by the product proteins. In this scenario, if two pathways contribute to sustain essential cellular processes, the inhibition of one is not lethal, because sufficiently compensated by the alternative pathway, but the combined inhibition results lethal for the cell due to the lack of compensatory effect.³³

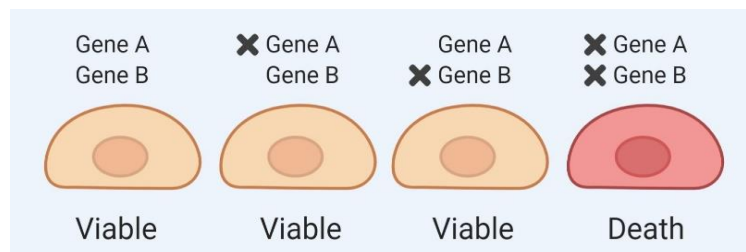


Figure 4. Synthetic lethality concept.

SL can be exploited in anticancer drug discovery to expand the repertoire of anticancer drug targets^{35,36} and overcome the genetic heterogeneity observed within tumor cells since it allows targeting multiple key interconnected processes.³⁷ Moreover, since SL takes advantage of altered or mutated genes present only in cancer cells to exploit tumor molecular vulnerabilities,³⁸ this approach has been included in the framework of precision medicine in cancer therapy.³⁹ Indeed, precision medicine, or precision oncology, proposes to tailor personalized treatments to each individual oncological patient, based on the genetic profile of the cancer and the individual.^{39,40} Ultimately this goal can be reached by applying SL to design the therapeutic options.

During the past decade, the advent of advanced genome-wide screening techniques has enabled the identification of biologically relevant SL interactions in human cancer cells,³⁷ with improved efficiency and accuracy.^{37,41} These techniques include RNA interference (RNAi)-

based largescale screens⁴² based on small interfering RNA (siRNAs) and short hairpin RNA (shRNAs), II) clustered regularly interspaced short palindromic repeats (CRISP), CRISPR/Cas9 systems,⁴³⁻⁴⁵ and recently III) RNA-targeting CRISPR/Cas9 systems.⁴⁶ In parallel to biotechnological platforms, high- and medium-throughput phenotypic approaches, in particular cellular-based drug screening, have been intensively exploited to provide information about the anticancer effect of drugs in presence of specific cancer mutations, detecting possible pharmacological and clinical outcomes. Moreover, computational approaches have also been applied to analyze collected data and map genetic interaction networks in tumors with the aim to predict SL interactions.^{47 48,49}

SL strategy can be employed mainly in two different approaches. One option can be targeting proteins encoded by genes that are synthetic lethal in presence of a known tumor-specific mutations (Figure 5A).^{34,36} In another option, SL can be exploited to identify specific drug combinations, which act simultaneously on two synthetic lethal partners, to induce cancer cell death (Figure 5B).⁵⁰

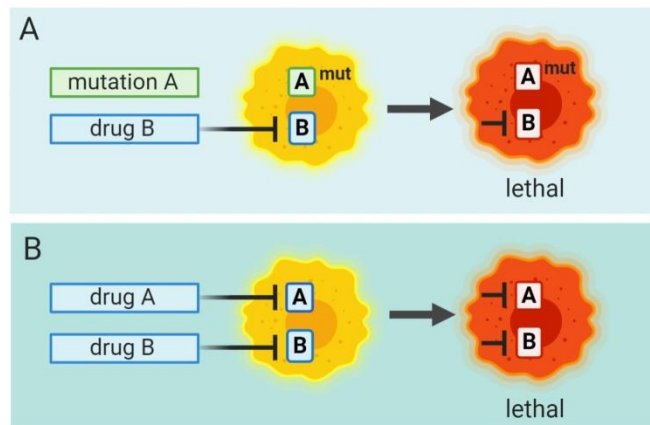


Figure 5. Synthetic lethality in anticancer therapy: A) Mutation A + drug B; B) drug A + drug B.

In the first approach, the combination of an endogenous tumor mutation and the targeted drug leads to cancer cell death, while normal cells are spared due to the lack of a specific genotype.³³⁻³⁶ This approach exploits tumor vulnerabilities induced by genetic alterations, facilitating the indirect targeting of undruggable cancer mutations through a druggable synthetic lethal partner. In fact, while the majority of available targeted therapies exploits tumor oncogene addiction by targeting *gain-of-function* mutations, SL provides the opportunity to target so far considered undruggable genetic alterations, including *loss-of-function* mutations and non-oncogene addiction.^{35,36}

SL has been validated clinically through the efficacy of poly(ADP-ribose) polymerase (PARP) inhibitor (PARPi),⁵¹ Olaparib (Lynparza ®) for the treatment of cancers harboring the germline *loss-of-function* mutations in either *BRCA1* or *BRCA2*.⁵² Indeed, *BRCA2* gene encodes for the homonym protein, which participates to the homologous recombination (HR) process to repair DNA double strand breaks (DSBs). The *loss-of-function* mutations in *BRCA2* gene sensitize cancer cells to the inhibition of other pathways and proteins involved in DNA damage response (DDR) network, including PARP, which plays a role in DNA single strand breaks (SSBs) for base excision repair (BER). Ultimately, the simultaneous impairment of *BRCA2* and PARP activities is able to induce the synthetic lethal effect in cancer cells.⁵³⁻⁵⁶

Following the clinical application of SL of PARPi in *BRCA2*-defective cancer, new SL interactions have been identified with the purpose to target cancers harboring specific genetic mutations. At this regard, S. Parameswaran *et al* ³⁷ has recently reported a detailed list of ongoing clinical trials for potential therapeutics that target specific cancer genotypes. In this context, authors clarified that an observed 'incomplete penetrance' of the lethal phenotype could be the reason of the limited results in clinic of this approach.³⁷

Despite the advantageous selectivity of targeting mutations harbored only by cancer cells, this strategy has been showing issues similar to those observed in classical targeted monotherapy, such as the onset of acquired resistance.⁵¹ Indeed, multiple potential mechanisms of drug resistance have been reported in *BRCA2*-defective cancers as effect of PARP inhibition.⁵¹ These include the restoration of *BRCA2* gene function, the inactivation of proteins involved in DNA repair^{57,58} and the loss of PARP1 protein.^{51,59} This negative outcome is in agreement with the adaptive nature of cancer, which drive the selection of resistant clones under the selective pressure of the PARPi. Ultimately, this clinical observation could suggest that SL could be better exploited to identify synergic drug combinations, rather than in monotherapy, in order to eradicate or at least reduce the risk of drug resistance.

1.4 Synthetic lethality as strategy for drug combination

If two drugs targeting two SL pathways are simultaneously administered, the exerted effect should be more than additive, thus synergic, due to pathways crosstalk. In this scenario, SL could provide a source of new synergic drug combinations, and novel molecular targets, overcoming the need of specific tumor mutations^{35,50} and ultimately broadening the spectrum of treatable cancers. Indeed, SL combinations have more possibilities to target intratumour heterogeneity.^{24,50} Moreover, unlike the treatment of *BRCA2* defective tumors with Olaparib, a SL combination promises to discourage the onset of acquired drug resistance caused by the restoration of genes harboring *loss-of-function* mutations.⁵¹ In line with these considerations, in the last years SL has becoming an attractive strategy to target pathways crosstalk and identify synergic combinations. In the most of cases, therapeutics, already used in clinic as single-agents, have been taken as starting points, followed by the search of potential SL drugs.

In 2015, Yi.Y.W. *et al*⁶⁰ reported the induction of SL death in triple-negative breast cancer (TNBC) cells in mesenchymal stem-like (MSL) subtype for the simultaneous inhibition of the epidermal growth factor receptor (EGFR) and mesenchymal-epithelial transition factor (MET). EGFR is a membrane receptor, essential for cell proliferation and survival, whose aberrant activation and overexpression are correlated to unregulated proliferation, invasion, metastasis and resistance to therapy of cancer cells.^{61,62} EGFR inhibitor, Gefitinib (Iressa ®) is an orally active agent, which has showed efficacy against cancers with EGFR activation such as breast, lung and colon cancers.⁶³⁻⁶⁵ Nevertheless, most TNBC cells expressing elevated level of EGFR exhibit innate resistance to EGFRi. To identify SL combinations in MSL subtype TNBC cells, authors performed a MTT screening in MDA-MB-231 cells with different receptor tyrosine kinase (RTK) inhibitors in presence of a fixed concentration of Gefitinib. Based on this phenotypic analysis, they characterized the MET inhibitor, SU11274, as SL agent in combination with Gefitinib. Further western blot analyses of treated cells lysates revealed that agent combination reduced the level of phosphor-EGFR (Y1068) and phosphor-MET (Y1234/1235) and, interestingly, decreased level of phosphor-ribosomal protein S6 (RPS6) (S235/236), more in combination than single-agent treatment. RPS6, a component of 40S ribosomal subunit, is involved in the regulation of protein synthesis and, ultimately in cell proliferation and glucose homeostasis,⁶⁶ and has been reported at high levels and hyperphosphorylated in cancers.⁶⁷⁻⁶⁹ RPS6 knockdown with siRNA exhibited reduction in cell proliferation in MDA-MB-231 cells, confirming the role of RPS6.⁶⁰ On these evidences, author suggested that the observed synthetic lethal effect of Gefitinib/SU11274 could be caused by the downregulation of RPS6 in

MDA-MB-231 cells, mediated by the two drugs.⁶⁰ This study has opened up to EGFR/MET inhibition as a strategy to address TNBC, and RPS6 as an unexplored oncological target (Table 1, entry 1).

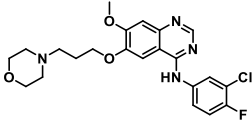
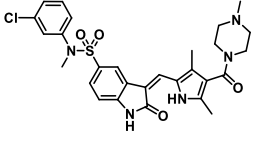
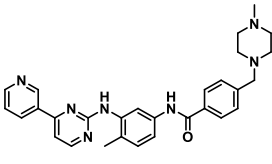
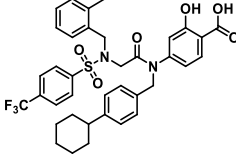
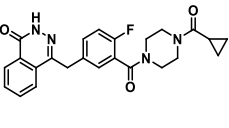
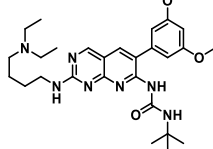
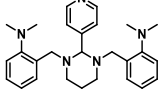
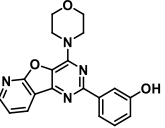
As attempt to overcome kinase independent-resistance to tyrosine kinase inhibitors (TKI) in chronic myeloid leukemia, AM Eiring *et al*⁷⁰ identified BP-5-087, an inhibitor of signal transducer and activator of transcription 3 (STAT3) to induce SL in combination with the BCR-ABL1 inhibitor, Imatinib. Despite targeting BCR-ABL1 with Imatinib has been effective in CML patients,⁷¹ the onset of resistance is highly frequent. While resistance due to point mutations in BCR-ABL1 kinase domain is clinically addressable with other approved TKIs,⁷²⁻⁷⁴ kinase-independent resistance is still an unmet need in CML treatment. In this case, the activation of alternative signaling pathways prevents the response to therapy and disease eradication in patients. It has been reported that STAT3 activation occurs upon TKIs treatments, and shSTAT3 reduced colony formation and increase apoptosis in intrinsically TKI-resistant K562^S cells. Authors firstly provided the proof of concept of SL by combining Imatinib and SF-1-0666, a salicylic acid-based compound previously reported to inhibit STAT3 by interacting with STAT3 SH2 domain.⁷⁵ Secondly, after structure-activity relationship (SAR) studies employed around SF-1-0666, among the up to 70 compounds synthesized, BP-5-087 has been characterized to increase the apoptosis in *intrinsically* resistant AR230^R cells when combined with Imatinib, opening the way to exploitation of SL to overcome intrinsic TKIs resistance in CML (Table 1, entry 2).

Recently, Lai SW *et al*⁷⁶ exploited the simultaneous inhibition of PARP1 by Olaparib, and fibroblast growth factor receptor 1 (FGFR1) by PD173074, to trigger synthetic lethality in PDAC cells. Firstly described by Connolly CJC *et al*,⁷⁷ PD173074 is a pyrido [2,3-d]pyrimidine-based compound, able to inhibit the tyrosine kinase activity of FGFR1⁷⁸ and suppress PDAC stem cell viability (Table 1).⁷⁹ FGFR1 and PARP1 seems to co-occur in PDAC cells and interact with each other forming complexes.⁷⁶ Thus, author proposed and proved that a SL combination can be exploited to enhance the efficacy of PD173034 and address acquired resistance to FGFR1 inhibitors (Table 1, entry 3).

In a further example, Graab U. *et al*⁸⁰ exploited the crosstalk between hedgehog (HH) and PI3K/AKT/mTOR signaling pathways to develop a SL combination for the treatment of rhabdomyosarcoma (RMS), one of the most common pediatric soft-tissue sarcoma.⁸⁰ HH pathway results aberrantly activated in RMS and it is proposed as possible target for

therapeutics.⁸¹ However the onset of acquired resistance for second transmembrane receptor smoothed (SMO) inhibitors underscores the need of alternative strategies. PI3K/AKT/mTOR pathway can activate via phosphorylation, in SMO-independent manner, GLI proteins, transcriptional factors of HH target genes. To reach the inhibition of HH pathway at multiple levels, authors combined the GLI1/2 inhibitor GANT61,^{82,83} and the PI3K/mTOR inhibitor PI103.⁸⁴ In RD cells, the combination proved to activate the apoptotic mitochondrial pathway via upregulation of the proapoptotic proteins, such as NOXA, BMF, BAX, and BAK, trigger caspase activation and suppress clonogenic survival and tumor growth *in vivo* (Table 1, entry 4).⁸⁰

Table 1. Synthetic lethal drug combinations.

Entry	Protein A	Protein B	Drug A	Drug B	Cell lines	Cancer type	Reference
1	EGFR	MET	 Gefitinib	 SU11274	MDA-MB-231	MSL subtype TNBC	Yi Y. W. <i>et al</i> 2015 ⁶⁰
2	BCR-ABL1	STAT3	 Imatinib	 BP-5-087	AR230 ^R cells	Kinase-independent TKI resistant-CML	Eiring A.M. <i>et al</i> 2015 ⁷⁰
3	PARP	FGFR1	 Olaparib	 PD173074	PDAC cells	Pancreatic cancer	Lai S.W <i>et al</i> 2020 ⁷⁶
4	GLI1/2	PI3K/mTOR	 GANT61	 PI103	RD cells	RMS	Graab U. <i>et al</i> 2015 ⁸⁰

Overcoming drug resistance is still an unmet need to treat human cancers, and it is clear that mutational analysis of resistant tumors is no longer sufficient to develop effective single agent

therapies. In this scenario, SL offers the possibility to develop combination therapies to adapt and engage the rapidly evolving heterogeneity, complexity and mutational set in cancer, exploiting non-oncogene addiction through the inhibition of alternative pathways.

1.4.1 Computational approaches to synthetic lethal drug combinations

Accumulating studies have been demonstrating that one drug can be synthetic lethal in combination with another in different types of cancer. Phenotypic assays and RNAi methods, as reported by examples above, have been intensively used to identify and demonstrate the mechanism of action of potential SL combinations. However, translation of SL into the clinic is still elusive and part of the problem is our incomplete knowledge of the complex network in which gene expressions converge.

Complexity and alternativity in biology can be simulated by *in silico* predictions based on system biology models.⁸⁵ For this reason, the use of computational tool has been exploited to integrate multiple datasets, predict lethal interactions and map these interactions into the cell signaling networks.⁸⁶ Phenotype is the result of the interaction of multiple degenerate pathways, and typical properties are robustness and resilience, comparably to a network.⁸⁷ These properties arise from redundancy and degeneracy, which are at the basis of pathways crosstalk that are therapeutically exploited by means of SL.

An example of how computational approach has been employed is Data-mining synthetic lethality identification pipeline (DAISY),⁸⁸ designed to deduce SL interactions at genome-wide level. This method performs a combinatorial analysis of collected genomic data, such as somatic copy number alterations, somatic mutations, pairs of genes co-inactivated at low frequency, and shRNA essentiality screens data. As integrative statistical analysis, DAISY led to the identification of thousands of biological pathways crosstalk as exploitable SL I interactions.⁸⁶

Another example of computational approach is represented by Synthetic Lethal Database (SynLethDB). SynLethDB is a source developed to integrate genomic, transcriptomic and drug sensitive data, which allows predictions about cancer responsiveness to drugs, based on SL interactions within a specific genomic context.^{48,86}

Interestingly, machine learning has been employed to explore synergistic combinations. DeepSynergy, reported by Preuer *et al*,⁸⁹ is a deep learning method whose inputs contain chemical descriptors of two drugs and information about cell line genomics in the absence of

drug. This method has been set up not only predictive on the existing dataset, but also to deduce unexplored drug combinations.

A further exploitation of computational approach toward SL has been reported by A. Heinzl *et al.*⁵⁰ Through the systematic analysis of drug combinations currently in use or at late phase III or IV clinical trials for ovarian cancer, they rank a series of novel drug combinations, not previously investigated or tested, which address SL targets.⁵⁰ Despite the lack of experimental validation, this study proves how computational mapping and analysis can open the way to unexplored SL combinations.

From these examples it is clear that databases, computational analyses and machine learning are growing as useful tool to collect, process and combine data derived from genetic studies and phenotypic assays. Indeed, mapping the SL network within cancer cell could promote the identification of new SL combinations and potentially predict the outcome of therapy in oncological patients. Noteworthy, these approaches need to be coupled to a growing collection of input data from biological studies to improve our knowledge about complex biological networks and elaborate more reliable predictions.

1.5 DNA double strand breaks (DSBs) repair pathways

Eukaryotic cells have evolved several coordinated and sophisticated processes to respond to DNA damages. This regulated effort, known as the DNA damage response (DDR), activates the DNA repair machineries or triggers cell death if DNA remains unrepaired, in response to genotoxic events.⁹⁰ Among DNA damages, DNA double strand breaks (DSBs) is one of the most harmful types of DNA lesions. DSBs can be the consequence of the exposure to ionizing radiation or chemical agents, or derive from natural cellular processes such as DNA replication. If unrepaired, DSBs compromise genetic integrity and stability, ultimately leading to cell death or carcinogenesis. In presence of DSBs, DDR machinery acts by activating cell cycle checkpoints to arrest cell cycle and allow time to restore genome integrity. Checkpoints G1/S, the intra-S and the G2/M transitions are the ones activated by DDR. In particular, G1/S checkpoint is the most sensitive to DNA damage and is reported to be defective in many human cancers.⁹¹

Two are the major processes involved in repair DSBs: end-joining (EJ) and homologous recombination (HR) (Figure 6).

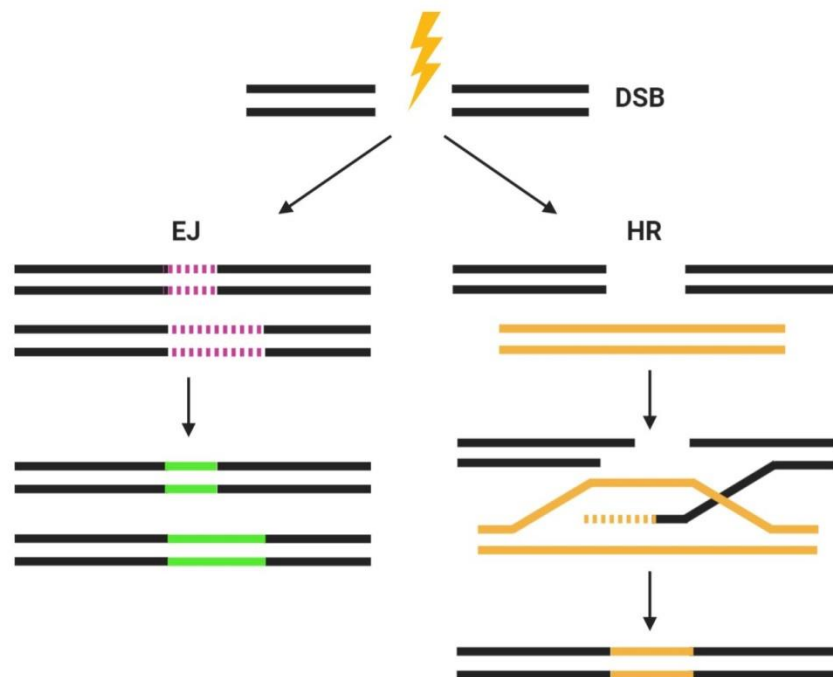


Figure 6. End join (EJ) and homologous recombination (HR).

EJ is a template independent process and can be classified into non-homologous EJ (NHEJ) and microhomology-mediated EJ. Due to the lack of a template or a sister chromatid, EJ can lead to the loss of genetic material or chromosomal rearrangements (Figure 6). On the other

hand, homologous recombination (HR) necessitates a DNA template to repair complex DNA damages, which include DNA gaps, DNA DSBs, and DNA interstrand crosslinks (ICLs). Indeed, HR provides an error-free, template-dependent, high-fidelity, and accurate repair, which restores genetic information lost in the DSB.^{92,90,93} In addition to DNA damage repair function, HR plays a prominent role in guaranteeing the faithful genome duplication, supporting telomere maintenance and DNA replication in the recovery of stalled or broken replication forks. Many proteins are involved in HR to orchestrate the recognition and the subsequent processing of DSBs.

1.5.1 Homologous recombination (HR) pathway

In the HR process, DSBs repair is initiated by MRN complex (Mre11, RAD50, and Nbs1), which binds to the broken DNA ends.⁹⁴ Mre11 and RAD50 enzymes form a heterodimeric complex of two Mre11 and two RAD50 molecules, while Nbs1 binds across the Mre11 dimer (Figure 7).^{94,95,96} The crucial role of MRN complex is to recognize DSBs and promote the resection of free DNA ends, involving the recruitment of exonuclease Exo1 and BLM complex (Figure 7).⁹⁷ Among its multiple functions, MRN complex mediates the loading of replication protein A (RPA) on single-stranded DNA (ssDNA) and the recruitment and activation of ATM (Ataxia Telangiectasia Mutated) kinase at damaged sites via its binding to Nbs1 (Figure 7).^{90,98} Upon its activation, ATM recruits additional DDR factors, by phosphorylation of a variety of proteins, including histone H2AX⁹⁹ and Chk2,¹⁰⁰ to follow up on DDR signal transduction. The resection process mediated by ATM-MRN, Exo1, and BLM produces long stretches of ssDNA, which are in turn coated by RPA. In parallel, ATR (ATM-related) kinase is recruited on RPA-coated ssDNA recruitment platform.^{101,102,103} As part of DDR signaling transduction, ATR kinase activity leads to the phosphorylation of other kinases, such as Chk1,^{100,104} involved in cell cycle checkpoints regulation. In the context of DDR, a critical role is played by serine/threonine protein kinases belonging to the family of phosphatidylinositol-3-kinase-like protein kinases (PIKKs), which include ATM, ATR and DNA-PK (DNA-dependent protein kinase), sharing structural similarities and domain organization typical of PIKK members.⁹⁰

RPA is a ubiquitous heterotrimeric ssDNA binding protein, which comprises three subunits RPA70, RPA32 and RPA14, containing oligonucleotide/oligosaccharide (OB)-folds to interact with ssDNA and proteins.^{90,105} The role of RPA is to coordinate the repair process, preserve the integrity of ssDNA and, most importantly, stimulate the exchange with RAD51 enzyme. RAD51

is an evolutionarily conserved ATP-dependent recombinase, which effectively catalyzes the repair of DSBs through strand exchange reactions. The direct interaction between RPA and RAD51 at the level of RPA70 subunit and RAD51 N-terminal domain is followed by the replacement of RPA and loading of RAD51 onto ssDNA.⁹⁰ Herein, the dynamic exchange of RPA facilitates RAD51 nucleation to form the nucleoprotein filament. In addition to that, RPA exhibits a regulating effect toward nucleoprotein filament formation as free RPA in solution, resulting from the displacement, can inhibit RAD51 nucleation.¹⁰⁶

RAD51 loading on ssDNA at DSB site and the subsequent nucleoprotein filament formation are a highly regulated process, where numerous proteins participate as mediators. Breast cancer type 2 susceptibility protein (BRCA2) is the principal mediator, since it recruits and loads RAD51 onto the RPA-ssDNA complex, produced by resection.¹⁰⁷ In turn, BRCA2 is recruited by Partner and Localizer of BRCA2 (PALB2) and breast cancer type 1 susceptibility protein (BRCA1) to DSB, ultimately binding ssDNA portion with its OB-domains at C-terminal (Figure 7). PALB2 acts as bridging protein to connect BRCA2 to BRCA1,¹⁰⁸ an E3 ubiquitin ligase, which structurally exhibits two major domains, an amino-terminal RING domain and a tandem BRCT repeats, and forms a heterodimer with BARD1 protein.^{107,108} Therefore, BRCA2 interacts with both PALB2 and BRCA1-BARD1 complex, suggesting that all these components are implied in the stabilization of RAD51 nucleoprotein filament during recombination and strand exchange reaction. Upon recruitment by BRCA2, RAD51 coats ssDNA substrate, forming helical nucleoprotein filaments, to perform homology search, invading duplex DNA, and find the undamaged DNA template. Base pairing between the RAD51-coated ssDNA and its dsDNA homolog triggers the DNA strand exchange for the genetic recombination. Moreover this generates the conversion of a RAD51-bound filament and its dsDNA complement into a RAD51-bound heteroduplex DNA (hDNA) within a displacement loop (D-loop).^{90,109} Nucleation of RAD51 on ssDNA and homology search are highly regulated by the actions of many HR proteins, including RAD52, RAD54 and RAD51 paralogs, such as RAD55, RAD57,¹¹⁰ BCDX2 (RAD51B-RAD51C-RAD51D-XRCC2) and CX3 (RAD51C-XRCC3) complexes.^{90,93,109,111,112} Upon dissociation of RAD51 from hDNA, the 3'-end invading ssDNA acts as primer for DNA synthesis, using the complementary strand in the hDNA as a template to restore missing sequence (Figure 7). DNA synthesis can be performed through different mechanisms, such as BIR, SDSA or dHJ, where DNA polymerase and DNA ligase go through damaged 3'-end extension and strands annealing, resulting in DNA repair. Many factors are involved in the regulation of RAD51 activities, suggesting that multiple proteins and steps of HR could be valuable targets to inhibit HR and face therapeutic needs in oncology.⁹³

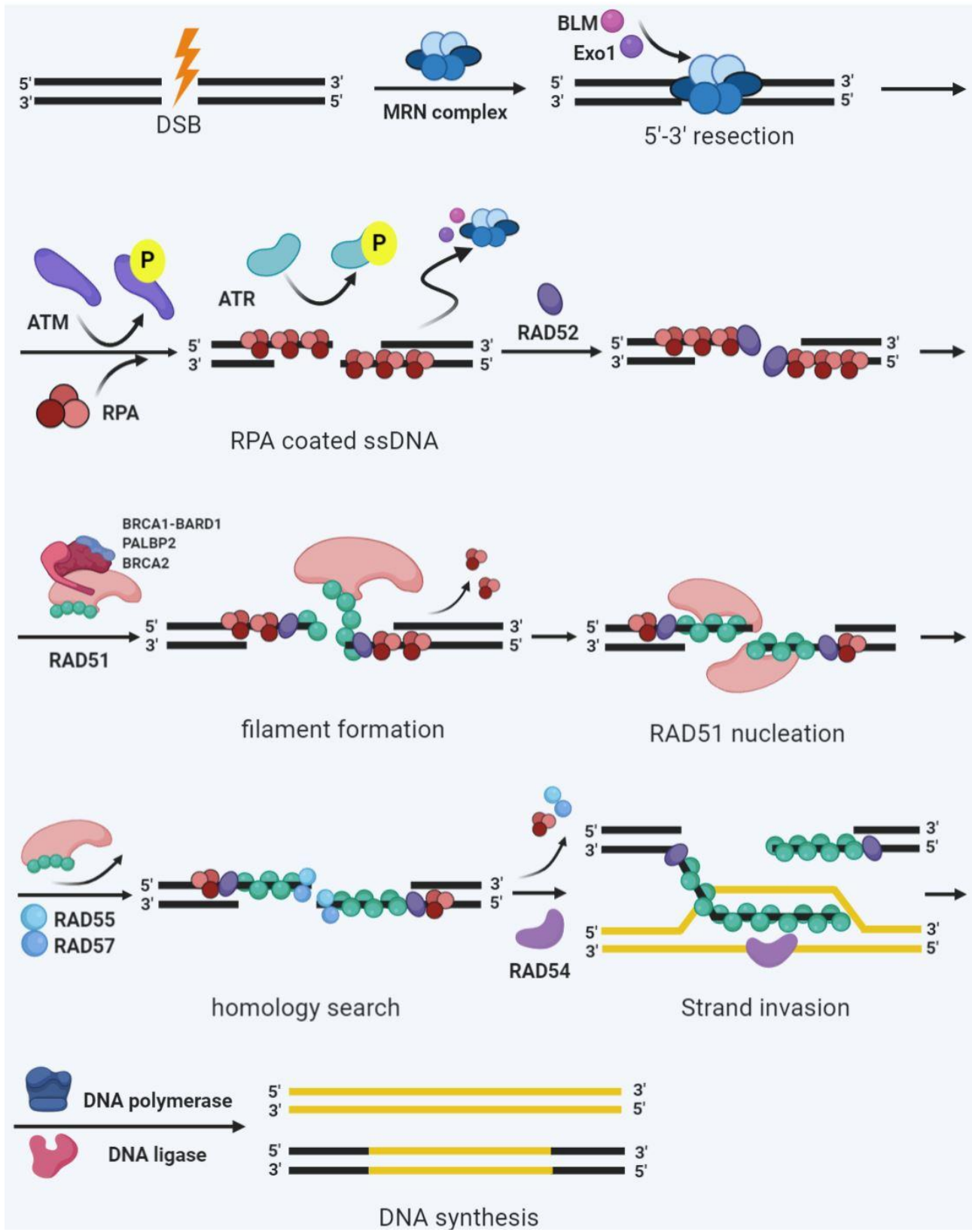


Figure 7. HR process for DNA DSBs repair.

1.5.1.1 BRCA2 protein: structure and functional domains

BRCA2 is a tumor suppressor protein, involved in the maintenance of genomic integrity.¹¹³ BRCA2 localizes to the nucleus during S and G2 phases of the cell cycle as part of mitosis process¹¹⁴ and DSBs repair by HR.¹⁰⁸ As its primary task, BRCA2 controls the function of RAD51 during the error-free HR process for the repair of DNA DSBs. Germline mutations in BRCA2 gene are associated to hereditary breast and ovarian cancer (HBOC) syndrome, correlated to predisposition to early onset of breast cancer and increased susceptibility to ovarian, pancreatic, stomach, laryngeal, fallopian tube and prostate cancers.¹⁰⁸

BRCA2 contains 3,418 amino acid residues and exhibits several and different functional domains (Figure 8), mainly described by three available crystal structures of isolated domains and regions, PDB ID 1N0W, PDB ID 1MJE, and EMDB ID 2779.¹¹⁴⁻¹¹⁶ The N terminal portion of BRCA2 is characterized by a PALB2-binding domain between 21 and 39 residues, with Trp31, Phe32 and Leu35 mainly responsible for the interaction (P),¹¹⁵ and eight highly conserved motifs about 30 amino acids each, BRC 1-8 repeats, which are the primary sites for RAD51 binding (987- 2113 residues) (Figure 8).¹¹⁴ In addition, BRCA2 contains a DNA-binding domain (DBD), which binds to ssDNA and dsDNA. The DBD domain is composed by five portions, an α -helical domain of 190 amino acids (H), three oligonucleotide binding (OB) folds (OB1, OB2, OB3), which are the ssDNA-binding modules, and a tower domain (TD), which protrudes from OB2 to bind dsDNA (Figure 8).^{90,108,116} Ultimately, at C terminus, BRCA2 contains a S3291 residue, substrate of cyclin-dependent kinase (CDK) phosphorylation, which represents a secondary binding site for RAD51 (Figure 8).¹⁰⁸

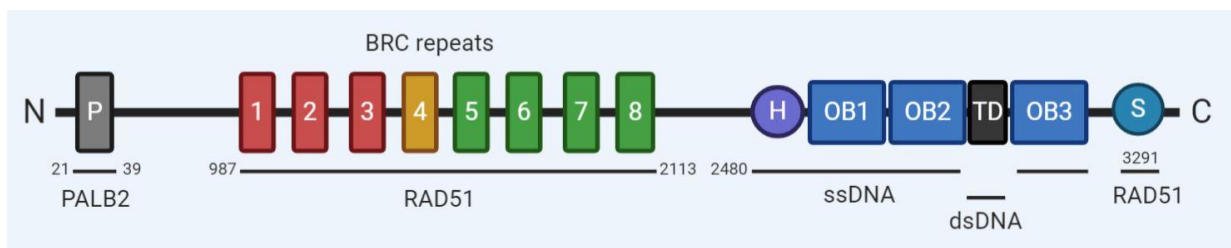


Figure 8. BRCA2 primary structure and functional domains.

1.5.1.2 RAD51 protein: structure and functional domains

RAD51 is an ATP-dependent recombinase, which forms a helical nucleoprotein filament on DNA to catalyze the strand exchange reaction in HR and lead to the free-error repair of DNA DSBs. Firstly discovered in yeast, RAD51 has been recognized as an orthologue of bacterial recombinase A (RecA). RAD51 is a 43 KDa protein composed by an α -helical N-terminal domain (NTD) of ~84 amino acids connected by a short helical linker to the C-terminal ATPase domain of ~240 amino acids (Figure 9).⁹⁰

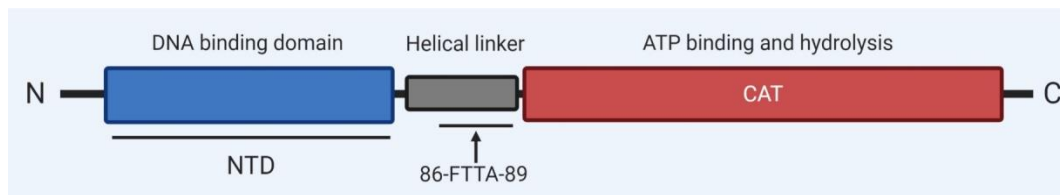


Figure 9. RAD51 primary structure and functional domains.

The NTD is primarily described as the DNA binding function, which regulates the recognition of ssDNA and dsDNA. RAD51 proved to interact with DNA through its phosphate backbone. In particular, each RAD51 monomer binds DNA in triplet clusters for intercalation of Arg235 and Val273. The complex is further stabilized by the interaction of Arg235 with the phosphate backbone of the complementary strand, opening the way to a mechanistic explanation about how homology search actually works in HR.¹¹⁷

On the other hand, the large C-terminal region comprises a Walker A/B motif, which is responsible for ATP binding and hydrolysis.¹¹⁸ The presence of ATP promotes RAD51 nucleoprotein filament formation by interaction of RAD51 monomers, whereas ATP hydrolysis fosters the nucleoprotein disassembly. In fact, ATP binding site localizes close to the interface area between RAD51 monomers, suggesting its role in RAD51 nucleation and oligomerization. Residues L133 and T134 result to interact directly with ATP, while a loop 315-323 of an adjacent monomer provides hydrophobic interactions with adenosine moiety (PDB ID: 5NWL).^{90,119}

In addition, the C-terminal region includes residues M158-M210 and M251-F259 forming hydrophobic pockets, which can lodge BRCA2 residues to mediate the protein-protein interaction (PPI) with RAD51, as essential step in HR.^{90,114} Ultimately, the short bridge, linking the two helical domains and bearing the motif 86-FTTA-89, appears to play a crucial role in the monomer-monomer recognition and oligomerization interaction.⁹⁰

1.6 RAD51-BRCA2 protein-protein interaction (PPI)

1.6.1 BRCA2 as principal RAD51 mediator in HR

BRCA2 has a central role in HR. There, BRCA2 recruits RAD51 recombinase to the site of DNA damage and mediates its loading and stabilization on RPA-ssDNA to promote homology search, strand invasion and strand exchange reactions. BRCA2 contains different highly conserved hallmark motifs.^{113,120} Despite the limited sequence similarity among BRCA2 orthologues, sequences of approximately 35 amino acids, repeated eight times in human protein, are highly conserved among mammalian species, suggesting their central role in BRCA2 biological functions. These sequences, known as BRC1-8 repeats, are located between 990 and 2100 residues and confer to BRCA2 the ability to bind RAD51 recombinase. Additionally, a region at the extreme C-terminus of BRCA2 has been mapped as secondary binding site for RAD51 and implied in the stabilization of RAD51 oligomeric assemblies. BRC repeats bind to the core region of RAD51, and the full-length BRCA2 has a binding capacity of at least six RAD51 monomers. Noteworthy, BRC repeats exhibit different binding affinities for RAD51 and displayed diverse effects in the modulation of loading, stabilization and ATPase activity of RAD51. Indeed, BRC repeats can be divided in two separate classes, based on their binding affinity for RAD51 and RAD51-ssDNA complex. As reported by Carreira *et al*¹¹³, BRC repeats 1–4 exhibit the strongest affinity for RAD51, with a binding stoichiometry of about 1:1. In addition, BRC 1–4 proved to block ATP hydrolysis mediated by RAD51, suggesting their role in the stabilization of RAD51-ssDNA complex. Moreover, BRCs 1–4 inhibit the formation of RAD51-dsDNA nucleoprotein and promote the DNA strand exchange. On the other hand, BRC 5–8 showed the weakest affinity for RAD51 and no effect on either ATPase activity or RAD51-dsDNA inhibition. However affinity increases significantly when RAD51 is in complex with ssDNA, suggesting their function in nucleoprotein filament stabilization during HR¹¹³. Based on these data, BRC repeats have evolved in two distinct groups, which together are necessary to guarantee efficient and correct DNA recombination.

When a DNA DSB occurs, followed by DNA resection, BRCA2 interacts with the free form of RAD51 through BRCs 1–4, altering RAD51 conformation to enhance ssDNA binding and promote the loading of numerous RAD51 monomers on ssDNA to form the nucleofilament. By means of the high affinity for RAD51, BRC repeats 1–4 modulate kinetically the nucleation of RAD51 on ssDNA, by preventing association with dsDNA and inhibiting ATP hydrolysis.^{113,120} After nucleation, BRC repeats 5–8 bind to RAD51 molecules of the nascent nucleofilament on

ssDNA. This second group of BRC repeats stabilizes the RAD51-ssDNA complex and, as chaperones, guide the filament growth. RAD51 filament grows in both directions to enable the fill of ssDNA gap in both sides. When filament starts to grow in BRCA2-independent manner and RPA are displaced from ssDNA, BRCA2 dissociates, as a free protein or in complex with four or five bound RAD51 molecules. RAD51 nucleofilament grows to form a complex, bound to ATP, and performs HR. During HR the cooperativity between BRC repeats results in the modulation of RAD51-DNA interaction and in turn RAD51 functions, such as RAD51 loading, homology search, DNA pairing, strand invasion and DNA recombination (Figure 10).^{113,120} Therefore by means of BRC repeats, BRCA2 ensures the efficiency and the fine regulation of HR crucial steps.

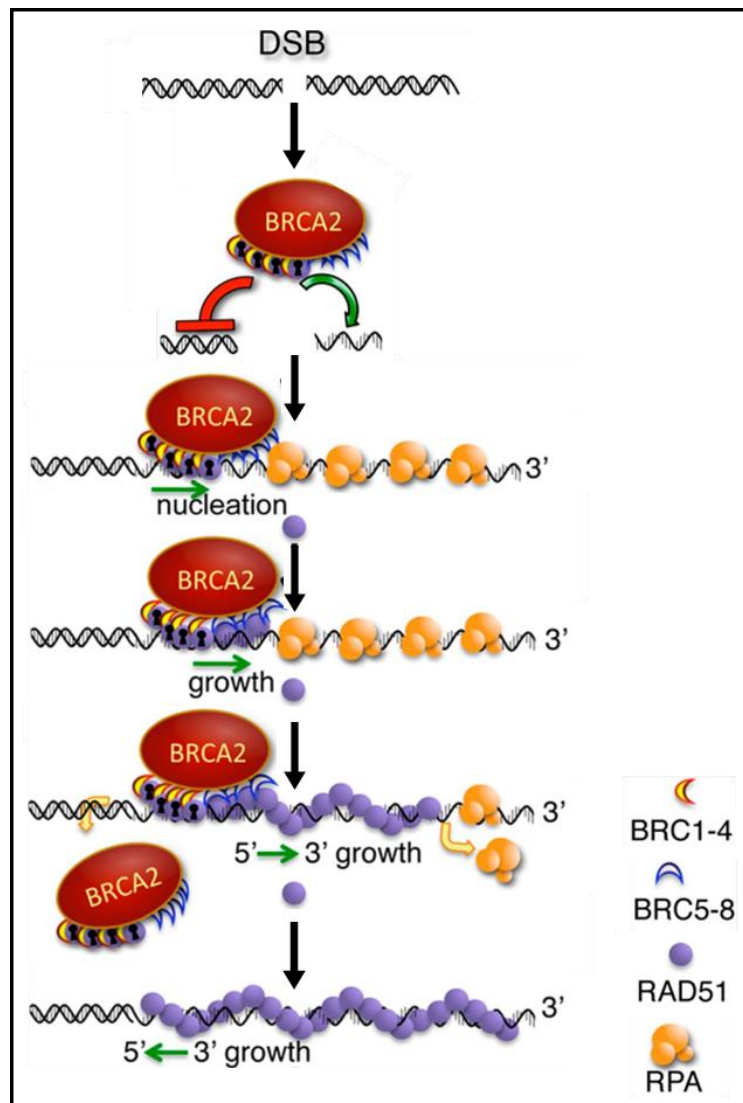


Figure 10. Role of the BRC repeats in the context of the BRCA2 protein in DSB repair (adapted from A. Carreira *et al*).¹¹³

1.6.2 RAD51-BRC4 interaction

BRC 1–8 repeats constitute the primary site of the RAD51-BRCA2 protein-protein interaction (PPI). Among the eight BRC repeats, BRC4 exhibits the highest binding affinity for RAD51, the strongest inhibition effect on DNA-dependent ATPase activity of RAD51 and the most stimulating effect on RAD51-ssDNA complex formation.¹¹³

In 2002 Pellegrini *et al*¹¹⁴ reported the high-resolution crystal structure of a fusion protein containing RAD51 in complex with BRC4, to provide mechanistic insights of the PPI. In this structure (PDB ID: N0W) the N-terminal region of RAD51 and the connecting domain 86-FTTA-89 necessary for RAD51 oligomerization have not been included to obtain RAD51 in the monomeric form (Figure 11).¹²¹

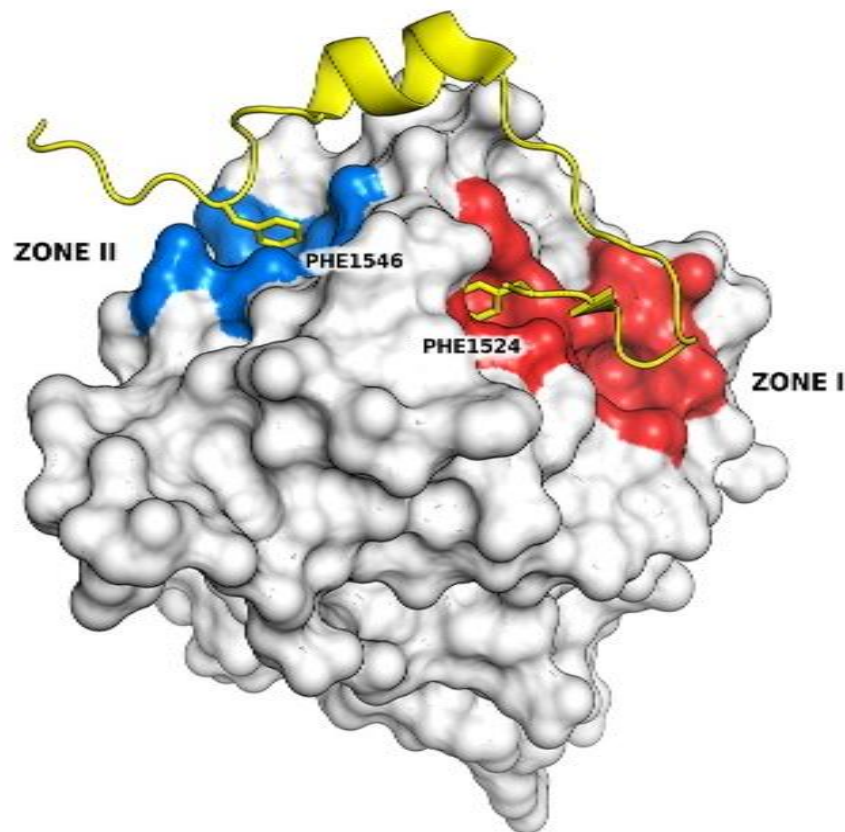


Figure 11. Crystal structure of RAD51-BRC4 complex (PDB ID_1N0W).

The crystal structure highlights the presence of two crucial tetrameric clusters in BRC4 repeat, FXXA and LFDE that interact with two distinct hydrophobic pockets on RAD51 surface. These two modules in BRC4 are essential for the binding to RAD51, and the two pockets on RAD51,

known as Zone I and Zone II, can be defined as hot spots of the RAD51-BRCA2 PPI (Figure 11).¹²¹ In details, RAD51-BRC4 covers an interface area of 2.026 Å, over a sequence of 28 amino acids, from L1521 to E1548, where hydrophobic interactions are prevalent, and BRC4 residues F1524, A1527, L1545 and F1546 are mainly involved in the interaction (Figure 11).¹¹⁴

Concerning the first PPI hot spot, 1524-FXXA-1527 tetrameric cluster of BRC4 is located at the level of a β -hairpin and interacts with the Zone I on RAD51 surface. This RAD51 hydrophobic pocket contains residues M158, I160, A190, A 192, L203, A207, M210, which form a cavity where the phenyl ring of F1524 is located, and residues F166, P168, L171, L186, V189, where A1527 is placed. Noteworthy, Zone I has been described as RAD51 oligomerization site. Indeed, Zone I RAD51 hydrophobic pocket can lodge the 86-FTTA-89 of another RAD51 molecule, mediating RAD51 monomer-monomer interaction. Thus, FTHA domain of BRC4 is a molecular mimic of RAD51 oligomerization sequence and has been considered a potential antagonist of RAD51 oligomerization, an essential step in nucleation and filament formation in HR.

As second PPI hot spot, 1545-LFDE-1548 motif at C-terminal domain of BRC4 engages the second hydrophobic pocket of RAD51, Zone II, distant from the oligomerization interface. In particular residues L1545 and F1546 fit between RAD51 helices A4 and A5, buried by residues L204, Y205, S208, M251, R254, L255, E258 and F259.^{114,121} As proof of the mechanistic importance of this second PPI hot spot, mutation of the LFDE binding pocket has been associated with failure of RAD51 foci assembly and cellular lethality.¹²¹

Additional interactions ensure the enhancement of the affinity between BRC4 and RAD51. In particular, it has been described an ionic interaction between E1548 of BRC4 and R250 of RAD51, forming a salt bridge, located at the interface area and proposed as stabilizer in RAD51 assembly.¹¹⁴

1.7 Targeting DNA repair machinery

1.7.1 PARP inhibitors

PARP1 and PARP2 are members of the PARP (poly (ADPribose) polymerase) protein family. These enzymes catalyze the polymerization of ADP-ribosyl units in target proteins (PARylation) with the use of NAD⁺ as a substrate, and the release of nicotinamide⁵¹. This modification often generates substrate proteins bearing negatively charged branched polymers of around 20-30 units, which modulate their conformation, stability or activity. PARP1 is one of the most representative member of PARP family, and plays a key role in the base excision repair (BER), to recognize, process and repair DNA SSBs. The primary structure of PARP1 shows different domains, a DNA-binding domain and a protein-recruitment domain (Figure 12).¹²² In particular, the N-terminus contains three Zn-finger domains, which mediate the interaction with DNA. The middle region is primarily involved in regulation of PARP1, containing BRCT (BRCA1 C terminus domain), and the site of auto-PARylation (P). Ultimately, the C-terminal portion contains WGR (tryptophan-, glycine-arginine-rich domain), responsible for interdomain contacts and DNA damage recognition, the HD domain and the catalytic domain, highly conserved among ADP-ribosyl transferases (Figure 12).^{122,123}

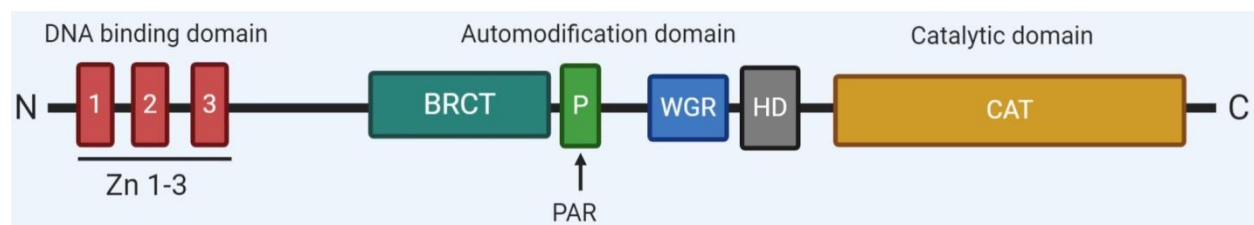


Figure 12. PARP1 primary structure and functional domains.

PARP1 enzymatic activation is triggered in presence of different types of DNA lesions, including SSBs, DSBs, DNA crosslinks, and stalled replication forks. Herein, the roles of PARP1 include the chromatin reorganization around the site of damage to promote DNA repair. PARP1 initiates the process by detecting and binding SSBs, and then the catalytic activity of PARP1 triggers the PARylation of PARP1 itself (auto-PARylation) and the PARylation of substrate proteins, including XRCC1 and the histones H1 and H2B.^{4,51} Interestingly, auto-PARylation appears to work as an autoregulation event, where the negative charge, endowed by PAR chains, triggers PARP1 dissociation from DNA.

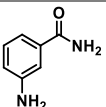
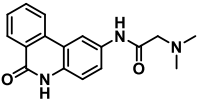
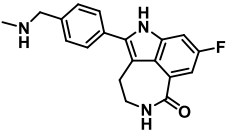
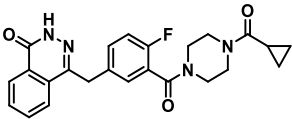
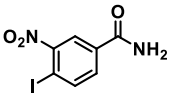
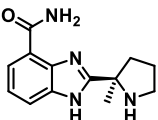
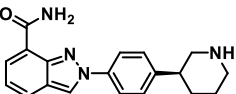
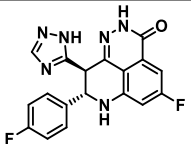
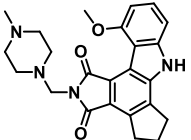
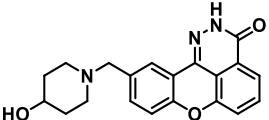
Inhibiting PARP1 activity compromises the efficient repair of DNA SSBs. Therefore PARP1 inhibition has been proposed as potential anticancer target to sensitize cancer cells to the treatment with DNA damaging agents.¹²² The initial hypothesis was that the impairment of PARP1 activity might leave DNA SSBs unpaired, in turn converted to DSBs by means of replication forks collapse. Since DSBs are repaired by HR, PARP1 inhibition is expected to be effective in cancer cells harboring HR deficiencies, such as cells lacking BRCA1/2 tumor suppressors.¹²² Indeed, PARP1 inhibition resulted synthetic lethal with biallelic defects in BRCA1, BRCA2 or PALB2 genes, found in a variety of breast and ovarian cancers.¹²²

In the 1980s, the development of the first generation of PARP1 inhibitors started from the observation that nicotinamide, a second product of the PARP1-catalyzed reaction, could induce moderate inhibition of the PARP. Modifications of the nicotinamide led to the development of a class of 3-aminobenzamides, which showed low selectivity and cytotoxic effects.¹²⁴

In the 1990s, a second generation of PARP1 inhibitors was developed on a class of quinazoline analogues, including isoquinolines, quinazolinediones, phthalazinones, and phenanthridinones, with PJ-34 as the most representative compound. The second generation proved to be more effective and target-specific and became the basis for the development of further drug groups.¹²⁴

The subsequent third generation of PARP1 included high potent and selective compounds, with Rucaparib as first characterized member.¹²⁵ This group includes also Olaparib,¹²⁶ Iniparib, Veliparib, Niraparib,¹²⁷ Talazoparib,¹²⁸ CEP-9722, and E7016 (Table 2).¹²⁴ The feasibility to exploit the pharmacologically induced SL led to the approval of PARP inhibitors Olaparib (Lynparza ®, 2014) and Rucaparib (Rubraca ®, 2016) for the treatment of advanced, chemotherapy resistant ovarian and breast cancer in BRCA1/2 deficient patients, and Niraparib (Zejula ®, 2017) for platinum-sensitive ovarian, fallopian tube, and primary peritoneal cancers.^{122,129} As proposed mechanism of action, PARP1 inhibitor block the catalytic activity of the enzyme. In particular, the second generation of PARP1 inhibitors bearing a quinazolinone moiety occupy both the nicotinamide-ribose and the adenosine-ribose binding sites of NAD⁺.¹²² Another proposed mechanism of action is the inhibition of the dissociation of PARP1 from the DNA damage site. This ‘trapping’ mechanism of PARP1 on DNA results in the accumulation of cytotoxic protein-DNA complexes, which prevents DNA replication and access to downstream DNA repair proteins in the damaged site.^{51,122} The trapping activity has been ascribed to a wide range of PARP1 inhibitors, including Niraparib and Veliparib¹²² (Table 2).^{4,130 122,131,132}

Table 2. Principal PARP inhibitor.

Inhibitor	Structure	Clinical applications	Trade name
3-Aminobenzamide		-	-
PJ-34		-	-
Rucaparib		2020 - Deleterious BRCA mutation (germline and/or somatic)-associated metastatic castration-resistant prostate cancer (mCRPC) who have been treated with androgen receptor-directed therapy and a taxane-based chemotherapy.	Rubraca®
Olaparib		2014 – FDA approved for germline BRCA-mutated advanced ovarian cancer	Lynparza®
Iniparib		-	-
Veliparib		-	-
Niraparib		2017 - FDA approved for platinum-sensitive ovarian, fallopian tube, and primary peritoneal cancers	Zejula®
Talazoparib		2018 - FDA approved for deleterious or suspected deleterious germline BRCA-mutated (gBRCAm), HER2-negative locally advanced or metastatic breast cancer	Talzenna®
CEP-9722		-	-
E7016		-	-

1.7.2 Inhibitors of HR proteins

1.7.2.1 RAD51 inhibitors

RAD51 plays an essential role in HR to repair DNA DSBs. During this process, RAD51 is implicated in several interactions, including RAD51/ssDNA, RAD51-RAD51, RAD51/dsDNA, and RAD51/nucleotide, and additionally it interacts with its protein partners, including RAD52 and RAD54.¹³³

Many common chemotherapies are based on cytotoxic compounds, which induce adducts, SSBs or DSBs in DNA. These anticancer drugs are often correlated to the onset of multiple mechanisms of drug resistance, either intrinsic or acquired. It is well understood that many pathways contribute to DNA repair by removing the DNA damage induced by radio- and chemotherapy in cancer cells. Therefore, targeting these pathways has raised as a potential therapeutic strategy to sensitize tumors and face the onset of drug resistance.¹³³

Concerning RAD51, high level of HR has been described in a wide range of cancers, including breast cancer, pancreatic, non-small-cell lung carcinoma and leukemia,^{134,135} and has been strictly correlated to RAD51 overexpression observed in tumor cells. In cancer cells showing increased level of HR, RAD51 overexpression is associated to drug resistance as it mediates the repair of DSBs and replication stalling lesions caused by radio- and chemotherapy. In addition, higher levels of RAD51 have been correlated to a shorter patient survival. Modulation or inhibition of HR has been proposed as option to potentiate the effect of available chemotherapies. As proof of concept, it has been demonstrated that reduced RAD51 expression, following antisense or ribozyme treatment, overcome resistance to radio- and chemotherapy.¹³³ The inhibition of RAD51 activity can be achieved either by inhibiting RAD51 catalytic function or by interfering with the established network of interactions between RAD51 and its partners.¹³³

Compounds acting directly on RAD51 catalytic recombinase activity have been identified by high-throughput screening of chemical libraries.¹³³ Reported by Ishida *et al*¹³⁶ in 2009, DIDS (4'-diisothiocyanostilbene-2,2'-disulfonic acid), a known inhibitor of chlorine ionic channel, proved to bind RAD51 and reduce HR by inhibiting both the binding of RAD51 to ssDNA and DNA strand exchange reactions (Table 3). In addition, in presence of DIDS, RAD51 showed to hydrolyze ATP, despite the absence of ssDNA. According to Ishida *et al*, this observation suggests that DIDS binds close to the DNA binding site of RAD51 and directly competes with ssDNA for RAD51, ultimately resulting in the stimulation of RAD51 DNA-independent ATPase activity.¹³⁶

As natural product firstly extracted from the marine sponge *Xestospongia exigua*, halenaquinone has been reported to inhibit HR during DNA pairing and D-loop formation steps (Table 3).¹³⁷ Halenaquinone proved to bind RAD51 by surface plasmon resonance (SPR) and to inhibit RAD51-dsDNA binding, and not RAD51-ssDNA, suggesting its interaction close to dsDNA domain of RAD51. Noteworthy, halenaquinone showed to inhibit the secondary dsDNA binding to the RAD51-ssDNA complex. In particular it inhibits the formation of both the D-loop and the ternary complex containing ssDNA, dsDNA and RAD51, which promotes the DNA homologous pairing step.¹³³

In 2011, Huang *et al*¹³⁸ reported the identification of B02 ((*E*)-3-benzyl-2-(2-(pyridine-3-yl) vinyl) quinazolin-4(3*H*)-one), which inhibits RAD51 binding to ssDNA, nucleoprotein filament formation and DNA strand exchange activity (Table 3). Subsequently, B02 proved to enhance sensitivity to ionizing radiations and cisplatin in triple negative breast cancer^{139,140} and, in combination with doxorubicin, reduce HR, increase apoptosis in multiple myeloma cells.^{122,141}

As further example of RAD51 inhibitors, Chicago Sky Blue (CSB) has been identified to inhibit RDA51-ssDNA interaction, by preventing the formation of stable filaments on ssDNA, as reported by Normand *et al* in 2014 (Table 3).¹⁴²

In 2012, Budke *et al*¹⁴³ reported the identification of RI-1, a chloromaleimide-based compound, which proved to form a covalent bond with the thiol group of RAD51 Cys319 by a Michael addition reaction, at the monomer-monomer interface. The reaction of RI-1, as Michael acceptor, provides the irreversible inhibition of RAD51 polymerization during nucleofilament formation. From subsequent SAR studies, RI-2, a RI-1 analogue, emerged as inhibitor of comparable potency and without the undesirable side effects linked to the Michael acceptor reactivity of RI-1 (Table 3).^{144,145}

The accumulation of complexes of RAD51 with undamaged chromatin exerts toxic effect in cancer cells overexpressing RAD51, thus the stabilization of RAD51-ssDNA complex has been proposed as potential strategy.¹⁴⁵ To this purpose, RS-1 has been reported to promote the accumulation of genotoxic nucleoprotein complexes in cancer cells, especially in case of RAD51 overexpression. Noteworthy, RS-1 exerted the highest effect in tumor cells expressing low level of RAD54L and RAD54B, two translocases that act as chromatin remodeling factors by removing RAD51 from dsDNA (Table 3).

RAD51 participates not only in DNA DSBs repair, but also in the stabilization of stalled replication forks. Compounds RI(dl)-1 and RI(dl)-2 has been reported as inhibitor of the

homologous strand exchange activity of RAD51, ultimately resulting in the prevention of D-loop formation.¹⁴⁵ This strategy proposes to block HR in cancer cells, preserving RAD51 ability to bind ssDNA and thus its protective role in replication stress tolerance (Table 3).

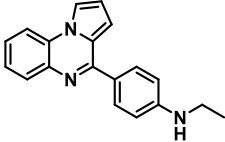
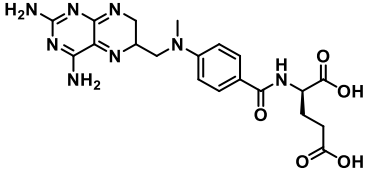
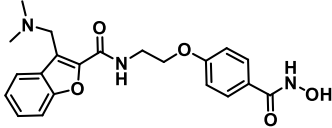
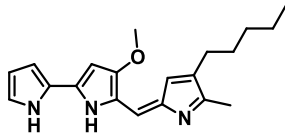
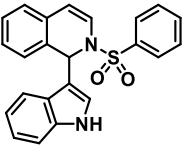
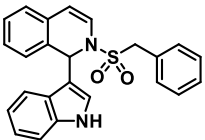
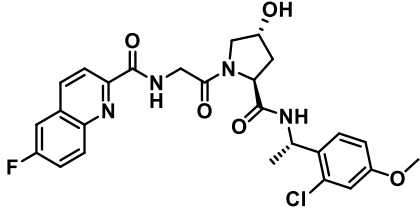
Methotrexate, Phenylhydroxamic acid and prodigiosin have been reported to inhibit HR by downregulation of RAD51 protein expression in different lines of tumor cells. In particular, methotrexate, used as dihydrofolate reductase inhibitor in chemotherapy, proved to induce lower level of RAD51 and decrease significantly RAD51 foci formation after irradiation in human osteosarcoma cell line (HOS) (Table 3).¹⁴⁶ Likewise, an inhibitor of histone deacetylases, phenylhydroxamic acid, showed to reduce RAD51 foci formation after irradiation, decrease RAD51 level and reduce HR response to DNA DSBs caused by chemotherapy in human colorectal carcinoma (HTC116).¹⁴⁷ With some differences, prodigiosin, a tripyrrole red pigment, exhibited a downregulating effect on RAD51 protein level, in particular by lowering the mRNA expression in several breast cancer cell lines (Table 3).¹⁴⁸

RAD51 nucleation to the site of DNA damage is a highly regulated process, where BRCA2 plays an essential role. Therefore, targeting the protein-protein interaction (PPI) between RAD51 and BRCA2 has been proposed as strategy to decrease HR level and sensitize cancer cells to chemotherapy. In 2013, Zhu *et al* ¹⁴⁹ reported the identification of two phenyl-sulfonyl indolyl isoquinoline compounds, IBR-1 and IBR-2, to disrupt the PPI and potentiate the effect of anticancer treatments (Table 3). In particular it has been proposed that the benzyl moiety of IBR-1/2 binds in the hydrophobic pocket of RAD51 involved in the monomer-monomer and RAD51-BRCA2 interaction, competing with RAD51 F86 and BRCA2 F1524, respectively.¹⁴⁹ In addition, IBR2 proved to impair HR and lower RAD51 foci formation in breast cancer cells (MCF-7) after irradiation.¹³³

Recently, Scott *et al* ¹⁵⁰ have reported the identification of CAM883A, as disruptor of the PPI interaction between RAD51 and BRCA2 (Table 3). In particular CAM883A has been described to bind the RAD51 oligomerization pocket and, in line with this, to reduce RAD51 foci assembly in the site of DNA damage and ultimately, reduce HR activity in non-small cell lung carcinoma (NSCLC) cell line.

Table 3. RAD51 inhibitors

Inhibitor	Structure	Mechanism of action
DIDS		Inhibition of DNA strand exchange activity of RAD51
Halenquinone		Inhibition of RAD51-dsDNA binding and formation of ternary complex, dsDNA, ssDNA, RAD51
B02		Inhibit RAD51 strand invasion and D-loop formation
CSB		Inhibition of RAD51-dsDNA binding and nucleoprotein formation
RI-1		Irreversible inhibition of RAD51 polymerization for covalent reaction with Cys319 at the monomer-monomer interface
RI-2		Interaction at the monomer-monomer interface and inhibition of nucleofilament formation
RS-1		Stabilization of RAD51-ssDNA complexes
RI(dl)-1		Inhibition of D-loop formation

RI(dl)-2		Inhibition of D-loop formation
Methotrexate		RAD51 downregulation
Phenylhydroxamic acid		RAD51 downregulation
Prodigiosin		RAD51 downregulation
IBR-1		Inhibition of RAD51-BRCA2 protein-protein interaction
IBR-2		Inhibition of RAD51-BRCA2 protein-protein interaction
CAM833A		Inhibition of RAD51-BRCA2 protein-protein interaction

1.7.2.2 RAD52 inhibitors

RAD52, a protein of 418 amino acids, participates in both DNA strand exchange and recovery of the stalled replication forks, and mediates the DNA-DNA interaction for complementary DNA strands annealing during HR. Its structure has a ring shape, formed by two main domains, the N-terminal domain (NTD), responsible for ssDNA binding and annealing actions of RAD52, and the C-terminal domain (CTD), involved in the interactions between RAD51 and RPA in HR.⁹³

RAD52 is an emerging therapeutic target for BRCA-deficient tumors. Indeed depletion of RAD52 results synthetically lethal in *BRCA1*-, *BRCA2*-, *PALB2*- and *RAD51C*-defective cancer cells.⁹³ This is due to the significant role played in genomic stability maintenance, which is enhanced when HR proteins such as BRCA1, BRCA2, PALB2, and RAD51 paralogs (RAD51B, C, D, and XRCC 2 and 3) are depleted or inactive.¹⁵¹⁻¹⁵³ RAD52 appears to have a postsynaptic role in HR, as a mediator of RAD51 and annealing protein, belonging to a single-strand annealing protein (SSAP) family, and its recruitment depends on RPA.⁹³ Seen its role in genomic stability maintenance and, recently reported, in carcinogenesis, RAD52 has been proposed as molecular target in anticancer therapy to exploit SL in *BRCA2*-, *BRCA1*- and *PALB2*- defective cancers. In particular, preliminary efforts have been focused on small molecule inhibitors targeting RAD52 oligomeric ring or DNA binding domain to prevent RAD52-DNA interaction. In 2015, 6-hydroxy-DL-DOPA has been firstly reported by Chandramouly *et al*¹⁵⁴ to interfere with RAD52 oligomerization and inhibit RAD52 foci assembly in murine hematopoietic cells deficient in *BRCA1* (Figure 13).

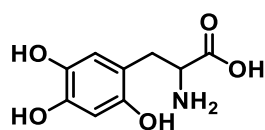


Figure 13. Structure of 6-hydroxy-DL-DOPA.

Subsequently, Huang *et al*¹⁵¹ identified two other compounds, D-103 and D-G23, bearing quinoline and quinazoline chemotypes, that target the DNA domain of RAD52, inhibiting RAD52 ssDNA annealing activity, preventing RAD52 foci assembly and reducing growth of in BCR-ABL1-positive BRCA1-deficient 32Dcl3 murine hematopoietic cell line (Figure 14).¹⁵¹

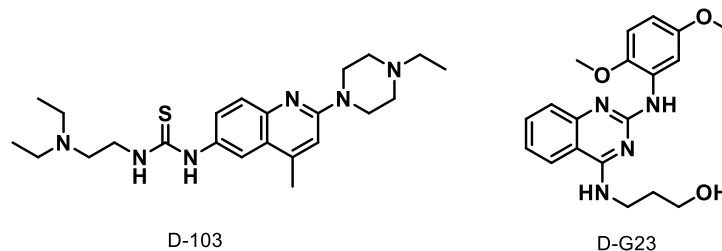


Figure 14. Structure of D-103 and D-G23.

Through a molecular docking study into the RAD52 DNA-binding site (PDB ID: 1KN0¹⁵⁵), 5-aminoimidazole-4-carboxamide ribonucleotide (AICAR) 5' phosphate (ZMP) was identified as potential inhibitor of RAD52-ssDNA interaction, which proved to kill *BRCA1*- and *BRCA2*-mutated cells.¹⁵⁶ Hengel *et al*¹⁵³ reported the identification of the macrocyclic compound NP-00425, emerging from *in silico* predictions as potential hit compounds, able to bind RAD52 and compete with ssDNA binding (Figure 15).¹²²

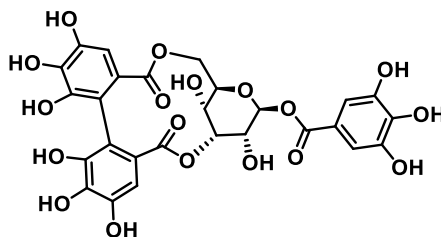


Figure 15. Structure of NP-00425.

1.7.2.3 RAD54 inhibitors

One of the several auxiliary proteins that stimulates RAD51 is RAD54, a member of the SNF2/SWI2 family of dsDNA-ATPase-dependent translocases.^{157,158} In mice, depletion of RAD54 sensitizes to ionizing radiation and to the DNA cross-linking agents, such as mitomycin C,¹⁵⁷ while mutations in RAD54 gene is associated to genetic instability and cancer. RAD54 directly interacts with RAD51, stimulating DNA strand exchange activity. In HR, RAD54 can bind specifically to Holliday junctions, forming oligomeric complexes, and promoting their ATPase-dependent branch migration by translocation along the DNA, during a postsynaptic stage when heteroduplex extension or dissociation is required to complete HR.^{157,159} RAD54 performs its functions in association with RAD51, stabilizing the nucleoprotein filament and regulating the stimulation of the RAD51-dependent strand exchange and heteroduplex extension.¹⁵⁸ Therefore, RAD54 exhibits diverse biochemical activities that can be potentially targeted to

inhibit HR, such as RAD51 modulation, DNA binding, oligomerization, ATPase activity, and DNA translocation.

In 2013, Deakne *et al*¹⁵⁷ recognized streptonigrin (SN), as a specific RAD54 inhibitor by high-throughput screening, to investigate the mechanisms of RAD54 (Figure 16). SN proved to target specifically RAD54 ATPase activity, through direct interaction with RAD54 and generation of reactive oxygen species, without affecting the DNA binding. In addition, SN showed to inhibit RAD54 branch migration, in agreement with the dependence on the ATPase-dependent DNA translocation of RAD54.¹⁵⁷ Noteworthy SN has been reported recently to enhance heterochromatin formation at low concentrations, a protective function toward genome integrity that suggests it as a good candidate in the context of epigenetic cancer therapy.¹⁶⁰

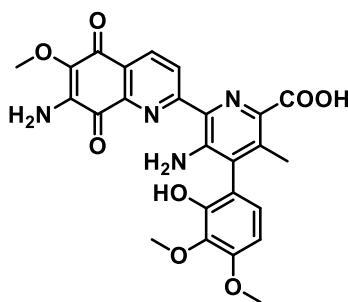


Figure 16. Structure of streptonigrin.

Recently, Ehmsen *et al*¹⁶¹ described the identification of two compounds, reported as 54i-1 and 54i-2, through high-throughput screening against RAD54 dsDNA-dependent ATPase activity (Figure 17). These compounds showed to inhibit RAD54, for interference in ssDNA-RAD54 interaction, and reduce cell growth alone and in combination with mitomycin C and cisplatin.¹⁶¹

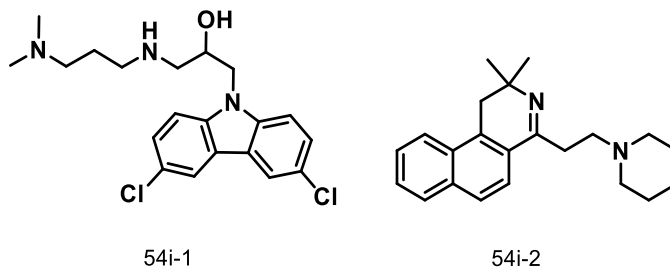


Figure 17. Structures of 54i-1 and 54i-2.

2. Motivations, aims and hit identification strategies

My PhD research project aims to develop small molecules as RAD51-BRCA2 protein-protein interaction (PPI) disruptors to synergize with PARPi Olaparib and induce synthetic lethality in pancreatic cancer.

Indeed, the concept of SL has been extensively studied in oncology, as an opportunity to discover new anticancer molecules for personalized targeted therapies.⁹³ The DNA repair and DNA damage response (DDR) pathways provide many opportunities to exploit SL. The application of this concept to DDR machinery assumes that, in the presence of an impaired DNA repair pathway, the inactivation of a compensatory pathway can trigger cancer cell death by the loss of buffering effect of the two complementary repair pathways.⁹³ Whereas, the inactivation of a single pathway is not enough to cause cell death, since the cell still tolerates DNA damage, sustaining cell survival. Genome instability is a hallmark of cancer and DNA damage occurs constantly in cells due to the continuous exposition to endogenous and exogenous stressors.¹⁶² Therefore, the complex and coordinated DDR network evolved by cells, to orchestrate the DNA repair and preserve genome integrity, becomes essential for cell survival. DDR prevents the transmission of altered genetic material to daughter cells and acts as a tumor-suppressive barrier.¹⁶² Defects in DDR are associated with the accumulation of oncogenic mutations and genome instability, and they contribute to cancer initiation and progression. Since cancer cells with defects in one DDR pathway can become reliant on other pathways, targeting other DDR pathways can potentially trigger selective cancer cell death through a mechanism of SL.

Initially, SL has been exploited to treat cancer cells with inactivating mutations in BRCA1 and BRCA2 genes, known as BRCAness condition, by poly adenosine-diphosphate ribose polymerase (PARP) inhibitor, Olaparib (Lynparza ®, 2014).⁹³ PARP is a crucial enzyme involved in the repair of DNA single-strand breaks (SSBs) through base excision repair (BER),⁴ whereas BRCA1/2 are essential proteins in DNA double-strand breaks (DSBs) repair by error-free homologous recombination (HR).¹¹³ The simultaneous impairment of both repair mechanisms, one due to the drug and one due to the mutation, results in cell-cycle arrest and apoptosis of cancer cells through SL (Figure 18A). Olaparib was firstly approved in 2014 by FDA as PARP inhibitor (PARPi) to treat advanced ovarian BRCAness cancers and later in 2018, it was extended to the treatment of metastatic breast tumors associated with germline BRCA mutations.¹⁶² Noteworthy, Olaparib has been approved in 2019 as first-line maintenance treatment of germline BRCAness metastatic pancreatic cancer, emerging as a new treatment

option for this unmet need in oncology.¹⁶³ In the context of DDR, BRCA2 plays its major role in HR, recruiting RAD51, the evolutionarily conserved recombinase, at the site of DSBs where it performs DSB repair through homology search and strand exchange reactions. DSBs represent a major risk of genetic loss and HR provides an error-free, template-dependent repair that guarantees the maintenance of genomic integrity. Indeed, the overexpression of RAD51 has been observed in a wide variety of cancers,¹³⁵ as well as the increased rate of RAD51-mediated HR. In parallel, the increased cellular amount of RAD51 is positively correlated to the onset of resistance to radio- or chemotherapies that induce DNA damage. Therefore, targeting HR represents a valuable starting point to sensitize cancer cells to DNA damaging agents and, ultimately, trigger SL in combination with the inhibition of complementary DNA repair pathways.

In this context, my PhD research project aims to chemically mimic a condition of BRCA2 mutation in BRCA2-functional cancer cells by inhibiting HR through a small molecule, and thus sensitize tumors to Olaparib treatment. Ultimately the combination of PARP inhibition and HR impairment would trigger cancer cell death by a fully small-molecules-induced SL, providing a new paradigm for the discovery of innovative anticancer therapies. This strategy could lead to the development of synergic drug combinations that target cancer cells genomic instability and reduce the onset of drug resistance.^{162,164}

To achieve significant HR inhibition and reproduce BRCAness condition, the PPI between RAD51 and BRCA2 has been chosen as molecular target. Indeed, RAD51 is essential in HR and a highly available molecular target due to its overexpression in cancer. On the other hand, BRCA2 mutation is the substrate required for the clinical success of PARP inhibition and the impairment of the protein function through a small molecule appears to be a valuable way to mimic BRCAness (Figure 18B).^{162,164}

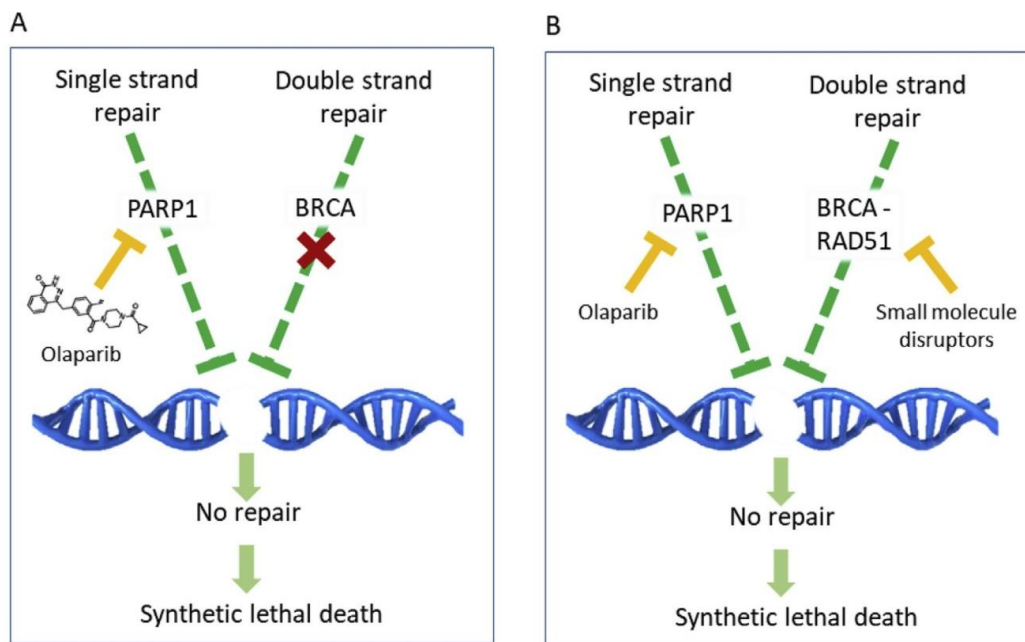


Figure 18. A) Synthetic lethal death induced by Olaparib in BRCA-defective cancer cells. B) Synthetic lethal death triggered by a combination of Olaparib and RAD51-BRCA2 PPI disruptors.

PPI interfaces have been emerging as an attractive, although challenging, class of potential targets for the development of anticancer drugs.¹⁶⁵ Indeed, the landscape of PPI networks in cancer has been constantly expanding by means of cancer genomics, targeted therapies, and network oncology, revealing the key roles of PPIs in driving and maintaining cancer growth. Therefore, the disruption of PPIs offers the possibility to inhibit the transmission of oncogenic signals.¹⁶⁵ Nevertheless, targeting PPI interactions by small molecules exhibits a number of challenges and concerns, including i) large and flat PPI interface areas, ii) lack of deep binding pockets, iii) presence of non-contiguous binding sites, and iv) the lack of natural ligands.¹⁶⁵ In contrast to the typically hydrophilic and well-defined ligand binding of many enzymes or receptors, the interface surfaces of protein-protein complexes are generally hydrophobic and relatively flat, often missing deep cavities where a small molecule can fit. However the presence of “hot spots” in the interface areas makes PPIs amenable for small molecule perturbations, providing the opportunity to perform a structure-based approach to drug design.^{166,167}

The RAD51-BRCA2 interaction is mediated by two critical hot spots on RAD51 surface, Zone I and Zone II, which can lodge eight highly conserved BRCA2 motifs. The X-ray crystallographic structure BRC4 (the fourth BRC repeat) is available in complex with the catalytic domain of RAD51.¹¹⁴ This makes the RAD51-BRCA2 interaction suitable for a structure-based design of PPI small molecule disruptors.

To identify potential RAD51-BRCA2 PPI disruptors, during my PhD research I have applied two distinct approaches for hit identification and optimization.¹⁶⁴

In the first approach (Part I), virtual screening campaign was exploited as tool for hit identification, followed by chemical exploration and SAR studies. A first virtual screening protocol, targeting Zone I, identified a 1,2,4-triazole hit compound **1** (Figure 19), which was exploited to develop a class of potential PPI 1,2,4-triazole-based disruptors and depict general SAR studies. Subsequently, as further step of my PhD project, a second virtual screening, performed targeting Zone II, led to the identification of a dihydroquinolone-pyrazoline hit compound **19** (Figure 25). A chemical modification campaign around the dihydroquinolone-pyrazoline core led to the development of a new PPI disruptor able to synergize with PARPi Olaparib and induce synthetic lethality in pancreatic cancer cells.

In the second approach (Part II), during the 6-months placement at HIPS, I explored the application of target-directed dynamic combinatorial chemistry (tdDCC) as hit identification tool to obtain new chemical scaffolds targeting RAD51 and enabling the displacement of BRCA2 interaction. As far as I knew, this technique has never been applied on RAD51. The approach allowed the identification of compounds able to bind to the target protein, which could be selected for biochemical tests in order to verify their ability to act as RAD51-BRCA2 PPI disruptors. Potential hit compounds identified by tdDCC can be adopted for chemical exploration to depict SAR studies and perform hit optimization.

For the sake of clarity, my PhD research activity has been focused on compounds design and synthesis and on the application of tdDCC. Biochemical, biophysical and biological profile evaluations have been performed in the context of the research group. Details about test protocols are reported in Appendix.

3. Part I: STRUCTURE-BASED DESIGN APPROACH TO THE IDENTIFICATION OF RAD51-BRCA2 PPI DISRUPTORS

To identify potential PPI disruptors, the research group where I carried out my PhD has recently conducted a successful Virtual Screening campaign using the available X-ray crystal structure of BRC4 (the fourth BRC repeat) in complex with the catalytic domain of RAD51 (PDB ID: 1N0W). The Virtual Screening was performed using the “FxxA” pocket, corresponding to the Zone I of the PPI. This allowed to identify a triazole-based hit compound **1**, which proved to disrupt RAD51-BRC4 interaction at the biochemical ELISA assay ($EC_{50} = 53 \pm 3 \mu\text{M}$) (Figure 19).¹⁶⁸ Upon preliminary SAR studies around **1**, focused on the linker connecting 1,2,4-triazole core and phenyl ring, triazole derivatives **2**, **3** and **4** were synthesized and tested. The propyl phenyl derivative **3** has been identified with the best PPI inhibitory activity ($EC_{50} = 25 \pm 2 \mu\text{M}$) (Figure 19) and submitted to cell-based assays. **3** proved to increase the sensitivity to Olaparib in pancreatic cancer cells BxPC-3, expressing fully functional BRCA2. However, compound **3** did not show the desired mechanism of action and, probably due to off-target effects via direct DNA damage, caused the increase of HR rate in treated BxPC-3 cells.¹⁶⁸

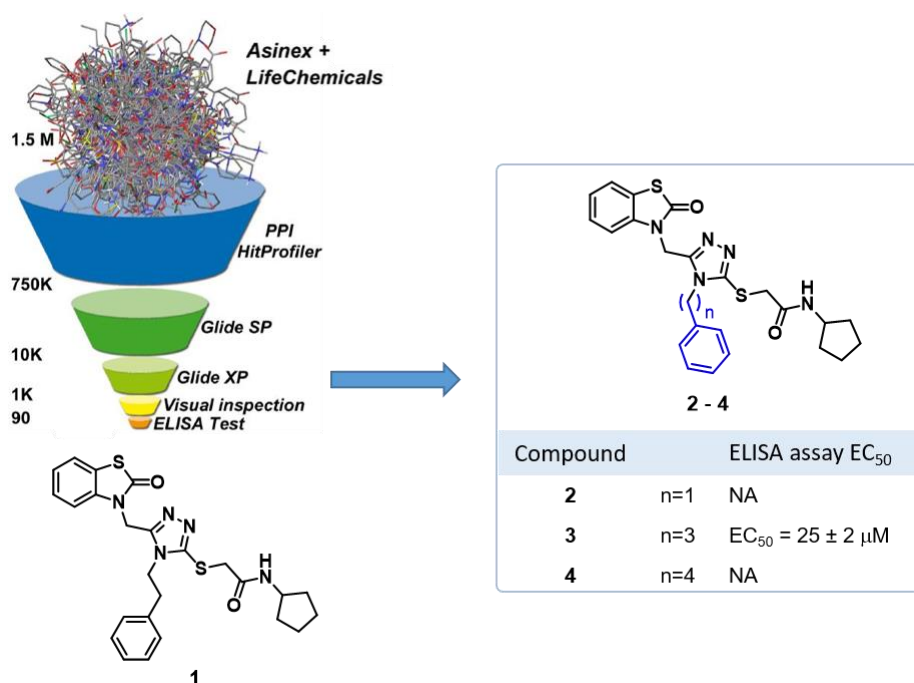


Figure 19. Identification of 1,2,4-triazole hit compound **1** by virtual screening on Zone I, followed by preliminary SAR studies, achieved **3**.

The binding mode of **3** to RAD51, obtained by docking simulations, exhibited similarities to the crystallographic structure of RAD51 in complex with BRC4 (Figure 20). Specifically, the docking model suggests that (i) the phenyl ring of the propyl phenyl group of **3** binds (similarly to the Phe1524 of BRC4) into the hydrophobic pocket outlined by the side chains of Met158, Ile160, Ala190, Leu203, Ala207, and Met210 of RAD51; (ii) the carbonyl group of the benzothiazolone moiety forms hydrogen bonds with the sidechains of RAD51, His199, and Gln206, similarly to the backbone carbonyl of Leu1522 of BRC4. Likewise, (iii) the acetamide carbonyl of **3** binds the backbone Tyr191 of RAD51, similarly to His1525 of BRC4 (Figure 20).¹⁶⁴

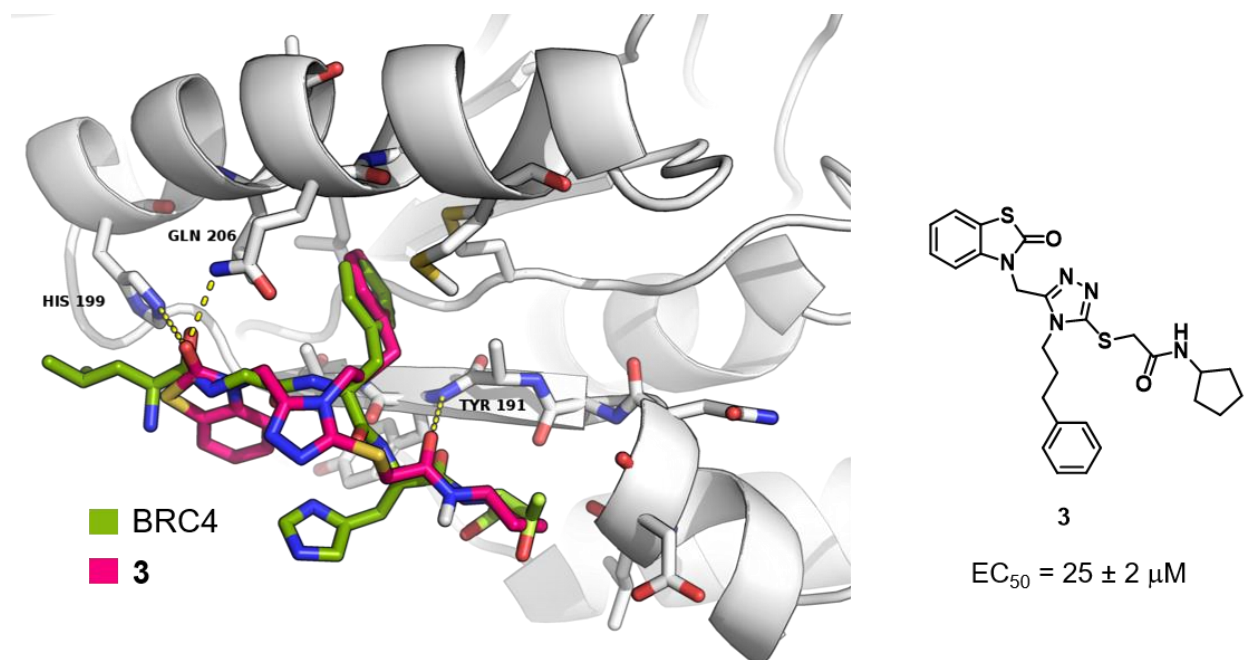


Figure 20. Compound **3** docked into the FxxA domain of RAD51. The small molecule recapitulates major interactions of the peptide BRC4.

To improve the PPI disruption activity of **3**, a chemical modification campaign was conducted around the 1,2,4-triazole moiety. In this context, taking advantage of the synthetic strategy previously optimized (Scheme 1), my PhD work started from the synthesis of new analogues of **3**, to depict general SAR studies and complete a library of 1,2,4-triazole derivatives.¹⁶⁴ Indeed, while benzothiazolone (green region, Figure 21) and alkyl phenyl (blue region, Figure 21) moieties have been formerly investigated, I explored the role of the acetamide moiety (red region, Figure 21), introducing different acetamide chains, bearing aromatic ring (**7**, Table 4) unsaturated rings and heterocycles (**5-6**, **8-10**, Table 4), leaving the carbonyl group unchanged (Figure 21).¹⁶⁴

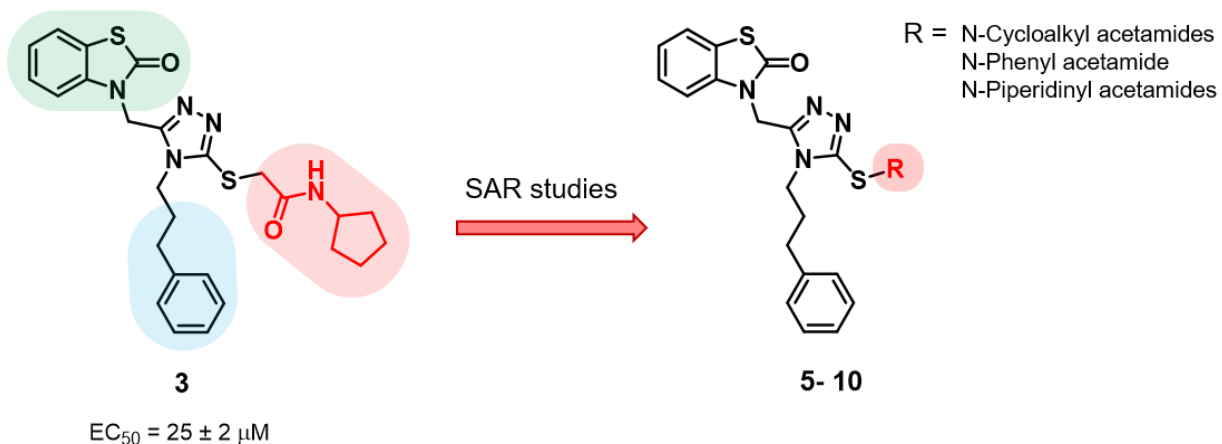
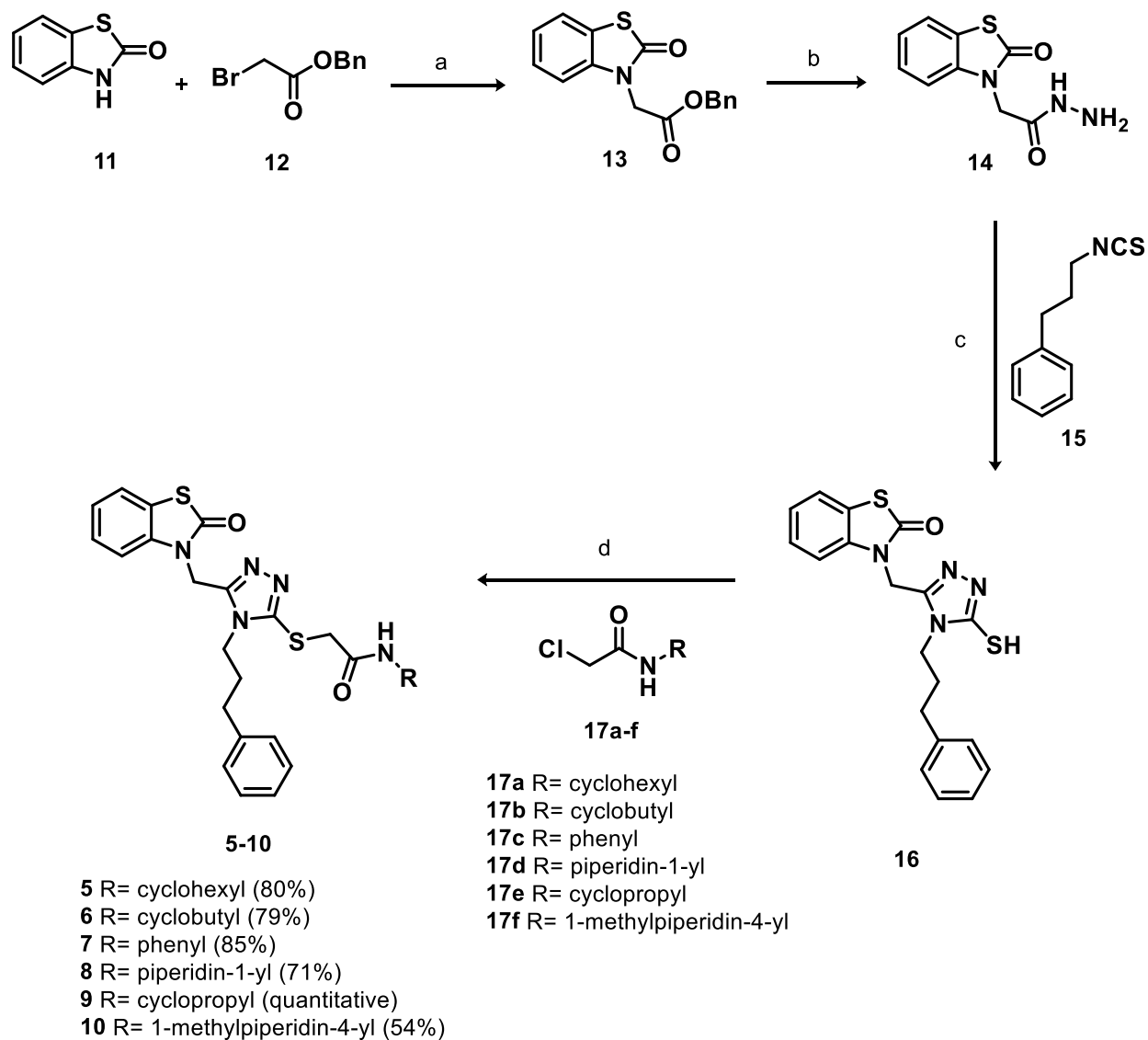


Figure 21. SAR studies on **3** with focus on the modifications of the acetamide group.

Chemistry

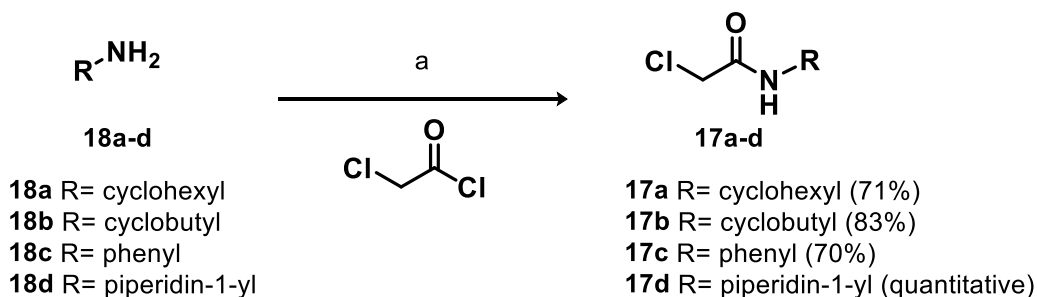
Scheme 1 illustrates the common synthetic strategy optimized to achieve the desired compounds (**5–10**). The N-alkylation of benzothiazolone **11** with benzyl bromoacetate **12** achieved the ester intermediate **13**, which in turn underwent hydrazinolysis to give the corresponding hydrazide **14**. The cyclocondensation of **14** and the commercially available isothiocyanate **15** in the presence of triethylamine gave 1,2,4-triazole-3-thiol intermediate **16**. Ultimately, the S-alkylation of **16** with appropriate 2-chloroacetamides **17a–f** led to final compounds **5–10**. The chloroacetamides **17a–d**, not commercially available, were synthesized through nucleophilic substitution reaction between the appropriate amine **18a–d** and chloroacetyl chloride (Scheme 2).¹⁶⁴

Scheme 1. General synthesis of 1,2,4-triazole compounds **5–10**.



Reagents and conditions: a) K_2CO_3 , NaI cat, acetone, reflux, 2h, yield 94%; b) $NH_2NH_2 \cdot H_2O$, EtOH, reflux, 90', yield 49%; c) EtOH, reflux, 12h; d) Cs_2CO_3 , NaI cat, MeCN, 40°C, 5-12h, yield 54%-quantitative.

Scheme 2. Synthesis of 2-chloro-acetamides **17 a-d**.



Reagents and conditions: a) TEA, DCM, 0°C, 1h, yield 70%-quantitative.

Biological evaluation and results

Our working hypothesis is that small molecule disruptors of RAD51-BRCA2 PPI could synergize with PARPi to treat pancreatic cancer. To investigate the mechanism of action of the new triazole derivatives different biological assays were performed. First, the ability of compounds **5–10** to inhibit RAD51-BRCA2 PPI was investigated with a competitive biochemical ELISA assay, performed by TES Pharma s.r.l, in comparison to the parent compound **3** ($EC_{50} = 25 \pm 2 \mu\text{M}$, Table 4).¹⁶⁴ This assay is effective in evaluating the ability of new molecules to compete with BRC4 to bind to RAD51.¹²¹ The 3-thio-N-cyclohexylacetamide **5** showed good potency with an EC_{50} of $8 \pm 2 \mu\text{M}$, three-fold higher than the parent **3**. Moreover derivatives **6** and **9** were active in the micromolar range (EC_{50} of $24 \pm 5 \mu\text{M}$ and $42 \pm 2 \mu\text{M}$, respectively), both similar to the initial hit compound. Indeed, activity appears to be marginally affected by replacing the cyclopentyl ring in the 3- thio-N-cyclopentylacetamide chain with different cycloalkyl rings such as cyclohexyl (**5**) and cyclobutyl (**6**) and cyclopropyl (**9**). Otherwise the replacement of cyclopentyl moiety with a phenyl ring (**7**) or piperidin-1-yl- (**8**) and 1-methylpiperidin-4-yl- (**10**) causes the complete loss of activity.¹⁶⁴

Table 4. Biochemical evaluation of 1,2,4-triazoles **5** –**10**

Cpd	R	EC ₅₀ ELISA assay	Cpd	R	EC ₅₀ ELISA assay
5		8 ± 2 μM	8		NA
6		42 ± 3 μM	9		24 ± 5 μM
7		NA	10		NA

To investigate the biological profile, derivatives **5**, **6** and **9** with the best EC₅₀ values, were selected to cell-based studies, performed in the laboratory of Professor Giuseppina Di Stefano, University of Bologna. Compound **6** was preliminarily discarded due to its poor solubility. Triazoles **5** and **9** were characterized in BxPC-3 cell line to evaluate firstly the inhibition of homologous recombination (HR) rate and then the presence of a synergistic effect in combination with PARPi Olaparib. BxPC3 cells were chosen for their clinical relevance and for the possibility to use Capan-1 cells, which lack functional BRCA2 protein, as negative control. As reported in Figure 22, while compound **3** increased the HR rate in treated cells, probably due to off-target effects via direct DNA damage, triazoles **5** and **9** reduced HR in treated BxPC3 cells. In particular, **5** had the strongest effect, with a statistically significant 40% inhibition at 20 μM, whereas **9** showed a less significant effect, with a 24% inhibition at 40 μM. Noteworthy, either **5** or **9** caused the inhibition of HR in Capan-1 cells which lack functional BRCA2, strongly supporting the disruption of the RAD51-BRCA2 PPI as their mechanism of action. Therefore **5** and **9** were tested in cell viability experiments in combination with Olaparib in both BxPC3 and Capan-1 (Figure 22). After 72 h, **9** did not affect Olaparib efficacy, whereas, **5** proved to increase significantly the efficacy of PARPi in BxPC3 cells, without any effect in Capan-1 (Figure 22). These results confirmed, in a dose-dependent manner, that HR inhibition might be

the mechanism of action that explains the synergistic effect of RAD51-BRCA2 inhibitor and PARPi in cell lines where PARPi are normally inactive. By the data of the cell viability experiments combination index calculated (CI) was 0.76 ± 0.03 , in agreement with a potential synergistic effect between Olaparib and **5**. However, the enhanced sensitivity to Olaparib did not provide evidence of increased cell death, as confirmed by immunoblotting evaluation of apoptosis markers. On the other hand, an immunoblotting evaluation of DNA damage, performed by measuring the phosphorylation of H2AX (γ -H2AX) revealed that the combination induced a DNA damage signal increased HR up to 70% more than untreated cells. All together these data suggested that disrupting RAD51-BRCA2 interaction could enable the sensitization of pancreatic cancer cells to Olaparib.

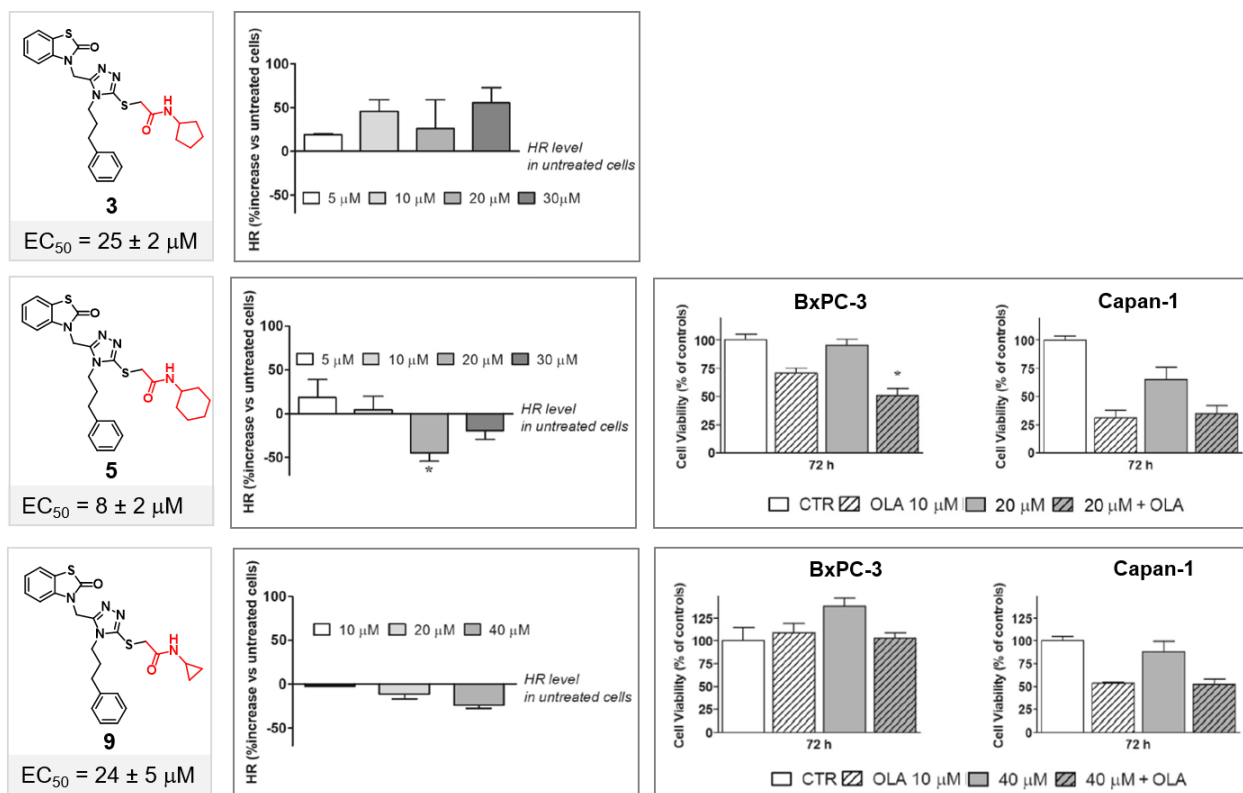


Figure 22. Biological evaluation of 1,2,4-triazoles **3**, **5** and **9**.

In summary, the synergistic effect of **5** in combination with Olaparib in BxPC-3 cells provided encouraging preliminary steps toward the proof of our working hypothesis. However, the paradigm of synthetic lethality was not fully reproduced, presumably due to the low potency of the compound and the insufficient HR inhibition no greater than 40%. Noteworthy, BxPC3 cells are characterized by inherent resistance to apoptosis, due to p53 mutation, and more potent combinations are necessary to trigger cancer cell death. Thus we envisaged the identification of

novel classes of potential RAD51-BRCA2 PPI disruptors by targeting the second PPI hotspot, Zone II.

3.1 Hit identification and optimization targeting Zone II

To obtain the new classes of PPI disruptors, a second Virtual Screening campaign was performed targeting the LFDE binding pocket, corresponding to Zone II of RAD51-BRCA2 PPI (Figure 23). This binding pocket is more evolutionarily conserved than the FxxA, suggesting an essential role in RAD51 biological functions. Moreover, mutations at the LFDE are reported to cause failure of RAD51 assembly in nuclear foci at the site of DNA breaks *in vivo* and cellular lethality.¹²¹ This further suggests this pocket as a critical site for RAD51's mechanism of action.

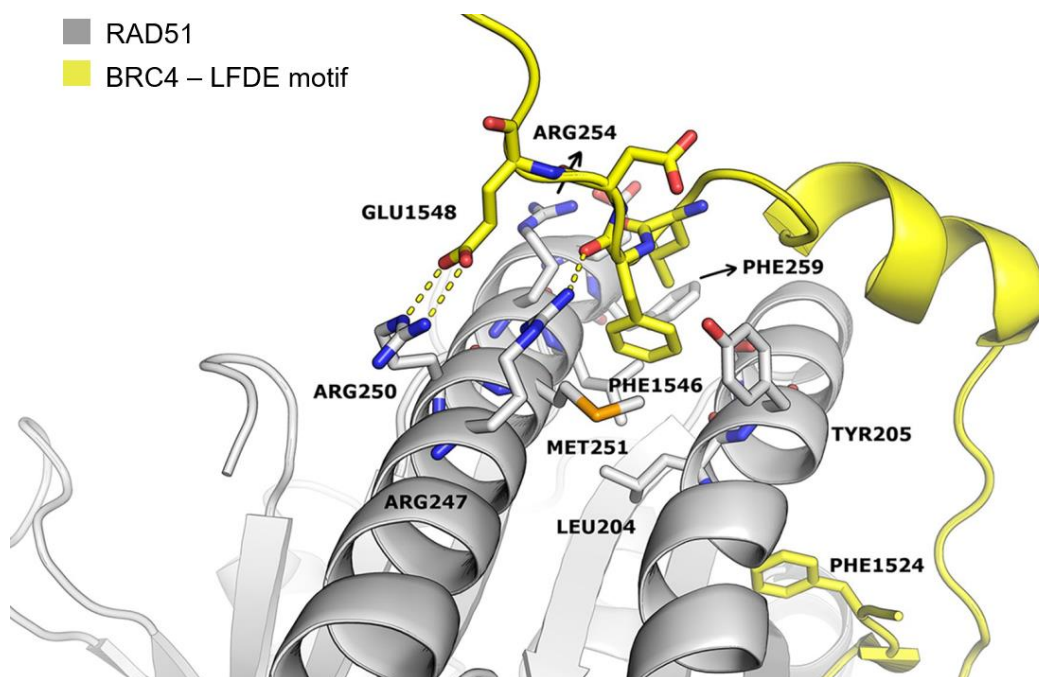


Figure 23. Zone II magnification showing the interacting residues of BRC4 (yellow) and RAD51 (grey) (PDB ID: 1N0W).

To the best of our knowledge, no inhibitor that binds the LFDE binding pocket has been reported so far in the literature. This may open up new possibilities for combining molecules targeting Zone I and Zone II toward a more in depth understanding of the mechanism of inhibition of RAD51-BRCA2 interaction.

To identify potential PPI inhibitors, a commercially available library of about 750K compounds composed of ASINEX and LifeChemicals databases collected from ZINC was prepared.

Compounds with more than 2 chiral centers, Pan-Assay Interference Compounds (PAINS), compounds with Michael acceptor groups, and frequent hitters were discarded. To enrich the database with potential Protein Protein Interaction Inhibitors, the database was filtered with the PPI-HitProfiler tool using the “soft” methods. After the VS campaign, 42 small molecules were selected by visual inspection, purchased, and tested for their inhibitory activity using a competitive biochemical ELISA assay, as previously described by Rajendra *et al.*¹²¹ Among the tested compounds, the commercially available dihydroquinolone pyrazoline derivative **19** was the best candidate in terms of EC₅₀ and chemical tractability (Figure 24). Indeed, the dihydroquinolone pyrazoline moiety is a core structure of compounds with different biological targets.^{169,170} Its activity was confirmed by retesting the newly synthesized compound **19** (Scheme 4). The racemic mixture was separated by semi-preparative chiral separation, as reported in Experimental section. The binding mode to RAD51 of both enantiomers of **19**, as obtained by induced-fit docking simulations, displays some points of interaction similar to those of the crystallographic BRC4-RAD51 complex (Figure 24).

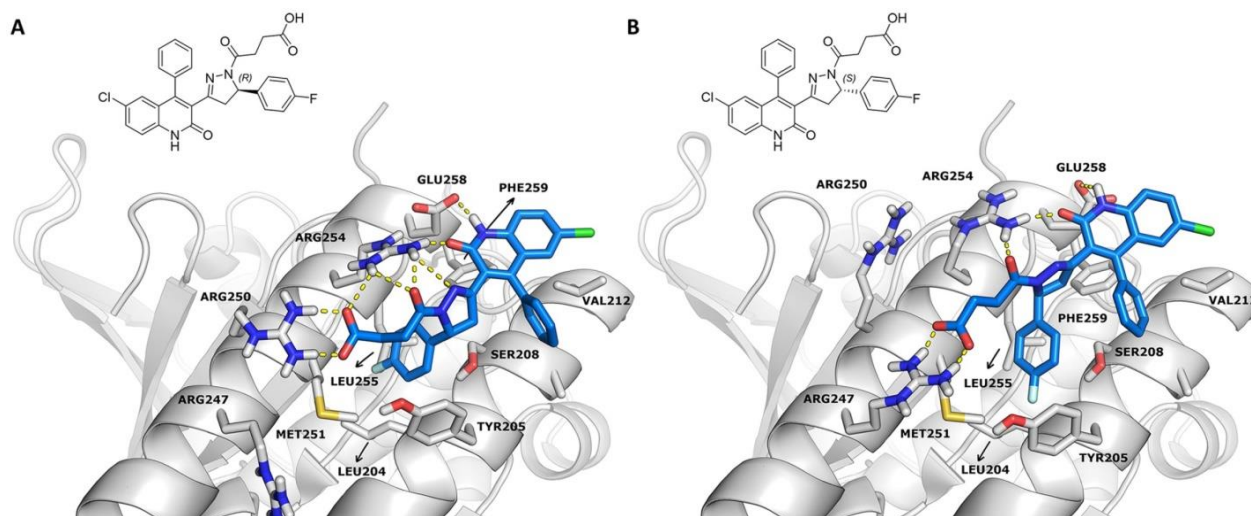


Figure 24. Docking simulations of both enantiomers of **19** into the LFDE binding site of RAD51 (PDB ID: 1N0W).

Specifically, the docking model suggests that (i) the fluorophenyl ring in position 5 of the pyrazoline lies (similar to the Phe1546 of BRC4) in a hydrophobic pocket outlined by the side chains of Leu204, Tyr205, Met251, Leu255, and Phe259 of RAD51 and (ii) the carboxyl group of the pyrazoline side chain forms an ionic interaction with the Arg250 (or Arg247) of RAD51, as does the side chain Glu1548 of BRC4. In addition, the model suggests that the carbonyl and the nitrogen of the dihydroquinolone moiety, together with the carbonyl group of the pyrazoline side

chain, establish hydrogen bonds with Arg254 and Glu258. Notably, both enantiomers show the same global pattern of interactions.¹⁶²

To improve the RAD51-BRCA2 inhibitory activity of **19** (Figure 25, Table 5), we conducted a chemical modification campaign around the dihydroquinolone pyrazoline scaffold. Firstly we investigated the role of the pyrazoline core, by the replacement with other heterocycles (blue region, Figure 25). Subsequently, leaving the central pyrazoline unchanged, we synthesized a chemical library that contained a variety of aromatic substitutions on ring A (orange region, Figure 25) in combination with modifications of the acyl chain moiety (red region, Figure 25). Ultimately we envisioned modifications of the dihydroquinolone group (green region, Figure 25).¹⁶²

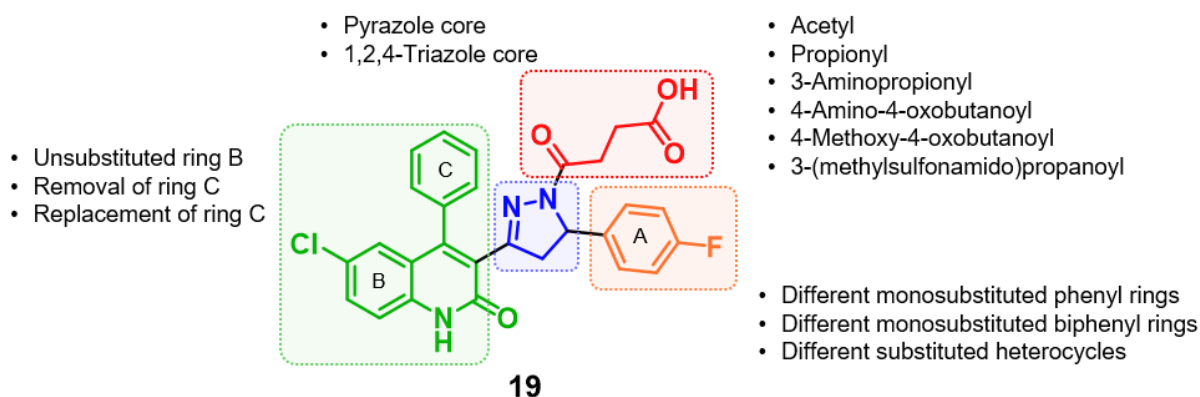


Figure 25. Overview of the optimization strategy of **19** for SAR exploration.

In attempt to explore alternative central cores, we replaced the pyrazoline with other 5-member, fully aromatic heterocycles, such as pyrazole and 1,2,4-triazole (**20–21**, Table 6). Indeed we intended to investigate if more rigid and aromatic systems could engage favorable π - π stacking interactions in the targeted pocket and improve the PPI inhibitory activity. Herein, the derivatization with 4-oxobutanoic chain did not work due to the poor reactivity of functionalizable nitrogen atom of heterocyclic cores. Thus pyrazole and 1,2,4-triazole analogues were functionalized exclusively with acetyl chain.

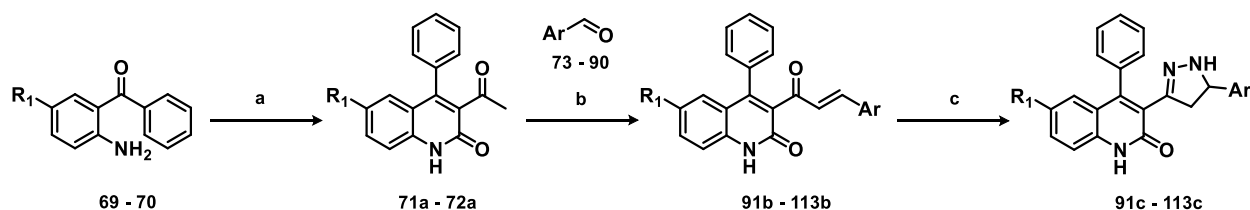
Then, we explored the role of the carboxylic region, which showed to mimic the ionic interaction of Glu1548 of BRC4 with Arg250 of RAD51, forming H bonds. Indeed we replaced the 4-oxobutanoic chain on the pyrazoline nitrogen with a series of different acyl chains, such as propionyl, acetyl, 3-aminopropionyl, 4-amino-4-oxobutanoyl, 4-methoxy-4-oxobutanoyl, 3-(methylsulfonamido)propanoyl groups (**22–27**, Table 5). Next, we moved to the ring A, which

showed to interact in the binding pocket of Phe1546 of BRC4 by docking simulation. The fluorine in para position was replaced by different substituents, including chlorine and bromine atoms and methoxy, tert-butyl, and trifluoromethyl groups, leaving the succinate acyl chain unchanged (**28–32**, Table 5). In addition, the moiety of the aromatic ring A was elongated by the replacement with different substituted biphenyl (**33–36**, Table 5) or heterocycle groups (**37–44**, Table 5) in order to probe its role in the hydrophobic cluster and try to increase π/π stacking interactions. The ring A was also modified in combination with the propionyl (**45–47**, Table 5) or acetyl substitution on the pyrazoline nitrogen (**48–61**, Table 5). Furthermore we investigated the role of rings B and C of the dihydroquinolone moiety. In particular the chlorine atom in the position 6 of the ring B was removed leaving the acyl chain unchanged and introducing some different substituents in the phenyl ring A (**62–66**, Table 5).¹⁶² Then the phenyl ring C was removed (**67**, Table 5) or replaced by methyl group (**68**, Table 5) to probe its role in possible π/π stacking interactions. The loss of phenyl ring C led to a drop in chemical reactivity of the pyrazoline nitrogen atom, and the functionalization with 4-oxobutanoic chain did not work. Thus derivatives **67** and **68** were functionalized exclusively with the acetyl chain (Table 5).

3.2 Chemistry

The desired dihydroquinolone pyrazoline derivatives **19**, **22–23** and **28–66** were achieved, taking advantage of a common synthetic strategy previously reported by Acker *et al.*¹⁷⁰ The commercially available 2-amino- benzophenones **69** and **70** treated with ethyl acetoacetate afforded the corresponding methyl ketones **71a** and **72a**, which underwent base-catalyzed condensation with the appropriate aryl aldehydes **73–90** yielding the α,β -unsaturated aryl ketones **91b–113b**, according to general procedure A (Scheme 3). In turn, **91b–113b** were treated with hydrazine monohydrate to yield the pyrazoline derivatives **91c–113c**, according to general procedure B (Scheme 3).¹⁶²

Scheme 3. Synthesis of dihydroquinolone pyrazoline intermediates **91c** – **113c**.^a



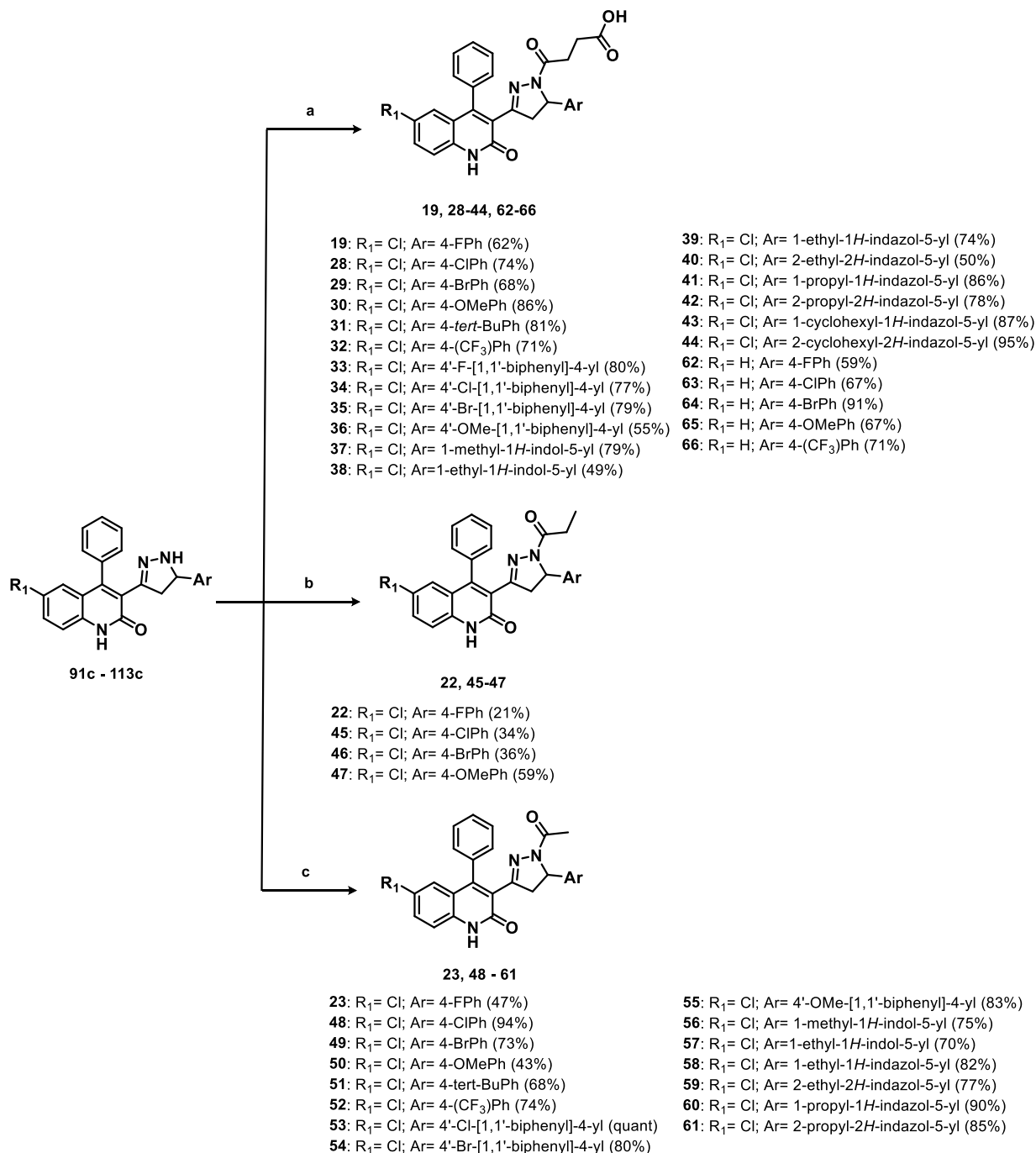
Cpd	R ₁	Ar	Cpd	R ₁	Ar
69	Cl	-	91b; 91c	Cl	4-FPh
70	H	-	92b; 92c	Cl	4-ClPh
71a	Cl	-	93b; 93c	Cl	4-BrPh
72a	H	-	94b; 94c	Cl	4-OMePh
73	-	4-FPh	95b; 95c	Cl	4-tert-BuPh
74	-	4-ClPh	96 b; 96c	Cl	4-(CF ₃)Ph
75	-	4-BrPh	97b; 97c	Cl	4'-F-[1,1'-biphenyl]-4-yl
76	-	4-OMePh	98b; 98c	Cl	4'-Cl-[1,1'-biphenyl]-4-yl
77	-	4-tert-BuPh	99b; 99c	Cl	4'-Br-[1,1'-biphenyl]-4-yl
78	-	4-(CF ₃)Ph	100b; 100c	Cl	4'-OMe-[1,1'-biphenyl]-4-yl
79	-	4'-F-[1,1'-biphenyl]-4-yl	101b; 101c	Cl	1-methyl-1 <i>H</i> -indol-5-yl
80	-	4'-Cl-[1,1'-biphenyl]-4-yl	102b; 102c	Cl	1-ethyl-1 <i>H</i> -indol-5-yl
81	-	4'-Br-[1,1'-biphenyl]-4-yl	103b; 103c	Cl	1-ethyl-1 <i>H</i> -indazol-5-yl
82	-	4'-OMe-[1,1'-biphenyl]-4-yl	104b; 104c	Cl	2-ethyl-2 <i>H</i> -indazol-5-yl
83	-	1-methyl-1 <i>H</i> -indol-5-yl	105b; 105c	Cl	1-propyl-1 <i>H</i> -indazol-5-yl
84	-	1-ethyl-1 <i>H</i> -indol-5-yl	106b; 106c	Cl	2-propyl-2 <i>H</i> -indazol-5-yl
85	-	1-ethyl-1 <i>H</i> -indazol-5-yl	107b; 107c	Cl	1-cyclohexyl-1 <i>H</i> -indazol-5-yl
86	-	2-ethyl-2 <i>H</i> -indazol-5-yl	108b; 108c	Cl	2-cyclohexyl-2 <i>H</i> -indazol-5-yl
87	-	1-propyl-1 <i>H</i> -indazol-5-yl	109b; 109c	H	4-FPh
88	-	2-propyl-2 <i>H</i> -indazol-5-yl	110b; 110c	H	4-ClPh
89	-	1-cyclohexyl-1 <i>H</i> -indazol-5-yl	111b; 111c	H	4-BrPh
90	-	2-cyclohexyl-2 <i>H</i> -indazol-5-yl	112b; 112c	H	4-OMePh
			113b; 113c	H	4-(CF ₃)Ph

^aReagents and conditions: (a) ethyl acetoacetate, DMF, 120 °C μ Wave or reflux, yield quantitative (**71a**), yield 53% (**72a**); (b) KOH, EtOH/H₂O 4:3 v/v (0.05 M), 0 °C to rt, yield 53%- quantitative; (c) hydrazine monohydrate, EtOH, 110 °C μ Wave , 45 min, yield 64%- quantitative.

The pyrazoline amines **91c–113c** functionalized with succinic anhydride **114** afforded the corresponding desired dihydroquinolone pyrazoline derivatives **19**, **28–44** and **62–66**, according to general procedure C₁ (Scheme 4). The pyrazoline amines **91c–94c** functionalized with propionic acid **115** afforded the corresponding derivatives **22**, **45–47**, according to general procedure C₂ (Scheme 4). The pyrazoline amines **91c–96c**, **98c–106c** functionalized with acetic anhydride **116** afforded the corresponding derivatives **23**, **48–61**, according to general

procedure C₃ (Scheme 4). The isolated enantiomers **19-I** and **19-II** were achieved by the chiral separation of the racemic hit compound **19**.

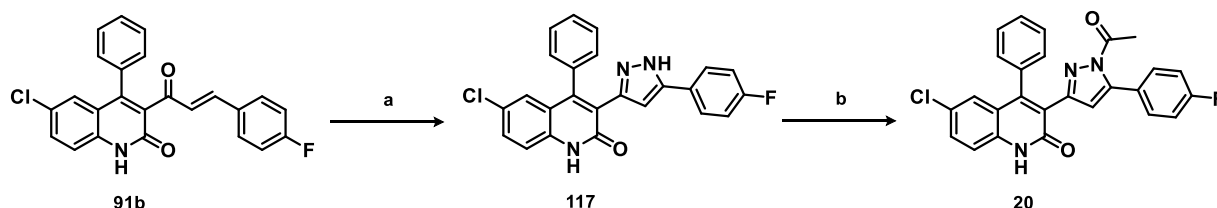
Scheme 4. Synthesis of final dihydroquinolone pyrazolines **19**, **22–23**, **28–66**.^a



^aReagents and conditions: (a) Succinic anhydride **114**, anhydrous THF, μ Wave, 120°C, 45 min, yield 49- 95%; (b) Propionic acid **115**, HOBT, EDCI, DCM, 3 h, yield 21- 59%; (c) Acetic anhydride **116**, anhydrous THF, μ Wave, 165°C, 45 min, yield 43%- quantitative.

To obtain **20**, the α,β -unsaturated aryl ketone **91b** was treated with *tert*-butyl hydrazide and I_2 which afforded the pyrazole intermediate **117** (Scheme 5). In turn **117** was functionalized with acetic anhydride **116** to give **20** (Scheme 5).

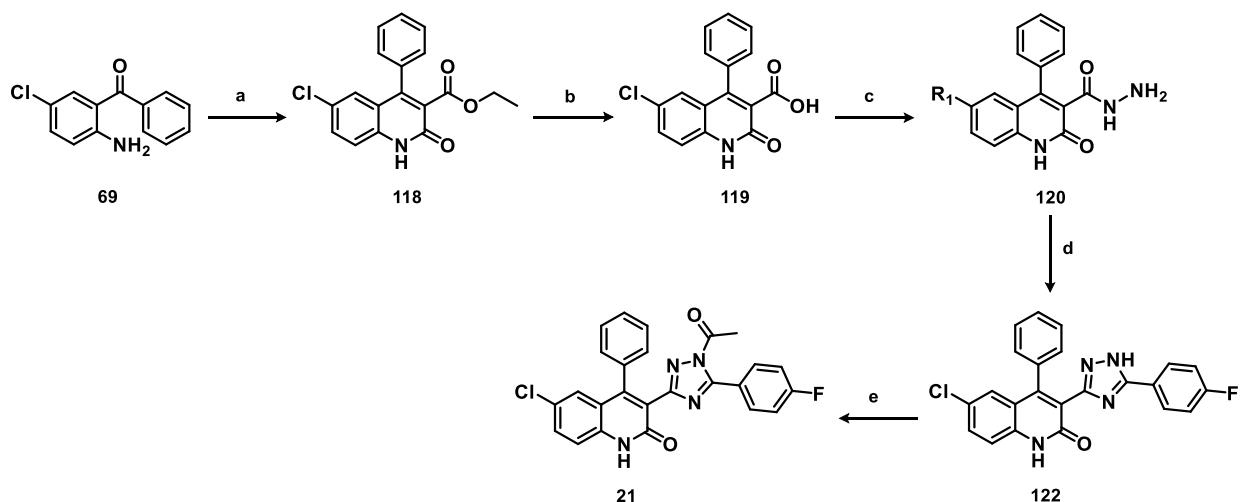
Scheme 5. Synthesis of compound **20**.^a



^aReagents and conditions: (a) *tert*-butyl-hydrazide, I_2 , reflux, overnight, yield 23%; (b) Acetic anhydride **116**, anhydrous THF, μ Wave, 165°C , 20 min, yield 16%.

To achieve **21**, the synthesis started from the cyclocondensation of 2-amino-benzophenone **69** with diethylmalonate in presence of DBU to give the intermediate ester **118** (Scheme 6). The ester basic hydrolysis afforded the carboxylic acid **119**, which was in turn treated with hydrazine hydrate to obtain the N-acylhydrazide **120**. The cyclocondensation of **120** with 4-fluoro benzonitrile **121** afforded the 1,2,4-triazole intermediate **122**, which was in turn functionalized with acetic anhydride **116** to obtain **21** (Scheme 6).

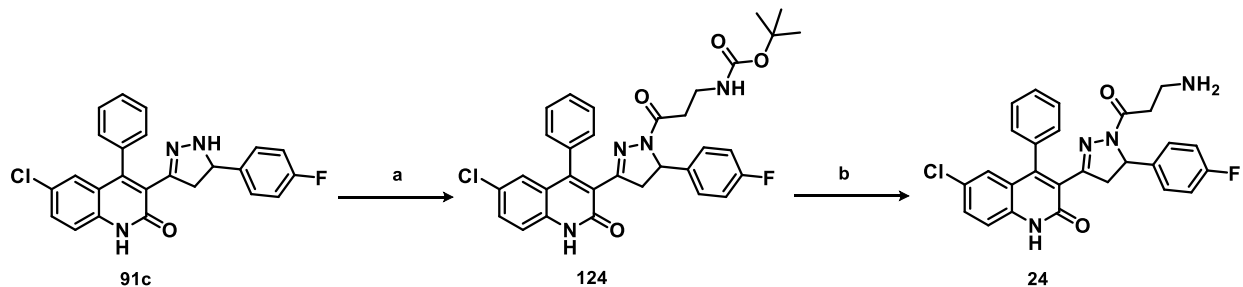
Scheme 6. Synthesis of compound **21**.^a



^aReagents and conditions: (a) diethyl malonate, DBU, anhydrous THF, μ Wave, 160°C, 2 h, yield 62%; (b) LiOH 2M, EtOH, reflux, 5 h, yield 99%; (c) i. HOBt, EDCI, MeCN, 0°C- rt, ii. Hydrazine hydrate, yield 51%; (d) 4-fluorobenzonitrile **121**, K₂CO₃, n-BuOH, μ Wave, 150°C, 4 h, yield 49%; (e) Acetic anhydride **116**, anhydrous THF, μ Wave, 165°C, 25 min, yield 50%.

Compound **24** was obtained by coupling **91c** with the commercially available 3-((*tert*-butoxycarbonyl)-amino)propanoic acid **123** to achieve the Boc-aminopyrazoline derivative **124** (Scheme 7). In turn, **124** was Boc-protected under acidic conditions to afford the desired **24** (Scheme 7).

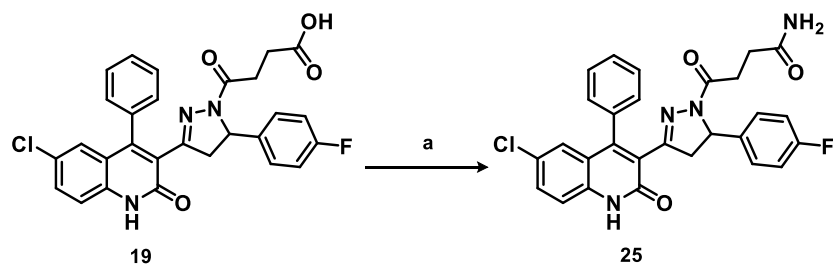
Scheme 7. Synthesis of compound **24**.^a



^aReagents and conditions: (a) HOBt, EDCI, TEA, 3-((*tert*-butoxycarbonyl)-amino)propanoic acid **123**, DCM, overnight, yield 25%; (b) i. HCl 4M in dioxane, rt, 15 min; ii. NaOH 0.5 M in EtOAc, rt, 15 min, yield 50%.

Compound **25** was obtained by HATU-mediated coupling of **19** with ammonium chloride (Scheme 8).

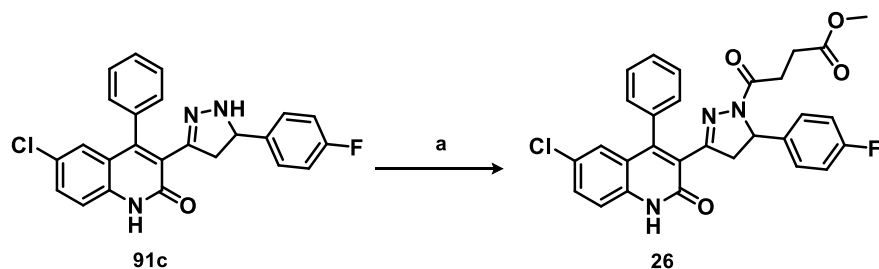
Scheme 8. Synthesis of compound **25**.^a



^aReagents and conditions: (a) HATU, EDC, DCM, DMF, ammonium chloride, DIPEA, rt, 26 h, yield 46%.

Compound **26** was afforded by coupling **91c** with the commercially available 4-methoxy-4-oxobutanoic acid **125** (Scheme 9).

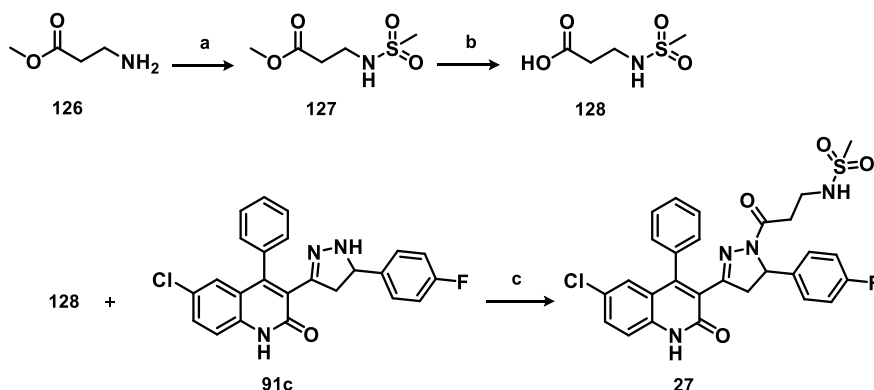
Scheme 9. Synthesis of compound **26**.^a



^aReagents and conditions: (a) 4-methoxy-4-oxobutanoic acid **125**, HOBT, EDC, TEA, DCM, rt, 16 h, yield 42%.

The synthesis of **27** began with the commercially available methyl 3-aminopropanoate **126**, which was treated with methansulfonyl chloride to afford the corresponding methyl 3-(methylsulfonamido) propanoate **127**, which in turn underwent basic hydrolysis to give 3-(methylsulfonamido) propanoic acid **128** (Scheme 10). The coupling reaction of **91c** with **128** afforded the desired **27** (Scheme 10).

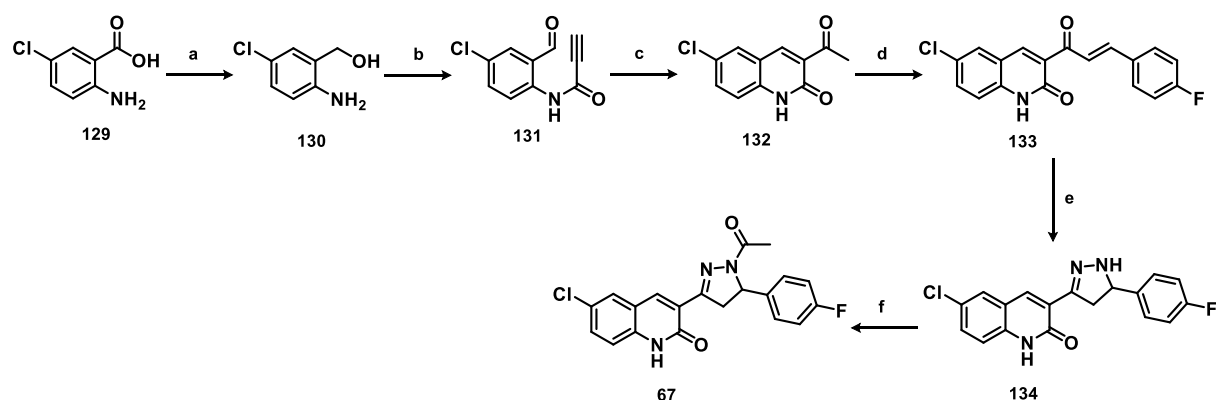
Scheme 10. Synthesis of compound **27**.^a



^aReagents and conditions: (a) TEA, anhydrous DCM, methanesulfonyl chloride, rt, 48 h, yield 82%; (b) MeOH/THF (1:1 v/v), LiOH 2M, rt, 16 h, yield 82%; (c) HOBt, EDC, TEA, DCM, rt, 16 h, yield 15%.

To obtain **67**, the synthesis began from the reduction of anthranilic acid **129** to the benzyl alcohol **130** (Scheme 11). The coupling with tetrolic acid and subsequent oxidation of alcoholic function achieved the alkynamidic benzaldehyde **131** (Scheme 11). The cyclization of **131** in presence of palladium acetate and 4-4'-dimethoxy-bipyridyl afforded the ketone intermediate **132**, which underwent basic condensation with benzaldehyde **73** to achieve the α,β -unsaturated ketone **133**. Then **133** was treated with hydrazine hydrate to give the corresponding pyrazoline **134**, which was coupled to acetic anhydride **116** to obtain **67** (Scheme 11).

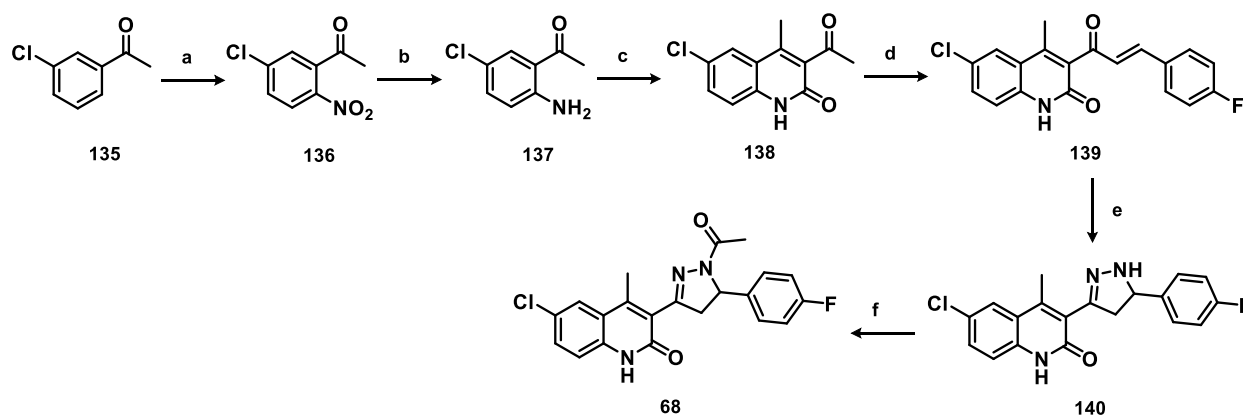
Scheme 11. Synthesis of compound **67**.^a



^aReagents and conditions: (a) i. LiAlH₄, anhydrous THF, 0°C - rt; ii. NaOH 1M, 0°C - rt, yield 96%; (b) i. Tetrolic acid, DCC, anhydrous DCM, 0°C - rt; ii. Pyridinium chlorochromate, DCM, rt, yield 70%; (c) Pd(OAc)₂, 4,4'-MeO-bpy, 4 Å MS, AcOH/DCE 1:1, 80°C, overnight, yield 67%; (d) **73**, KOH, EtOH/H₂O 4:3 v/v (0.05 M), 0°C to rt, yield quantitative; (e) hydrazine monohydrate, EtOH, 110 °C μ Wave, 30 min, yield 59%; (f) Acetic anhydride **116**, anhydrous THF, 165 °C μ Wave, 30 min, yield 82%.

The synthesis of **68** started from the nitration of 3-chloroacetophenone **135** to give the corresponding **136** (Scheme 12). The subsequent reduction of **136** afforded the 1-(2-amino-5-chlorophenyl) ethanone **137** (Scheme 12). Cyclocondensation of **137** with ethylacetoacetate achieved the ketone intermediate **138**, which in turn underwent basic condensation with **73** to afford **139**. The treatment of **139** with hydrazine hydrate gave the corresponding pyrazoline **140**, which was coupled to acetic anhydride **116** to achieve **68** (Scheme 12).

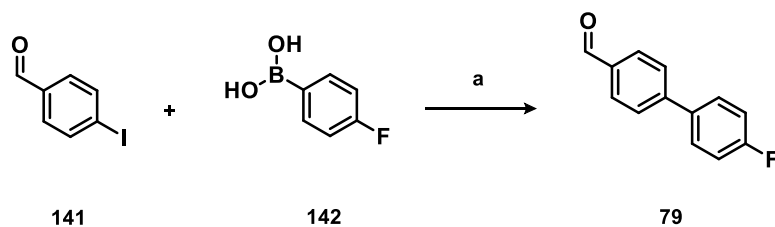
Scheme 12. Synthesis of compound **68**.^a



^aReagents and conditions: (a) Nitric acid, sulfuric acid, -20°C-(-10°C), 75 min, yield 80%; (b) Sn⁰, HCl conc, reflux, 12 h, yield 96%; (c) Ethyl acetoacetate, anhydrous THF, 140 °C μ Wave, 75 min, yield 30%; (d) **73**, KOH, EtOH/H₂O 4:3 v/v (0.05 M), 0 °C to rt, yield quantitative; (e) hydrazine monohydrate, EtOH, 110 °C μ Wave, 30 min, yield 37%; (f) Acetic anhydride **116**, anhydrous THF, 165 °C μ Wave, 30 min, yield 40%.

The aldehydes **79**, **83–90**, not commercially available, were prepared following standard procedures as reported in Experimental section (Schemes 13-18). 4'-Fluoro-[1,1'-biphenyl]-4-carbaldehyde **79** was synthesized taking advantage of Suzuki coupling reaction between the commercially available 4-iodobenzaldehyde **141** and (4-fluorophenyl) boronic acid **142** in presence of palladium(0) catalyst (Scheme 13).

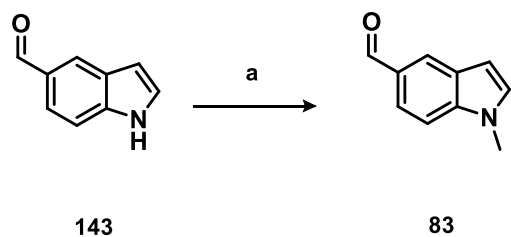
Scheme 13. Synthesis of compound **79**.^a



^aReagents and conditions: (a) i. Anhydrous sodium carbonate (3.0 equiv); ii. DMF, H₂O, rt, 15 min; iii. Tetrakis (triphenylphosphine) palladium(0) (0.15 equiv), 110 °C, 20 h yield 66%.

1-Methyl-1*H*-indole-5-carbaldehyde **83** was achieved by the alkylation of the commercially available 1*H*-indole-5-carboxaldehyde **143** with methyl iodide under basic conditions (Scheme 14).

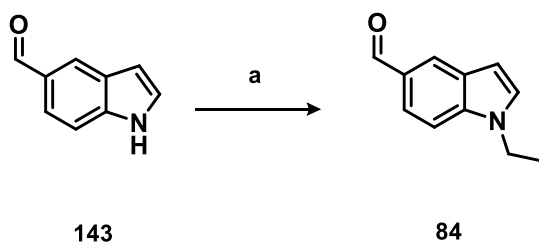
Scheme 14. Synthesis of compound **83**.^a



^aReagents and conditions: (a) Potassium carbonate (2.0 equiv), anhydrous DMF, methyl iodide (2.0 equiv), 35°C, 18 h, yield 81%.

1-Ethyl-1*H*-indole-5-carbaldehyde **84** was achieved by the alkylation of the commercially available 1*H*-indole-5-carboxaldehyde **143** with iodoethane under basic conditions (Scheme 15).

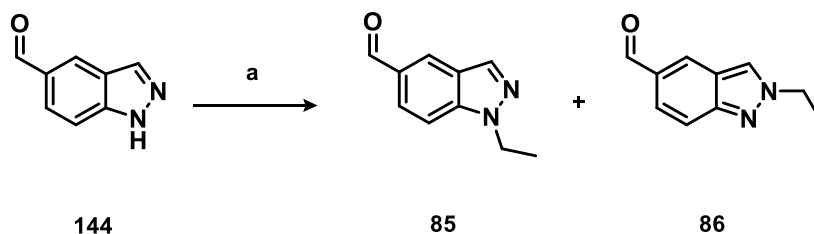
Scheme 15. Synthesis of compound **84**.^a



^aReagents and conditions: (a) Potassium carbonate (2.0 equiv), anhydrous DMF, iodoethane (2.0 equiv), 35°C, 18 h, yield 91%.

Ethylindazole-5-carbaldehyde isomers **85** and **86** were synthesized by the alkylation of the commercially available 1H-indazole-5-carboxaldehyde **144** with ethyl bromide under basic conditions (Scheme 16).

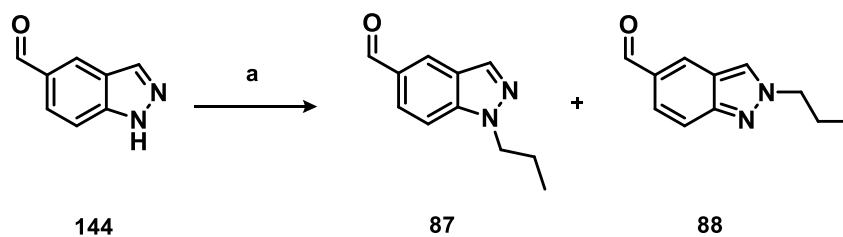
Scheme 16. Synthesis of compound **85-86**.^a



^aReagents and conditions: (a) Potassium carbonate (3.0 equiv), anhydrous DMF, ethyl bromide (1.1 equiv), 40°C, 5 h, yield 50% (**85**); yield 34% (**86**).

Propylindazole-5-carbaldehyde isomers **87** and **88** were synthesized by the alkylation of the commercially available 1H-indazole-5-carboxaldehyde **144** with 1-bromopropane under basic conditions (Scheme 17).

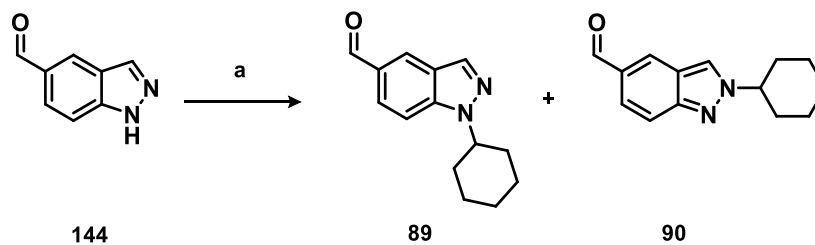
Scheme 17. Synthesis of compound **87-88**.^a



^aReagents and conditions: (a) Potassium carbonate (2.6 equiv), anhydrous DMF, 1-bromopropane (2.0 equiv), rt, 14 h; yield 50% (**87**); yield 34% (**88**).

Cyclohexylindazole-5-carbaldehyde isomers **89** and **90** were synthesized by the alkylation of the commercially available 1*H*-indazole-5-carboxaldehyde **144** with 1-bromocyclohexane under basic conditions (Scheme 18).

Scheme 18. Synthesis of compound **89-90**.^a



^aReagents and conditions: (a) Potassium carbonate (2.1 equiv), anhydrous DMF, 1-bromocyclohexane (2.1 equiv), rt, 6 days; yield 21% (**89**); yield 14% (**90**).

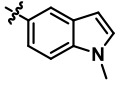
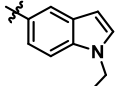
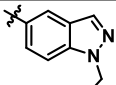
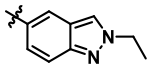
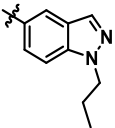
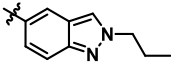
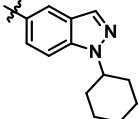
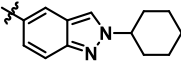
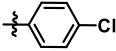
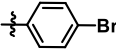
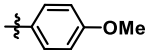
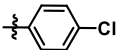
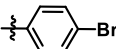
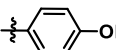
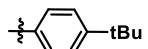
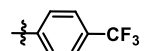
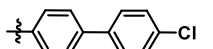
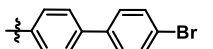
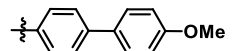
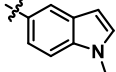
Structures of the isomers **85–90** were confirmed by mono- and bi-dimensional ¹H- and ¹³C-NMR (HMBC) analyses, as reported in Experimental section.

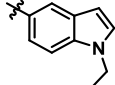
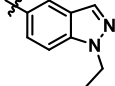
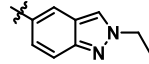
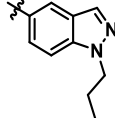
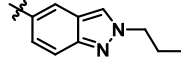
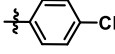
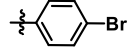
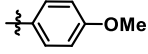
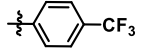
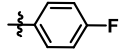
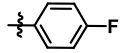
3.3 SAR studies and biological evaluation

As a primary screening, the ability of compounds **20–68** to inhibit RAD51-BRCA2 PP interaction was investigated with a competitive biochemical ELISA assay against the parent compound **19** (Tables 5, 6).

Table 5. Structures and EC₅₀ of compounds **19**, **22–68** on ELISA assay.

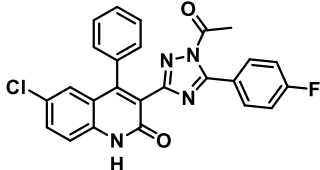
Cpd ^a	R ₁	R ₂	Ar	R ₃	EC ₅₀ ELISA assay (μM)
19	Cl	-CH ₂ CH ₂ COOH		-Ph	16 ± 4
22	Cl	-CH ₂ CH ₃		-Ph	34 ± 3
23	Cl	-CH ₃		-Ph	50 ± 10
24	Cl	-CH ₂ CH ₂ NH ₂		-Ph	NA ^b
25	Cl	-CH ₂ CH ₂ CONH ₂		-Ph	NA ^b
26	Cl	-CH ₂ CH ₂ COOCH ₃		-Ph	NA ^b
27	Cl	-CH ₂ CH ₂ NHS(O) ₂ CH ₃		-Ph	NA ^b
28	Cl	-CH ₂ CH ₂ COOH		-Ph	59 ± 8
29	Cl	-CH ₂ CH ₂ COOH		-Ph	16 ± 2
30	Cl	-CH ₂ CH ₂ COOH		-Ph	NA ^b
31	Cl	-CH ₂ CH ₂ COOH		-Ph	NA ^b
32	Cl	-CH ₂ CH ₂ COOH		-Ph	29 ± 2
33	Cl	-CH ₂ CH ₂ COOH		-Ph	13 ± 1
34	Cl	-CH ₂ CH ₂ COOH		-Ph	25 ± 5
35	Cl	-CH ₂ CH ₂ COOH		-Ph	20 ± 2
36	Cl	-CH ₂ CH ₂ COOH		-Ph	20 ± 4

37	Cl	-CH ₂ CH ₂ COOH		-Ph	2 ± 0.5
38	Cl	-CH ₂ CH ₂ COOH		-Ph	10 ± 2
39	Cl	-CH ₂ CH ₂ COOH		-Ph	NA ^b
40	Cl	-CH ₂ CH ₂ COOH		-Ph	28 ± 4
41	Cl	-CH ₂ CH ₂ COOH		-Ph	NA ^b
42	Cl	-CH ₂ CH ₂ COOH		-Ph	NA ^b
43	Cl	-CH ₂ CH ₂ COOH		-Ph	NA ^b
44	Cl	-CH ₂ CH ₂ COOH		-Ph	NA ^b
45	Cl	-CH ₂ CH ₃		-Ph	8 ± 2
46	Cl	-CH ₂ CH ₃		-Ph	19 ± 1
47	Cl	-CH ₂ CH ₃		-Ph	19 ± 1
48	Cl	-CH ₃		-Ph	10 ± 0.7
49	Cl	-CH ₃		-Ph	38 ± 7
50	Cl	-CH ₃		-Ph	NA ^b
51	Cl	-CH ₃		-Ph	15 ± 4
52	Cl	-CH ₃		-Ph	NA ^b
53	Cl	-CH ₃		-Ph	45 ± 8
54	Cl	-CH ₃		-Ph	70 ± 15
55	Cl	-CH ₃		-Ph	70 ± 6
56	Cl	-CH ₃		-Ph	18 ± 1

57	Cl	-CH ₃		-Ph	50 ± 15
58	Cl	-CH ₃		-Ph	40 ± 3
59	Cl	-CH ₃		-Ph	NA ^b
60	Cl	-CH ₃		-Ph	0.95 ± 0.05
61	Cl	-CH ₃		-Ph	NA ^b
62	H	-CH ₂ CH ₂ COOH		-Ph	NA ^b
63	H	-CH ₂ CH ₂ COOH		-Ph	NA ^b
64	H	-CH ₂ CH ₂ COOH		-Ph	NA ^b
65	H	-CH ₂ CH ₂ COOH		-Ph	NA ^b
66	H	-CH ₂ CH ₂ COOH		-Ph	NA ^b
67	Cl	-CH ₃		-H	18 ± 3 μM
68	Cl	-CH ₃		-CH ₃	55 ± 15 μM

Footnotes: ^a Structures and EC₅₀ of compounds **20** and **21** are reported in Table 6. ^b NA, not active.

Table 6. Structures and EC₅₀ of compounds **20** and **21** on ELISA Assay.

Cpd	Structure	EC ₅₀ ELISA assay (μM)
20		33 ± 3
21		NA ^a

Footnotes: ^a NA, not active.

The replacement of the pyrazoline central core with pyrazole, functionalized with the acetyl chain, led to a drop in activity (**20**, $EC_{50} = 33 \pm 3 \mu\text{M}$, Table 6). Whereas, the substitution with 1,2,4-triazole, combined to the acetyl chain, in compound **21** resulted in the complete loss of activity (Table 6). Together these results suggested that the partially aromaticity and the flexible system of the pyrazoline core could be preferred to engage favorable interactions at the targeted pocket, ultimately being indispensable for the PPI inhibitory activity.

The separated enantiomers (**19-I** and **19-II**) of the racemic hit compound **19** were tested and showed a very similar inhibitory activity (**19-I**, $EC_{50} = 4 \pm 0.5 \mu\text{M}$; **19-II**, $10 \pm 1 \mu\text{M}$), in agreement with the docking model (Figure 24). This suggested no stereochemical preference of these compounds for the hypothesized molecular target RAD51. Thus all pyrazoline-based compounds **22–68** were synthesized and tested as racemic mixtures.

The replacement of the 4-oxobutanoic acyl chain of the pyrazoline nitrogen led to compounds (**22–27**, Table 5) with reduced inhibitory activity (**22**, $EC_{50} = 34 \pm 3 \mu\text{M}$; **23**, $EC_{50} = 50 \pm 10 \mu\text{M}$) or totally inactive (**24–27**). These results indicate that no improvement in RAD51-BRCA2 PPI inhibitory activity was achieved with this subset of compounds relative to the parent **19** ($EC_{50} = 16 \pm 4 \mu\text{M}$). Replacing the fluorine atom on ring A with bromine led to **29** ($EC_{50} = 16 \pm 2 \mu\text{M}$), which shows a comparable activity as the initial hit **19**. The activity was affected when the fluorine was replaced with chlorine (**28**, $EC_{50} = 59 \pm 8 \mu\text{M}$) and trifluoromethyl groups (**32**, $EC_{50} = 29 \pm 2 \mu\text{M}$). The replacement with electron-donating groups in para position of ring A yielded the inactive compounds (**30–31**). For the subset of dihydroquinolone pyrazolines, in which the aromatic ring A was replaced by different substituted biphenyl (**33–36**) or heterocycle groups (**37–44**, Table 5) the N-methyl indole derivative **37** showed a good potency with an $EC_{50} = 2 \pm 0.5 \mu\text{M}$, at low micromolar. **33–36**, **38** and **40** were active at micromolar range, all comparable to the initial hit. Whereas derivatives **39**, **41–44** were completely inactive. The replacement of the aromatic ring A in combination with the substitution of the pyrazoline nitrogen with either propionyl or acetyl chain yielded compounds **45–61**. The 1-N-acetyl-5-(1-N-propyl)- indazolyl pyrazoline **60** showed the best activity of the series with $EC_{50} = 0.95 \pm 0.05 \mu\text{M}$, while **45–48**, **51** and **56** showed an activity very similar to that of the initial hit. A drop in potency was observed with for compounds **49**, **53–55**, **57** and **58**, while **50**, **52**, **59**, and **61** the activity was completely lost. Removing the chlorine atom in position 6 on the dihydroquinolone core led to the completely inactive compounds **62–66**, suggesting an active role for the halogen. The removal of phenyl ring C in presence of acetyl chain led to **67** with inhibitory activity comparable to the hit

compound. Whereas the replacement of ring C with a methyl group, combined with acetic chain, resulted in a drop of activity (**68**, EC₅₀ = 55 ± 15 μM).

As expected for PPI disruptors, the SARs of the new series of dihydroquinolone pyrazoline were rather complex to rationalize, with many cliffs and spikes that were difficult to understand.¹⁶²

Nonetheless, the SAR campaign efforts allowed us to identify several compounds with interesting EC₅₀ values ranging from 0.95 to 20 μM, **19**, **29**, **33**, **35–38**, **45–48**, **51**, **56**, **60** and **67** (Table 5, 6), which were selected for further cell-based studies (Table 7).

Interestingly, contrary to what expected from the docking model of **19** (Figure 24), the carboxylic function appeared to be not essential for the activity, with compounds bearing propionyl and acetyl chains showing comparable or increased activities. Moreover the enlargement of the ring A region with heterocyclic groups in compounds **37**, **60** led to an increase of potency, suggesting the possible engagement of π-π stacking interactions, in particular in proximity of Tyr205.

Table 7. Preliminary biological evaluation of compounds with EC₅₀ within 20 μM.

Cpd	EC ₅₀ ELISA assay (μM)	Preliminary biological evaluation
19	16 ± 4	HR inhibition = 10% at 40 μM
29	16 ± 2	HR inhibition = not present Olaparib association = not present
33	13 ± 1	Olaparib association = not present
35	20 ± 2	Olaparib association = not present
36	20 ± 4	NE ^a
37	2 ± 0.5	HR inhibition = not present Olaparib association = not present at 5 μM
38	10 ± 2	Olaparib association = not present
45	8 ± 2	HR inhibition = not present Olaparib association = not present
46	19 ± 1	HR inhibition = not present Olaparib association = NE ^a
47	19 ± 1	HR inhibition = 54% at 20 μM Olaparib association = present at 15 μM
48	10 ± 0.7	HR inhibition = 24% at 10 μM Olaparib association = not present

51	15 ± 4	HR inhibition = NDD ^b
56	18 ± 1	HR inhibition = not present
60	0.95 ± 0.05	HR inhibition = not present Olaparib association = not present
67	18 ± 3 μM	Olaparib association = not present

Footnotes: ^aNE, not evaluable. ^bNDD, not dose dependent.

Our working hypothesis is that compounds disrupting RAD51-BRCA2 PPI should affect HR repair, resulting in the increase of efficacy of PARPi in breast, ovarian and pancreatic cancer cells. To validate the hypothesis, a preliminary biological screening was performed, that envisaged the evaluation of cell HR inhibition and/or the measurement of cell viability in combination with Olaparib. The pancreatic adenocarcinoma BxPC3 cell line was selected as cell model for a direct comparison with the previously reported 1,2,4-triazole-based derivatives.

From these first preliminary investigations, we could discarded compounds exhibiting (i) low or no activity (**19**, **29**, **33**, **35**, **37**, **38**, **45**, **56**, **60**, **67**), (ii) poor solubility (**36**, **46**), (iii) discrepancy between data obtained from HR inhibition assay and cell viability assay in combination with Olaparib (**48**), and (iv) a non-dose-dependent effect (**51**). For 4-oxobutanoic acid-containing compounds (**19**, **29**, **33**, **35–38**), a general poor cell permeability was proposed as reason for their lower potency in cell-based study, likely related to the ionizable acid moiety. As reported in Table 7, **47** resulted the most promising compound in the HR activity test. Thus **47** was selected for further evaluations of the biophysical and biological profile.

The binding affinity of **47** for RAD51 was assessed by microscale thermophoresis (MST) assay on the recombinant human RAD51 (Figure 26). The dissociation constant (K_d) value for RAD51-**47** interaction was estimated of 11 ± 6 μM, supporting the hypothesis that **47** could act as a RAD51-BRCA2 disruptor, in agreement with the ELISA assay.

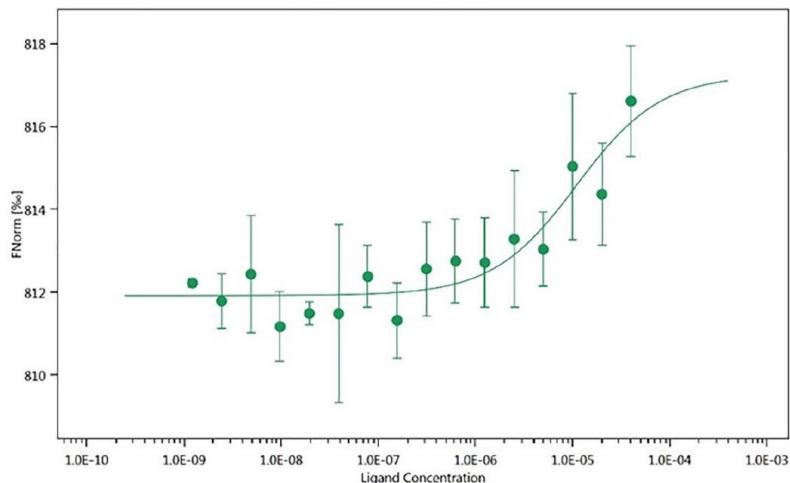


Figure 26. MST analysis of His-hRAD51-**47** binding. Titration curve of (RED-tris-NTA 2nd Generation)-His-hRAD51 (80 nM) with increasing concentrations of **47**.

In cell-based HR inhibition assay at different doses, **47** reduced cell HR in a statistically significant dose–response trend, with an estimated EC₅₀ value of 18.4 μM (Figure 27A). Noteworthy, this assay had an upper concentration limit of 40 μM due to compound solubility. In addition, further cell-based experiments demonstrated that **47** compromises cell HR. Indeed evidences showed that **47** (i) reduced the nuclear foci formation of RAD51, upon cisplatin treatment, (ii) increased the percentage of γ-H2AX nuclear foci, upon combination with Olaparib, and (iii) induced the increment of cells bearing chromosomal aberrations, such as micronuclei, alone or in combination with Olaparib. These results supported the requested mechanism of action for **47**. Therefore, to test whether the combination of **47** and Olaparib could induce synthetic lethality, cell viability and cell death were simultaneously measured at 72 h in BxPC3 cells exposed to **47** alone or in combination with 10μM olaparib (Figure 27B, C). In cultures treated with 10 μM Olaparib and 20 μM **47**, the concentration corresponding to the highest HR inhibitory effect, cell death was markedly evident and increased in a statistically significant manner (Figure 27B, C).

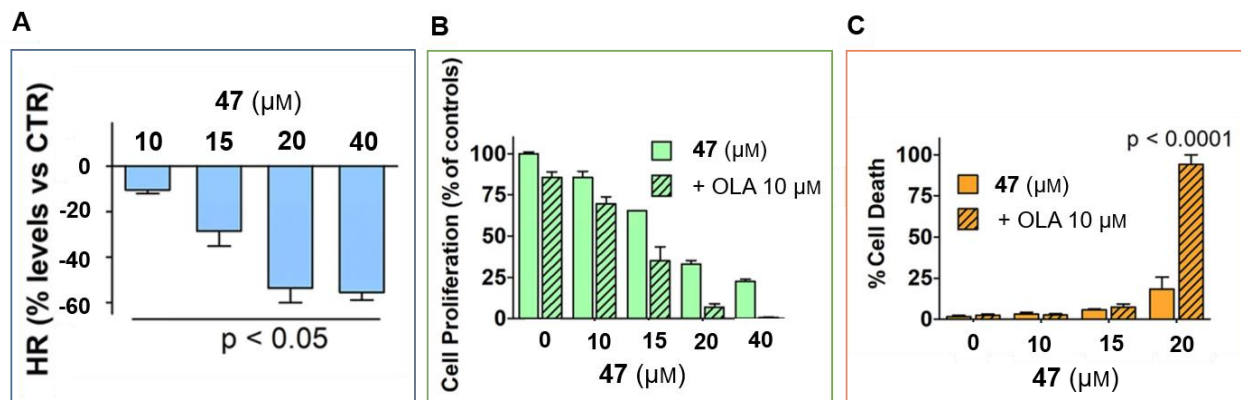


Figure 27. A) Effect on HR caused by **47** in BxPC3 cells (5 h); B) and C) BxPC3 cell viability and death after 72 h exposure to **47** and 10 μM Olaparib, given alone or in combination.

The lethality effect of the combination was investigated more in depth by observing cell morphology and reaction to vital dyes, DAPI and PI, after the 72 h treatment. The simultaneous marked staining of both dyes suggested an event of apoptosis in BxPC-3 treated with the combination. The mutated p53 status of BxPC3 cells conferred more relevance to these results, since p53 mutation endows cells with an intrinsic resistance to mechanisms of induced cell death.

The association effect between **47** and Olaparib was evaluated by the calculation of the combination index (CI), where $CI < 0.8$ indicates synergism, while $0.8 < CI < 1.2$ additive effect. In BxPC-3, CI resulted lower than 0.8, indicating a synergism between the two compounds (Figure 28). Noteworthy, in Capan-1 cells, which lack functional BRCA2 and are HR-defective, the combination of **47** and Olaparib produced an increased antiproliferative effect, if compared to the single agent treatment. However the statistical evaluation excluded the presence of synergism, indicating an additive effect with CI not significantly different from 1 (Figure 28).

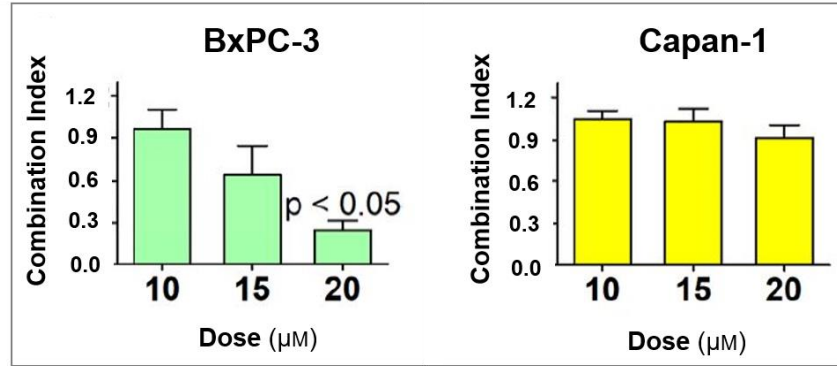


Figure 28. Combination indexes of the **47** and Olaparib in association, measured in BxPC-3 and Capan-1 cell lines.

Biochemical, biophysical and biological evaluations suggested that the disruption of RAD51-BRCA2 PPI could be a valuable strategy to impair RAD51 function and inhibit HR in pancreatic cancer cells. Moreover the sustained and increased DNA damage due to the simultaneous inhibition of different DNA repair pathways could induce a synthetic lethal effect, as suggested by in-depth biological studies. Ultimately these findings supported the working hypothesis that the combination of a RAD51-BRCA2 small molecule disruptor and Olaparib could reproduce the mechanism of synthetic lethality in pancreatic cancer cell lines with fully functional BRCA genes and HR.

3.4 Conclusions

In continuation of a research for the discovery of potential RAD51-BRCA2 PPI small molecule disruptors, able to trigger SL in pancreatic cancer with Olaparib, a series of dihydroquinolone pyrazoline derivatives has been identified.

To improve the PPI inhibitory activity of previously identified compound **3**, a chemical modification campaign was conducted around the 1,2,4 triazole core. This led to the identification of compound **5**, which proved to synergize with Olaparib, providing encouraging preliminary steps toward the proof of our working hypothesis. However the paradigm of SL was not fully reproduced. Thus, we envisaged the identification of novel classes of potential RAD51-BRCA2 PPI disruptors. Through a virtual screening campaign on Zone II, **19** was selected as a promising hit, and subsequently, SAR efforts led to compound **47** with the desired biological profile. Indeed, **47** bound to RAD51 and inhibited PPI between RAD51 and BRCA2. Noteworthy, **47** proved to synergize with Olaparib and induce synthetic lethal death in pancreatic cancer cells where it reduced significantly cell HR, as proof of its mechanism of action. This promising achievement supports the working hypothesis that synthetic lethality can be triggered by using only small organic molecules. Herein synthetic lethality resulted as valuable paradigm for the discovery of novel anticancer therapies, which include the treatment of pancreatic cancer, one of the major unmet oncological need. Notably, the observed synthetic lethality was triggered by targeting two biochemically different mechanisms: enzyme inhibition (PARP) and protein-protein disruption (RAD51-BRCA2). This highlights how complex and diverse mechanisms of action can synergistically contribute to the same physiological and, in turn, pharmacological activity. However, low solubility of **47** may influence its metabolic and pharmacokinetic profile (DM/PK), preventing it from further *in vivo* studies in cancer models. Therefore, structural tuning is currently ongoing to discover more drug-like dihydroquinolone pyrazoline derivatives.¹⁶²

4. Part II: DISCOVERY OF RAD51-BRCA2 PPI DISRUPTORS VIA TARGET DIRECTED DYNAMIC COMBINATORIAL CHEMISTRY

4.1 Introduction to dynamic combinatorial chemistry

Over the past decades, target-directed dynamic combinatorial chemistry (tdDCC) has become an attractive strategy to identify novel chemical structures for binding to a target protein.¹⁷¹ The concept of tdDCC was firstly coined in the late 1990s as a branch of supramolecular chemistry,¹⁷¹⁻¹⁷³ and, since then, it has been developed as an efficient tool to accelerate hit identification and, more recently, hit optimization in drug discovery.¹⁷⁴

In tdDCC, dynamic combinatorial libraries (DCL) are generated by reversible reactions of appropriate building blocks. In this system, building blocks and products are continuously interconverting, reaching an equilibrium state under thermodynamic control. Upon addition of the target protein, the equilibrium is shifted as a response to the external stimulus, according to Le Châtelier's principle (Figure 29).

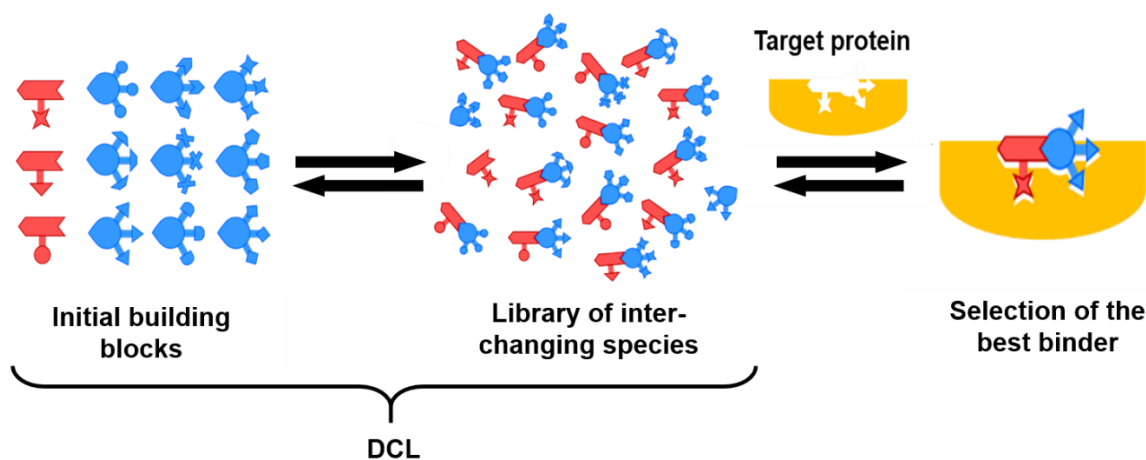


Figure 29. Target directed dynamic combinatorial chemistry (tdDCC) concept.

The protein acts as a template changing the DCL composition by interaction with mixture components, and, ultimately resulting in the amplification of its best binders, at the expense of non-binders.¹⁷¹ This technique broadens the number of chemical scaffolds that can be identified as binders, overcoming, or limiting the need for individual synthesis and tests for a large number of compounds.

In general, two different approaches can be adopted in td-DCC: comparative and non-comparative.¹⁷¹ In the comparative approach, a blank reaction in absence of the target protein is run concurrently with the templated reaction. The amplification of compounds is calculated by comparing the library composition of both templated and blank reactions. This approach commonly employs HPLC-MS as an analytical method. Noteworthy prior to the analysis, the equilibrium of the reaction should be frozen to avoid re-equilibration of the library, followed by the denaturation of the protein to release the bound ligands. In the non-comparative approach, ligands are identified without comparison to a blank reaction. This approach gives the possibility to analyze both the ligand–protein complex and the released ligand, by many different analytical techniques. For the ligand–protein complex analysis, non-denaturing MS and X-ray analysis can also be performed.¹⁷¹

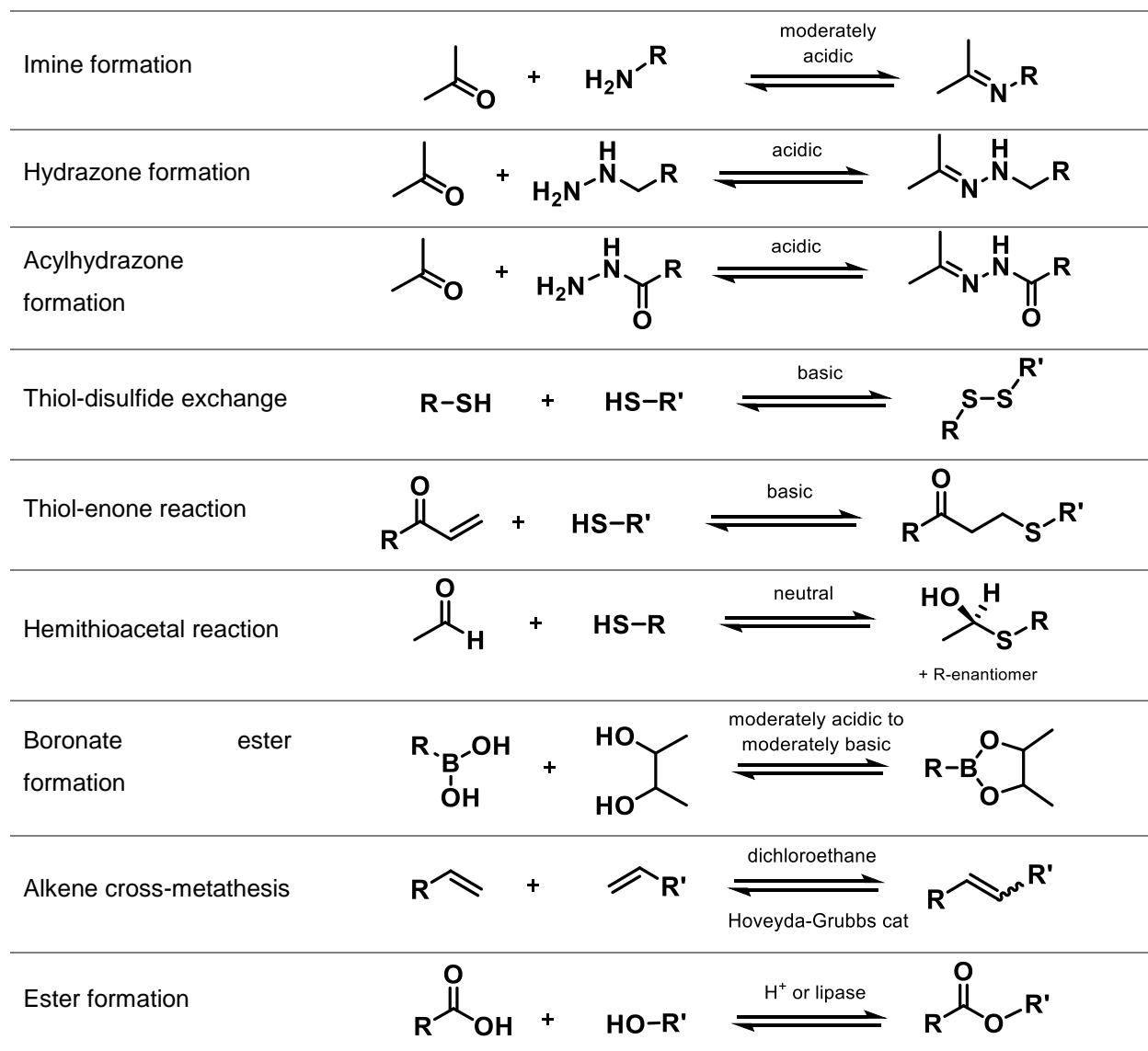
To generate active hits and obtain meaningful results, the tdDCC experiment setup should carefully consider: (i) reversible reaction, (ii) design of DCLs, (iii) templating protein, (iv) analytical methodology.¹⁷⁵

i. Reversible reactions suitable for tdDCC

The selection of the appropriate reversible reaction is an important step in tdDCC. The reversible reaction must be biocompatible, which means occurring at physiological pH, at room temperature, and reaching the equilibrium in a short timescale. The reaction must not affect protein activity, exert a denaturing effect, and must avoid off-site reactions with protein functional groups.¹⁷³ Considering the biocompatibility, only a limited number of reactions can be employed in tdDCC.

The dynamic reversible reactions adopted so far include condensation reactions (imine, hydrazone, and acylhydrazone formation), thiol exchange reactions (thiol-disulfide exchange, thiol-enone reaction, and hemithioacetal reaction), and boronate ester formation. Ultimately, also alkene cross-metathesis and ester formation have been reported (Scheme 19).

Scheme 19. Reversible reactions applied in tdDCC.



Imine formation is one of the first examples of reversible reactions in tdDCC. The reaction occurs between amine and aldehyde building blocks at neutral pH, and the equilibrium is reached within 12–24 h.^{171,173} As the generated imines are labile, the DCL analysis with HPLC for ligand detection requires the reduction of the imine bond with sodium cyanoborohydride or tetrabutylammonium cyanoborohydride, to form the corresponding stable amines. Despite the loss of information on the *E* and *Z* conformation of the imines upon reduction of C=N bond and the risk of protein denaturation by reductive agents, imine formation remains one of the most widely reported reactions in tdDCC.¹⁷¹

Acylhydrazone formation is another example of an addition-elimination reaction. In contrast to imines, acylhydrazone linkages have the advantage to be sufficiently stable to allow for direct HPLC analysis. The reaction occurs between aldehydes and hydrazides at acidic pH. For the DCL analysis, the equilibrium of the reaction should be quenched by increasing the pH using base. However, the low pH often is not compatible with protein stability, and the acylhydrazone formation is significantly slowed down at neutral pH, greatly limiting practical application in tdDCC. In this case, the use of a nucleophilic catalyst is required to activate the aldehyde through transformation into an intermediate Schiff base. Aniline is one of the most widely used catalysts, which allows the reaction to be reversible even at higher pH (6.0–7.5).¹⁷⁵⁻¹⁷⁷ The catalyst can be used at high concentrations, as aniline Schiff bases are not stable in water. At millimolar concentration, the catalyst enables the system to reach the equilibrium within a day at room temperature, avoiding the use of large amounts of DCL reactants. Additionally, aniline derivatives with electron-donating substituents on the aromatic ring proved to be even more effective in speeding up the equilibrium rate of reactions and find application in tdDCC.^{175,178,179}

Amongst thiol reactions, the reversible thiol-disulfide exchange is one of the most commonly reported examples. The reaction typically occurs under neutral to slightly basic pH. The intrinsic long incubation time of 1–2 weeks can be reduced to 24 h with redox buffers containing glutathione (GSH/GS-GS) or dithiothreitol (DTT). For HPLC analysis, the equilibrium is frozen by decreasing pH using different acids.

Boronate ester formation represents another approach employed in tdDCC. The reaction occurs from boronic acids and diol building blocks, at pH values resembling the pK_a value of boronic acids. Since pK_a values of arylboronic and alkylboronic acids are around ~ 8 and ~ 10 – 12 respectively, arylboronic acids are more suitable for reversible reactions at neutral pH. For analysis of DCL composition, ^{11}B NMR spectroscopy has been successfully employed.¹⁷³

ii. Design of dynamic combinatorial libraries (DCLs)

The design of a dynamic library is usually guided by protein structural information. Following a structure-based-approach, the design and selection of promising building blocks can be inspired by existing binders, by analysis of the target protein structure, or by molecular modeling. Once the scaffold is chosen, the functional groups for the reversible reaction should be placed where they do not hamper the interaction with the target protein.

To this end, a particular advantage of the acylhydrazone linkage is the resemblance to the amide functionality and the presence of H-bond donor and H-bond acceptor sites.

A structure-based approach is supposed to increase the probability of running a successful tdDCC. Indeed it enables the recognition of the specific chemical groups required for the interaction with the target protein, and which should be included in the library. Although a completely random ligand selection is discouraged, tdDCC can be exploited to broaden the chemical diversity of known binders. To this aim, the DCLs can include building blocks with different structures, which do not necessarily display a protein-binding affinity, to cover different geometrical and functional spaces. In this way, successful tdDCC can lead to the identification of new chemical entities able to bind the protein.¹⁷⁵

iii. Templating protein

In tdDCC, significant results are correlated to the quality of the input template. Indeed, the equilibrium shift in DCL composition is mediated by the templating effect of the target protein, thus the protein must stay as close to its native state as possible. The quantity of the target protein should be chosen to guarantee the templating effect that can be detected, avoiding protein aggregation, and precipitation. Protein concentration is normally low (μM – nM range). Variables, like purity, concentration, the tertiary and quaternary structure of the added protein, presence of additives, and contaminations, as well as the pH value and buffer components, must be considered to design correctly a tdDCC experiment. Protein degradation and precipitation could occur during the experiment, with the risk to alter or bias experimental results. Thus it is important to properly select suitable experimental conditions and envisage those factors.¹⁷⁵

Stability

The assessment of protein stability should be checked by preliminary tests before setting up a tdDCC experiment. Precipitation, aggregation, and degradation of the protein must be avoided. Precipitation causes the removal of the template from the solution, whereas the denaturation leads to a completely new template, which can alter the DCL composition with consequent amplification of compounds, which do not bind in the native state. In all these cases, random and irreproducible results can be generated with the loss of the best binders from the DCL.

pH, buffer, ionic strength

The effect of pH, buffer, and ionic strength on the protein state should be evaluated, to select the most appropriate experimental conditions. For most of the target proteins, the optimal buffer conditions and the stability at room temperature are usually unknown. Thus, it can be convenient to screen the protein over a wide range of pH, buffer, and ionic strength values in parallel, to select the best combinations. Subsequently, two or more buffers can be evaluated per pH value to distinguish the effect of buffer components and pH on the protein. The determination of the melting point of the target protein via thermal-shift assay/differential scanning fluorimetry (TSA/DSF) is a useful method to evaluate the protein state during the screening. This technique offers the possibility of a high-throughput analysis in relatively short times. The method exploits the presence of a lipophilic dye, which increases in fluorescence by binding to hydrophobic parts of the protein, typically located inside of the protein. These portions become exposed due to the melting/unfolding process, induced by an increase in temperature. The temperature-dependent fluorescence is measured and the protein conformational change is evaluated as a function of the shift in protein melting temperature (T_m). Amongst other methods, differential scanning calorimetry (DSC), isothermal titration calorimetry (ITC), and circular dichroism (CD) can be used to collect information about the interaction of the protein with buffer components. In general, any side reactions and competition effects of buffer components with the target protein must be avoided.¹⁷⁵

DMSO

In tdDCC experiments, DCL building blocks are solubilized in DMSO stock solutions at known concentrations. Thus, in all experiments, DMSO is commonly present in variable percentages, depending on the number of DCL components and the library composition. The DMSO concentration should be kept constant through all the experiments to provide comparable data. The fixed DMSO concentration is a parameter to choose carefully as it can exert a wide range of effects on the protein structure. A decrease in solubility, denaturation, and precipitation can occur if the DMSO concentration is not well tolerated by the protein. The evaluation of T_m shift by TSA/DSF technique helps the selection of the compatible DMSO percentage. In the case of enzymes, the determination of the enzymatic activity can be performed, if a specific enzymatic assay is available. In general, the DMSO concentration should be kept as low as possible, to guarantee the solubility of products and protein in solution during all the experimental time.¹⁷⁵

Temperature

To reach the DCL equilibrium, experiments are performed at room temperature. As the temperature can potentially interfere with protein stability, it can be lowered to help the protein stabilization. As a result, the equilibration rate of the reactions will decrease with consequent prolonged incubation time.¹⁷⁵

iv. Analytical methodologies in tdDCC

According to the tdDCC approach, different analytical techniques have been employed to examine DCL composition and amplification of library components. These mainly include HPLC, native, non-denaturing mass spectroscopy, and ligand-observed NMR spectroscopy.

In tdDCC comparative approaches, the library is usually analyzed by recording HPLC-MS chromatograms of the DCL mixture. In the chromatogram, signals of each library component are recognized and the peak areas are integrated as a function of compound concentration. This method concerns the analysis of the ligand, thus the dissociation of the ligand–protein complex is a prerequisite for the analysis since a bound ligand is not reliably detectable. The release of the ligands from the complex can be achieved by denaturation of the protein with organic solvents, heat, acids, bases, or ethylenediaminetetraacetic acid (EDTA), or for displacement by the addition of a competitive ligand.¹⁷¹ The subsequent sample treatment, including centrifugation, filtration, and precipitation, to avoid column obstruction during HPLC runs. To calculate the amplification rate of library components, HPLC data should be accurately interpreted. The superimposition of chromatograms from the template and blank reactions do not fulfill the requirements for an accurate analysis of the library and can be limited to experiments where large variations of compound peaks are observed. To detect smaller changes and derive the amplification factor, the relative peak area (RPA) of each compound is calculated. RPA value represents the single peak area of each compound relative to the total peak area in the blank and template reactions. The amplification factor is then derived by dividing RPAs from the template and blank reactions respectively, as shown in Equation (1), or following Equation (2) to calculate the relative change.^{171,175}

$$\text{Amplification factor \%} = (\text{RPA}_{\text{template}} / \text{RPA}_{\text{blank}}) \times 100 \quad (1)$$

$$\text{Normalized change of RPA} = (\text{RPA}_{\text{template}} - \text{RPA}_{\text{blank}}) / \text{RPA}_{\text{blank}} \quad (2)$$

However, this approach can include disadvantages, like a time-consuming peak assignment, and risk of signal overlap, which at least can limit the size of DCLs per experiment. Moreover, since HPLC relies on UV detection, the extinction coefficient values of each compound should be comparable to assure a meaningful comparison of UV signal intensity.

MS analysis is preferentially exploited in non-comparative approaches to detect DCL composition. In this case, native non-denaturing mass spectrometry is applied to analyze the native ligand–protein complex and, in comparative approaches, the concentration of free ligand.

HPLC-MS and MS analysis can both provide a quantification of concentration for each library component, relative to the dynamic mixture.

NMR analysis found application in tdDCC, in particular with techniques like ^{11}B NMR spectroscopy, in boronate ester chemistry, and ligand-observed NMR spectroscopy. The latter generally includes nuclear Overhauser effect (NOE)-based ligand-observe NMR techniques such as saturation transfer difference (STD) and water ligand-observed via gradient spectroscopy (waterLOGSY). However, a disadvantage can be the ligand exchange dynamics, which can hamper the analysis. Indeed, the exchange can be too fast compared to the NMR timescale, resulting in broadened resonance signals. Moreover, STD-NMR and waterLOGSY mainly enable the detection of weak binders with K_D in the μM – nM range, with the risk of false-negative results and loss of strong binders.¹⁷³

4.2 Application of tdDCC on RAD51

Cancer cells are strictly dependent on efficient DNA repair machinery to guarantee their survival. Thus DNA repair pathways can provide a source of biological targets for the development of anticancer treatments. RAD51, an evolutionarily conserved recombinase enzyme,⁹⁰ is involved in homologous recombination (HR), one of the cellular pathways responsible for the repair of DNA double-strand breaks (DSBs). In this process, RAD51 is recruited by BRCA2 to reach the DNA damage site into the nucleus.¹¹³ Indeed, RAD51 overexpression has been observed in a wide variety of cancers,¹³⁴ suggesting the dependence of cancer cells on efficient HR. Thus, the inhibition of HR by targeting RAD51-BRCA2 protein-protein interaction represents a valuable tool to sensitize cancer cells to the treatment with chemotherapeutic agents and synergize with the PARP inhibitor Olaparib.

In the present work, the DCC approach has been exploited for the identification of new chemical scaffolds targeting RAD51 and enabling the displacement of BRCA2 interaction. For DCC experiments, RAD51 has been used as a templating protein and *N*-acylhydrazone formation has been chosen as a reversible reaction.

N-acylhydrazone derivatives as a privileged structure in drug discovery

In tdDCC, the use of *N*-acylhydrazone linkage is well established because the reaction is reversible at acidic pH, occurs in aqueous media, resembling physiological conditions, and generates compounds quite stable to hydrolysis at physiological pH.^{173,175}

In addition to its successful use in tdDCC, the *N*-acylhydrazone (NAH) core has been considered a privileged structure with great potential in medicinal chemistry. A huge number of hit and lead compounds bearing the NAH core have been reported and included in many drug discovery pipelines.¹⁸⁰ Indeed, NAH-based derivatives can display a broad range of activities, with possibilities for the development of new, therapeutically useful bioactive NAH candidates to face many diseases, including viral,¹⁸¹⁻¹⁸³ bacterial infections,¹⁸⁴ metabolic disorders,¹⁸⁵ and cancer.^{180,186}

NAH bioactive framework can display ligand interactions with various biological targets. This characteristic can be correlated to the typical NAH chemical properties, which include a relatively weak N-N bond, the presence of an acidic proton, and an acyl group. NAH scaffold shows significant chemical versatility, based on its synthetic feasibility. Indeed the chemical

synthesis, which occurs by condensation between aldehydes or ketones and hydrazides, allows broad modifications of the subunits bonded to its acyl and imine functions. Ultimately, this results in the possibility to synthesize several derivatives with varying chemical compositions and possible target modulations.^{187,188} Generally NAHs display a stable *E* configuration of the imine double bond, except in cases of intramolecular interactions, which stabilize and favor the *Z* isomer (Figure 30).

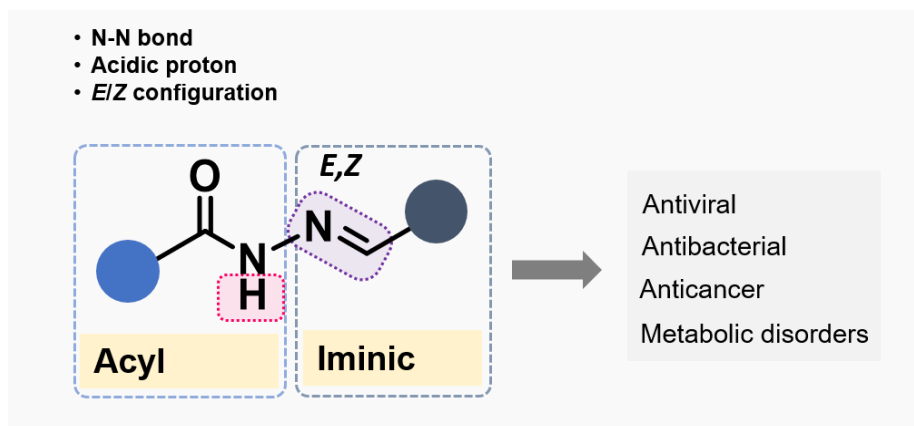


Figure 30. NAH framework as a useful bioactive chemical entity.

Nevertheless, NAH-based compounds are generally correlated to disadvantages linked to their chemistry. Indeed, NAHs chemical class has been included among the pan-assay interference compounds (PAINS) family.¹⁸⁹ Noteworthy, a certain PAINS activity has been ascribed only to compounds with an ortho-hydroxyl aryl or a para-hydroxyl aryl group in the imine subunit of the NAH core as it enables the formation of the tautomeric reactive ortho and para quinone methide, respectively, as real PAINS species.¹⁸⁹ Moreover, examples of photo-induced *E/Z* isomerization have been reported and cannot be excluded.^{190,191}

Along with this, the major issue of NAHs relies on their chemical stability. Indeed, depending on the substituents on the amide nitrogen and the imine carbon, the acylhydrazone linkage can undergo hydrolysis into the corresponding aldehyde and hydrazide under acidic pH. NAHs chemical instability can be disadvantageous, resulting in activity loss, poor pharmacokinetic profile, and even increased toxicity.¹⁹¹ To overcome this issue, the replacement of *N*-acylhydrazone linker with bioisosteres has been successfully applied to generate more stable compounds with a comparable activity toward the biological target, as reported by V. R. Jumde *et al.*¹⁹¹

Thus, despite the relevant biological importance of NAH-based compounds, chemical stability and PAINS activity should be carefully checked and, if necessary, it is recommended to

envisage chemical modification strategies, which include bioisosteric replacement of the NAH core.

4.2.1 Protein stability assessment

RAD51 has been chosen as a templating protein and used in the oligomeric form, which more resembles more closely its physiological state in the cell.

RAD51 is stored in solution at pH 7.5 in well-optimized buffer composition, containing HEPES 20 mM, KCl 300 mM, glycerol 10%, EDTA 0.1 mM, and DTT 2 mM (storage buffer). High salt and glycerol concentrations and the presence of additives were not previously reported to be compatible in tdDCC experiments. Thus, as a prerequisite for acylhydrazone-based tdDCC, we analyzed the stability of RAD51 under different experimental conditions, screening different protein concentrations, buffers, pH values, glycerol amounts, salt concentrations, and DMSO percentages.¹⁷⁵ We decided to include also the storage buffer in the analysis and keep it as a reference condition. The stability assessment was performed by measuring the melting temperature (T_m) of the protein via thermal-shift assay/differential scanning fluorimetry (TSA/DSF) within two days. In more than one condition, we observed the formation of multiple melting curves, probably due to changes in the oligomeric state of the protein.

From the buffer screening, performed at a fixed concentration of KCl 300 mM and glycerol 5%, RAD51 proved to be unstable in acetate buffer and, in general, to poorly tolerate pH lower than 6.0. In MES and TRIS-Bis buffers, the protein showed reasonable stability for 24h at pH 6.0–6.5. However the significant difference in T_m , in comparison to the storage conditions, suggested undefined conformational changes of the protein, thus these buffer compositions were discarded. Finally, we found that RAD51 was stable in phosphate buffer at pH 7.0 and 7.5 for 24h, which is comparable to the stability observed in storage conditions. Since pH 7.5 is too high to be compatible with *N*-acylhydrazone chemistry in the tdDCC experiments, we selected phosphate 50 mM at 7.0 pH for further DCC experiments (Figure 31). The screening suggested that tdDCC is compatible with our target protein. Ultimately, we decided to select both storage buffer conditions and phosphate buffer (50 mM) at 7.0 pH for the first tdDCC experiments. However, protein exhibited stability at pH higher than 6.0, values that could slow down the rate of acylhydrazone formation reversibility. Thus the use of aniline as a nucleophilic catalyst is required to ensure the reversibility of the reaction in both the selected conditions.

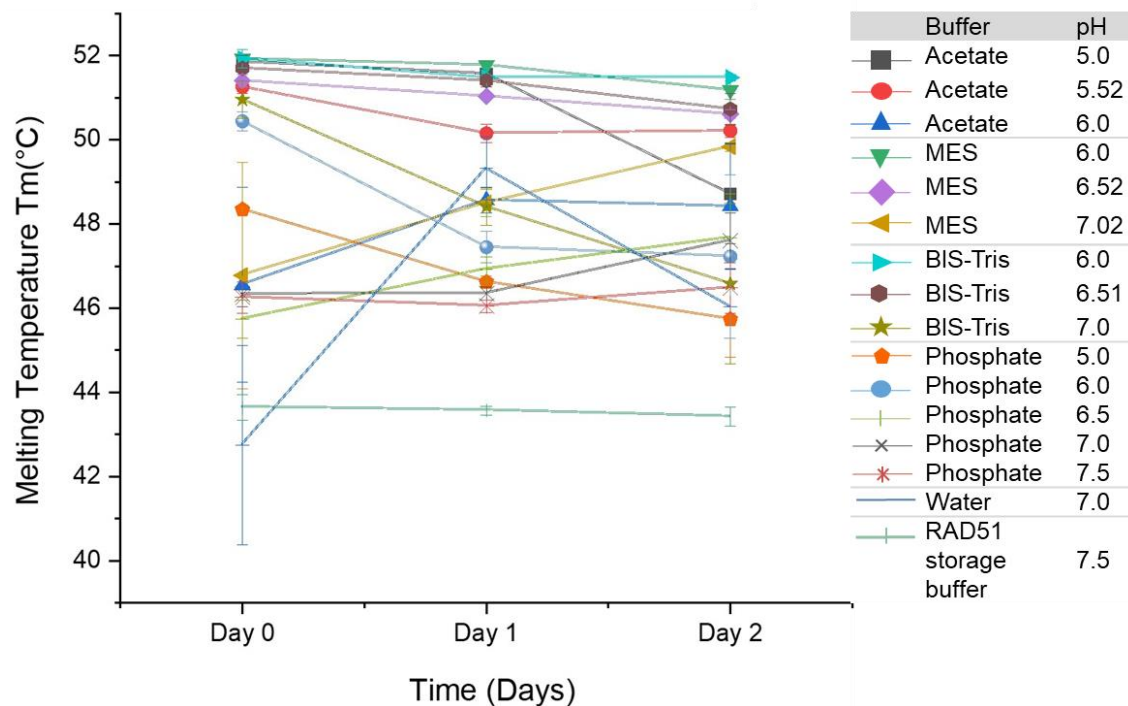


Figure 31. Buffer and pH values screening on RAD51 through TSA/DSF assay.

Regarding other components, we observed that the RAD51 protein stability was not affected by the absence of EDTA and DTT within 24 h. Ultimately, we assessed the optimal concentrations of other buffer components, in particular KCl 300 mM, glycerol 5%, DMSO 5%.

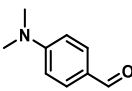
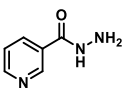
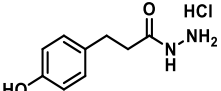
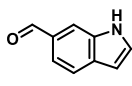
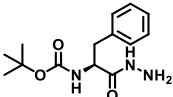
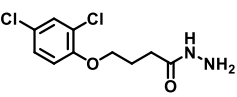
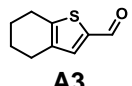
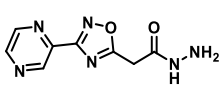
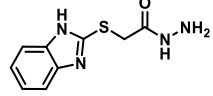
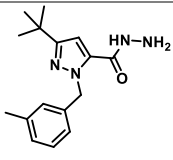
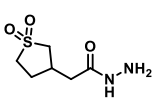
To guarantee RAD51 stability for prolonged times at room temperature, tdDCC experiments were performed following the listed conditions.

4.2.2 tdDCC-1

We designed the DCL1 to explore the tdDCC approach on RAD51 for the first time. In this preliminary phase, the choice of building blocks was meant to broaden the chemical diversity of known RAD51 binders and lead to the identification of new chemical classes able to display binding-affinity for RAD51.

DCL1 consisted of three aldehydes (**A1–A3**) and eight hydrazides (**H1–H8**), corresponding to twenty-four possible compounds (Table 8). After a given time, the library was analyzed via UPLC-MS, after protein denaturation by the addition of methanol and equilibrium freezing by increasing the pH.

Table 8. Dynamic combinatorial library 1 (DCL1) composition.

DCL1		
A1-3		H1-8
 A1	 H1	 H2
 A2	 H3	 H4
 A3	 H5	 H6
	 H7	 H8

The first tdDCC experiment was performed in RAD51 storage buffer to ensure the highest protein stability in solution at room temperature (Table 9, entry 1). We ran protein-templated and blank reactions in parallel, taking samples at 8 h, 24 h, and 48 h. We assessed the amplification of DCL components using the equations (1) and (2) previously reported. The presence of RAD51 successfully influenced the library composition and, indeed, compounds **A1H3**, **A1H7**, **A2H4**, **A2H7**, **A3H4**, and **A3H7** were significantly amplified in the templated reaction. However, we observed that the equilibrium state in the blank reaction was not completely reached in the given time. To understand the possible reasons for fluctuations in the equilibrium state of the blank reaction, we checked the effect of other experimental conditions, like interfering buffer components, the pH values, and the library composition.

To evaluate the effect of storage buffer components, we screened three different experimental setups, taking advantage of RAD51 stability assessment assay reported in Figure 31 (Table 9). Moreover, we decided to monitor the DCC blank reaction every two hours for 12 h, to match the correct window of the maximum templating effect of RAD51.

Phosphate buffer is commonly used in *N*-acylhydrazone based DCC and was selected to facilitate the NAH formation in DCC conditions. The thermodynamic equilibrium was reached in the blank reaction between 2–8 h. However, after 6 h of experiment, RAD51 solubility significantly decreased and at 8 h, the protein precipitation occurred. Nonetheless, the

calculated amplification factors matched with the experimental results observed in the storage buffer experiment at 24 h (Table 9, entry 1). Due to the protein instability after six hours in DCC conditions, we decided to further investigate the effect of other parameters to obtain more reliable results (Table 9, entry 2).

Subsequently, we performed an experiment using conditions, which resembled the storage buffer, without EDTA and DTT and with a reduced glycerol amount (Table 9, entry 3). We reasoned that it could foster protein solubility and interfere less with the equilibrium state. Indeed, at pH 7.0 the system proved to reach the equilibrium in the blank reaction (Figure 32).

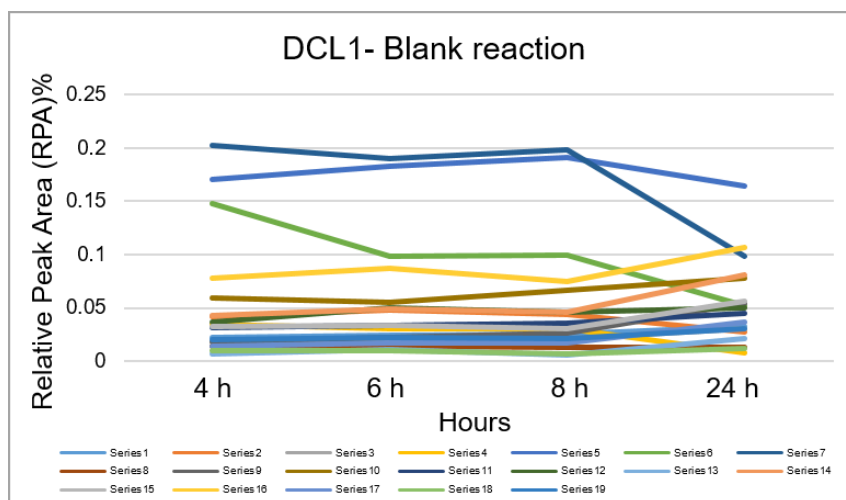


Figure 32. RPA trend in DCL1 blank reaction between 4–24 h.

Then we ran the protein-templated reaction and calculated the amplification factors by comparing its composition with the blank DCL1. In agreement with the first experiment in RAD51 storage buffer, compounds **A1H3**, **A1H7**, **A2H4**, **A2H7**, **A3H4**, **A3H7**, corresponding to LC-MS chromatogram peaks number 13, 14, 16, 17, 18 and 19 respectively, were most significantly amplified and thus selected for further synthesis and tests in biochemical assay with the target protein (Table 9, Figure 33).

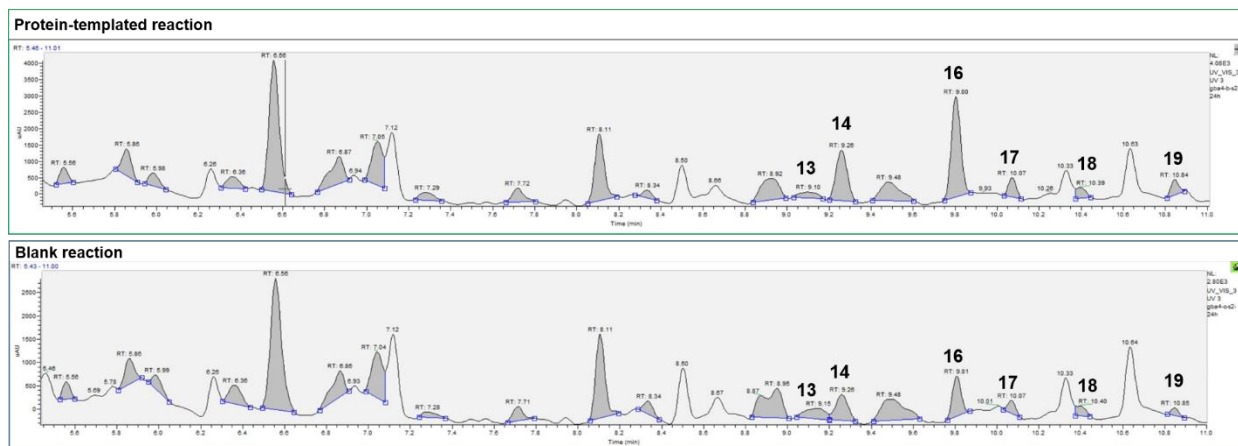
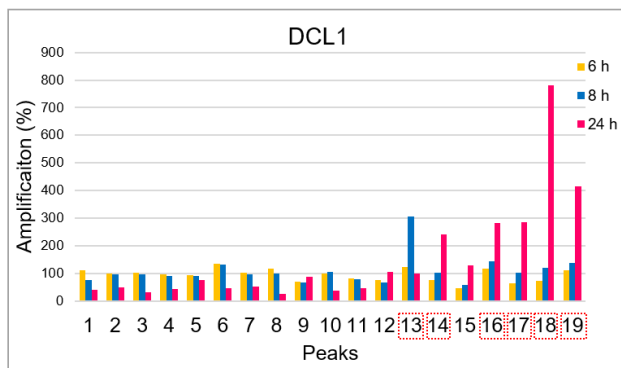
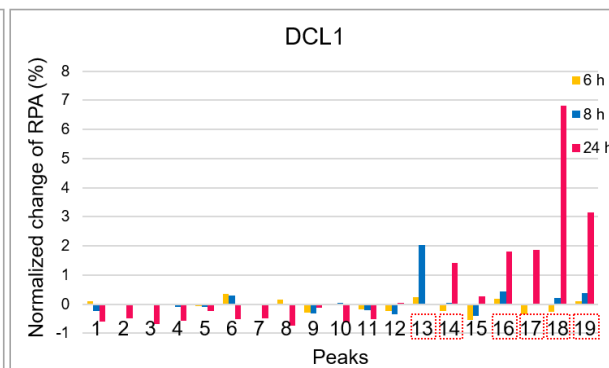
A**B****C**

Figure 33. A) LC-MS chromatogram of protein-templated and blank reactions at 24 h; B) DCL1 amplification% calculated from RPA values (Equation 1); C) DCL1 normalized change of RPA (%), (Equation 2).

In addition to the previous experiments, we envisaged evaluating the effect of pH on the equilibrium state. For this reason, we set up an experiment in HEPES 20 mM at pH value 7.5 (Table 9, entry 4). As previously hypothesized, despite the presence of aniline as a nucleophilic catalyst, high pH values hampered the product formation and the equilibrium state was not reached.

In conclusion, using DCL1, we screened different experimental conditions and selected an optimal buffer composition for further DCC experiments (Table 9, entry 3).

Table 9. Screening for experimental condition setup with DCL1.

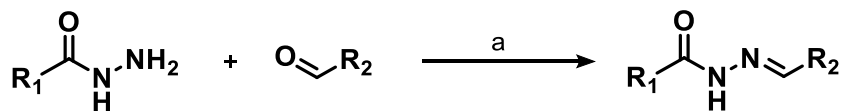
Entry	Buffer	Issues	Amplified compounds
1	HEPES 20 mM, pH 7.54 KCl 300 mM Glycerol 10%, EDTA 0.1 mM DTT 2 mM	Equilibrium not stable in the blank reaction	A1H3, A1H7, A2H4, A2H7, A3H4, A3H7
2	Phosphate 50 mM, pH 7.00 KCl 300 mM Glycerol 5%	Protein precipitation, visible after 6 h	-
3	HEPES 20 mM pH 7.02 KCl 300 mM Glycerol 5%	-	A1H3, A1H7, A2H4, A2H7, A3H4, A3H7
4	HEPES 20 mM, pH 7.43 KCl 300 mM Glycerol 5%	Equilibrium not reached	-

4.2.3 Biochemical evaluation and results

From DCL1 experiments, we observed the significant signal amplification of NAHs **A1H3, A1H7, A2H4, A2H7, A3H4, and A3H7** (Figure 33). Thus, we proceeded with the chemical synthesis of these compounds to test their ability to inhibit RAD51-BRCA2 PPI in the competitive biochemical ELISA assay, reported by Rajendra *et al*²¹, and evaluate the presence of a correlation between amplification observed in tdDCC and activity against the target protein.

All the amplified compounds amplified were re-synthesized from the corresponding commercially available aldehydes and hydrazides, according to the general synthetic route reported in Scheme 20. Synthetic procedures and characterizations are reported in the Experimental section. Results from the biochemical ELISA assay are reported in Table 10.

Scheme 20. Synthesis of *N*-acylhydrazones.



Reagents and conditions: a) MeOH, 65 °C, overnight, yield 65%–quantitative

Table 10. EC₅₀ from ELISA assay of dynamic combinatorial library 1 (DCL1) amplified *N*-acylhydrazones.

Entry	Cpd	Structure	EC ₅₀ (μM)	Entry	Cpd	Structure	EC ₅₀ (μM)
1	A1H3		70 ± 25	4	A2H7		NA ^a
2	A1H7		130 ± 20	5	A3H4		86 ± 30
3	A2H4		50 ± 5	6	A3H7		NA ^a

Footnote: ^aNA, not active.

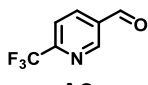
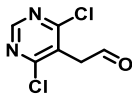
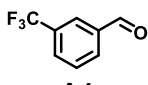
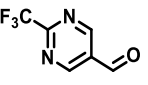
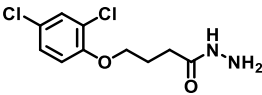
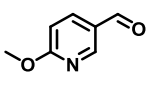
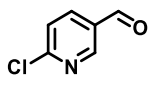
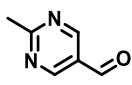
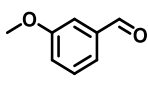
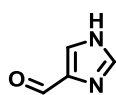
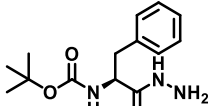
Compounds containing 4-(2,4-Dichlorophenoxy)butanoyl (**A2H4**, **A3H4**, Table 10, entry 3 and 5) and Boc-phenylalanine (**A1H3**, Table 10, entry 1) moieties proved to inhibit the PPI with EC₅₀ values in the range of 50–86 μM. Whereas compounds bearing 3-(*tert*-butyl)-1-(3-methylbenzyl)-1*H*-pyrazole-5-carboxyl moiety proved to be inactive (**A2H7**, **A3H7**, Table 10, entry 4 and 6) or poorly active (**A1H7**, Table 10, entry 2). These ELISA assay results suggest that the activity of compounds was influenced more by the substituents on the hydrazide part than on the iminic part. To corroborate these preliminary results, the synthesis of not amplified NAH, **A1H1**, is ongoing, to provide a negative control compound in biochemical tests.

4.2.4 tdDCC-2

To further improve the activity of hits from DCL1, we design two tailored libraries (DCL2 and DCL3) inspired by the initial DCL1 hits. We assumed that using the common structural motifs of the best hits from DCL1 as building blocks in the subsequent DCC experiments, along with new

aldehyde and/or hydrazide counterparts would provide better chances of identifying improved hits. We decided to keep the 4-(2,4-dichlorophenoxy)butanoyl and *Boc*-phenylalanine hydrazides from DCL1, which emerged as common structural motifs in hits **A2H4**, **A3H4**, and hit **A1H3**, respectively. Thus we explored the combination of hydrazides **H1** and **H2** with mono aromatic ring systems, and we included monosubstituted phenyl rings, **A4**, **A9**, monosubstituted pyridines, **A1**, **A2**, **A6** and **A7**, mono- and disubstituted pyrimidines **A3**, **A5**, **A8**, and 1,3-imidazole moiety, **A10** (Table 11). DCL2 was composed of ten aldehydes (**A1–A10**) along with the two hydrazides (**H1–H2**), which could provide twenty possible NAH products (Table 11).

Table 11. Dynamic combinatorial library 2 (DCL2) composition.

DCL2					
A1–10					H1 and 2
					
					

The composition of the DCL2 was analyzed via UPLC-MS periodically. The blank reaction reached the equilibrium between 8–10 h (Figure 34).

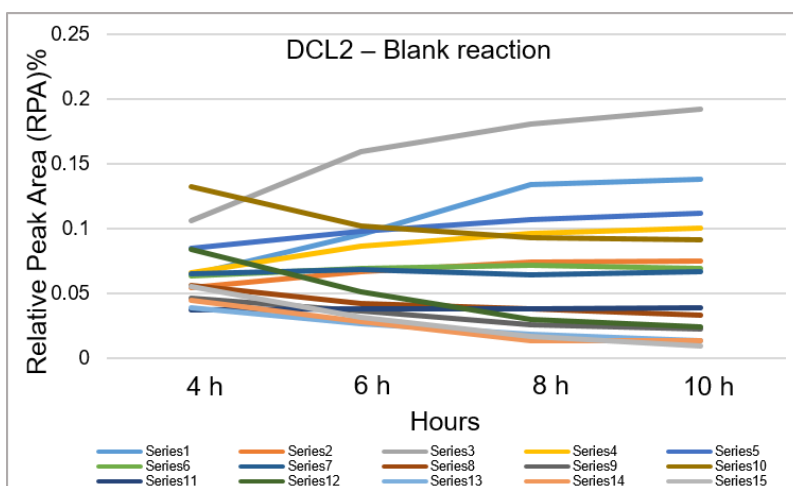


Figure 34. RPA trend in DCL2 blank reaction between 4–10 h.

Taking into account amplification factors at 8 and 10 h, the analysis of the library revealed the amplification of six compounds **H1A1**, **H1A6**, **H1A9**, **H1A2**, **H2A4**, and **H1A4** corresponding to LC-MS chromatogram peaks number 8, 9, 12, 13, 14 and 15, respectively (Figure 35).

Noteworthy, NAHs bearing monosubstituted pyridines and monosubstituted phenyl rings have mainly emerged from amplification data. Amplified *N*-acylhydrazones were re-synthesized, according to the general synthesis reported in Scheme 20 (Table 12).

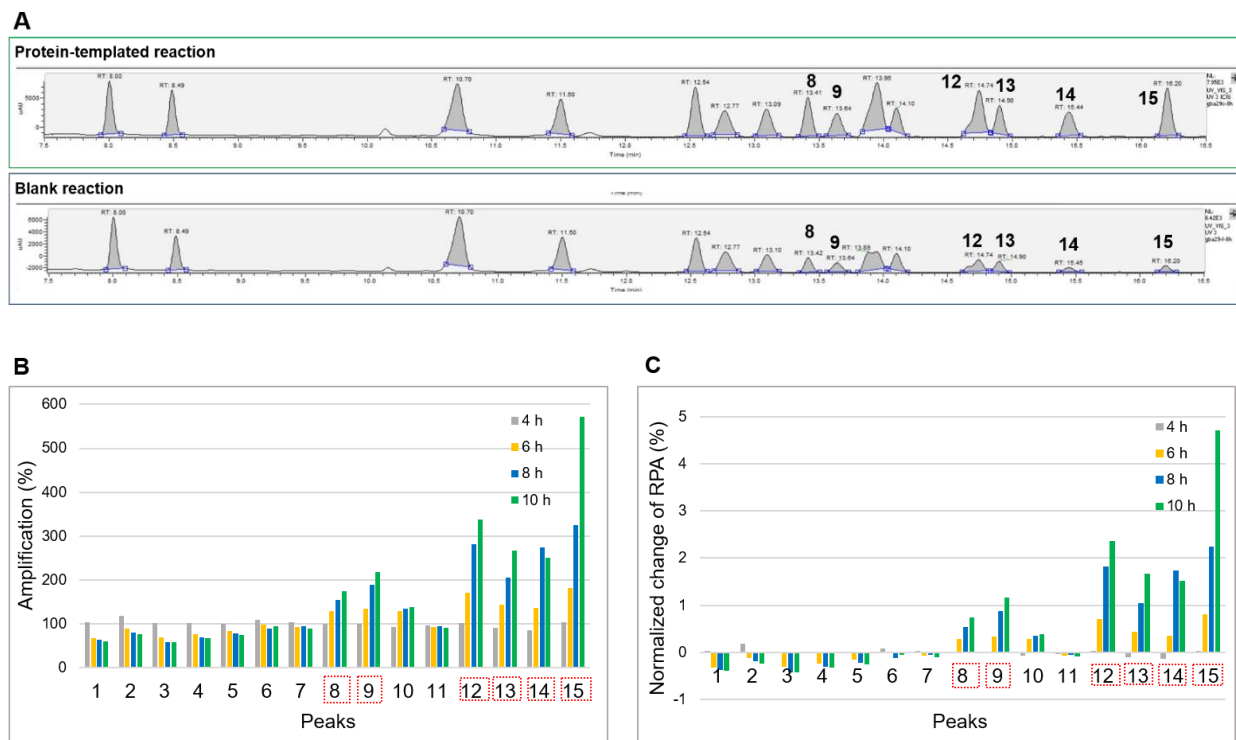
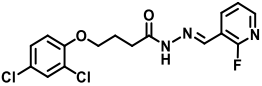
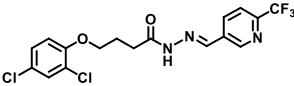
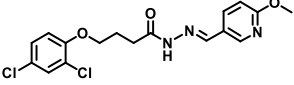
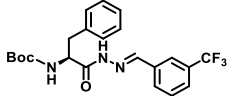
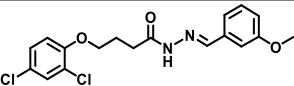
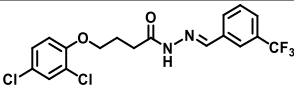


Figure 35. A) LC-MS chromatogram of protein-templated and blank reactions at 8 h; B) DCL2 amplification(%) calculated from RPA values (Equation 1); C) DCL2 normalized change of RPA (%), (Equation 2).

Table 12. Dynamic combinatorial library 2 (DCL2) amplified compounds.

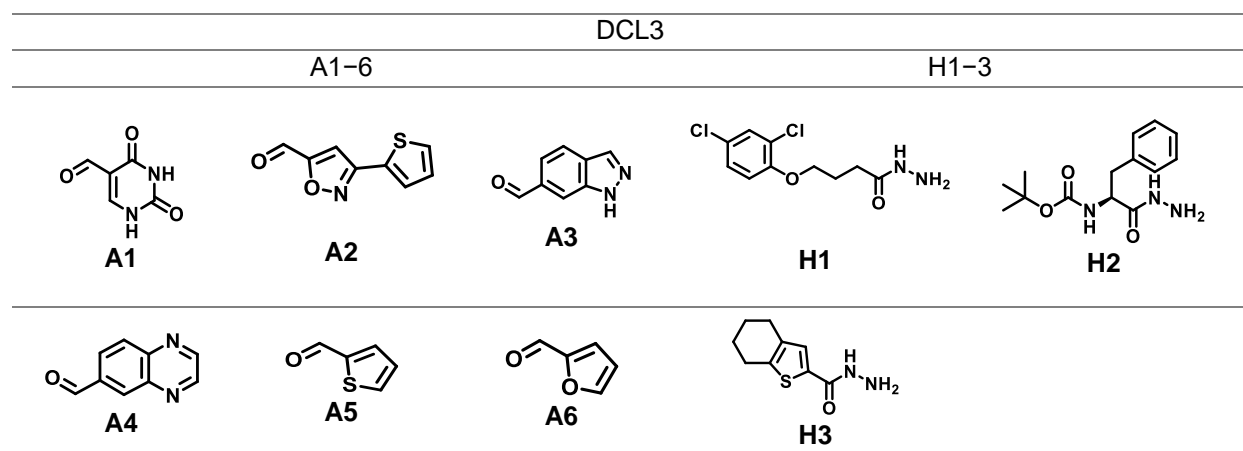
Entry	Cpd	Structure	Entry	Cpd	Structure
1	H1A1		4	H1A2	
2	H1A6		5	H2A4	
3	H1A9		6	H1A4	

Synthetic procedures and characterizations of NAH are reported in the Experimental section. The evaluation of the biochemical profile of the newly synthesized NAHs is now ongoing. The EC₅₀ values will clarify if combining 4-(2,4-dichlorophenoxy)butanoyl and *Boc*-phenylalanine moieties with substituted pyridines and phenyl rings results in the improvement of the activity toward RAD51-BRCA2 PPI displacement.

4.2.5 tdDCC-3

The DCL3 has been designed, taking inspiration from the results of the biochemical activity of DCL1 hits. We kept both 4-(2,4-dichlorophenoxy)butanoyl **H1** and *Boc*-phenylalanine **H2** as hydrazide moieties and included the 4,5,6,7-tetrahydrobenzothiophene from the hits in DCL1. To investigate the effect of inverting the position of 4,5,6,7-tetrahydrobenzothiophene in the acylhydrazone, we included it as a hydrazide **H3** instead of aldehyde **A3**. In DCL3, we decided to expand the chemical diversity of potential hit compounds by combining the emerged hydrazides with aldehydes bearing groups with different chemical properties. Thus, we included aldehydes with a uracil group as a hydrophilic component **A1**, an aromatic system of two heterocycles **A2**, bi-cyclic heterocycles with two heteroatoms, **A3** and **A4**, and five-membered heterocycles, **A5** and **A6** (Table 13). DCL3 was composed of six aldehydes (**A1–A6**) and three hydrazides (**H1–H3**), corresponding to eighteen possible compounds (Table 13). The composition of the DCL3 was analyzed *via* UPLC-MS periodically.

Table 13. Dynamic combinatorial library 3 (DCL3) composition.



The blank reaction showed to reach the equilibrium after 8 h (Figure 36).

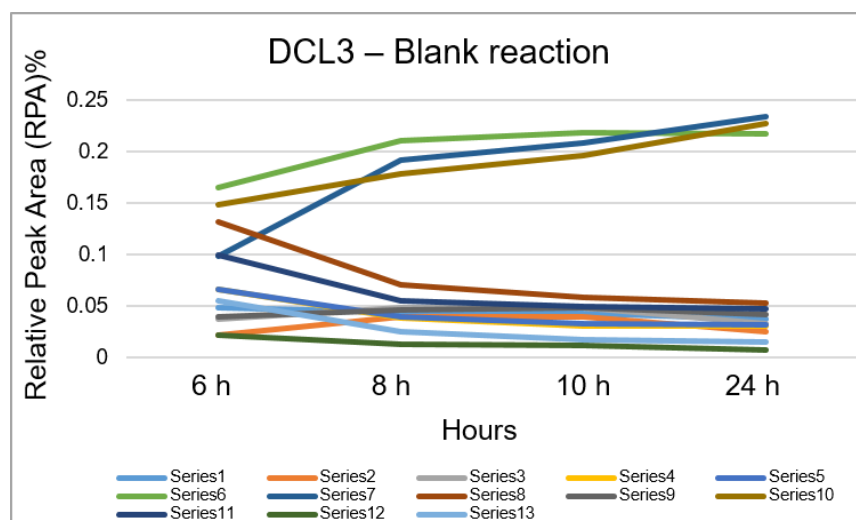


Figure 36. RPA trend in DCL3 blank reaction between 6–24 h.

After 8 hours, a significant amplification was registered for compounds **H3A3** and **H1A3** with indazole group, **H3A4** and **H1A4** with quinoxaline ring, and **H3A2**, **H2A2**, **H1A2** with 3-(thiophen-2-yl)isoxazolyl moiety, corresponding to chromatogram peaks number 4, 5, 8, 11, 12 and 13 respectively (Figure 37). Compounds reported in Table 14 have been selected for further evaluation of the biochemical profile. To this aim, *N*-acylhydrazones **H3A4**, **H3A3**, **H1A4**, and **H1A3** (Table 14, entry 1–4) have been re-synthesized and synthetic procedures and characterizations of NAH are reported in the Experimental section. The synthesis of **H3A2**, **H2A2**, **H1A2** (Table 14, entry 5–7) is still ongoing and will be soon completed.

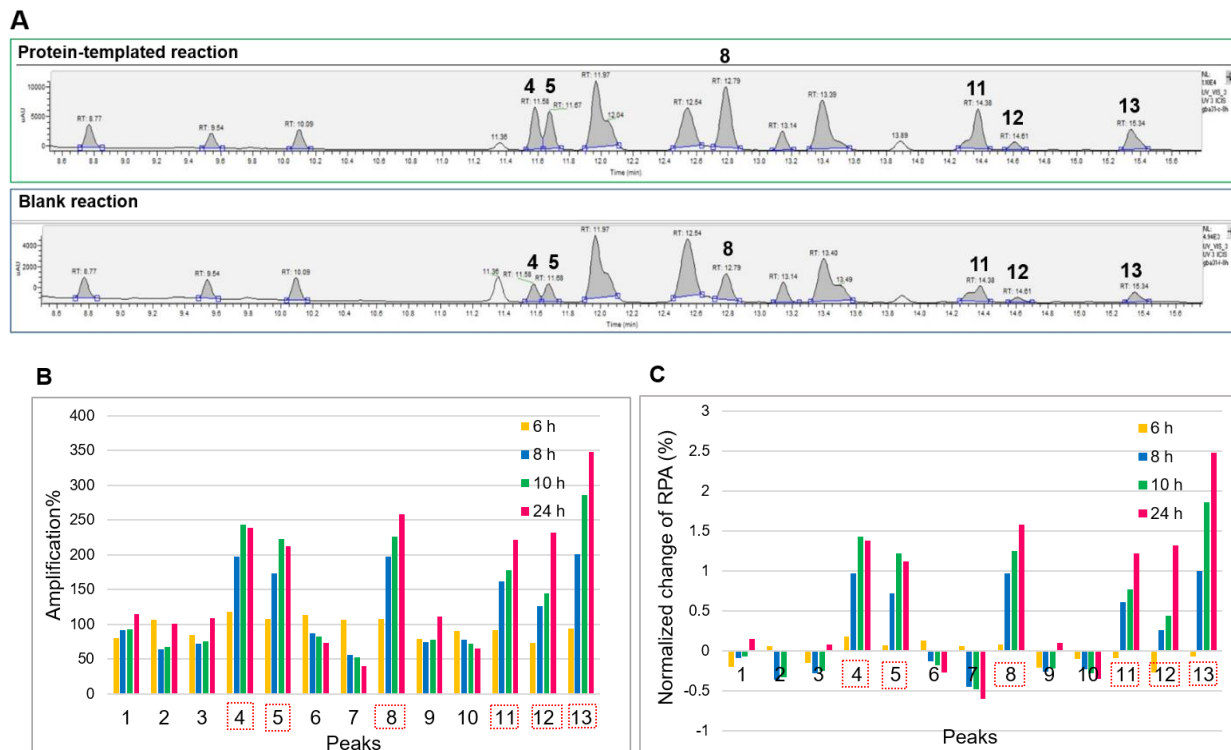


Figure 37. A) LC-MS chromatogram of protein-templated and blank reactions at 8 h; B) DCL3 amplification% calculated from RPA values (Equation 1); C) DCL3 normalized change of RPA (%), (Equation 2).

Table 14. Dynamic combinatorial library 3 (DCL3) amplified compounds.

Entry	Cpd	Structure	Entry	Cpd	Structure
1	H3A4		5	H3A2	
2	H3A3		6	H2A2	
3	H1A4		7	H1A2	
4	H1A3				

4.3 Conclusions

As an emerging hit- identification tool, tdDCC promises to accelerate the drug discovery process, enabling the development of potential binders against the target with potentially interesting biological activities.

In the context of anticancer drug discovery, we investigated for the first time the possibility to exploit tdDCC on RAD51.

Upon RAD51 protein stability assessment and optimization of experimental conditions, the first dynamic combinatorial library (DCL1), based on *N*-acylhydrazone formation, was designed to explore a broad range of chemical moieties. Indeed, we could observe the amplification of six *N*-acylhydrazones (NAH) in the templated-reactions (Figure 33). Once re-synthesized and tested, three of the six NAH proved to interact with RAD51 and displace BRCA2 interaction in the biochemical ELISA assay (Table 10). Noteworthy, 4-(2,4-dichlorophenoxy)butanoyl, Boc-phenylalanine, and 4,5,6,7-tetrahydro benzothiophene moieties emerged as common structural motifs from these first hits, providing encouraging premises for identification of potential hit compounds able to bind RAD51. The subsequent DCL2 and DCL3 were tailored based on results from DCL1 and provided the amplification of the other 13 novel *N*-acylhydrazones (Table 12, Table 14), which will undergo a biochemical evaluation.

5. Concluding remarks and future perspectives

The main achievement of my PhD research has been to provide a proof-of-concept that synthetic lethality can be exploited as paradigm for the development of new combination strategies in anticancer therapy. To this aim, my work focused on the design and the synthesis of small organic molecules as potential disruptors of RAD51-BRCA2 PPI, able to induce SL in combination with PARPi Olaparib to target pancreatic cancer, one of the major unmet needs in oncology.

In the context of this project, I explored the application of two distinct approaches for the identification of potential RAD51-BRCA2 PPI disruptors.

In the first part of the project, following a structure-based drug design, a virtual screening campaign has been exploited as an approach to hit identification. Two different campaigns were performed, targeting respectively, Zone I and Zone II of RAD51-BRCA2 PPI. The first virtual screening on Zone I allowed the selection of a 1,2,4-triazole-based hit compound **1**, able to inhibit BRCA2-RAD51 PPI in biochemical assay. The exploration of the chemical space of **1** led to the identification of **5**, which proved to increase the response to Olaparib in pancreatic cancer cells BxPC-3. This encouraging result supported the idea that RAD51-BRCA2 PPI could be targeted by small organic molecules, thus mimicking the condition observed in BRCA2-mutated cells. However, the mechanism of SL was not fully reproduced, since no evidences of cell death were revealed. Thus, in order to discover more potent compounds and new chemical classes of potential PPI disruptors, the second hotspot of the PPI, Zone II, has been explored as target for structure-based design of novel disruptors. The second virtual screening campaign identified the dihydroquinolone pyrazoline-based hit compound **19**, able to inhibit RAD51-BRCA2 PPI. The optimization of a general synthetic strategy led to the synthesis of a library of dihydroquinolone pyrazoline-based analogs. Compound **47** emerged as the best compound of the series, proving to inhibit HR and induce cancer cell death in combination with Olaparib in BxPC-3 cells. Indeed, compound **47** exhibited the desired biological profile and reproduced the paradigm of a fully small-molecule-induced SL in combination with the PARPi, providing the proof-of-concept that SL can be exploited to develop new anticancer drug combinations.

In the second part of the thesis, to explore an innovative process to hit identification, I joined the research group of Prof. Anna K.H. Hirsch at HIPS. During the six-month activity, I applied an approach of target directed dynamic combinatorial chemistry (tdDCC) on RAD51. To the best of my knowledge, no previous applications of this technique on RAD51 have ever been reported.

Upon design of three dynamic combinatorial libraries (DCLs), I could select three amplified *N*-acylhydrazones from the first DCL, which showed to inhibit RAD51-BRCA2 PPI in biochemical assay in micromolar range. So far these preliminary achievements appeared to support the idea that tdDCC could be employed on RAD51 as hit identification tool. Biochemical evaluation of compounds emerged from the second and the third DCL and further biological evaluation of first DCL compounds are ongoing to confirm if tdDCC could open the way to the discovery of novel classes of RAD51-BRCA2 PPI disruptors. For compounds with significant activity in the ELISA assay, we will envisage designed chemical modifications to improve chemical stability. In particular, we will evaluate if the activity is affected by the replacement of the acid-sensitive and hydrolyzable NAH linker with bioisosteres such as amide and ester linkers, or heterocycles. If the activity is preserved, we will consider exploring the chemical space of the newly identified hit compounds, leading to a hit-to-lead process. Ultimately, this would demonstrate that tdDCC could be applied as a hit identification tool for the discovery of novel chemical classes of RAD51 inhibitors.

6. Experimental section

6.1 Experimental section: Part I

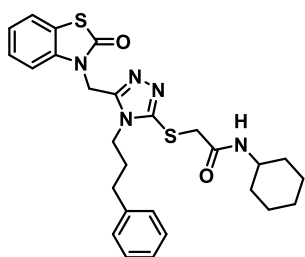
6.1.1 Material and methods

Solvents and reagents were obtained from commercial suppliers and used without further purification. If required, solvents were distilled prior to use. For simplicity, solvents and reagents are indicated as follows: acetonitrile (MeCN), , cyclohexane (Cy), dichloromethane (DCM), diethyl ether (Et₂O), petroleum ether (PE), dimethyl sulfoxide (DMSO), ethanol (EtOH), ethyl acetate (EtOAc), methanol (MeOH), triethylamine (TEA). Thin layer chromatography analyses were performed using pre-coated Supelco silica gel on TLC Al foils 0.2 mm and visualized by UV (254 nm), and/or KMnO₄ stain. Automated column chromatography purifications were conducted using a Teledyne ISCO apparatus (CombiFlash Rf) with prepacked silica gel columns of different sizes (from 4 to 120 g). Mixtures of increasing polarity of Cy and EtOAc or DCM and MeOH were used as eluents. NMR experiments were run on a Bruker Avance III 400 system (400.13 MHz for ¹H, and 100.62 MHz for ¹³C), equipped with a BBI probe and Z-gradients. Spectra were acquired at 300 K, using deuterated dimethyl sulfoxide (DMSO-*d*₆) or deuterated chloroform (Chloroform-*d*) as solvent. Chemical shifts for ¹H and ¹³C spectra were recorded in parts per million using the residual non-deuterated solvent as the internal standard (for DMSO-*d*₆: 2.50 ppm, ¹H; 39.52 ppm, ¹³C; for Chloroform-*d*: 7.26 ppm, ¹H; 77.16 ppm, ¹³C). Data are reported as follows: chemical shift (ppm), multiplicity (indicated as: bs, broad signal; s, singlet; d, doublet; t, triplet; q, quartet; m, multiplet), coupling constants (*J*) in Hertz (Hz) and integrated intensity. UPLC/MS analyses were run on a Waters ACQUITY UPLC/MS system consisting of an SQD (Single Quadrupole Detector) Mass Spectrometer equipped with an Electrospray Ionization interface and a Photodiode Array Detector. PDA range was 210-400 nm. Analyses were performed on an ACQUITY UPLC BEH C18 column (50 x 2.1 mmID, particle size 1.7 mm) with a VanGuard BEH C18 pre-column (5 x 2.1 mmID, particle size 1.7 mm). Mobile phase was 10mM NH₄OAc in H₂O at pH 5 adjusted with AcOH (A) and 10mM NH₄OAc in CH₃CN/H₂O (95:5) at pH 5 (B). Electrospray ionization in positive and negative mode was applied. Analyses were performed with a gradient: 5-95% B over 3 min; flow rate 0.5 mL/min; temperature 40°C. Compounds were named using the naming algorithm developed by CambridgeSoft Corporation and used in ChemBioDraw Ultra 16.0. All final compounds displayed >96% purity as determined by UPLC/MS analysis.

6.1.2 General procedure for synthesis of final 1,2,4-triazoles (**5–10**)

The 1,2,4-triazole-3-thiol intermediate (**16**, 1.0 equiv) and the appropriate 2-chloroacetamide (**17 a-f**, 1.1 equiv) in presence of Cs₂CO₃ (1.1 equiv) and NaI (0.05 equiv) were stirred in dry MeCN at 50°C, and reaction progress was monitored by UPLC/MS. Then water was added, and the final compounds **5–10** were purified by washing the precipitated powder or by silica gel flash chromatography (Scheme 1).

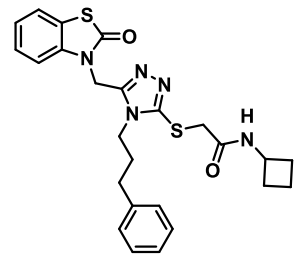
N-cyclohexyl-2-((5-((2-oxobenzo[d]thiazol-3(2H)-yl)methyl)-4-(3-phenylpropyl)-4H-1,2,4-triazol-3-yl)thio)acetamide (**5**).



3-((5-mercapto-4-(3-phenylpropyl)-4H-1,2,4-triazol-3-yl)methyl)benzo[d]thiazol-2(3H)-one **16** (80 mg, 0.21 mmol), 2-chloro-N-cyclohexylacetamide **17a** (40 mg, 0.23 mmol), Cs₂CO₃ (75 mg, 0.23 mmol), and a catalytic amount of NaI in 8 mL of dry MeCN were allowed to react for 4 h according to general procedure. The desired product precipitated from water, and washed with water, Et₂O and

dried. Precipitate was purified by column chromatography (SiO₂, A= Cyclohexane, B= EtOAc, gradient 0–100% B) to afford **5** (89 mg, 80% yield) as a white solid. ¹H NMR (400 MHz, DMSO-*d*₆) δ 7.99 (d, J = 7.7 Hz, 1H), 7.69 (dd, J = 7.8, 1.2 Hz, 1H), 7.47 (dd, J = 8.2, 1.1 Hz, 1H), 7.36 (td, J = 7.8, 1.3 Hz, 1H), 7.30-7.17 (m, 6H), 5.39 (s, 2H), 4.06 (t, 2H), 3.82 (s, 2H), 3.47-3.49 (m, 1H), 2.59 (t, 2H), 1.87-1.79 (m, 2H), 1.63-1.58 (m, 4H), 1.23-1.02 (m, 6H) ppm. ¹³C NMR (101 MHz, DMSO-*d*₆) δ 169.1, 165.53, 150.3, 150.2, 140.5, 136.5, 128.3 (2C), 128.1 (2C), 126.6, 126.0, 123.6, 122.9, 121.2, 112.1, 47.9, 43.6, 37.0, 36.9, 32.1 (2C), 32.0, 31.0, 25.1, 24.3 (2C) ppm. UPLC-MS (ESI, m/z) Rt = 2.45 min, 522 [M+ H]⁺; UPLC-MS purity (UV 215 nm) >99.5%.

N-cyclobutyl-2-((5-((2-oxobenzo[d]thiazol-3(2H)-yl)methyl)-4-(3-phenylpropyl)-4H-1,2,4-triazol-3-yl)thio)acetamide (**6**).

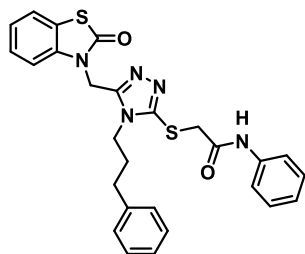


3-((5-mercapto-4-(3-phenylpropyl)-4H-1,2,4-triazol-3-yl)methyl)benzo[d]thiazol-2(3H)-one **16** (100 mg, 0.26 mmol), 2-chloro-N-cyclobutylacetamide **17b** (43 mg, 0.29 mmol), Cs₂CO₃ (95 mg, 0.29 mmol) and a catalytic amount of NaI in 5 mL of dry MeCN were allowed to react overnight according to general procedure. The desired product precipitated from water, and was washed with water, Et₂O and dried.

Precipitate was purified by column chromatography (SiO₂, A= DCM, B= MeOH, gradient 0–4%

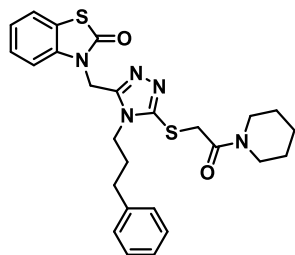
B) to afford **6** (102 mg, 79% yield) as a white solid. ^1H NMR (400 MHz, $\text{DMSO-}d_6$) δ 8.39 (d, J = 7.6 Hz, 1H), 7.69 (dd, J = 7.8, 1.2 Hz, 1H), 7.47 (dd, J = 8.1, 1.1 Hz, 1H), 7.41-7.29 (m, 1H), 7.32-7.16 (m, 6H), 5.39 (s, 2H), 4.14-4.07 (m, 1H), 4.06-4.03 (m, 2H), 3.82 (s, 2H), 2.62-2.55 (m, 2H), 2.13-1.98 (m, 2H), 1.90-1.69 (m, 4H), 1.64-1.50 (m, 2H) ppm. ^{13}C NMR (101 MHz, $\text{DMSO-}d_6$) δ 169.1, 165.3, 150.3, 140.5, 136.6, 128.4 (2C), 128.1 (2C), 126.6, 126.0, 123.6, 122.9, 121.2, 112.1, 99.5, 43.6, 43.5, 36.9, 36.7, 32.0, 31.0, 30.0 (2C), 14.6 ppm. UPLC-MS (ESI, m/z) R_t = 2.25 min, 494 $[\text{M} + \text{H}]^+$; UPLCMS purity (UV 215 nm) >99.5%.

2-((5-((2-oxobenzo[d]thiazol-3(2H)-yl)methyl)-4-(3-phenylpropyl)-4H-1,2,4-triazol-3-yl)thio)-N-phenylacetamide (7)



3-((5-mercapto-4-(3-phenylpropyl)-4H-1,2,4-triazol-3-yl)methyl)benzo[d]thiazol-2(3H)-one **16** (80 mg, 0.21 mmol), 2-chloro-N-phenylacetamide **17c** (39 mg, 0.23 mmol), Cs_2CO_3 (112 mg, 0.23 mmol) and a catalytic amount of NaI in 4 mL of dry MeCN were allowed to react for 2 h according to general procedure. The desired product precipitated from water, and was washed with water, Et_2O and dried overnight under vacuum at 60 $^\circ\text{C}$ to give **7** (93 mg, 85 %) as a white powder. ^1H NMR (400 MHz, $\text{DMSO-}d_6$) δ 10.25 (s, 1H), 7.69 (dd, J = 7.8, 1.2 Hz, 1H), 7.51 (d, J = 7.7 Hz, 2H), 7.45 (d, J = 7.9 Hz, 1H), 7.36 – 7.17 (m, 9H), 7.05 (t, J = 7.4 Hz, 1H), 5.39 (s, 2H), 4.11 (s, 2H), 4.08 (t, J = 7.9 Hz, 2H), 2.60 (t, 2H, J = 7.9 Hz), 1.89-1.82 (m, 2H) ppm; ^{13}C NMR (101 MHz, $\text{DMSO-}d_6$) δ 169.1, 165.4, 150.4, 150.2, 140.4, 138.7, 136.5, 128.7 (2C), 128.4 (2C), 128.1 (2C), 126.6, 126.0, 123.6, 123.5, 122.9, 121.2, 119.1 (2C), 112.1, 43.6, 37.5, 36.9, 32.0, 31.0 ppm. UPLC-MS (ESI, m/z) R_t = 2.45 min, 516 $[\text{M} + \text{H}]^+$; UPLC-MS purity (UV 215 nm) 99 %

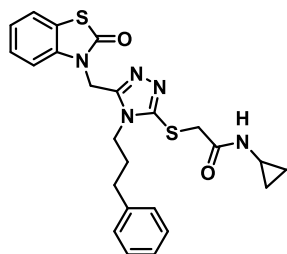
3-((5-((2-oxo-2-(piperidin-1-yl)ethyl)thio)-4-(3-phenylpropyl)-4H-1,2,4-triazol-3-yl)methyl)benzo[d]thiazol-2(3H)-one (8)



3-((5-mercapto-4-(3-phenylpropyl)-4H-1,2,4-triazol-3-yl)methyl)benzo[d]thiazol-2(3H)-one **16** (122 mg, 0.32 mmol), 2-chloro-1-(piperidin-1-yl)ethan-1-one **17d** (58 mg, 0.36 mmol), Cs_2CO_3 (115 mg, 0.36 mmol) and a catalytic amount of NaI in 5 mL of dry MeCN were allowed to react for 3 h according to general procedure. The reaction was cooled down, water was added and the aqueous phase was extracted with EtOAc (3 x 10 mL) and DCM (3 x 10 mL). The collected organic phases were washed with brine, dried over MgSO_4 , filtered and concentrated in vacuum. The crude was purified by flash

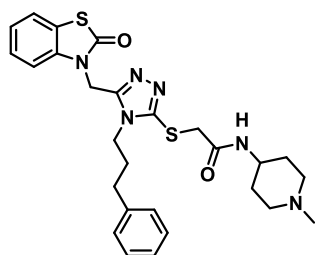
chromatography (SiO₂, A= Cyclohexane, B= EtOAc, gradient 0–100% B) to afford **8** (115 mg, 71 % yield) as a white solid. ¹H NMR (400 MHz, DMSO-*d*₆) δ 7.70 (dd, J = 7.8, 1.2 Hz, 1H), 7.48 (dd, J = 8.2, 1.1 Hz, 1H), 7.36 (td, J = 7.8, 1.3 Hz, 1H), 7.31 – 7.14 (m, 6H), 5.40 (s, 2H), 4.23 (s, 2H), 4.12 – 3.94 (m, 2H), 3.38-3.34 (m, 4H), 2.62 – 2.58 (m, 2H), 1.86 – 1.78 (m, 2H), 1.53 – 1.36 (m, 6H) ppm. ¹³C NMR (101 MHz, DMSO-*d*₆) δ 169.1, 164.7, 150.3, 150.3, 140.5, 136.5, 128.4 (2C), 128.1 (2C), 126.6, 126.0, 123.6, 123.0, 121.2, 112.2, 46.4, 43.6, 42.4, 37.0, 36.9, 32.0, 31.1, 25.8, 25.1, 23.7 ppm. UPLC-MS (ESI, m/z) Rt = 2.34 min, 508 [M+H]⁺; UPLC-MS purity (UV 215 nm): > 99.5 %.

N-cyclopropyl-2-((5-((2-oxobenzo[d]thiazol-3(2H)-yl)methyl)-4-(3-phenylpropyl)-4H-1,2,4-triazol-3-yl)thio)acetamide (9).



3-((5-mercapto-4-(3-phenylpropyl)-4H-1,2,4-triazol-3-yl)methyl)benzo[d]thiazol-2(3H)-one **16** (100 mg, 0.26 mmol), commercially available 2-chloro-N-cyclopropylacetamide **17e** (39 mg, 0.29 mmol), Cs₂CO₃ (95 mg, 0.29 mmol) and a catalytic amount of NaI in 5mL of dry MeCN were allowed to react overnight according to general procedure. The desired product precipitated from water, and was washed with water, Et₂O and dried overnight under vacuum at 60°C to give **9** (120 mg, quantitative yield) as a white powder. ¹H NMR (400 MHz, DMSO-*d*₆) δ 8.23 (d, J = 4.1 Hz, 1H), 7.70 (dd, J = 7.8, 1.2 Hz, 1H), 7.48-7.46 (m, 2H), 7.36 (td, J = 7.8, 1.3 Hz, 1H), 7.30-7.17 (m, 7H), 5.39 (s, 2H), 4.05 (t, J = 7.9 Hz, 2H), 3.81 (s, 2H), 2.61-2.53 (m, 3H), 1.87-1.79 (m, 2H), 0.59-0.54 (m, 2H), 0.34-0.30 (m, 2H) ppm. ¹³C NMR (101 MHz, DMSO-*d*₆) δ 169.1, 167.6, 150.3, 150.2, 140.5, 136.5, 128.4 (2C), 128.1 (2C), 126.6, 126.0, 123.6, 122.9, 121.2, 112.1, 43.6, 36.9, 36.5, 32.0, 31.0, 22.5, 5.5 (2C) ppm. UPLC-MS (ESI, m/z) Rt = 2.15 min, 480 [M + H]⁺; UPLC-MS purity (UV 215 nm) >99.5%.

N-(1-methylpiperidin-4-yl)-2-((5-((2-oxobenzo[d]thiazol-3(2H)-yl)methyl)-4-(3-phenylpropyl)-4H-1,2,4-triazol-3-yl)thio)acetamide (10)

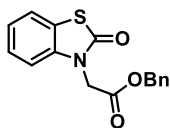


3-((5-mercapto-4-(3-phenylpropyl)-4H-1,2,4-triazol-3-yl)methyl)benzo[d]thiazol-2(3H)-one **16** (120 mg, 0.31 mmol), commercially available 2-chloro-N-(1-methylpiperidin-4-yl)acetamide **17f** (66 mg, 0.35 mmol), Cs₂CO₃ (112 mg, 0.35 mmol) and a catalytic amount of NaI in 5 mL of dry MeCN were allowed to react for 4 h according to general procedure. The reaction was cooled down, water was added and the aqueous phase was extracted with EtOAc (3 x 10 mL). The collected organic phases were washed with brine, dried over MgSO₄, filtered and concentrated in vacuum. The crude was

purified by flash chromatography (SiO₂, A= DCM, B= MeOH, gradient 0–10% B) to afford **10** (90 mg, 54 % yield) as a white solid. ¹H NMR (401 MHz, DMSO-*d*₆) δ 8.10 (d, J = 7.5 Hz, 1H), 7.70 (d, J = 7.4 Hz, 1H), 7.47 (d, J = 8.1 Hz, 1H), 7.36 (t, J = 7.8 Hz, 1H), 7.32 – 7.21 (m, 3H), 7.21 – 7.15 (m, 3H), 5.39 (s, 2H), 4.06 (t, J = 7.9 Hz, 2H), 3.83 (s, 2H), 3.50 – 3.38 (m, 1H), 2.69 – 2.61 (m, 2H), 2.61 – 2.55 (m, 2H), 2.14 (s, 3H), 2.00 – 1.87 (m, 2H), 1.87 – 1.75 (m, 2H), 1.64 – 1.53 (m, 2H), 1.38 – 1.24 (m, 2H) ppm. ¹³C NMR (101 MHz, DMSO-*d*₆) δ 169.1, 165.8, 150.3, 150.2, 140.5, 136.6, 128.4 (2C), 128.1 (2C), 126.7, 126.1, 123.6, 123.0, 121.2, 112.1, 53.7, 45.8, 45.7, 43.6, 37.0, 36.9, 32.0 (2C), 31.1 (2C), 31.0 ppm. UPLC-MS (ESI, m/z) Rt = 3.58 min, 537 [M+H]⁺; UPLC-MS purity (UV 215 nm): > 99.5 %.

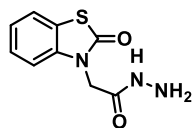
6.1.3 Synthesis of intermediates **13**, **14**, **16**

Benzyl 2-(2-oxobenzo[d]thiazol-3(2H)-yl) acetate (**13**)



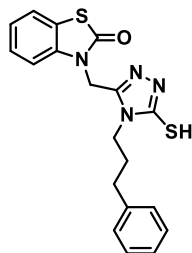
A mixture of benzothiazolone **11** (2.00 g, 13.23 mmol), K₂CO₃ (1.92 g, 13.89 mmol), a catalytic amount of NaI and 20 mL of acetone was stirred at room temperature. Benzyl bromoacetate **12** (2.3 mL, 14.55 mmol) was added dropwise to the mixture which was then refluxed for 2 h. The reaction mixture was next cooled and poured into ice water (300 mL). The yellow granulose precipitate formed was filtered and recrystallized from ethanol (80 mL) to give **13** (3.74 g, 94% yield) as white needles. ¹H NMR (400 MHz, Chloroform-*d*) δ 7.42 – 7.27 (m, 6H), 7.25 (t, J = 7.8 Hz, 1H), 7.14 (t, J = 7.5 Hz, 1H), 6.87 (d, J = 8.1 Hz, 1H), 5.18 (s, 2H), 4.69 (s, 2H); ¹³C NMR (101 MHz, Chloroform -*d*) δ 170.1, 166.9, 136.6, 135.1, 128.7 (2C), 128.6, 128.3 (2C), 126.6, 123.7, 122.8, 122.2, 110.5, 67.5, 43.5; UPLC-MS (ESI, m/z) Rt = 2.55 min, 300 [M+H]⁺.

2-(2-oxobenzo[d]thiazol-3(2H)-yl) acetohydrazide (**14**)



Compound **13** (2 g, 6.34 mmol, 1.0 equiv) was dissolved in 15 mL of EtOH and hydrazine hydrate (7.5 mL, 154 mmol, 23 equiv) was added. The mixture was refluxed for 90 min, cooled down and after 5 min stirred was stopped, and the reaction flask is placed in an ice bath for 20 min then filtered, washed with EtOH and dried under vacuum to give **14** (1.37 g, 49% yield) as a white powder. ¹H NMR (400 MHz, DMSO-*d*₆) δ 9.46 (s, 1H), 7.65 (d, J = 7.4 Hz, 1H), 7.42 – 7.27 (m, 1H), 7.26 – 7.13 (m, 2H), 4.56 (s, 2H), 4.32 (s, 2H); ¹³C NMR (101 MHz, DMSO-*d*₆) δ 169.6, 165.8, 137.7, 126.9, 123.7, 123.2, 121.7, 111.8, 43.8; UPLC-MS (ESI, m/z) Rt = 1.30 min, 224 [M+H]⁺.

3-((5-mercapto-4-(3-phenylpropyl)-4H-1,2,4-triazol-3-yl)methyl)benzo[d]thiazol-2(3H)-one (16)

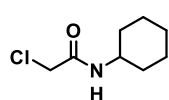


A mixture of hydrazide **14** (100 mg, 0.45 mmol) and commercially available isothiocyanate **15** (78 μ L, 0.47 mmol) in 5 mL of ethanol containing TEA (130 μ L, 0.95 mmol) were refluxed overnight. The reaction was cooled, the solvent was evaporated, and dried under vacuum for few hours to give **16** (195 mg, crude product) that was used in the next step without further purification. ^1H NMR (400 MHz, DMSO- d_6) δ 13.73 (s, 1H), 7.76 – 7.66 (m, 1H), 7.43 – 7.33 (m, 2H), 7.33 – 7.16 (m, 6H), 5.36 (s, 2H), 4.09 – 4.01 (m, 2H), 2.68 – 2.55 (m, 2H), 1.95 – 1.84 (m, 2H); ^{13}C NMR (101 MHz, DMSO- d_6) δ 169.1, 167.3, 147.0, 140.7, 136.4, 128.3 (2C), 128.1 (2C), 126.7, 125.9, 123.7, 123.1, 121.1, 111.8, 43.3, 37.2, 32.1, 29.1; UPLC-MS (ESI, m/z) R_t = 2.32 min, 383 [M+H] $^+$.

6.1.4 General procedure for synthesis of chloroacetamides (**17a–d**)

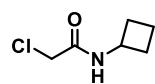
To the appropriate substituted amines (**18a–d**, 1.0 equiv) in DCM was added chloroacetyl chloride (1.1 equiv) followed by the addition of TEA (2.8 equiv) at 0-10 $^\circ\text{C}$. The reaction was continued at the same temperature for 1 h. Then, the reaction mixture was washed with saturated NaHCO_3 solution, HCl 2N, and brine solution. The excess of organic solvent was removed under reduced pressure and the crude compounds were purified by flash chromatography, eluting with Cyclohexane/EtOAc 50:50, otherwise noted (Scheme 2).

2-chloro-N-cyclohexylacetamide (**17a**).



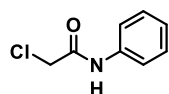
Cyclohexylamine **18a** (911 mL, 7.97 mmol), chloroacetyl chloride (705 mL, 8.85 mmol), TEA (3.08 mL, 22.14 mmol) in DCM (20 mL) were allowed to react, and clean compound was purified according to the general procedure, giving **17a** (995 mg, 71% yield) as white solid. ^1H NMR (400 MHz, Chloroform- d) δ 6.45 (s, 1H), 4.04 (s, 2H), 3.89e3.72 (m, 1H), 1.94 (dq, J = 12.0, 3.7 Hz, 2H), 1.74 (dp, J = 10.5, 3.5, 2.9 Hz, 2H), 1.64 (dq, J = 12.7, 3.5 Hz, 1H), 1.48-1.31 (m, 2H), 1.21 (dddd, J = 15.4, 11.4, 7.2, 3.4 Hz, 3H). UPLC-MS (ESI, m/z) R_t = 1.82 min, 176, 178 [M+H] $^+$.

2-chloro-N-cyclobutylacetamide (17b).



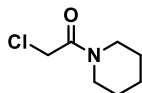
Cyclobutylamine **18b** (240 mL, 2.81 mmol), chloroacetyl chloride (248 mL, 3.12 mmol), TEA (1.09 mL, 7.8 mmol) in DCM (6 mL) were allowed to react according to the general procedure. Clean compound was purified over silica gel flash chromatography (SiO₂, A= Cyclohexane, B= EtOAc, gradient 0–30% B) to **17b** (380 mg, 83% yield) as white solid. ¹H NMR (400 MHz, DMSO-*d*₆) δ 8.43 (s, 1H), 4.28-4.09 (m, 1H), 3.98 (s, 2H), 2.21-2.08 (m, 2H), 2.00-1.80 (m, 2H), 1.70-1.59 (m, 2H). UPLC-MS (ESI, m/z) Rt= 1.23 min, 148 [M+H]⁺.

2-chloro-N-phenylacetamide (17c)



Aniline **18c** (726 μL, 7.97 mmol), chloroacetyl chloride (705 μL, 8.85 mmol), TEA (3.08 mL, 22.14 mmol) in DCM (20 mL) were allowed to react and clean compound was purified according the general procedure giving **17c** (986mg, 70 % yield) as an off-white solid. ¹H NMR (400 MHz, Chloroform -*d*) δ 8.27 (s, 1H), 7.57 (dt, J = 8.7, 1.7 Hz, 2H), 7.41 – 7.36 (m, 2H), 7.20 (tt, J = 7.0, 1.1 Hz, 1H), 4.21 (s, 2H) ppm. UPLC-MS (ESI, m/z) Rt = 1.67 min, 170, 172 [M+H]⁺.

2-chloro-1-(piperidin-1-yl) ethan-1-one (17d)



Piperidine **18d** (787 μL, 7.97 mmol), chloroacetyl chloride (705 μL, 8.85 mmol), TEA (3.08 mL, 22.14 mmol) in DCM (20 mL) were allowed to react and clean compound was purified according the general procedure giving **17d** (1.28 g, quantitative yield) as an orange oil. ¹H NMR (400 MHz, Chloroform -*d*) δ 3.98 (s, 2H), 3.48 – 3.41 (m, 2H), 3.38 – 3.31 (m, 2H), 1.62 – 1.50 (m, 4H), 1.50 – 1.41 (m, 2H) ppm. UPLC-MS (ESI, m/z) Rt = 1.54 min, 162, 164 [M+H]⁺.

6.2.1 General Procedure A for the synthesis of acroyl intermediates (**91b–113b**, **133**, **139**)

In a round-bottomed flask, the appropriate quinolin-2(1H)-one (**71a–72a**, **132**, **138**, 1.00 equiv) and potassium hydroxide (25.00 equiv) were stirred in EtOH/H₂O (4:3 v/v, 0.05 M) at 0 °C for 45 min prior to the addition of an appropriately substituted aryl aldehyde (**73–90**, 1.00 equiv). The reaction mixture was stirred overnight as it gradually reached room temperature. The reaction was quenched by slow addition of acetic acid (25.00 equiv). The crude was extracted with DCM/H₂O (3 × 50 mL), the organic layer was then dried over Na₂SO₄, and the solvent was removed under reduced pressure. The desired compound was obtained after purification over silica gel unless otherwise noted (Scheme 3, Scheme 11, and Scheme 12).

6.2.2 General Procedure B for synthesis of pyrazoline intermediates (**91c–113c**, **134**, **140**)

In a microwaveable vessel, the appropriate quinolin-2(1H)-one acroyl intermediate (**91b–113b**, **133**, **139**, 1.00 equiv) was dissolved in EtOH absolute (0.2 M), and hydrazine monohydrate (2.00 equiv) was added. The mixture was microwaved with stirring for 45 min at 110 °C (200 W). The EtOH was removed under reduced pressure. Crude was purified over silica gel, unless otherwise noted, to afford desired compounds (Scheme 3, Scheme 11, and Scheme 12).

6.2.3 General procedures C₁ for final dihydroquinolone pyrazolines (**19**, **28–44**, **62–66**).

In a microwaveable vessel, the appropriate pyrazol-3-ylquinolin-2(1H)-one intermediate (**91c–113c**, 1.00 equiv) was dissolved in anhydrous THF (0.5 M) in presence of MS 4Å. The succinic anhydride **114** (2.00 equiv) was added. The solution was microwaved (200 W) with stirring for 45 min at the appropriate temperature. The THF was removed under reduced pressure, and the organic layers were dissolved in DCM, washed with HCl_{aq} pH 2 (3 × 30 mL), and dried over Na₂SO₄. The solvent was removed under reduced pressure, and the crude was purified over silica gel (Scheme 4).

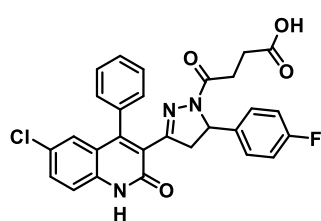
6.2.4 General procedures C₂ for final dihydroquinolone pyrazolines (**22**, **45–47**).

In a round-bottomed flask, propionic acid **115** (1.80 equiv), HOBt (1.80 equiv), and EDCI (1.80 equiv) were stirred in DCM (0.50 M) at room temperature for 1 h. Then a solution of the pyrazol-3-ylquinolin-2(1H)-one intermediate **91c–94c** (1.00 equiv) in DCM (0.50 M) was added. The reaction was stirred at room temperature for 3 h. The organic layer was washed with NaHCO₃ aq 1 M (1 × 50 mL), citric acid 10% (1 × 50 mL), and H₂O (1 × 50 mL), dried over Na₂SO₄, and the solvent was removed under reduced pressure. The desired compound was obtained after purification over silica gel unless otherwise noted (Scheme 4).

6.2.5 General procedures C₃ for final dihydroquinolone pyrazolines (**20**, **21**, **23**, **48–61**, **67**, **68**)

In a microwaveable vessel, the appropriate intermediate (**91c–96c**, **98c–116c**, **117**, **122**, **134**, **140**, 1.00 equiv) was dissolved in anhydrous THF (0.5 M). The acetic anhydride **116** (2.00 equiv) was added. The solution was microwaved (200 W) with stirring for 45 min at the appropriate temperature. The THF was removed under reduced pressure, and the organic layers were dissolved in DCM, washed with H₂O (3 × 30 mL), and dried over Na₂SO₄. The solvent was removed under reduced pressure, and the crude was purified over silica gel (Scheme 4, Scheme 5, Scheme 6, Scheme 11, and Scheme 12).

4-(3-(6-Chloro-2-oxo-4-phenyl-1,2-dihydroquinolin-3-yl)-5-(4-fluorophenyl)-4,5-dihydro-1H-pyrazol-1-yl)-4-oxobutanoic Acid (**19**).

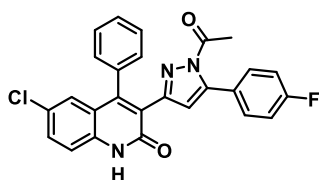


6-Chloro-3-(5-(4-fluorophenyl)-4,5-dihydro-1H-pyrazol-3-yl)-4-phenylquinolin-2(1H)-one **91c** (270 mg, 0.65 mmol) and succinic anhydride **114** (130 mg, 1.30 mmol) were microwaved (120 °C, 200 W) according to general procedure C₁. The crude was purified by flash column chromatography (SiO₂ gold 24 g, A= DCM, B= EtOH, gradient 0–50% B) to afford the desired **19** (208 mg, 62% yield). ¹H NMR (400 MHz, DMSO-*d*₆) δ 12.38 (s, 1H), 12.02 (s, 1H), 7.64 (dd, J = 8.8, 2.4 Hz, 1H), 7.60–7.37 (m, 5H), 7.28 (dt, J = 6.8, 2.0 Hz, 1H), 7.04 (t, J = 8.9 Hz, 2H), 6.94 (d, J = 2.3 Hz, 1H), 6.88–6.76 (m, 2H), 5.32 (dd, J = 12.0, 4.5 Hz, 1H), 3.73 (dd, J = 18.5, 12.0 Hz, 1H), 2.79 (dd, J = 18.4, 4.5 Hz, 1H), 2.48–2.40

(m, 2H), 2.32–2.26 (m, 2H). ^{13}C NMR (101 MHz, $\text{DMSO-}d_6$) δ 173.95, 169.09, 160.56, 152.85, 150.38, 137.78, 135.00, 131.68, 129.88, 128.97, 128.88, 128.81, 127.99, 127.90, 126.57, 126.51, 125.07, 121.14, 118.09, 115.67, 115.46, 95.62, 58.69, 45.66, 29.04, 28.69. In agreement with that previously reported by Acker *et al.*¹⁷⁰ tR = 2.04 min. ESI-MS for $\text{C}_{28}\text{H}_{21}\text{ClFN}_3\text{O}_4$: calculated 517.1, found m/z 518.4, 520.4 $[\text{M} + \text{H}]^+$; 516.4, 518.4 $[\text{M} - \text{H}]^-$. UPLC-MS purity (UV at 215 nm) 98%.

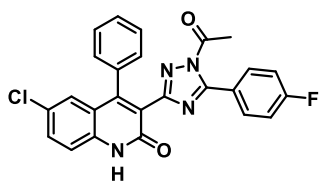
3-(1-acetyl-5-(4-fluorophenyl)-1H-pyrazol-3-yl)-6-chloro-4-phenylquinolin-2(1H)-one (20)

(Scheme 5)



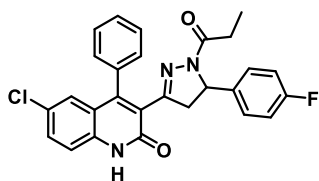
Compound **20** was synthesized via general procedure C₃ using **117** (85 mg, 0.20 mmol) and acetic anhydride **116** (20.0 μL , 0.20 mmol). Purification was performed by direct phase flash chromatography (SiO_2 , A= DCM, B= EtOAc, gradient 0–10% B) to afford **20** (55 mg, yield 16%). ^1H NMR (400 MHz, $\text{DMSO-}d_6$) δ 12.28 (s, 1H), 7.81 (dd, J = 8.5, 5.6 Hz, 2H), 7.64 (dd, J = 8.8, 2.1 Hz, 1H), 7.46 (d, J = 8.8 Hz, 3H), 7.35 (s, 2H), 7.27 (t, J = 8.8 Hz, 2H), 6.94 (d, J = 2.1 Hz, 2H), 6.72 (s, 1H), 2.66 (s, 3H). ^{13}C NMR (101 MHz, $\text{DMSO-}d_6$) δ 170.44, 162.02, 160.22, 152.29, 147.71, 140.27, 137.94, 135.33, 131.47, 129.17, 128.65, 128.57, 128.26, 126.61, 126.31, 125.84, 121.10, 118.18, 116.60, 116.39, 111.09, 23.20. $\text{C}_{26}\text{H}_{17}\text{ClFN}_3\text{O}_2$: calculated 457.10, found m/z 458.36 $[\text{M} + \text{H}]^+$.

3-(1-acetyl-5-(4-fluorophenyl)-1H-1,2,4-triazol-3-yl)-6-chloro-4-phenylquinolin-2(1H)-one (21) (Scheme 6)



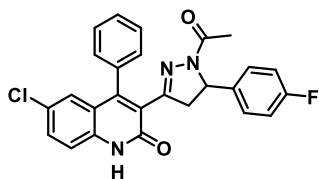
Compound **21** was synthesized via general procedure C₃ using **122** (90 mg, 0.22 mmol) and acetic anhydride **116** (125.0 μL , 1.32 mmol). Purification was performed by precipitation from EtOAc and filtration to afford **21** (50 mg, yield 50%). ^1H NMR (400 MHz, $\text{DMSO-}d_6$) δ 12.50 (s, 1H), 8.01 – 7.90 (m, 2H), 7.72 (dd, J = 8.8, 2.4 Hz, 1H), 7.53 (t, J = 11.2 Hz, 1H), 7.47 – 7.36 (m, 3H), 7.36 – 7.29 (m, 2H), 7.23 (s, 1H), 7.06 (d, J = 2.3 Hz, 1H), 2.71 (s, 3H). ^{13}C NMR (101 MHz, $\text{DMSO-}d_6$) δ 168.54, 164.61, 162.15, 159.94, 159.07, 152.06, 149.34, 137.79, 133.59, 131.70, 128.96, 128.72, 128.64, 128.50, 126.36, 125.87, 125.50, 125.47, 123.50, 119.91, 117.94, 116.19, 115.97, 39.52, 22.96. $\text{C}_{25}\text{H}_{16}\text{ClFN}_4\text{O}_2$: calculated 458.09, found m/z 459.36 $[\text{M} + \text{H}]^+$.

6-Chloro-3-(5-(4-fluorophenyl)-1-propionyl-4,5-dihydro-1H-pyrazol-3-yl)-4-phenylquinolin-2(1H)-one (22).



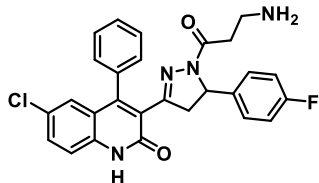
Compound **22** was synthesized via general procedure C₂ using **91c** (250 mg, 0.60 mmol) and propionic acid **115** (80.8 μ L, 1.08 mmol). Purification was performed by direct phase flash chromatography (SiO₂, A= DCM, B= MeOH, gradient 0–1% B) to afford **22** (60 mg, yield 21%). ¹H NMR (400 MHz, DMSO-*d*₆) δ 12.38 (s, 1H), 7.64 (dd, J = 2.0, 8.0 Hz, 1H), 7.58–7.50 (m, 3H), 7.45 (d, J = 8.8 Hz, 1H), 7.41–7.39 (m, 1H), 7.28 (d, J = 5.6 Hz, 1H), 7.06 (t, J = 8.8 Hz, 2H), 6.93 (d, J = 2.0 Hz, 1H), 6.84 (dd, J = 4.0, 8.0, Hz, 2H), 5.32 (dd, J = 8.0, 12.0 Hz, 1H), 3.73 (dd, J = 12.0, 16.0 Hz, 1H), 2.81 (dd, J = 4.0, 16.0 Hz, 1H), 2.30–2.16 (m, 2H), 0.83 (t, J = 7.6 Hz, 3H). ¹³C NMR (101 MHz, DMSO- *d*₆) δ 206.89, 170.93, 162.79, 160.57, 160.38, 152.63, 150.30, 139.00, 138.98, 137.75, 135.12, 131.63, 129.79, 128.97, 128.95, 128.86, 128.80, 127.96, 127.88, 126.53, 126.47, 125.10, 121.11, 118.07, 115.67, 115.46, 58.54, 45.54, 29.44, 9.27. ESI-MS for C₂₇H₂₁ClFN₃O₂: calculated 473.1, found m/z 474.2, 476.2 [M + H]⁺; 472.3, 474.3 [M – H][–]. UPLC–MS purity (UV at 215 nm) 99%.

3-(1-Acetyl-5-(4-fluorophenyl)-4,5-dihydro-1H-pyrazol-3-yl)-6-chloro-4-phenylquinolin-2(1H)-one (23).



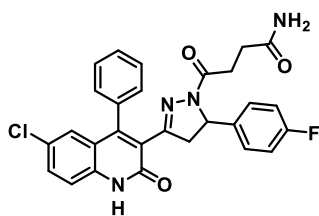
6-Chloro-3-(5-(4-fluorophenyl)-4,5-dihydro-1H-pyrazol-3-yl)-4-phenylquinolin-2(1H)-one **91c** (200 mg, 0.48 mmol) and acetic anhydride **116** (91 μ L, 0.96 mmol) were microwaved (120 °C, 200 W) according to general procedure C₃. The crude was purified by direct phase flash column chromatography (SiO₂, A= DCM, B= MeOH, gradient 0–20% B) to afford the desired **23** (207 mg, yield 47%). ¹H NMR (400 MHz, DMSO-*d*₆) δ 12.38 (s, 1H), 7.64 (dd, J = 8.8, 2.4 Hz, 1H), 7.61–7.50 (m, 3H), 7.46 (d, J = 8.8 Hz, 1H), 7.41 (dt, J = 6.6, 1.9 Hz, 1H), 7.29 (dt, J = 6.4, 1.9 Hz, 1H), 7.06 (t, J = 8.9 Hz, 2H), 6.94 (d, J = 2.3 Hz, 1H), 6.84 (dd, J = 8.6, 5.6 Hz, 2H), 5.32 (dd, J = 12.0, 4.5 Hz, 1H), 3.73 (dd, J = 18.4, 12.1 Hz, 1H), 2.84 (dd, J = 18.5, 4.5 Hz, 1H), 1.88 (s, 3H). ¹³C NMR (101 MHz, DMSO- *d*₆) δ 167.53, 162.80, 160.57, 160.39, 152.67, 150.35, 138.87, 138.84, 137.79, 135.12, 131.64, 129.84, 129.04, 128.96, 128.80, 128.76, 128.00, 127.93, 126.53, 126.49, 125.02, 121.11, 118.09, 115.67, 115.45, 58.49, 45.71, 21.85. tR = 2.38 min. ESI-MS for C₂₆H₁₉ClFN₃O₂: calculated 459.1, found m/z 460.1, 462.1 [M + H]⁺; 458.1, 460.1 [M – H][–]. UPLC–MS purity (UV at 215 nm) >99.5%.

3-(1-(3-Aminopropanoyl)-5-(4-fluorophenyl)-4,5-dihydro-1H-pyrazol-3-yl)-6-chloro-4-phenylquinolin-2(1H)-one (24) (Scheme 7).



In round-bottom flask **124** (200 mg, 0.34 mmol) was treated with 4 M HCl in dioxane (4.0 mL) and stirred at rt for 15 min. The solvent was removed under reduced pressure. In a round-bottom flask the solid residue (110 mg, 0.21 mmol) was treated with NaOH 0.5 M (420 μ L) in EtOAc (5.0 mL) stirring at rt for 30 min. The mixture was then diluted with further EtOAc and washed twice with H₂O. The organic layer was dried over Na₂SO₄, filtered, and evaporated to dryness. Purification was performed by direct phase flash chromatography (SiO₂, A= DCM, B= MeOH, gradient 0–10% B, 0–0.1% NH₄OH) to afford the desired **24** (50 mg, yield 50%). ¹H NMR (400 MHz, DMSO-*d*₆) δ 7.63 (dd, *J* = 12.0, 4.0 Hz, 1H), 7.57–7.50 (m, 3H), 7.54 (d, *J* = 4.8 Hz, 1H), 7.42–7.40 (m, 1H), 7.26 (d, *J* = 7.2 Hz, 1H), 7.03 (t, *J* = 8.8 Hz, 2H), 6.92 (d, *J* = 2.0 Hz, 1H), 6.81 (dd, *J* = 2.0, 8.0 Hz, 2H), 5.32 (dd, *J* = 2.0, 12.0 Hz, 1H), 3.72 (dd, *J* = 12.0, 20.0 Hz, 1H), 2.76 (dd, *J* = 4.0, 16.0 Hz, 1H), 2.57 (t, *J* = 6.6 Hz, 2H), 2.42–2.28 (m, 2H). ¹³C NMR (101 MHz, DMSO-*d*₆) δ 169.42, 162.77, 160.56, 160.36, 152.76, 150.29, 138.96, 138.93, 137.78, 135.02, 131.63, 129.86, 128.99, 128.92, 128.89, 128.80, 127.95, 127.86, 126.52, 126.45, 125.09, 121.11, 118.10, 115.66, 115.45, 110.00, 58.53, 45.61, 38.06, 38.04. ESI-MS for C₂₇H₂₂ClFN₄O₂: calculated 488.1, found *m/z* 489.4, 491.4 [M + H]⁺, 487.3, 489.4 [M – H][–]. UPLC–MS purity (UV at 215 nm) >99.5%.

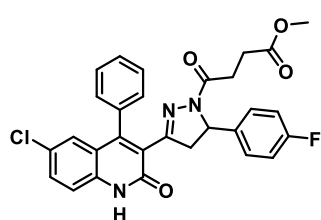
4-(3-(6-Chloro-2-oxo-4-phenyl-1,2-dihydroquinolin-3-yl)-5-(4-fluorophenyl)-4,5-dihydro-1H-pyrazol-1-yl)-4-oxobutanamide (25) (Scheme 8).



In a round bottomed flask 4-(3-(6-chloro-2-oxo-4-phenyl-1,2-dihydroquinolin-3-yl)-5-(4-fluorophenyl)-4,5-dihydro-1H-pyrazol-1-yl)-4-oxobutanamide **19** (258 mg, 0.50 mmol) was dissolved with 3.2 mL of anhydrous DCM, then HATU (285 mg, 0.75 mmol), EDC (144 mg, 0.75 mmol), and 1.8 mL of anhydrous DMF were added. The mixture was stirred at rt for 10 min. Ammonium chloride (144 mg 2.50 mmol) and soon after DIPEA (348 μ L, 2.00 mmol) were added. The reaction mixture was thus stirred at rt for 26 h. Purification was performed by direct phase chromatography (SiO₂ gold 24 g, A= DCM, B= EtOH, gradient 2.5–50% B) to afford the desired **25** (120 mg, yield 46%). ¹H NMR (400 MHz, DMSO-*d*₆) δ 12.38 (s, 1H), 7.64 (dd, *J* = 8.8, 2.4 Hz, 1H), 7.60–7.38 (m, 5H), 7.28 (d, *J* = 7.4 Hz, 1H), 7.19 (s, 1H), 7.04 (dd, *J* = 9.9, 7.7 Hz, 2H), 6.93 (d, *J* = 2.3 Hz, 1H), 6.84–6.78 (m, 2H), 6.68 (s, 1H), 5.31 (dd, *J* = 12.0, 4.5 Hz, 1H), 3.71 (dd, *J* = 18.5, 12.1 Hz, 1H), 2.76 (dd, *J* = 18.4,

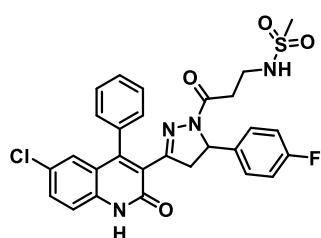
4.5 Hz, 1H), 2.54–2.45 (m, 2H), 2.15 (t, $J = 7.4$ Hz, 2H). ^{13}C NMR (101 MHz, $\text{DMSO-}d_6$) δ 173.51, 169.56, 160.65, 160.38, 152.73, 150.28, 138.90, 137.94, 135.00, 131.61, 129.94, 129.94, 129.02, 128.99, 128.87, 128.79, 127.99, 127.90, 126.48, 125.10, 121.14, 118.19, 115.66, 115.45, 58.66, 45.64, 29.82, 29.38. $t_R = 2.09$ min. ESI-MS for $\text{C}_{28}\text{H}_{22}\text{ClFN}_4\text{O}_3$: calculated 516.1, found m/z 517.4, 519.3 $[\text{M} + \text{H}]^+$; 515.4, 517.4 $[\text{M} - \text{H}]^-$. UPLC-MS purity (UV at 215 nm) 99%.

Methyl 4-(3-(6-Chloro-2-oxo-4-phenyl-1,2-dihydroquinolin-3-yl)-5-(4-fluorophenyl)-4,5-dihydro-1H-pyrazol-1-yl)-4-oxobutanoate (26) (Scheme 9).



In a round-bottomed flask, commercially available 4-methoxy-4-oxobutanoic acid **125** (153 mg, 1.16 mmol), 6-chloro-3-(5-(4-fluorophenyl)-4,5-dihydro-1H-pyrazol-3-yl)-4-phenylquinolin-2(1H)-one **91c** (486 mg, 1.16 mmol), HOBT (173 mg, 1.28 mmol) were dissolved in DCM. Then TEA (355.8 μL , 2.55 mmol) was added, followed by EDCI (245 mg, 1.28 mmol) suspended in DCM. The mixture was stirred overnight at rt. The solvent was removed under vacuum, the residue was dissolved in ethyl acetate and washed with H_2O , NaHCO_3 sat. solution and 5% citric acid. The organic phase was dried over Na_2SO_4 and evaporated to dryness. The title compound was obtained after purification by direct phase flash column chromatography (SiO_2 , A= DCM, B= EtOAc, gradient 0–30% B) to afford the desired **26** (256 mg, yield 42%). ^1H NMR (400 MHz, $\text{DMSO-}d_6$) δ 12.36 (s, 1H), 7.60 (dd, $J = 2.2, 9.0$ Hz, 1H), 7.53–7.48 (m, 3 H), 7.41 (d, $J = 8.8$ Hz, 1H), 7.37 (dd, $J = 2.2, 4.6$ Hz, 1H), 7.23 (d, $J = 6.8$ Hz, 1H), 7.01 (t, $J = 8.8$ Hz, 2H), 6.89 (d, $J = 2.0$, 1H), 6.77 (dd, $J = 5.4, 8.6$ Hz, 2H), 5.28 (dd, $J = 12.0, 4.0$ Hz, 1H), 3.50 (s, 3H), 3.67 (dd, $J = 12.0, 18.0$ Hz, 1H), 2.75 (dd, $J = 4.0, 18.0$ Hz, 1H). ^{13}C NMR (101 MHz, $\text{DMSO-}d_6$) 172.9, 168.8, 160.0, 153.1, 150.1, 139.0, 135.0, 131.9, 129.8, 128.9, 127.9, 126.5, 125.0, 120.9, 118.0, 115.6, 115.4, 58.7, 21.7, 45.0, 28.9, 28.4. UPLC-MS purity (UV at 215 nm) 98%.

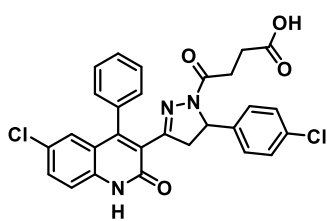
N-(3-(3-(6-Chloro-2-oxo-4-phenyl-1,2-dihydroquinolin-3-yl)-5-(4-fluorophenyl)-4,5-dihydro-1H-pyrazol-1-yl)-3-oxopropyl) methane sulfonamide (27) (Scheme 10).



In a round bottom flask, 6-chloro-3-(5-(4-fluorophenyl)-4,5-dihydro-1H-pyrazol-3-yl)-4-phenylquinolin-2(1H)-one **91c** (500 mg, 1.20 mmol), 3-(methylsulfonamido)propanoic acid **128** (200 mg, 1.20 mmol), HOBT (178 mg, 1.32 mmol) were stirred in DCM prior to the addition of triethylamine (367.7 mL, 2.64 mmol) and EDCI (253 mg,

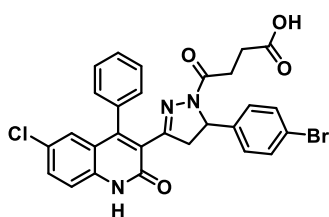
1.32 mmol) at 0 °C. The reaction was stirred overnight while the mixture gradually reached rt. The solvent was removed under vacuum, and the residue was dissolved in DCM. The organic layer was washed with H₂O, NaHCO₃ sat solution, and 5% citric acid, dried over Na₂SO₄, filtered, and evaporated to dryness. The title compound was obtained after purification over direct phase flash column chromatography (SiO₂, A= DCM, B= EtOAc, gradient 0–60% B) to afford the desired **27** (100 mg, yield 15%). ¹H NMR (400 MHz, DMSO-*d*₆) δ 12.35 (s, 1H), 7.60 (dd, J = 2.0, 8.0 Hz, 1H), 7.55–7.49 (m, 3H), 7.41 (d, J = 8.0 Hz, 1H), 7.38 (d, J = 6.0 Hz, 1H), 7.24 (d, J = 6.0 Hz, 1H), 7.00 (t, J = 8.0 Hz, 2H), 6.89 (d, J = 2.0 Hz, 2H), 6.77 (dd, J = 4.0, 8.0 Hz, 2H), 5.29 (dd, J = 4.0, 12.0 Hz, 1H), 3.69 (dd, J = 12.0, 20.0 Hz, 1H), 3.03–2.98 (m, 2H), 2.80 (s, 3H), 2.72 (dd, J = 4.0, 20.0 Hz, 1H), 2.51–2.47 (m, 2H). ¹³C NMR (101 MHz, DMSO-*d*₆) δ 168.01, 162.81, 160.49, 160.40, 153.25, 150.39, 138.71, 137.78, 134.86, 131.68, 129.94, 129.10, 128.94, 128.91, 128.83, 128.02, 127.94, 126.57, 125.01, 121.07, 118.09, 115.69, 115.48, 58.63, 45.67, 38.61, 34.73. UPLC–MS purity (UV at 215 nm) 99%.

4-(3-(6-Chloro-2-oxo-4-phenyl-1,2-dihydroquinolin-3-yl)-5-(4-chlorophenyl)-4,5-dihydro-1H-pyrazol-1-yl)-4-oxobutanoic Acid (28**).**



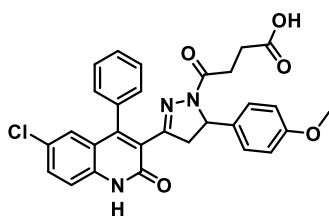
Compound **28** was synthesized via general procedure C₁ using **92c** (253 mg, 0.58 mmol) with succinic anhydride **114** (116 mg, 1.16 mmol) (120 °C, 200 W). Purification was performed by direct phase flash chromatography (SiO₂ gold 24 g, A= DCM, B= EtOH, gradient 0–60% B) to afford **28** (231 mg, yield 74%). ¹H NMR (400 MHz, DMSO-*d*₆) δ 12.38 (s, 1H), 12.03 (s, 1H), 7.64 (dd, J = 8.8, 2.4 Hz, 1H), 7.59–7.48 (m, 3H), 7.45 (d, J = 8.8 Hz, 1H), 7.41 (dt, J = 6.3, 2.0 Hz, 1H), 7.31–7.23 (m, 3H), 6.93 (d, J = 2.4 Hz, 1H), 6.83–6.76 (m, 2H), 5.32 (dd, J = 12.0, 4.6 Hz, 1H), 3.74 (dd, J = 18.5, 12.1 Hz, 1H), 2.78 (dd, J = 18.5, 4.6 Hz, 1H), 2.48–2.41 (m, 2H), 2.29 (t, J = 7.1 Hz, 2H). In agreement with that previously reported by Acker *et al.*¹⁷⁰ tR = 2.16 min. ESI-MS for C₂₈H₂₁Cl₂N₃O₄: calculated 533.1, found m/z 534.4, 536.4, 538.3 [M + H]⁺; 532.4, 534.4, 536.4 [M – H][–]. UPLC–MS purity (UV at 215 nm) 99%.

4-(5-(4-Bromophenyl)-3-(6-chloro-2-oxo-4-phenyl-1,2-dihydroquinolin-3-yl)-4,5-dihydro-1H-pyrazol-1-yl)-4-oxobutanoic Acid (29).



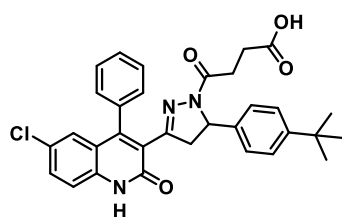
Compound **29** was synthesized via general procedure C₁ using **93c** (330 mg, 0.69 mmol) with succinic anhydride **114** (138 mg, 1.38 mmol) (120 °C, 200 W). Purification was performed by direct phase flash chromatography (SiO₂ gold 24 g, A= DCM, B= EtOH, gradient 0–50% B) to afford **29** (275 mg, yield 68%). ¹H NMR (400 MHz, DMSO-*d*₆) δ 12.38 (s, 1H), 12.03 (s, 1H), 7.63 (dd, *J* = 8.8, 2.3 Hz, 1H), 7.59–7.47 (m, 3H), 7.45 (d, *J* = 8.8 Hz, 1H), 7.40 (d, *J* = 8.4 Hz, 2H), 7.27 (dd, *J* = 6.5, 1.8 Hz, 1H), 6.93 (d, *J* = 2.3 Hz, 1H), 6.73 (d, *J* = 8.5 Hz, 2H), 5.30 (dd, *J* = 12.0, 4.6 Hz, 1H), 3.74 (dd, *J* = 18.5, 12.1 Hz, 1H), 2.77 (dd, *J* = 18.5, 4.6 Hz, 1H), 2.48–2.36 (m, 2H), 2.28 (t, *J* = 7.1 Hz, 2H). In agreement with that previously reported by Acker *et al.*¹⁷⁰ tR = 2.18 min. ESI-MS for C₂₈H₂₁BrClN₃O₄: calculated 577.0, found *m/z* 578.2, 580.2, 582.3 [M + H]⁺; 576.1, 578.1, 580.0 [M – H][–]. UPLC–MS purity (UV at 215 nm) >99.5%.

4-(3-(6-Chloro-2-oxo-4-phenyl-1,2-dihydroquinolin-3-yl)-5-(4-methoxyphenyl)-4,5-dihydro-1H-pyrazol-1-yl)-4-oxobutanoic Acid (30).



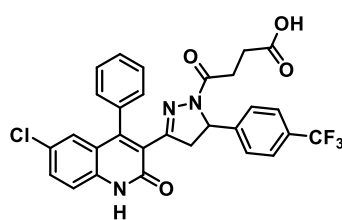
Compound **30** was synthesized via general procedure C₁ using **94c** (320 mg, 0.74 mmol) with succinic anhydride **114** (148 mg, 1.48 mmol) (120 °C, 200 W). Purification was performed by direct phase flash chromatography (SiO₂ gold 24 g, A= DCM, B= EtOH, gradient 0–15% B) to afford **30** (339 mg, yield 86%). ¹H NMR (400 MHz, DMSO-*d*₆) δ 12.19 (s, 1H), 7.57 (dd, *J* = 8.8, 2.3 Hz, 1H), 7.51 (m, 3H), 7.42 (d, *J* = 8.8 Hz, 1H), 7.36–7.31 (m, 1H), 7.27–7.21 (m, 1H), 7.02 (dd, *J* = 8.9, 5.9 Hz, 3H), 6.90 (d, *J* = 2.3 Hz, 1H), 6.80 (d, *J* = 8.7 Hz, 2H), 4.52 (td, *J* = 10.4, 2.9 Hz, 1H), 3.73 (s, 3H), 3.18 (dd, *J* = 16.4, 10.9 Hz, 1H), 2.58–2.52 (m, 5H). In agreement with that previously reported by Acker *et al.*¹⁷⁰ tR = 1.99 min. ESI-MS for C₂₉H₂₄ClN₃O₅: calculated 529.1, found *m/z* 530.5, 532.4 [M + H]⁺; 528.4, 530.4 [M – H][–]. UPLC–MS purity (UV at 215 nm) >99.5%.

4-(5-(4-(tert-Butyl)phenyl)-3-(6-chloro-2-oxo-4-phenyl-1,2-dihydroquinolin-3-yl)-4,5-dihydro-1H-pyrazol-1-yl)-4-oxobutanoic Acid (31).



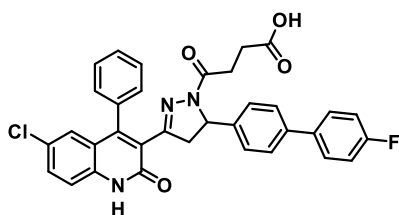
Compound **31** was synthesized via general procedure C₁ using **95c** (124 mg, 0.27 mmol) with succinic anhydride **114** (54 mg, 0.54 mmol) (120 °C, 200 W). Purification was performed by direct phase flash chromatography (SiO₂ gold 24 g, A= DCM, B= EtOH, gradient 0–20% B) to afford **31** (121 mg, yield 81%). ¹H NMR (400 MHz, DMSO-*d*₆) δ 12.27 (d, J = 78.0 Hz, 1H), 12.08 (s, 1H), 7.64 (dd, J = 8.8, 2.3 Hz, 1H), 7.59–7.47 (m, 3H), 7.47–7.43 (m, 1H), 7.40 (dd, J = 4.6, 2.1 Hz, 1H), 7.28 (d, J = 7.5 Hz, 1H), 7.23 (d, J = 8.3 Hz, 2H), 6.93 (d, J = 2.3 Hz, 1H), 6.73 (d, J = 8.3 Hz, 2H), 5.26 (dd, J = 11.9, 4.5 Hz, 1H), 3.69 (dt, J = 24.9, 12.5 Hz, 1H), 2.85 (ddd, J = 23.0, 18.2, 4.3 Hz, 1H), 2.47 (dd, J = 6.7, 4.0 Hz, 2H), 2.36–2.22 (m, 2H), 1.27 (s, 9H). ¹³C NMR (101 MHz, DMSO-*d*₆) δ 173.52, 168.56, 160.09, 152.41, 149.87, 149.19, 139.24, 137.30, 134.59, 131.15, 129.30, 128.57, 128.47, 128.33, 126.06, 126.03, 125.13, 125.09, 124.67, 120.69, 117.60, 58.62, 45.26, 34.12, 31.11, 28.57, 28.21, 26.32. tR = 2.39 min. ESI-MS for C₃₂H₃₀ClN₃O₄: calculated 555.2, found m/z 556.5, 558.4 [M + H]⁺; 554.4, 556.4 [M – H][–]. UPLC–MS purity (UV at 215 nm) 97%.

4-(3-(6-Chloro-2-oxo-4-phenyl-1,2-dihydroquinolin-3-yl)-5-(4-(trifluoromethyl)phenyl)-4,5-dihydro-1H-pyrazol-1-yl)-4-oxobutanoic Acid (32).



Compound **32** was synthesized via general procedure C₁ using **96c** (309 mg, 0.66 mmol) with succinic anhydride **114** (132 mg, 1.32 mmol) (120 °C, 200 W). Purification was performed by direct phase flash chromatography (SiO₂ gold 40 g, A= DCM, B= EtOH, gradient 0–10% B) to afford **32** (266 mg, yield 71%). ¹H NMR (400 MHz, DMSO-*d*₆) δ 12.38 (s, 1H), 12.05 (s, 1H), 7.63 (dd, J = 8.8, 2.4 Hz, 1H), 7.60–7.39 (m, 7H), 7.31–7.19 (m, 1H), 7.00 (d, J = 8.1 Hz, 2H), 6.93 (d, J = 2.3 Hz, 1H), 5.42 (dd, J = 12.1, 4.7 Hz, 1H), 3.78 (dd, J = 18.5, 12.2 Hz, 1H), 2.80 (dd, J = 18.5, 4.7 Hz, 1H), 2.59–2.38 (m, 2H), 2.36–2.26 (m, 2H). ¹³C NMR (101 MHz, DMSO-*d*₆) δ 173.45, 168.78, 160.05, 152.42, 150.01, 146.65, 137.33, 134.55, 131.24, 129.42, 128.54, 128.44, 128.38, 128.35, 127.85, 127.53, 127.22, 126.20, 126.12, 126.04, 125.54, 125.39, 125.35, 124.45, 122.83, 120.63, 117.63, 58.51, 45.05, 28.49, 28.18, 26.32. In agreement with that previously reported by Acker *et al.*¹⁷⁰ tR = 2.22 min. ESI-MS for C₂₉H₂₁ClF₃N₃O₄: calculated 567.1, found m/z 568.5, 570.4, [M + H]⁺; 566.4, 568.4 [M – H][–]. UPLC–MS purity (UV at 215 nm) 99%.

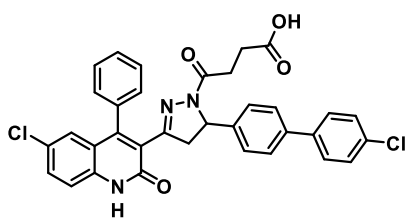
4-(3-(6-Chloro-2-oxo-4-phenyl-1,2-dihydroquinolin-3-yl)-5-(4'-fluoro-[1,1'-biphenyl]-4-yl)-4,5-dihydro-1H-pyrazol-1-yl)-4-oxobutanoic Acid (33).



Compound **33** was synthesized via general procedure C₁ using **97c** (171 mg, 0.35 mmol) with succinic anhydride **114** (70 mg, 0.70 mmol) (120 °C, 200 W). Purification was performed by direct phase flash chromatography (SiO₂ gold 24 g, A= DCM, B= EtOH, gradient 0–10% B) to afford **33** (167 mg, yield 80%).

¹H NMR (400 MHz, DMSO-*d*₆) δ 12.38 (s, 1H), 12.08 (s, 1H), 7.71–7.61 (m, 3H), 7.55 (ddt, J = 10.6, 9.5, 4.0 Hz, 3H), 7.50–7.40 (m, 4H), 7.33– 7.25 (m, 3H), 6.94 (d, J = 2.3 Hz, 1H), 6.87 (d, J = 8.3 Hz, 2H), 5.35 (dd, J = 12.0, 4.6 Hz, 1H), 3.77 (dd, J = 18.5, 12.1 Hz, 1H), 2.84 (dd, J = 18.4, 4.7 Hz, 1H), 2.57–2.44 (m, 2H), 2.30 (t, J = 6.8 Hz, 2H). ¹³C NMR (101 MHz, DMSO-*d*₆) δ 173.63, 173.50, 168.63, 163.05, 160.62, 160.11, 152.46, 149.94, 141.37, 137.96, 137.31, 136.34, 136.31, 134.60, 131.19, 129.41, 128.64, 128.56, 128.47, 128.33, 126.73, 126.08, 124.64, 120.69, 117.62, 115.78, 115.57, 58.66, 45.22, 28.96, 28.60, 28.23. tR = 2.36 min. ESI-MS for C₃₄H₂₅ClFN₃O₄: calculated 593.1, found m/z 594.1, 596.1 [M + H]⁺, 592.2, 594.2 [M – H][–]. UPLC–MS purity (UV at 215 nm) >99.5%.

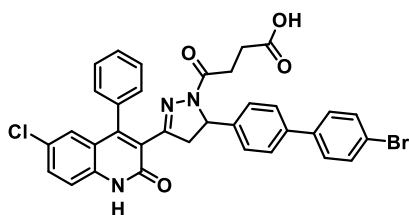
4-(3-(6-Chloro-2-oxo-4-phenyl-1,2-dihydroquinolin-3-yl)-5-(4'-chloro-[1,1'-biphenyl]-4-yl)-4,5-dihydro-1H-pyrazol-1-yl)-4-oxobutanoic Acid (34).



Compound **34** was synthesized via general procedure C₁ using **98c** (227 mg, 0.44 mmol) with succinic anhydride **114** (88 mg, 0.88 mmol) (120 °C, 200 W). Purification was performed by direct phase flash chromatography (SiO₂ gold 24 g, A= DCM, B= EtOH, gradient 0–10% B) to afford **34** (205 mg, yield 77%).

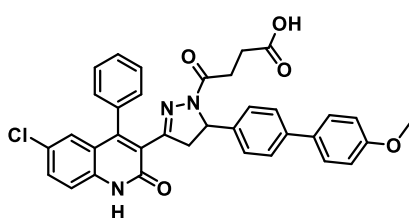
¹H NMR (400 MHz, DMSO-*d*₆) δ 12.38 (s, 1H), 12.04 (s, 1H), 7.67 (d, J = 8.6 Hz, 2H), 7.63 (dd, J = 8.8, 2.4 Hz, 1H), 7.59–7.48 (m, 7H), 7.47– 7.39 (m, 2H), 7.29 (dd, J = 6.5, 2.0 Hz, 1H), 6.94 (d, J = 2.4 Hz, 1H), 6.88 (d, J = 8.3 Hz, 2H), 5.35 (dd, J = 12.0, 4.6 Hz, 1H), 3.77 (dd, J = 18.5, 12.1 Hz, 1H), 2.84 (dd, J = 18.5, 4.6 Hz, 1H), 2.50 (m, 2H), 2.29 (t, J = 6.8 Hz, 2H). ¹³C NMR (101 MHz, DMSO-*d*₆) δ 173.58, 173.49, 168.64, 160.10, 152.44, 149.94, 141.77, 138.63, 137.62, 137.31, 134.60, 132.26, 131.18, 129.40, 128.84, 128.52, 128.45, 128.37, 128.32, 126.72, 126.14, 126.10, 126.05, 124.62, 120.68, 117.61, 58.66, 45.21, 28.60, 28.23. tR = 2.51 min. ESI-MS for C₃₄H₂₅Cl₂N₃O₄: calculated 609.1, found m/z 610.0, 612.0, 614.2 [M + H]⁺; 608.1, 610.1, 612.0 [M – H][–]. UPLC–MS purity (UV at 215 nm) >99.5%.

4- [3- [4- (4- (5- (4'-Bromo- [1,1'-biphenyl] -4-yl)-3- (6-chloro- 2-oxo-4-phenyl-1,2-dihydroquinolin-3-yl)-4,5-dihydro-1H-pyrazol- 1-yl)-4-oxobutanoic Acid (35).



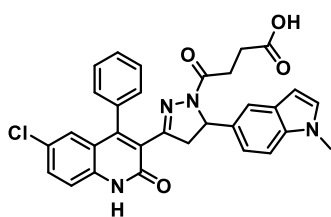
Compound **35** was synthesized via general procedure C₁ using **99c** (214 mg, 0.38 mmol) with succinic anhydride **114** (76 mg, 0.76 mmol) (120 °C, 200 W). Purification was performed by direct phase flash chromatography (SiO₂ gold 24 g, A= DCM, B= EtOH, gradient 0–20% B) to afford **35** (197 mg, yield 79%). ¹H NMR (400 MHz, DMSO-*d*₆) δ 12.37 (s, 1H), 12.08 (s, 1H), 7.68–7.38 (m, 12H), 7.30–7.26 (m, 1H), 6.94 (d, J = 2.4 Hz, 1H), 6.89 (d, J = 8.4 Hz, 2H), 5.35 (dd, J = 12.0, 4.6 Hz, 1H), 3.78 (dd, J = 18.5, 12.1 Hz, 1H), 2.84 (dd, J = 18.5, 4.7 Hz, 1H), 2.58–2.43 (m, J = 3.7 Hz, 2H), 2.30 (t, J = 6.9 Hz, 2H). ¹³C NMR (101 MHz, DMSO-*d*₆) δ 173.50, 168.66, 160.11, 152.44, 149.95, 141.81, 139.00, 137.67, 137.31, 134.60, 131.76, 131.18, 129.40, 128.71, 128.52, 128.45, 128.33, 126.68, 126.16, 126.11, 126.05, 124.62, 120.84, 120.68, 117.61, 58.67, 45.20, 28.61, 28.24. tR = 2.52 min. ESI-MS for C₃₄H₂₅BrClN₃O₄: calculated 653.1, found m/z 653.9, 655.9, 657.9 [M + H]⁺; 652.0, 654.0, 655.8 [M – H][–]. UPLC–MS purity (UV at 215 nm) >99.5%.

4-(3-(6-Chloro-2-oxo-4-phenyl-1,2-dihydroquinolin-3-yl)-5- (4'-methoxy-[1,1'-biphenyl]-4-yl)-4,5-dihydro-1H-pyrazol-1-yl)-4-oxobutanoic Acid (36).



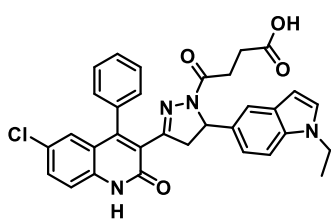
Compound **36** was synthesized via general procedure C₁ using **100c** (545 mg, 1.10 mmol) with succinic anhydride **114** (220 mg, 2.20 mmol) (120 °C, 200 W). Purification was performed by direct phase flash chromatography (SiO₂ gold 40 g, A= DCM, B= EtOH, gradient 0–10% B) to afford **36** (359 mg, yield 55%). ¹H NMR (400 MHz, DMSO-*d*₆) δ 12.38 (s, 1H), 12.03 (s, 1H), 7.67–7.50 (m, 6H), 7.44 (dt, J = 7.7, 5.9 Hz, 4H), 7.29 (dd, J = 6.7, 2.1 Hz, 1H), 7.02 (d, J = 8.8 Hz, 2H), 6.94 (d, J = 2.3 Hz, 1H), 6.84 (d, J = 8.3 Hz, 2H), 5.33 (dd, J = 12.0, 4.6 Hz, 1H), 3.79 (s, 4H), 2.84 (dd, J = 18.4, 4.6 Hz, 1H), 2.30 (t, J = 6.9 Hz, 2H). ¹³C NMR (101 MHz, DMSO-*d*₆) δ 173.51, 168.62, 160.12, 158.85, 152.44, 149.92, 140.63, 138.67, 137.31, 134.60, 132.23, 131.17, 129.40, 128.54, 128.44, 128.32, 127.68, 126.23, 126.10, 126.00, 124.66, 120.69, 117.61, 114.34, 58.70, 55.14, 45.24, 28.62, 28.25. tR = 2.30 min. ESI-MS for C₃₅H₂₈ClN₃O₅: calculated 605.2, found m/z 606.0, 608.0 [M + H]⁺; 604.0, 606.0 [M – H][–]. UPLC–MS purity (UV at 215 nm) >99.5%.

4-(3-(6-Chloro-2-oxo-4-phenyl-1,2-dihydroquinolin-3-yl)-5-(1-methyl-1H-indol-5-yl)-4,5-dihydro-1H-pyrazol-1-yl)-4-oxobutanoic Acid (37).



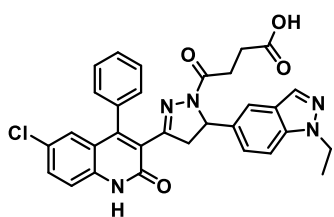
Compound **37** was synthesized via general procedure C₁ using **101c** (153 mg, 0.34 mmol) with succinic anhydride **114** (68 mg, 0.68 mmol) (120 °C, 200 W). Purification was performed by direct phase flash chromatography (SiO₂ gold 24 g, A= DCM, B= EtOH, gradient 0–20% B) to afford **37** (150 mg, yield 79%). ¹H NMR (400 MHz, DMSO-*d*₆) δ 12.37 (s, 1H), 12.18 (s, 1H), 7.63 (dd, *J* = 8.8, 2.3 Hz, 1H), 7.60–7.55 (m, 2H), 7.55–7.49 (m, 1H), 7.44 (dd, *J* = 7.7, 4.3 Hz, 2H), 7.31–7.20 (m, 3H), 6.98 (d, *J* = 1.7 Hz, 1H), 6.93 (d, *J* = 2.3 Hz, 1H), 6.61 (dd, *J* = 8.5, 1.7 Hz, 1H), 6.34 (dd, *J* = 3.0, 0.8 Hz, 1H), 5.35 (dd, *J* = 12.0, 4.6 Hz, 1H), 3.84–3.69 (m, 4H), 2.85 (dd, *J* = 18.4, 4.6 Hz, 1H), 2.53–2.45 (m, 2H), 2.26 (t, *J* = 6.9 Hz, 2H). ¹³C NMR (101 MHz, DMSO-*d*₆) δ 173.72, 173.52, 168.43, 160.17, 152.27, 149.80, 137.29, 135.60, 134.66, 133.04, 131.11, 129.90, 129.47, 128.52, 128.43, 128.25, 127.73, 126.06, 124.84, 120.75, 118.98, 117.58, 117.22, 109.64, 100.28, 59.51, 45.76, 32.46, 29.17, 28.70, 28.27. tR = 2.09 min. ESI-MS for C₃₁H₂₅ClN₄O₄: calculated 552.2, found *m/z* 553.1, 555.2 [M + H]⁺; 551.2, 553.2 [M – H][–]. UPLC–MS purity (UV at 215 nm) >99.5%.

4-(3-(6-Chloro-2-oxo-4-phenyl-1,2-dihydroquinolin-3-yl)-5-(1-ethyl-1H-indol-5-yl)-4,5-dihydro-1H-pyrazol-1-yl)-4-oxobutanoic Acid (38).



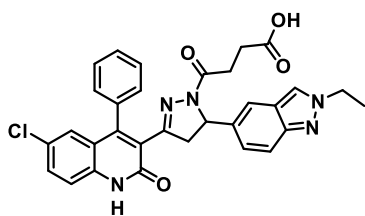
Compound **38** was synthesized via general procedure C₁ using **102c** (153 mg, 0.33 mmol) with succinic anhydride **114** (66 mg, 0.66 mmol) (120 °C, 200 W). Purification was performed by direct phase flash chromatography (SiO₂ gold 24 g, A= DCM, B= EtOH, gradient 0–10% B) to afford **38** (92 mg, yield 49%). ¹H NMR (400 MHz, DMSO-*d*₆) δ 12.37 (s, 1H), 12.02 (s, 1H), 7.63 (dd, *J* = 8.8, 2.4 Hz, 1H), 7.58 (dd, *J* = 5.5, 3.3 Hz, 2H), 7.52 (ddd, *J* = 8.9, 5.2, 3.1 Hz, 1H), 7.44 (dd, *J* = 8.7, 4.4 Hz, 2H), 7.35 (d, *J* = 3.1 Hz, 1H), 7.29 (dd, *J* = 8.5, 2.2 Hz, 2H), 6.95 (dd, *J* = 15.5, 2.0 Hz, 2H), 6.60 (dd, *J* = 8.5, 1.7 Hz, 1H), 6.34 (d, *J* = 3.1 Hz, 1H), 5.34 (dd, *J* = 12.0, 4.7 Hz, 1H), 4.17 (q, *J* = 7.2 Hz, 2H), 3.77 (dd, *J* = 18.4, 12.1 Hz, 1H), 2.86 (dd, *J* = 18.4, 4.7 Hz, 1H), 2.48–2.42 (m, 2H), 2.26 (t, *J* = 6.9 Hz, 2H), 1.34 (t, *J* = 7.2 Hz, 3H). ¹³C NMR (101 MHz, DMSO-*d*₆) δ 173.53, 168.45, 160.17, 152.28, 149.80, 137.29, 134.66, 134.56, 133.01, 131.11, 129.45, 128.53, 128.42, 128.28, 127.89, 126.05, 124.84, 120.74, 118.93, 117.58, 117.32, 109.62, 100.49, 59.51, 45.75, 40.26, 28.72, 28.30, 15.53. tR = 2.20 min. ESI-MS for C₃₂H₂₇ClN₄O₄: calculated 566.2, found *m/z* 567.2, 569.2 [M + H]⁺; 565.3, 567.3 [M – H][–]. UPLC–MS purity (UV at 215 nm) >99.5%.

4-(3-(6-Chloro-2-oxo-4-phenyl-1,2-dihydroquinolin-3-yl)-5-(1-ethyl-1*H*-indazol-5-yl)-4,5-dihydro-1*H*-pyrazol-1-yl)-4-oxobutanoic Acid (39).



Compound **39** was synthesized via general procedure C₁ using **103c** (196 mg, 0.42 mmol) with succinic anhydride **114** (84 mg, 0.84 mmol) (120 °C, 200 W). Purification was performed by direct phase flash chromatography (SiO₂ gold 24 g, A= DCM, B= EtOH, gradient 0–10% B) to afford **39** (177 mg, yield 74%). ¹H NMR (400 MHz, DMSO-*d*₆) δ 12.39 (s, 1H), 12.03 (s, 1H), 7.98 (s, 1H), 7.64 (dd, J = 8.8, 2.4 Hz, 1H), 7.59 (dd, J = 5.4, 3.5 Hz, 2H), 7.52 (dd, J = 10.0, 6.6 Hz, 2H), 7.48–7.43 (m, 2H), 7.29 (d, J = 7.5 Hz, 1H), 7.14 (d, J = 1.5 Hz, 1H), 6.94 (d, J = 2.3 Hz, 1H), 6.83 (dd, J = 8.7, 1.6 Hz, 1H), 5.42 (dd, J = 12.0, 4.6 Hz, 1H), 4.42 (q, J = 7.2 Hz, 2H), 3.80 (dd, J = 18.5, 12.1 Hz, 1H), 2.85 (dd, J = 18.5, 4.6 Hz, 1H), 2.54–2.48 (m, 2H), 2.28 (t, J = 6.9 Hz, 2H), 1.38 (t, J = 7.2 Hz, 3H). ¹³C NMR (101 MHz, DMSO-*d*₆) δ 173.99, 169.05, 160.62, 152.86, 150.36, 138.51, 137.79, 135.07, 134.85, 132.81, 131.65, 130.00, 129.09, 128.97, 128.93, 128.78, 126.57, 126.54, 125.22, 124.57, 123.78, 121.19, 118.09, 117.79, 110.22, 59.57, 45.96, 43.53, 29.13, 28.72, 15.43. tR = 1.95 min. ESI-MS for C₃₁H₂₆ClN₅O₄: calculated 567.2, found m/z 568.5, 570.4 [M + H]⁺, 566.4, 568.4 [M – H][–]. UPLC–MS purity (UV at 215 nm) >99.5%.

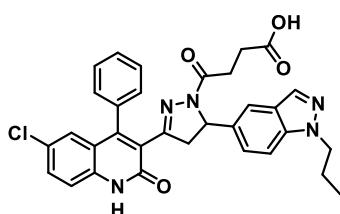
4-(3-(6-Chloro-2-oxo-4-phenyl-1,2-dihydroquinolin-3-yl)-5-(2-ethyl-2*H*-indazol-5-yl)-4,5-dihydro-1*H*-pyrazol-1-yl)-4-oxobutanoic Acid (40).



Compound **40** was synthesized via general procedure C₁ using **104c** (198 mg, 0.42 mmol) with succinic anhydride **114** (84 mg, 0.84 mmol) (120 °C, 200 W). Purification was performed by direct phase flash chromatography (SiO₂ gold 24 g, A= DCM, B= EtOH, gradient 0–20% B) to afford **40** (120 mg, yield 50%). ¹H NMR (400 MHz, DMSO-*d*₆) δ 12.37 (s, 1H), 12.04 (s, 1H), 8.29 (s, 1H), 7.66–7.55 (m, 3H), 7.51 (td, J = 6.6, 5.5, 3.3 Hz, 1H), 7.44 (dd, J = 10.0, 6.8 Hz, 3H), 7.28 (d, J = 7.5 Hz, 1H), 7.07 (d, J = 1.6 Hz, 1H), 6.93 (d, J = 2.4 Hz, 1H), 6.61 (dd, J = 8.9, 1.7 Hz, 1H), 5.35 (dd, J = 12.0, 4.6 Hz, 1H), 4.43 (q, J = 7.3 Hz, 2H), 3.77 (dd, J = 18.4, 12.1 Hz, 1H), 2.82 (dd, J = 18.4, 4.6 Hz, 1H), 2.54–2.44 (m, 2H), 2.28 (t, J = 6.9 Hz, 2H), 1.49 (t, J = 7.2 Hz, 3H). ¹³C NMR (101 MHz, DMSO-*d*₆) δ 173.50, 168.55, 160.12, 152.37, 149.84, 147.32, 137.29, 134.57, 134.39, 131.15, 129.53, 128.57, 128.49, 128.42, 128.28, 126.07, 126.04, 124.75, 123.57, 123.00, 120.94, 120.72, 117.60, 117.32, 116.68, 59.31, 47.68, 45.24, 28.67, 28.26, 15.84. tR = 1.85 min. ESI-MS for

C₃₁H₂₆ClN₅O₄: calculated 567.2, found m/z 568.4, 570.4 [M + H]⁺, 566.5, 568.4 [M - H]⁻. UPLC-MS purity (UV at 215 nm) >99.5%.

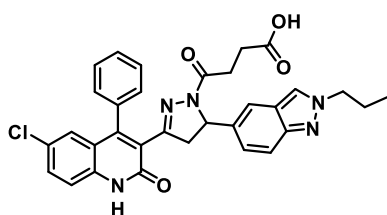
4-(3-(6-Chloro-2-oxo-4-phenyl-1,2-dihydroquinolin-3-yl)-5-(1-propyl-1*H*-indazol-5-yl)-4,5-dihydro-1*H*-pyrazol-1-yl)-4-oxobutanoic Acid (41).



Compound **41** was synthesized via general procedure C₁ using **105c** (176 mg, 0.36 mmol) with succinic anhydride **114** (72 mg, 0.72 mmol) (120 °C, 200 W). Purification was performed by direct phase flash chromatography (SiO₂ gold 24 g, A= DCM, B= EtOH, gradient 0–25% B) to afford **41** (178 mg, yield 86%). ¹H NMR (400

MHz, DMSO-*d*₆) δ 12.36 (s, 1H), 12.05 (s, 1H), 7.97 (d, J = 0.9 Hz, 1H), 7.62 (dd, J = 8.8, 2.4 Hz, 1H), 7.57 (qd, J = 4.0, 1.0 Hz, 2H), 7.53–7.47 (m, 2H), 7.47–7.41 (m, 2H), 7.30–7.25 (m, 1H), 7.16–7.11 (m, 1H), 6.94 (d, J = 2.3 Hz, 1H), 6.84 (dd, J = 8.8, 1.6 Hz, 1H), 5.42 (dd, J = 12.0, 4.6 Hz, 1H), 4.33 (t, J = 6.9 Hz, 2H), 3.78 (dd, J = 18.5, 12.0 Hz, 1H), 2.85 (dd, J = 18.5, 4.6 Hz, 1H), 2.54–2.48 (m, 2H), 2.28 (t, J = 6.9 Hz, 2H), 1.83 (h, J = 7.2 Hz, 2H), 0.83 (t, J = 7.4 Hz, 3H). ¹³C NMR (101 MHz, DMSO-*d*₆) δ 173.53, 168.61, 160.15, 152.41, 149.89, 138.59, 137.31, 134.60, 134.31, 132.32, 131.17, 129.50, 128.60, 128.49, 128.43, 128.32, 126.11, 126.06, 124.73, 124.13, 123.19, 120.71, 117.62, 117.28, 109.80, 59.09, 49.64, 45.49, 28.67, 28.26, 22.83, 11.17. tR = 2.06 min. ESI-MS for C₃₂H₂₈ClN₅O₄: calculated 581.2, found m/z 582.1, 584.1 [M + H]⁺, 580.4, 582.0 [M - H]⁻. UPLC-MS purity (UV at 215 nm) >99.5%.

4-(3-(6-Chloro-2-oxo-4-phenyl-1,2-dihydroquinolin-3-yl)-5-(2-propyl-2*H*-indazol-5-yl)-4,5-dihydro-1*H*-pyrazol-1-yl)-4-oxobutanoic Acid (42).

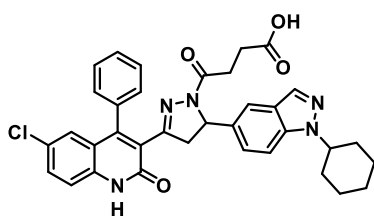


Compound **42** was synthesized via general procedure C₁ using **106c** (173 mg, 0.36 mmol) with succinic anhydride **114** (72 mg, 0.72 mmol) (120 °C, 200 W). Purification was performed by direct phase flash chromatography (SiO₂ gold 24 g, A= DCM, B= EtOH, gradient 0–20% B) to afford **42** (162 mg, yield 78%).

¹H NMR (400 MHz, DMSO-*d*₆) δ 12.37 (s, 2H), 8.28 (d, J = 0.9 Hz, 1H), 7.63–7.54 (m, 3H), 7.50 (td, J = 6.6, 5.5, 3.3 Hz, 1H), 7.47–7.40 (m, 3H), 7.30–7.24 (m, 1H), 7.08 (t, J = 1.2 Hz, 1H), 6.93 (d, J = 2.4 Hz, 1H), 6.62 (dd, J = 8.9, 1.7 Hz, 1H), 5.36 (dd, J = 12.0, 4.6 Hz, 1H), 4.35 (t, J = 6.9 Hz, 2H), 3.77 (dd, J = 18.5, 12.0 Hz, 1H), 2.83 (dd, J = 18.5, 4.6 Hz, 1H), 2.54–2.50 (m, 2H), 2.29 (t, J = 6.9 Hz, 2H), 1.96–1.87 (m, 2H), 0.83 (t, J = 7.4 Hz, 3H). ¹³C NMR (101 MHz, DMSO-*d*₆) δ 173.57, 168.64, 160.16, 152.44, 149.89, 147.41, 137.31, 134.59, 134.40, 131.16,

129.56, 128.60, 128.52, 128.43, 128.31, 126.13, 126.07, 124.77, 123.75, 123.60, 120.86, 120.74, 117.62, 117.39, 116.71, 59.36, 54.27, 45.27, 28.73, 28.32, 23.44, 10.91. tR = 2.00 min. ESI-MS for C₃₂H₂₈ClN₅O₄: calculated 581.2, found m/z 582.2, 584.3 [M + H]⁺, 580.3, 582.4 [M - H]⁻. UPLC-MS purity (UV at 215 nm) >99.5%.

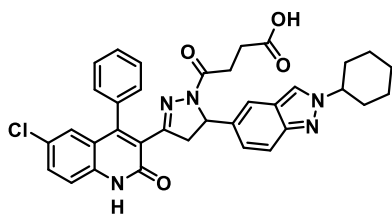
4-(3-(6-Chloro-2-oxo-4-phenyl-1,2-dihydroquinolin-3-yl)-5-(1-cyclohexyl-1H-indazol-5-yl)-4,5-dihydro-1H-pyrazol-1-yl)-4-oxobutanoic Acid (43).



Compound **43** was synthesized via general procedure C₁ using **107c** (164 mg, 0.31 mmol) with succinic anhydride **114** (62 mg, 0.62 mmol) (120 °C, 200 W). Purification was performed by direct phase flash chromatography (SiO₂ gold 24 g, A= DCM, B= EtOH, gradient 0–12% B) to afford **43** (169 mg, yield 87%). ¹H

NMR (400 MHz, DMSO-*d*₆) δ 12.38 (s, 1H), 12.07 (s, 1H), 7.96 (s, 1H), 7.65–7.49 (m, 5H), 7.48–7.41 (m, 2H), 7.28 (dd, J = 7.5, 1.8 Hz, 1H), 7.11 (d, J = 1.6 Hz, 1H), 6.94 (d, J = 2.3 Hz, 1H), 6.84 (dd, J = 8.8, 1.6 Hz, 1H), 5.41 (dd, J = 12.0, 4.6 Hz, 1H), 4.54 (tt, J = 10.0, 5.5 Hz, 1H), 3.80 (dd, J = 18.5, 12.1 Hz, 1H), 2.85 (dd, J = 18.5, 4.7 Hz, 1H), 2.53–2.46 (m, 2H), 2.28 (t, J = 6.9 Hz, 2H), 2.01–1.81 (m, 6H), 1.70 (dt, J = 12.8, 3.4 Hz, 1H), 1.58–1.43 (m, 2H), 1.26 (qt, J = 12.7, 3.5 Hz, 1H). ¹³C NMR (101 MHz, DMSO- *d*₆) δ 173.74, 173.51, 168.59, 160.16, 152.36, 149.90, 137.70, 137.31, 134.64, 134.41, 132.08, 131.16, 129.51, 128.59, 128.48, 128.45, 128.30, 126.12, 126.07, 124.73, 123.92, 123.18, 120.71, 117.61, 117.24, 109.77, 59.12, 56.63, 45.50, 32.34, 28.67, 28.26, 25.08. tR = 2.33 min. ESI-MS for C₃₅H₃₂ClN₅O₄: calculated 621.2, found m/z 622.3, 624.2 [M + H]⁺, 620.3, 622.4 [M - H]⁻. UPLC-MS purity (UV at 215 nm) >99.5%.

4-(3-(6-Chloro-2-oxo-4-phenyl-1,2-dihydroquinolin-3-yl)-5-(2-cyclohexyl-2H-indazol-5-yl)-4,5-dihydro-1H-pyrazol-1-yl)-4-oxobutanoic Acid (44).

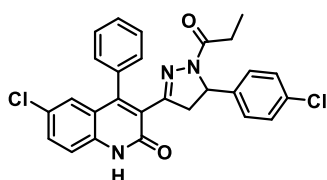


Compound **44** was synthesized via general procedure C₁ using **108c** (100 mg, 0.19 mmol) with succinic anhydride **114** (38 mg, 0.38 mmol) (120 °C, 200 W). Purification was performed by direct phase flash chromatography (SiO₂ gold 24 g, A= DCM, B= EtOH, gradient 0–20% B) to afford **44** (113 mg, yield 95%).

¹H NMR (400 MHz, DMSO-*d*₆) δ 12.37 (s, 1H), 12.10 (s, 1H), 8.29 (d, J = 1.0 Hz, 1H), 7.65–7.55 (m, 3H), 7.53–7.48 (m, 1H), 7.44 (t, J = 8.7 Hz, 3H), 7.30–7.24 (m, 1H), 7.10–7.05 (m, 1H), 6.93 (d, J = 2.4 Hz, 1H), 6.60 (dd, J = 9.0, 1.7 Hz, 1H), 5.35 (dd, J = 12.0, 4.6 Hz, 1H),

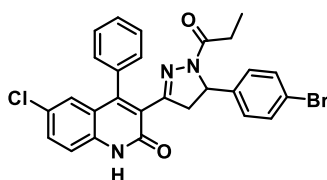
4.44 (tt, $J = 11.2, 3.8$ Hz, 1H), 3.77 (dd, $J = 18.4, 12.1$ Hz, 1H), 2.82 (dd, $J = 18.4, 4.7$ Hz, 1H), 2.55–2.46 (m, 2H), 2.28 (t, $J = 6.9$ Hz, 2H), 2.14–2.02 (m, 2H), 1.95–1.81 (m, 4H), 1.70 (dd, $J = 12.6, 3.7$ Hz, 1H), 1.45 (qt, $J = 12.5, 3.4$ Hz, 2H), 1.25 (tdd, $J = 15.6, 11.7, 7.8$ Hz, 1H). ^{13}C NMR (101 MHz, DMSO- d_6) δ 173.72, 173.52, 168.56, 160.14, 152.38, 149.87, 146.88, 137.30, 134.58, 134.35, 131.15, 129.52, 128.59, 128.51, 128.44, 128.30, 126.09, 126.05, 124.76, 123.49, 121.57, 120.73, 120.62, 117.61, 117.47, 116.76, 61.63, 59.36, 45.25, 33.29, 29.13, 28.69, 28.28, 24.92, 24.89. $t_R = 2.20$ min. ESI-MS for $\text{C}_{35}\text{H}_{32}\text{ClN}_5\text{O}_4$: calculated 621.2, found m/z 622.2, 624.2 $[\text{M} + \text{H}]^+$, 620.3, 622.3 $[\text{M} - \text{H}]^-$. UPLC-MS purity (UV at 215 nm) 99%.

6-Chloro-3-(5-(4-chlorophenyl)-1-propionyl-4,5-dihydro-1H-pyrazol-3-yl)-4-phenylquinolin-2(1H)-one (45).



Compound **45** was synthesized via general procedure C₂ using **92c** (200 mg, 0.46 mmol) and propionic acid **115** (60.5 μL , 0.83 mmol). Purification was performed by direct phase flash chromatography (SiO_2 , A= DCM, B= MeOH, gradient 0–2% B) to afford **45** (76 mg, yield 34%). ^1H NMR (400 MHz, DMSO- d_6) δ 12.38 (s, 1H), 7.63 (dd, $J = 9.0, 2.4$ Hz, 1H), 7.54–7.49 (m, 3H), 7.44 (d, $J = 8.8$ Hz, 1H), 7.41–7.39 (m, 1H), 7.30–7.27 (m, 3H), 6.92 (d, $J = 2.4$ Hz, 1H), 6.80 (d, $J = 8.8$ Hz, 2H), 5.31 (dd, $J = 12.2, 4.6$ Hz, 1H), 3.74 (dd, $J = 18.4, 12.0$ Hz, 1H), 2.80 (dd, $J = 18.4, 4.0$ Hz, 1H), 2.31–2.14 (m, 2H), 0.82 (t, $J = 7.2$ Hz, 3H). ^{13}C NMR (101 MHz, DMSO- d_6) δ 206.88, 170.96, 160.55, 152.65, 150.33, 141.76, 137.75, 135.13, 132.03, 131.64, 129.80, 128.95, 128.87, 128.82, 128.79, 127.81, 126.55, 126.48, 125.04, 121.10, 118.07, 110.00, 58.61, 45.45, 31.11, 27.06, 9.26. ESI MS for $\text{C}_{27}\text{H}_{21}\text{Cl}_2\text{N}_3\text{O}_2$: calculated 489.1, found m/z 490.2, 492.1, 494.1 $[\text{M} + \text{H}]^+$; 488.3, 490.3, 492.1 $[\text{M} - \text{H}]^-$. UPLC-MS purity (UV at 215 nm) 98%.

3-(5-(4-Bromophenyl)-1-propionyl-4,5-dihydro-1H-pyrazol-3-yl)-6-chloro-4-phenylquinolin-2(1H)-one (46).

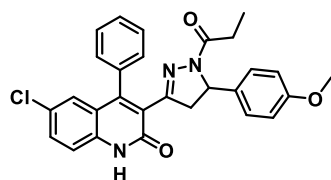


Compound **46** was synthesized via general procedure C₂ using **93c** (150 mg, 0.31 mmol) and propionic acid **115** (41.8 μL , 0.56 mmol). Purification was performed by direct phase flash chromatography (SiO_2 , A= DCM, B= MeOH, gradient 0–0.5% B) to afford **46** (60 mg, yield 36%). ^1H NMR (400 MHz, DMSO- d_6) δ 12.41 (s, 1H), 7.64 (dd, $J = 12.8, 1.6$ Hz, 1H), 7.55–7.50 (m, 3H), 7.46–7.41 (m, 4H), 7.28 (d, $J = 6.8$ Hz, 1H), 6.93 (d, $J = 2.0$ Hz, 1H), 6.75 (d, $J = 8.0$ Hz, 2H), 5.30 (dd, $J = 12.4, 4.0$ Hz, 1H), 3.75 (dd, $J = 18.4, 12.0$ Hz, 1H), 2.80 (dd, $J =$

18.2, 4.6 Hz, 1H), 2.31–2.14 (m, 2H), 0.83 (t, $J = 7.6$ Hz, 3H). ^{13}C NMR (101 MHz, $\text{DMSO-}d_6$) δ 206.78, 171.02, 160.54, 152.60, 150.33, 142.18, 137.77, 135.16, 131.72, 131.61, 129.79, 128.97, 128.92, 128.84, 128.78, 128.18, 126.56, 126.49, 125.03, 121.13, 120.51, 118.06, 58.73, 45.40, 31.08, 27.05, 9.23. ESI-MS for $\text{C}_{27}\text{H}_{21}\text{BrClN}_3\text{O}_2$: calculated 533.0, found m/z 534.2, 536.1, 538.1 $[\text{M} + \text{H}]^+$; 532.2, 534.1, 536.2 $[\text{M} - \text{H}]^-$. UPLC-MS purity (UV at 215 nm) 97%.

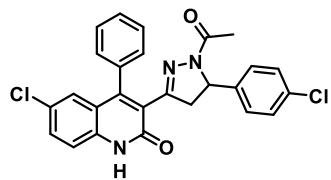
6-Chloro-3-(5-(4-methoxyphenyl)-1-propionyl-4,5-dihydro-phenylquinolin-2(1H)-one (47).

1H-pyrazol-3-yl)-4-



Compound **47** was synthesized via general procedure C_2 using **94c** (150 mg, 0.36 mmol) and propionic acid **115** (48.5 μL , 0.65 mmol). The crude was purified by direct phase flash column chromatography (SiO_2 , A= DCM, B= MeOH, gradient 0–2% B), to afford **47** (100 mg, yield 59%). ^1H NMR (400 MHz, $\text{DMSO-}d_6$) δ 12.36 (s, 1H), 7.64 (dd, $J = 8.6, 2.4$ Hz, 1H), 7.56–7.52 (m, 3H), 7.45 (d, $J = 8.4$ Hz, 1H), 7.40–7.38 (m, 1H), 7.29–7.27 (m, 1H), 6.92 (d, $J = 2.0$ Hz, 1H), 6.75 (dd, $J = 15.2, 9.2$ Hz, 4H), 5.24 (dd, $J = 12.0, 4.8$ Hz, 1H), 3.72 (s, 3H), 3.70 (dd, $J = 16.0, 12.0$ Hz, 1H), 2.81 (dd, $J = 20.0, 4.4$ Hz, 1H), 2.29–2.12 (m, 2H), 0.82 (t, $J = 8.0$ Hz, 3H). ^{13}C NMR (101 MHz, $\text{DMSO-}d_6$) δ 170.80, 160.60, 158.67, 152.56, 150.23, 137.74, 135.16, 134.94, 131.58, 129.76, 129.03, 128.89, 128.84, 128.77, 127.20, 126.51, 126.47, 125.22, 121.15, 118.05, 114.15, 58.73, 55.49, 45.59, 27.12, 9.31. ESI-MS for $\text{C}_{28}\text{H}_{24}\text{ClN}_3\text{O}_3$: calculated 485.1, found m/z 486.4, 488.4 $[\text{M} + \text{H}]^+$; 484.3, 486.3 $[\text{M} - \text{H}]^-$. UPLC-MS purity (UV at 215 nm) 98%.

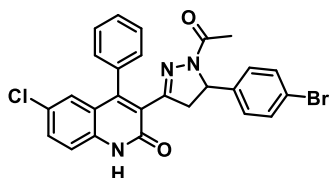
3-(1-Acetyl-5-(4-chlorophenyl)-4,5-dihydro-1H-pyrazol-3-yl)-6-chloro-4-phenylquinolin-2(1H)-one (48).



Compound **48** was synthesized via general procedure C_3 using **92c** (210 mg, 0.48 mmol) with acetic anhydride **116** (888 μL , 0.96 mmol) (165 $^\circ\text{C}$, 200 W). Purification was performed by direct phase flash chromatography (SiO_2 , A= DCM, B= MeOH, gradient 0–1.5% B) to afford **48** (200 mg, yield 94%). ^1H NMR (400 MHz, $\text{DMSO-}d_6$) δ 12.41 (s, 1H), 7.64 (dt, $J = 8.0, 1.2$ Hz, 1H), 7.58–7.53 (m, 3H), 7.44 (d, $J = 8.0$ Hz, 1H), 7.41–7.39 (m, 1H), 7.30–7.28 (m, 3H), 6.93 (d, $J = 0.8$ Hz, 1H), 6.80 (d, $J = 7.6$ Hz, 2H), 5.32 (dd, $J = 12.0, 8.0$ Hz, 1H), 3.74 (dd, $J = 20.0, 12.0$ Hz, 1H), 2.82 (dd, $J = 16.0, 4.0$ Hz, 1H), 1.87 (s, 3H). ^{13}C NMR (101 MHz, $\text{DMSO-}d_6$) δ 167.56, 160.54, 152.67, 150.39, 141.60, 137.75, 135.11, 132.05, 131.65, 129.86, 129.01, 128.96, 128.81, 128.75, 127.83, 126.55, 126.49, 124.96, 121.10, 118.06, 58.56, 45.62, 21.82.

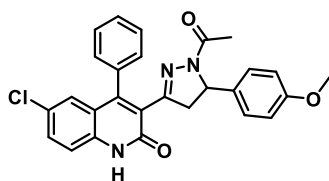
ESI-MS for $C_{26}H_{19}ClN_3O_2$: calculated 475.1, found m/z 476.3, 478.4, 480.4 $[M + H]^+$; 474.3, 476.3, 478.1 $[M - H]^-$. UPLC-MS purity (UV at 215 nm) 99%.

3-(1-Acetyl-5-(4-bromophenyl)-4,5-dihydro-1H-pyrazol-3-yl)-6-chloro-4-phenylquinolin-2(1H)-one (49).



Compound **49** was synthesized via general procedure C₃ using **93c** (100 mg, 0.21 mmol) with acetic anhydride **116** (40 μ L, 0.42 mmol) (165 °C, 200 W). Purification was performed by direct phase flash chromatography (SiO₂, A= DCM, B= MeOH, gradient 0–2% B) to afford **49** (80 mg, yield 73%). ¹H NMR (400 MHz, DMSO-*d*₆) δ 12.39 (s, 1H), 7.64 (dd, *J* = 8.0, 4.0 Hz, 1H), 7.57–7.53 (m, 3H), 7.45–7.39 (m, 4H), 7.28 (dd, *J* = 6.0, 1.6 Hz, 1H), 6.93 (d, *J* = 2.0 Hz, 1H), 6.75 (d, *J* = 8.8 Hz, 2H), 5.30 (dd, *J* = 12.0, 4.4 Hz, 1H), 3.74 (dd, *J* = 18.5, 12.0 Hz, 1H), 2.82 (dd, *J* = 4.0, 20.0 Hz, 1H), 1.86 (s, 3H). ¹³C NMR (101 MHz, DMSO-*d*₆) δ 167.58, 160.54, 152.64, 150.39, 142.02, 137.78, 135.15, 131.72, 131.63, 129.83, 129.03, 128.94, 128.78, 128.74, 128.20, 126.56, 126.50, 124.96, 121.13, 120.54, 118.06, 58.67, 45.58, 21.78. ESI-MS for $C_{26}H_{19}BrClN_3O_2$: calculated 519.0, found m/z 520.1, 522.1, 524.1 $[M + H]^+$; 518.1, 520.1, 522.2 $[M - H]^-$. UPLC-MS purity (UV at 215 nm) 99%.

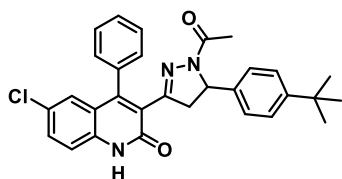
3-(1-Acetyl-5-(4-methoxyphenyl)-4,5-dihydro-1H-pyrazol-3-yl)-6-chloro-4-phenylquinolin-2(1H)-one (50).



Compound **50** was synthesized via general procedure C₃ using **94c** (65 mg, 0.15 mmol) with acetic anhydride **116** (28 μ L, 0.30 mmol) (165 °C, 200 W). Purification was performed by direct phase flash chromatography (SiO₂, A= DCM, B= MeOH, gradient 0–1.5% B) to afford **50** (30 mg, yield 43%). ¹H NMR (400 MHz, DMSO-*d*₆) δ 12.37 (s, 1H), 7.63 (dd, *J* = 8.8, 2.0 Hz, 1H), 7.55–7.52 (m, 3H), 7.45 (d, *J* = 8.8 Hz, 1H), 7.40–7.39 (m, 1H), 7.29 (d, *J* = 6.8 Hz, 1H), 6.93 (d, *J* = 2.0 Hz, 1H), 6.75 (dd, *J* = 8.8, 16.0 Hz, 4H), 5.24 (dd, *J* = 12.0, 4.0 Hz, 1H), 3.72 (s, 3H), 3.70–3.65 (m, 1H), 2.83 (dd, *J* = 4.4, 18.4 Hz, 2H), 1.84 (s, 3H). ¹³C NMR (101 MHz, DMSO-*d*₆) δ 167.42, 160.60, 158.70, 152.63, 150.29, 137.75, 135.14, 134.79, 131.60, 129.80, 129.09, 128.92, 128.78, 128.75, 127.24, 126.52, 126.49, 125.13, 121.14, 118.07, 114.15, 58.67, 55.49, 45.74, 21.90. ESI-MS for $C_{27}H_{22}ClN_3O_3$: calculated 471.1, found m/z 472.2, 474.2, $[M + H]^+$; 470.3, 472.3 $[M - H]^-$. UPLC-MS purity (UV at 215 nm) 99%.

3-(1-Acetyl-5-(4-(tert-butyl)phenyl)-4,5-dihydro-1H-pyrazol-3-yl)-6-chloro-4-phenylquinolin-2(1H)-one (51).

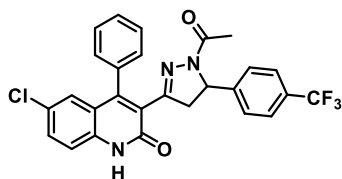
3-yl)-6-chloro-4-



Compound **51** was synthesized via general procedure C₃ using **95c** (141 mg, 0.31 mmol) with acetic anhydride **116** (59 μ L, 0.62 mmol) (165 $^{\circ}$ C, 200 W). Purification was performed by direct phase flash chromatography (SiO₂ gold 24 g, A= DCM, B= EtOH, gradient 0–5% B) to afford **51** (105 mg, yield 68%). ¹H NMR (400 MHz, DMSO-*d*₆) δ 12.36 (s, 1H), 7.63 (dt, *J* = 9.8, 4.9 Hz, 1H), 7.60–7.48 (m, 3H), 7.44 (t, *J* = 9.5 Hz, 1H), 7.41–7.36 (m, 1H), 7.30 (d, *J* = 7.1 Hz, 1H), 7.24 (d, *J* = 8.3 Hz, 2H), 6.94 (d, *J* = 2.3 Hz, 1H), 6.75 (d, *J* = 8.3 Hz, 2H), 5.32–5.17 (m, 1H), 3.69 (dt, *J* = 28.5, 14.3 Hz, 1H), 2.86 (dd, *J* = 18.4, 4.6 Hz, 1H), 1.86 (s, 3H), 1.27 (s, 9H). ¹³C NMR (101 MHz, DMSO-*d*₆) δ 167.01, 160.12, 152.20, 149.87, 149.25, 139.30, 137.30, 134.72, 131.14, 129.30, 128.66, 128.44, 128.31, 128.29, 126.07, 126.04, 125.16, 125.13, 124.65, 120.69, 117.60, 58.45, 45.30, 34.12, 31.10, 21.42. tR = 1.83 min. ESI-MS for C₃₀H₂₈ClN₃O₂: calculated 497.2, found *m/z* 498.5, 500.5 [M + H]⁺; 494.4, 496.4 [M – H][–]. UPLC–MS purity (UV at 215 nm) >99.5%.

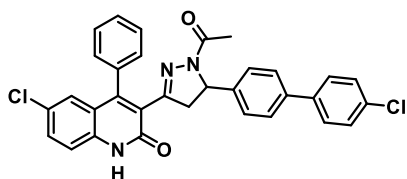
3-(1-Acetyl-5-(4-(trifluoromethyl)phenyl)-4,5-dihydro-1H-pyrazol-3-yl)-6-chloro-4-phenylquinolin-2(1H)-one (52).

3-yl)-6-chloro-4-



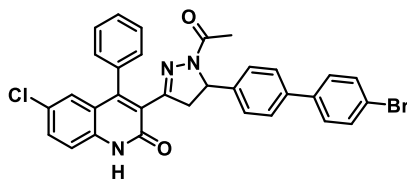
Compound **52** was synthesized via general procedure C₃ using **96c** (326 mg, 0.70 mmol) with acetic anhydride **116** (132 μ L, 1.40 mmol) (165 $^{\circ}$ C, 200 W). Purification was performed by direct phase flash chromatography (SiO₂ gold 24 g, A= DCM, B= EtOH, gradient 0–5% B) to afford **52** (268 mg, yield 74%). ¹H NMR (400 MHz, DMSO-*d*₆) δ 12.39 (s, 1H), 7.67–7.49 (m, 6H), 7.46 (d, *J* = 8.8 Hz, 1H), 7.44–7.39 (m, 1H), 7.32–7.25 (m, 1H), 7.03 (d, *J* = 8.0 Hz, 2H), 6.95 (d, *J* = 2.4 Hz, 1H), 5.42 (dd, *J* = 12.1, 4.7 Hz, 1H), 3.79 (dd, *J* = 18.5, 12.1 Hz, 1H), 2.87 (dd, *J* = 18.5, 4.8 Hz, 1H), 1.89 (s, 3H). ¹³C NMR (101 MHz, DMSO-*d*₆) δ 167.21, 160.08, 152.27, 150.01, 146.70, 137.34, 134.69, 131.23, 129.39, 128.54, 128.51, 128.33, 127.90, 127.58, 126.24, 126.11, 126.05, 125.52, 125.43, 125.39, 125.35, 124.41, 122.82, 120.62, 117.63, 58.36, 45.14, 21.30. tR = 2.55 min. ESI-MS for C₂₇H₁₉ClF₃N₃O₂: calculated 509.1, found *m/z* 510.5, 513.5 [M + H]⁺; 508.4, 510.4 [M – H][–]. UPLC–MS purity (UV at 215 nm) 99%.

3-(1-Acetyl-5-(4'-chloro-[1,1'-biphenyl]-4-yl)-4,5-dihydro-phenylquinolin-2(1H)-one (53). 1H-pyrazol-3-yl)-6-chloro-4-



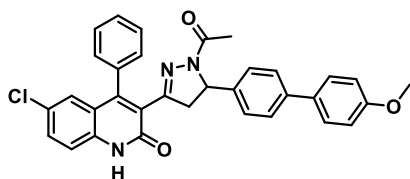
Compound **53** was synthesized via general procedure C₃ using **98c** (224 mg, 0.44 mmol) with acetic anhydride **116** (83 μ L, 0.88 mmol) (165 °C, 200 W). Purification was performed by direct phase flash chromatography (SiO₂ gold 24 g, A= DCM, B= EtOH, gradient 0–10% B) to afford **53** (245 mg, quantitative yield). ¹H NMR (400 MHz, DMSO-*d*₆) δ 12.37 (s, 1H), 7.71–7.48 (m, 10H), 7.48–7.39 (m, 2H), 7.29 (dt, *J* = 5.2, 2.0 Hz, 1H), 6.94 (d, *J* = 2.4 Hz, 1H), 6.90 (d, *J* = 8.3 Hz, 2H), 5.35 (dd, *J* = 12.1, 4.6 Hz, 1H), 3.78 (dd, *J* = 18.4, 12.1 Hz, 1H), 2.88 (dd, *J* = 18.5, 4.6 Hz, 1H), 1.88 (s, 3H). ¹³C NMR (101 MHz, DMSO-*d*₆) δ 167.09, 160.12, 152.23, 149.93, 141.80, 138.63, 137.66, 137.30, 134.73, 132.26, 131.16, 129.39, 128.82, 128.59, 128.49, 128.40, 128.37, 128.29, 126.74, 126.15, 126.10, 126.05, 124.60, 120.67, 117.60, 58.48, 45.29, 21.41. tR = 2.00 min. ESI-MS for C₃₂H₂₃Cl₂N₃O₂: calculated 551.1, found *m/z* 552.0, 554.0, 556.1 [M + H]⁺; 550.1, 552.1, 554.0 [M – H][–]. UPLC–MS purity (UV at 215 nm) 99%.

3-(1-Acetyl-5-(4'-bromo-[1,1'-biphenyl]-4-yl)-4,5-dihydro-phenylquinolin-2(1H)-one (54). 1H-pyrazol-3-yl)-6-chloro-4-



Compound **54** was synthesized via general procedure C₃ using **99c** (203 mg, 0.36 mmol) with acetic anhydride **116** (68 μ L, 0.72 mmol) (165 °C, 200 W). Purification was performed by direct phase flash chromatography (SiO₂ gold 24 g, A= DCM, B= EtOH, gradient 0–10% B) to afford **54** (175 mg, yield 80%). ¹H NMR (400 MHz, DMSO-*d*₆) δ 12.37 (s, 1H), 7.66–7.36 (m, 12H), 7.32–7.24 (m, 1H), 6.98–6.85 (m, 3H), 5.35 (dd, *J* = 12.0, 4.6 Hz, 1H), 3.78 (dd, *J* = 18.4, 12.1 Hz, 1H), 2.90 (dd, *J* = 18.4, 4.6 Hz, 1H), 1.88 (s, 3H). ¹³C NMR (101 MHz, DMSO-*d*₆) δ 167.10, 160.12, 152.20, 149.92, 141.81, 138.97, 137.70, 137.30, 134.73, 131.71, 131.12, 129.36, 128.67, 128.58, 128.46, 128.36, 128.27, 126.67, 126.17, 126.12, 126.04, 124.57, 120.84, 120.65, 117.58, 79.15, 58.51, 45.28, 21.39. tR = 2.52 min. ESI-MS for C₃₂H₂₃BrClN₃O₂: calculated 595.1, found *m/z* 595.9, 597.9, 600.0 [M + H]⁺; 594.0, 596.0, 597.9 [M – H][–]. UPLC–MS purity (UV at 215 nm) 99%.

3-(1-Acetyl-5-(4'-methoxy-[1,1'-biphenyl]-4-yl)-4,5-dihydro-1H-pyrazol-3-yl)-6-chloro-4-phenylquinolin-2(1H)-one (55).



Compound **55** was synthesized via general procedure C₃ using **100c** (179 mg, 0.35 mmol) with acetic anhydride **116** (66 μ L, 0.70 mmol) (165 °C, 200 W). Purification was performed by direct phase flash chromatography (SiO₂ gold 24 g, A= DCM, B= EtOH, gradient 0–8% B) to afford **55** (158 mg, yield 83%). ¹H NMR (400 MHz, DMSO-*d*₆) δ 12.39 (s, 1H), 7.63 (dd, *J* = 8.8, 2.4 Hz, 1H), 7.60–7.53 (m, 5H), 7.45 (d, *J* = 8.5 Hz, 3H), 7.43–7.39 (m, 1H), 7.31–7.27 (m, 1H), 7.03–6.99 (m, 2H), 6.94 (d, *J* = 2.4 Hz, 1H), 6.86 (d, *J* = 8.3 Hz, 2H), 5.33 (dd, *J* = 12.1, 4.6 Hz, 1H), 3.79 (s, 4H), 2.88 (dd, *J* = 18.5, 4.6 Hz, 1H), 1.88 (s, 3H). ¹³C NMR (101 MHz, DMSO-*d*₆) δ 167.09, 160.17, 158.87, 152.28, 149.95, 140.70, 138.74, 137.33, 134.75, 132.24, 131.20, 129.43, 128.64, 128.53, 128.43, 128.33, 127.72, 126.28, 126.12, 126.08, 126.04, 124.66, 120.71, 117.64, 114.35, 58.53, 55.16, 45.34, 21.47. *t*R = 1.65 min. ESI-MS for C₃₃H₂₆ClN₃O₃: calculated 547.2, found *m/z* 548.0, 550.0 [*M* + *H*]⁺; 546.0, 548.0 [*M* – *H*][–]. UPLC–MS purity (UV at 215 nm) >99.5%.

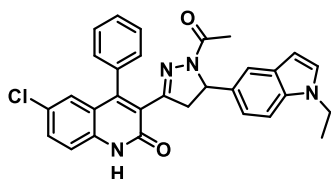
3-(1-Acetyl-5-(1-methyl-1H-indol-5-yl)-4,5-dihydro-1H-pyrazol-3-yl)-6-chloro-4-phenylquinolin-2(1H)-one (56).



Compound **56** was synthesized via general procedure C₃ using **101c** (127 mg, 0.28 mmol) with acetic anhydride **116** (53 μ L, 0.56 mmol) (165 °C, 200 W). Purification was performed by direct phase flash chromatography (SiO₂ gold 24 g, A= DCM, B= EtOH, gradient 0–10% B) to afford **56** (107 mg, yield 75%). ¹H NMR (400 MHz, DMSO-*d*₆) δ 12.36 (s, 1H), 7.64–7.56 (m, 3H), 7.53 (ddd, *J* = 8.9, 5.6, 3.3 Hz, 1H), 7.47– 7.40 (m, 2H), 7.31–7.23 (m, 3H), 6.99 (d, *J* = 1.7 Hz, 1H), 6.94 (d, *J* = 2.3 Hz, 1H), 6.65 (dd, *J* = 8.5, 1.7 Hz, 1H), 6.35 (dd, *J* = 3.1, 0.8 Hz, 1H), 5.36 (dd, *J* = 12.0, 4.5 Hz, 1H), 3.75 (s, 4H), 2.90 (dd, *J* = 18.4, 4.6 Hz, 1H), 1.86 (s, 3H). ¹³C NMR (101 MHz, DMSO- *d*₆) δ 166.93, 160.20, 152.06, 149.80, 137.30, 135.61, 134.79, 133.10, 131.09, 129.92, 129.46, 128.59, 128.47, 128.37, 128.23, 127.74, 126.06, 124.81, 120.74, 119.02, 117.58, 117.16, 109.63, 100.26, 59.32, 45.86, 32.45, 21.54. *t*R = 2.41 min. ESI-MS for C₂₉H₂₃ClN₄O₂: calculated 494.1, found *m/z* 495.2, 497.2 [*M* + *H*]⁺; 493.3, 495.3 [*M* – *H*][–]. UPLC–MS purity (UV at 215 nm) >99.5%.

3-(1-Acetyl-5-(1-ethyl-1*H*-indol-5-yl)-4,5-dihydro-1*H*-pyrazol-3-yl)-6-chloro-4-phenylquinolin-2(1*H*)-one (57).

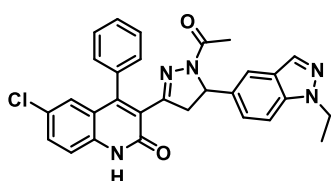
3-yl)-6-chloro-4-



Compound **57** was synthesized via general procedure C₃ using **102c** (168 mg, 0.36 mmol) with acetic anhydride **116** (68 μ L, 0.72 mmol) (165 $^{\circ}$ C, 200 W). Purification was performed by direct phase flash chromatography (SiO₂ gold 24 g, A= DCM, B= EtOH, gradient 0–10% B) to afford **57** (128 mg, yield 70%). ¹H NMR (400 MHz, DMSO-*d*₆) δ 12.36 (s, 1H), 7.64–7.50 (m, 4H), 7.47–7.40 (m, 2H), 7.35 (d, *J* = 3.1 Hz, 1H), 7.32–7.27 (m, 2H), 6.97 (dd, *J* = 22.0, 2.0 Hz, 2H), 6.64 (dd, *J* = 8.5, 1.7 Hz, 1H), 6.35 (dd, *J* = 3.1, 0.8 Hz, 1H), 5.35 (dd, *J* = 12.0, 4.6 Hz, 1H), 4.16 (q, *J* = 7.2 Hz, 2H), 3.78 (dd, *J* = 18.4, 12.0 Hz, 1H), 2.91 (dd, *J* = 18.4, 4.6 Hz, 1H), 1.86 (s, 3H), 1.33 (t, *J* = 7.2 Hz, 3H). ¹³C NMR (101 MHz, DMSO-*d*₆) δ 166.95, 160.20, 152.07, 149.81, 137.29, 134.80, 134.57, 133.07, 131.09, 129.43, 128.61, 128.47, 128.36, 128.31, 128.24, 127.90, 126.07, 124.82, 120.74, 118.97, 117.58, 117.29, 109.62, 100.48, 59.33, 45.85, 40.28, 21.55, 21.18, 15.52. *t*R = 2.51 min. ESI-MS for C₃₀H₂₅ClN₄O₂: calculated 508.2, found *m/z* 509.3, 511.2 [M + H]⁺; 507.3, 509.3 [M – H][–]. UPLC–MS purity (UV at 215 nm) >99.5%.

3-(1-Acetyl-5-(1-ethyl-1*H*-indazol-5-yl)-4,5-dihydro-1*H*-pyrazol-3-yl)-6-chloro-4-phenylquinolin-2(1*H*)-one (58).

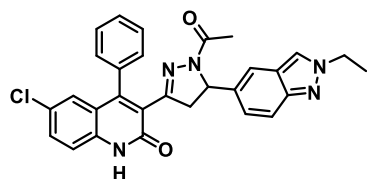
3-yl)-6-chloro-4-



Compound **58** was synthesized via general procedure C₃ using **103c** (131 mg, 0.28 mmol) with acetic anhydride **116** (53 μ L, 0.56 mmol) (165 $^{\circ}$ C, 200 W). Purification was performed by direct phase flash chromatography (SiO₂ gold 12 g, A= DCM, B= EtOH, gradient 0–5% B) to afford **58** (118 mg, yield 82%). ¹H NMR (400 MHz, DMSO-*d*₆) δ 12.37 (s, 1H), 7.98 (d, *J* = 0.9 Hz, 1H), 7.66–7.57 (m, 3H), 7.57–7.49 (m, 2H), 7.48–7.40 (m, 2H), 7.29 (ddt, *J* = 7.6, 2.0, 1.0 Hz, 1H), 7.15 (t, *J* = 1.1 Hz, 1H), 6.94 (d, *J* = 2.3 Hz, 1H), 6.84 (dd, *J* = 8.7, 1.6 Hz, 1H), 5.41 (dd, *J* = 12.0, 4.5 Hz, 1H), 4.41 (q, *J* = 7.2 Hz, 2H), 3.79 (dd, *J* = 18.5, 12.1 Hz, 1H), 2.88 (dd, *J* = 18.4, 4.6 Hz, 1H), 1.88 (s, 3H), 1.37 (t, *J* = 7.2 Hz, 3H). ¹³C NMR (101 MHz, DMSO-*d*₆) δ 167.05, 160.18, 152.21, 149.88, 138.03, 137.33, 134.72, 134.44, 132.33, 131.16, 129.51, 128.57, 128.41, 128.29, 126.08, 124.71, 124.11, 123.28, 120.72, 117.63, 117.30, 109.78, 58.90, 45.57, 43.06, 21.50, 14.95. *t*R = 2.29 min. ESI-MS for C₂₉H₂₄ClN₅O₂: calculated 509.2, found *m/z* 510.2, 512.2 [M + H]⁺, 508.3, 510.4 [M – H][–]. UPLC–MS purity (UV at 215 nm) 99%.

3-(1-Acetyl-5-(2-ethyl-2H-indazol-5-yl)-4,5-dihydro-1H-pyrazol-phenylquinolin-2(1H)-one (59).

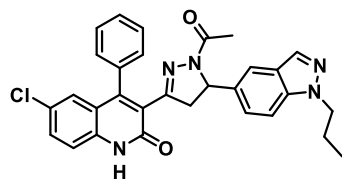
3-yl)-6-chloro-4-



Compound **59** was synthesized via general procedure C₃ using **104c** (80 mg, 0.17 mmol) with acetic anhydride **116** (32 μ L, 0.34 mmol) (165 °C, 200 W). Purification was performed by direct phase flash chromatography (SiO₂ gold 24 g, A= DCM, B= EtOH, gradient 0–10% B) to afford **59** (67 mg, yield 77%). ¹H NMR (400 MHz, DMSO-*d*₆) δ 12.37 (s, 1H), 8.31 (d, *J* = 0.9 Hz, 1H), 7.67–7.50 (m, 4H), 7.48–7.42 (m, 3H), 7.36–7.26 (m, 1H), 7.13–7.05 (m, 1H), 6.94 (d, *J* = 2.4 Hz, 1H), 6.65 (dd, *J* = 9.0, 1.7 Hz, 1H), 5.36 (dd, *J* = 12.0, 4.6 Hz, 1H), 4.44 (q, *J* = 7.3 Hz, 2H), 3.78 (dd, *J* = 18.4, 12.0 Hz, 1H), 2.87 (dd, *J* = 18.4, 4.6 Hz, 1H), 1.89 (s, 3H), 1.50 (t, *J* = 7.2 Hz, 3H). ¹³C NMR (101 MHz, DMSO-*d*₆) δ 167.04, 160.18, 152.20, 149.83, 147.32, 137.35, 134.71, 134.46, 131.13, 129.52, 128.57, 128.54, 128.37, 128.27, 126.04, 124.73, 123.59, 123.01, 120.93, 120.72, 117.63, 117.34, 116.65, 59.13, 47.69, 45.35, 21.52, 15.84. *t*R = 2.14 min. ESI-MS for C₂₉H₂₄ClN₅O₂: calculated 509.2, found *m/z* 510.2, 512.2 [M + H]⁺, 508.2, 510.3 [M – H][–]. UPLC– MS purity (UV at 215 nm) 99%.

3-(1-Acetyl-5-(1-propyl-1H-indazol-5-yl)-4,5-dihydro-1Hpyrazol-phenylquinolin-2(1H)-one (60).

3-yl)-6-chloro-4-



Compound **60** was synthesized via general procedure C₃ using **105c** (188 mg, 0.39 mmol) with acetic anhydride **116** (74 μ L, 0.78 mmol) (165 °C, 200 W). Purification was performed by direct phase flash chromatography (SiO₂ gold 24 g, A= DCM, B= EtOH, gradient 0–10% B) to afford **60** (184 mg, yield 90%). ¹H NMR (400 MHz, DMSO-*d*₆) δ 12.37 (s, 1H), 7.99 (d, *J* = 0.9 Hz, 1H), 7.65–7.57 (m, 3H), 7.56– 7.50 (m, 2H), 7.47–7.41 (m, 2H), 7.36–7.25 (m, 1H), 7.17–7.09 (m, 1H), 6.94 (d, *J* = 2.3 Hz, 1H), 6.85 (dd, *J* = 8.8, 1.7 Hz, 1H), 5.41 (dd, *J* = 12.0, 4.6 Hz, 1H), 4.33 (t, *J* = 6.9 Hz, 2H), 3.78 (dd, *J* = 18.5, 12.0 Hz, 1H), 2.89 (dd, *J* = 18.5, 4.6 Hz, 1H), 1.90–1.77 (m, 5H), 0.82 (t, *J* = 7.4 Hz, 3H). ¹³C NMR (101 MHz, DMSO-*d*₆) δ 167.06, 160.14, 152.20, 149.85, 147.37, 137.29, 134.69, 134.43, 131.13, 129.52, 128.53, 128.35, 128.26, 126.07, 124.73, 123.73, 123.58, 120.81, 120.71, 117.59, 117.37, 116.65, 59.13, 54.23, 45.34, 23.40, 21.51, 10.86. *t*R = 1.21 min. ESI-MS for C₃₀H₂₆ClN₅O₂: calculated 523.2, found *m/z* 524.1, 526.2 [M + H]⁺, 522.3, 524.2 [M – H][–]. UPLC–MS purity (UV at 215 nm) 94%.

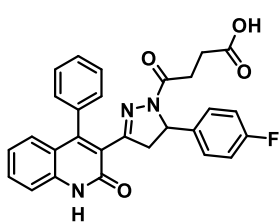
3-(1-Acetyl-5-(2-propyl-2H-indazol-5-yl)-4,5-dihydro-1H-pyrazol-3-yl)-6-chloro-4-phenylquinolin-2(1H)-one (61).

3-yl)-6-chloro-4-



Compound **61** was synthesized via general procedure C₃ using **106c** (132 mg, 0.27 mmol) with acetic anhydride **116** (51 μ L, 0.54 mmol) (165 °C, 200 W). Purification was performed by direct phase flash chromatography (SiO₂ gold 24 g, A= DCM, B= EtOH, gradient 0–10% B) to afford **61** (120 mg, yield 85%). ¹H NMR (400 MHz, DMSO-*d*₆) δ 12.37 (s, 1H), 8.29 (d, J = 1.0 Hz, 1H), 7.65–7.56 (m, 3H), 7.56–7.49 (m, 1H), 7.48–7.40 (m, 3H), 7.32–7.26 (m, 1H), 7.08 (t, J = 1.2 Hz, 1H), 6.93 (d, J = 2.3 Hz, 1H), 6.64 (dd, J = 8.9, 1.7 Hz, 1H), 5.35 (dd, J = 12.0, 4.5 Hz, 1H), 4.36 (t, J = 6.9 Hz, 2H), 3.77 (dd, J = 18.4, 12.0 Hz, 1H), 2.87 (dd, J = 18.4, 4.6 Hz, 1H), 1.97–1.83 (m, 5H), 0.83 (t, J = 7.4 Hz, 3H). ¹³C NMR (101 MHz, DMSO-*d*₆) δ 167.07, 160.15, 152.21, 149.85, 147.38, 137.31, 134.69, 134.43, 131.13, 129.52, 128.57, 128.53, 128.36, 128.26, 126.07, 126.04, 124.74, 123.74, 123.58, 120.81, 120.72, 117.61, 117.38, 116.65, 59.13, 54.24, 45.35, 23.41, 21.52, 10.87. tR = 1.01 min (apolar method). ESIMS for C₃₀H₂₆ClN₅O₂: calculated 523.2, found m/z 524.2, 526.2 [M + H]⁺, 522.3, 524.3 [M – H]⁻. UPLC–MS purity (UV at 215 nm) 99%.

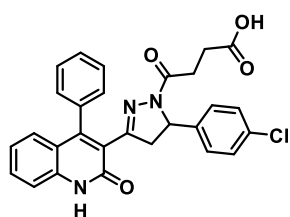
4-(5-(4-Fluorophenyl)-3-(2-oxo-4-phenyl-1,2-dihydroquinolin-3-yl)-4,5-dihydro-1H-pyrazol-1-yl)-4-oxobutanoic Acid (62).



Compound **62** was synthesized via general procedure C₁ using **109c** (150 mg, 0.39 mmol) with succinic anhydride **114** (78 mg, 0.78 mmol) (120 °C, 200 W). Purification was performed by direct phase flash chromatography (SiO₂ gold 24 g, A= DCM, B= EtOH, gradient 20–50% B) to afford **62** (114 mg, yield 59%). ¹H NMR (400 MHz, DMSO-*d*₆) δ 12.22 (s, 1H), 12.01 (s, 1H), 7.63–7.34 (m, 6H), 7.25 (dt, J = 6.8, 1.9 Hz, 1H), 7.14 (ddd, J = 8.2, 7.0, 1.2 Hz, 1H), 7.07–6.98 (m, 3H), 6.86–6.78 (m, 2H), 5.31 (dd, J = 12.0, 4.5 Hz, 1H), 3.72 (dd, J = 18.4, 12.0 Hz, 1H), 2.78 (dd, J = 18.4, 4.6 Hz, 1H), 2.47 (m, 2H), 2.32–2.25 (m, 2H). ¹³C NMR (101 MHz, DMSO-*d*₆) δ 173.48, 168.56, 160.25, 152.77, 151.05, 141.11, 138.53, 138.42, 135.16, 131.27, 129.38, 128.53, 128.22, 128.20, 128.13, 127.54, 127.45, 127.38, 123.30, 122.25, 119.35, 115.51, 115.16, 114.95, 58.16, 45.27, 28.58, 28.23. tR = 1.90 min. ESIMS for C₂₈H₂₂FN₃O₄: calculated 483.2, found m/z 484.5 [M + H]⁺, 482.5 [M – H]⁻. UPLC–MS purity (UV at 215 nm) >99.5%.

**4-(5-(4-Chlorophenyl)-3-(2-oxo-4-phenyl-1,2-dihydroquinolin-
pyrazol-1-yl)-4-oxobutanoic Acid (63).**

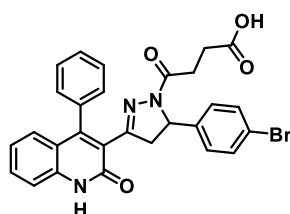
3-yl)-4,5-dihydro-1H-



Compound **63** was synthesized via general procedure C₁ using **110c** (121 mg, 0.27 mmol) with succinic anhydride **114** (54 mg, 0.54 mmol) (120 °C, 200 W). Purification was performed by direct phase flash chromatography (SiO₂ gold 24 g, A= DCM, B= EtOH, gradient 4–20% B) to afford **63** (130 mg, yield 67%). ¹H NMR (400 MHz, DMSO-*d*₆) δ 12.23 (s, 1H), 12.05 (s, 1H), 7.61–7.46 (m, 4H), 7.43 (dd, J = 8.3, 1.1 Hz, 1H), 7.39 (dt, J = 6.0, 2.0 Hz, 1H), 7.30–7.23 (m, 3H), 7.15 (ddd, J = 8.3, 7.0, 1.2 Hz, 1H), 7.05 (dd, J = 8.2, 1.4 Hz, 1H), 6.81 (d, J = 8.5 Hz, 2H), 5.31 (dd, J = 12.0, 4.6 Hz, 1H), 3.75 (dd, J = 18.5, 12.1 Hz, 1H), 2.78 (dd, J = 18.5, 4.6 Hz, 1H), 2.58–2.44 (m, 2H), 2.30 (t, J = 7.1 Hz, 2H). ¹³C NMR (101 MHz, DMSO-*d*₆) δ 173.95, 169.08, 160.73, 153.27, 151.57, 141.65, 139.02, 135.65, 132.01, 131.77, 129.89, 129.00, 128.79, 128.69, 128.62, 127.88, 123.73, 122.74, 119.83, 116.01, 58.72, 45.66, 29.04, 28.70. tR = 1.97 min. ESI-MS for C₂₈H₂₂ClN₃O₄: calculated 499.1, found m/z 500.4, 502.4 [M + H]⁺; 498.4, 500.3 [M – H][–]. UPLC–MS purity (UV at 215 nm) >99.5%.

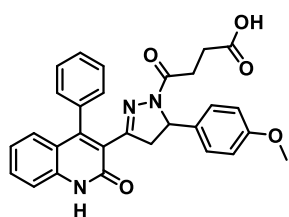
**4-(5-(4-Bromophenyl)-3-(2-oxo-4-phenyl-1,2-dihydroquinolin-
pyrazol-1-yl)-4-oxobutanoic Acid (64).**

3-yl)- 4,5-dihydro-1H-



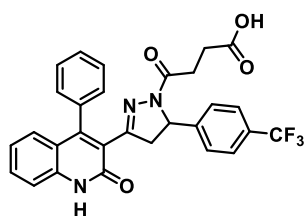
Compound **64** was synthesized via general procedure C₁ using **111c** (41 mg, 0.09 mmol) with succinic anhydride **114** (18 mg, 0.18 mmol) (120 °C, 200 W). Title compound **64** was obtained after the acidic workup (46 mg, yield 91%). ¹H NMR (400 MHz, DMSO-*d*₆) δ 12.22 (s, 1H), 12.01 (s, 1H), 7.61–7.45 (m, 4H), 7.45–7.36 (m, 4H), 7.25 (dt, J = 6.8, 1.9 Hz, 1H), 7.14 (ddd, J = 8.3, 7.0, 1.2 Hz, 1H), 7.04 (dd, J = 8.2, 1.4 Hz, 1H), 6.74 (d, J = 8.4 Hz, 2H), 5.29 (dd, J = 12.0, 4.6 Hz, 1H), 3.74 (dd, J = 18.4, 12.1 Hz, 1H), 2.77 (dd, J = 18.5, 4.6 Hz, 1H), 2.50 (m, 2H), 2.28 (t, J = 7.1 Hz, 2H). ¹³C NMR (101 MHz, DMSO- *d*₆) δ 173.46, 168.60, 160.25, 152.78, 151.09, 141.60, 138.54, 135.17, 131.29, 131.23, 129.41, 128.51, 128.21, 128.14, 127.75, 127.39, 123.23, 122.27, 121.42, 120.03, 119.35, 115.53, 58.30, 45.12, 28.55, 28.22. tR = 2.03 min. ESI-MS for C₂₈H₂₂BrN₃O₄: calculated 543.1, found m/z 544.5, 546.5 [M + H]⁺; 542.5, 544.4. UPLC–MS purity (UV at 215 nm) >99.5%.

4-(5-(4-Methoxyphenyl)-3-(2-oxo-4-phenyl-1,2-dihydroquinolin-3-yl)-4,5-dihydro-1H-pyrazol-1-yl)-4-oxobutanoic Acid (65).



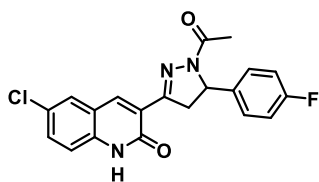
Compound **65** was synthesized via general procedure C₁ using **112c** (120 mg, 0.30 mmol) with succinic anhydride **114** (60 mg, 0.60 mmol) (120 °C, 200 W). Purification was performed by direct phase flash chromatography (SiO₂ gold 24 g, A= DCM, B= EtOH, gradient 5–35% B) to afford **65** (99 mg, yield 67%). ¹H NMR (400 MHz, DMSO-*d*₆) δ 12.21 (s, 1H), 12.00 (s, 1H), 7.61–7.34 (m, 6H), 7.29– 7.23 (m, 1H), 7.14 (ddd, J = 8.2, 7.0, 1.2 Hz, 1H), 7.04 (dd, J = 8.2, 1.4 Hz, 1H), 6.79–6.66 (m, 4H), 5.23 (dd, J = 11.9, 4.5 Hz, 1H), 3.72 (s, 4H), 2.79 (dd, J = 18.4, 4.5 Hz, 1H), 2.46 (dd, J = 6.8, 2.4 Hz, 2H), 2.27 (t, J = 6.9 Hz, 2H). ¹³C NMR (101 MHz, DMSO- *d*₆) δ 173.99, 168.91, 160.78, 158.68, 153.22, 151.47, 139.00, 135.70, 134.85, 131.71, 129.84, 129.08, 128.66, 128.60, 127.87, 127.27, 123.91, 122.71, 119.88, 115.99, 114.16, 58.85, 55.51, 45.80, 29.11, 28.74. tR = 1.83 min. ESI-MS for C₂₉H₂₅N₃O₅: calculated 495.1, found m/z 496.5 [M + H]⁺; 494.5 [M – H]⁻. UPLC–MS purity (UV at 215 nm) >99.5%.

4-Oxo-4-(3-(2-oxo-4-phenyl-1,2-dihydroquinolin-3-yl)-5-(4-(trifluoromethyl)phenyl)-4,5-dihydro-1H-pyrazol-1-yl)- butanoic Acid (66).



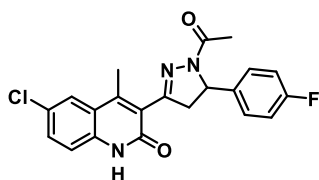
66 was synthesized via general procedure C₁ using **113c** (189 mg, 0.45 mmol) with succinic anhydride **114** (90 mg, 0.90 mmol) (120 °C, 200 W). Purification was performed by direct phase flash chromatography (SiO₂ gold 24 g, A= DCM, B= EtOH, gradient 2–50% B) to afford **66** (173 mg, yield 71%). ¹H NMR (400 MHz, DMSO-*d*₆) δ 12.23 (s, 1H), 12.02 (s, 1H), 7.64–7.36 (m, 8H), 7.25 (d, J = 7.3 Hz, 1H), 7.15 (ddd, J = 8.3, 7.1, 1.2 Hz, 1H), 7.08–6.98 (m, 3H), 5.42 (dd, J = 12.1, 4.7 Hz, 1H), 3.79 (dd, J = 18.5, 12.1 Hz, 1H), 2.81 (dd, J = 18.5, 4.7 Hz, 1H), 2.59–2.48 (m, 2H), 2.36–2.26 (m, 2H). ¹³C NMR (101 MHz, DMSO-*d*₆) δ 173.94, 169.21, 160.71, 153.30, 151.65, 147.20, 139.03, 135.67, 131.80, 129.88, 128.96, 128.70, 128.65, 128.29, 127.88, 126.70, 126.02, 125.84, 125.80, 123.63, 123.31, 122.76, 119.81, 116.02, 58.95, 45.63, 28.99, 28.68. tR = 2.06 min. ESI-MS for C₂₉H₂₂F₃N₃O₄: calculated 533.2, found m/z 534.5 [M + H]⁺; 532.5 [M – H]⁻. UPLC–MS purity (UV at 215 nm) >99.5%.

3-(1-Acetyl-5-(4-fluorophenyl)-4,5-dihydro-1H-pyrazol-3-yl)-6-chloroquinolin-2(1H)-one (67)



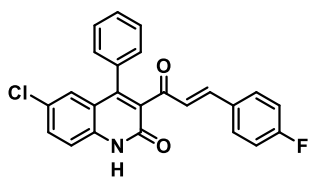
Compound **67** was synthesized via general procedure C₃ using **134** (200 mg, 0.59 mmol) with acetic anhydride **116** (67 μ L, 0.71 mmol) (165 °C, 200 W). Purification was performed by washing with cold THF to afford **67** as white-yellow pure solid (185 mg, yield 82%). ¹H NMR (400 MHz, DMSO-*d*₆) δ 12.17 (s, 1H), 8.50 (s, 1H), 7.96 (d, *J* = 1.9 Hz, 1H), 7.58 (dd, *J* = 8.8, 2.1 Hz, 1H), 7.33 (d, *J* = 8.8 Hz, 1H), 7.27 – 7.20 (m, 2H), 7.15 (t, *J* = 8.8 Hz, 2H), 5.52 (dd, *J* = 11.8, 4.3 Hz, 1H), 3.94 (dd, *J* = 18.8, 12.0 Hz, 1H), 3.27 (d, *J* = 4.4 Hz, 1H), 2.31 (s, 3H). ¹³C NMR (101 MHz, DMSO-*d*₆) δ 167.98, 160.52, 152.91, 138.33, 137.86, 131.74, 128.10, 127.98, 127.90, 126.50, 124.97, 120.28, 117.31, 115.87, 115.65, 59.22, 44.77, 22.14. ESI-MS for C₂₀H₁₅ClFN₃O₂: calculated 383.80, found *m/z* 383.00 [*M* - H]⁻. UPLC-MS purity (UV at 215 nm) 96%.

3-(1-acetyl-5-(4-fluorophenyl)-4,5-dihydro-1H-pyrazol-3-yl)-6-chloro-4-methylquinolin-2(1H)-one (68)



Compound **68** was synthesized via general procedure C₃ using **140** (200 mg, 0.56 mmol) with acetic anhydride **116** (64 μ L, 0.67 mmol) (165 °C, 200 W). Purification was performed by direct phase flash chromatography (SiO₂, A= DCM, B= MeOH, gradient 1–2% B) to afford **68** as white-off pure solid (90 mg, yield 40%). ¹H NMR (401 MHz, DMSO-*d*₆) δ 12.07 (s, 1H), 7.89 (d, *J* = 2.2 Hz, 1H), 7.61 (dd, *J* = 8.8, 2.2 Hz, 1H), 7.36 (dd, *J* = 8.6, 4.7 Hz, 3H), 7.18 (t, *J* = 8.8 Hz, 2H), 5.53 (dd, *J* = 12.0, 4.6 Hz, 1H), 3.79 (dd, *J* = 18.4, 12.0 Hz, 1H), 3.12 (dd, *J* = 18.4, 4.6 Hz, 1H), 2.53 (s, 3H), 2.22 (s, 3H). ¹³C NMR (101 MHz, DMSO-*d*₆) δ 167.50, 160.07, 153.64, 146.43, 138.51, 136.80, 130.99, 127.93, 126.26, 125.07, 124.08, 120.59, 117.37, 115.36, 115.15, 58.34, 44.98, 21.77, 16.14. ESI-MS for C₂₁H₁₇ClFN₃O₂: calculated 397.09, found *m/z* 397.00 [*M* - H]⁻. UPLC-MS purity (UV at 215 nm) 97%.

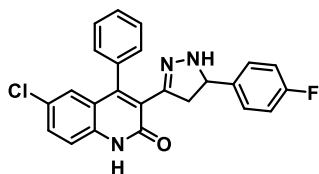
(E)-6-Chloro-3-(3-(4-fluorophenyl)acryloyl)-4-phenylquinolin-2(1H)-one (91b).



3-Acetyl-6-chloro-4-phenylquinolin-2(1H)-one **71a** (2.517 g, 8.45 mmol) and 4-fluorobenzaldehyde **73** (906 μ L, 8.45 mmol) were allowed to react overnight according to general procedure A. Purification was performed by direct phase flash chromatography (SiO₂ gold 40 g; A= DCM, B= EtOH, gradient 0–20% B) to afford **91b** (2.548 g, 75% yield). ¹H

NMR (400 MHz, DMSO- d_6) δ 12.35 (s, 1H), 7.81–7.70 (m, 2H), 7.66 (dd, J = 8.8, 2.4 Hz, 1H), 7.54–7.41 (m, 5H), 7.36–7.30 (m, 2H), 7.28–7.19 (m, 2H), 6.98 (d, J = 2.4 Hz, 1H), 6.73 (d, J = 16.4 Hz, 1H). t_R = 2.42 min. ESIMS for $C_{24}H_{15}ClFNO_2$: calculated 403.1, found m/z 404.1, 406.1 $[M + H]^+$; 402.1, 404.1 $[M - H]^-$.

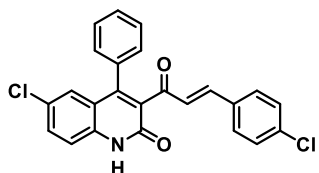
6-Chloro-3-(5-(4-fluorophenyl)-4,5-dihydro-1H-pyrazol-3-yl)-4-phenylquinolin-2(1H)-one (91c).



(*E*)-6-Chloro-3-(3-(4-fluorophenyl)acryloyl)-4-phenylquinolin-2(1H)-one **91b** (317 mg, 0.78 mmol) and hydrazine monohydrate (76 μ L, 1.56 mmol) were allowed to react according to general procedure B.

Crude compound was purified by flash column chromatography (SiO₂ gold 40 g; A= DCM, B= EtOH, gradient 0–20% B) to afford **91c** (303 mg, yield 92%). ¹H NMR (400 MHz, DMSO- d_6) δ 12.19 (s, 1H), 7.57 (dd, J = 8.8, 2.4 Hz, 1H), 7.50 (m, 2H), 7.41 (d, J = 8.8 Hz, 1H), 7.33 (dt, J = 6.9, 1.5 Hz, 1H), 7.23 (dt, J = 6.8, 2.0 Hz, 1H), 7.14 (d, J = 3.2 Hz, 1H), 7.13–7.02 (m, 4H), 6.89 (d, J = 2.3 Hz, 1H), 4.59 (td, J = 10.9, 10.2, 3.1 Hz, 1H), 3.23 (dd, J = 16.5, 11.0 Hz, 1H), 2.59–2.52 (m, 1H). t_R = 2.31 min. ESI-MS for $C_{24}H_{17}ClFN_3O$: calculated 417.1, found m/z 418.4, 420.4 $[M + H]^+$; 416.4, 418.3 $[M - H]^-$.

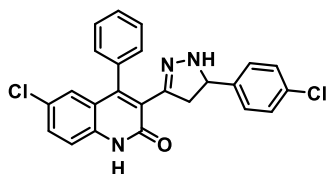
(*E*)-6-Chloro-3-(3-(4-chlorophenyl)acryloyl)-4-phenylquinolin-2(1H)-one (92b).



Compound **92b** was synthesized via general procedure A using **71a** (304 mg, 1.00 mmol) and 4-chlorobenzaldehyde **74** (140 mg, 1.00 mmol). Title compound **92b** was obtained by precipitation and filtration from the reaction crude (429 mg, quantitative yield). ¹H NMR

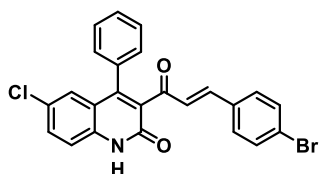
(400 MHz, DMSO- d_6) δ 7.70 (d, J = 8.6 Hz, 2H), 7.63 (dd, J = 8.8, 2.4 Hz, 1H), 7.55–7.37 (m, 7H), 7.32 (dd, J = 7.6, 1.9 Hz, 2H), 6.96 (d, J = 2.4 Hz, 1H), 6.78 (d, J = 16.4 Hz, 1H). t_R = 2.55 min. ESI-MS for $C_{24}H_{15}Cl_2NO_2$: calculated 419.0, found m/z 420.4, 422.4, 424.4 $[M + H]^+$; 418.5, 420.4, 422.3 $[M - H]^-$.

6-Chloro-3-(5-(4-chlorophenyl)-4,5-dihydro-1H-pyrazol-3-yl)-4-phenylquinolin-2(1H)-one (92c).



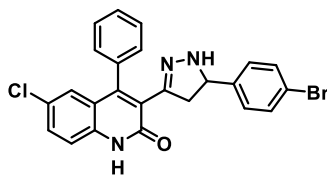
Compound **92c** was synthesized via general procedure B using **92b** (429 mg, 1.00 mmol) with hydrazine hydrate (97 μ L, 2.00 mmol). Purification was performed by direct phase flash chromatography (SiO₂ gold 24 g; A= DCM, B= EtOH, gradient 0–10% B) to afford **92c** (301 mg, yield 68%). ¹H NMR (400 MHz, DMSO-*d*₆) δ 12.20 (s, 1H), 7.58 (dd, J = 8.8, 2.4 Hz, 1H), 7.50 (tt, J = 7.5, 2.9 Hz, 3H), 7.42 (d, J = 8.8 Hz, 1H), 7.34 (dt, J = 7.0, 1.7 Hz, 1H), 7.30 (d, J = 8.4 Hz, 2H), 7.23 (dt, J = 7.3, 2.0 Hz, 1H), 7.18 (d, J = 3.2 Hz, 1H), 7.09 (d, J = 8.4 Hz, 2H), 6.90 (d, J = 2.3 Hz, 1H), 4.59 (td, J = 11.6, 9.3, 3.1 Hz, 1H), 3.25 (dd, J = 16.5, 11.1 Hz, 1H), 2.58–2.53 (m, 1H). tR = 2.45 min. ESI-MS for C₂₄H₁₇Cl₂N₃O: calculated 433.1, found m/z 434.4, 436.4, 438.5 [M + H]⁺; 432.4, 434.4, 436.4 [M – H]⁻.

(E)-3-(3-(4-Bromophenyl)acryloyl)-6-chloro-4-phenylquinolin-2(1H)-one (93b).



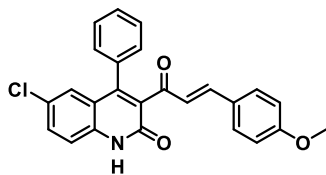
Compound **93b** was synthesized via general procedure A using **71a** (328 mg, 1.10 mmol) and 4-bromobenzaldehyde **75** (204 mg, 1.10 mmol). Title compound **93b** was obtained by precipitation and filtration from the reaction crude (511 mg, quantitative yield). ¹H NMR (400 MHz, DMSO-*d*₆) δ 7.67–7.47 (m, 6H), 7.46–7.35 (m, 4H), 7.30 (dd, J = 7.7, 1.8 Hz, 2H), 6.93 (d, J = 2.3 Hz, 1H), 6.80 (d, J = 16.4 Hz, 1H). tR = 2.59 min. ESI-MS for C₂₄H₁₅BrClNO₂: calculated 463.0, found m/z 464.3, 466.2, 468.2 [M + H]⁺; 462.2, 464.2, 466.2 [M – H]⁻.

3-(5-(4-Bromophenyl)-4,5-dihydro-1H-pyrazol-3-yl)-6-chloro-4-phenylquinolin-2(1H)-one (93c).



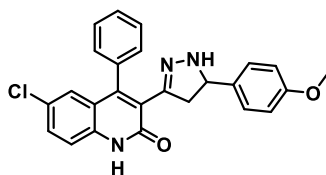
Compound **93c** was synthesized via general procedure B using **93b** (510 mg, 1.10 mmol) with hydrazine hydrate (110 μ L, 2.20 mmol). Purification was performed by direct phase flash chromatography (SiO₂, A= DCM, B= EtOH, gradient 0–8% B) to afford **93c** (349 mg, yield 64%). ¹H NMR (400 MHz, DMSO-*d*₆) δ 12.20 (s, 1H), 7.58 (dd, J = 8.8, 2.4 Hz, 1H), 7.56–7.45 (m, 3H), 7.42 (dd, J = 8.6, 5.5 Hz, 3H), 7.34 (dt, J = 7.2, 1.6 Hz, 1H), 7.23 (dt, J = 7.2, 2.0 Hz, 1H), 7.18 (d, J = 3.2 Hz, 1H), 7.07–6.99 (m, 2H), 6.89 (d, J = 2.3 Hz, 1H), 4.58 (td, J = 11.6, 9.3, 3.2 Hz, 1H), 3.25 (dd, J = 16.5, 11.1 Hz, 1H), 2.57–2.53 (m, 1H). tR = 2.50 min. ESI-MS for C₂₄H₁₇BrClN₃O: calculated 477.0, found m/z 478.2, 480.2, 482.2 [M + H]⁺; 476.3, 478.2, 480.3 [M – H]⁻.

(E)-6-Chloro-3-(3-(4-methoxyphenyl)acryloyl)-4-phenylquinolin-2(1H)-one (94b).



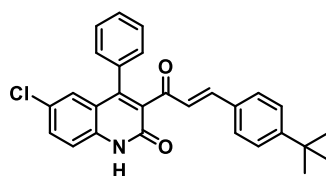
3-Acetyl-6-chloro-4-phenylquinolin-2(1H)-one **71a** (611 mg, 2.00 mmol) and p-anisaldehyde **76** (243 μ L, 2.00 mmol) were allowed to react overnight according to general procedure A. Purification was performed by direct phase flash chromatography (SiO₂ gold 40 g, A= DCM, B= EtOH, gradient 0–5% B), affording the desired **94b** (867 mg, quantitative yield). ¹H NMR (400 MHz, DMSO-*d*₆) δ 12.31 (s, 1H), 7.68–7.58 (m, 3H), 7.49–7.38 (m, 5H), 7.34–7.29 (m, 2H), 6.99–6.89 (m, 3H), 6.60 (d, *J* = 16.3 Hz, 1H), 3.78 (s, 3H). *t*R = 1.19 min. ESI-MS for C₂₅H₁₈ClNO₃: calculated 415.1, found *m/z* 416.4, 418.4 [M + H]⁺; 414.4, 416.4 [M – H][–].

6-Chloro-3-(5-(4-methoxyphenyl)-4,5-dihydro-1H-pyrazol-3-yl)-4-phenylquinolin-2(1H)-one (94c).



(*E*)-6-Chloro-3-(3-(4-methoxyphenyl)acryloyl)-4-phenylquinolin-2(1H)-one **94b** (780 mg, 1.9 mmol) and hydrazine monohydrate (185 μ L, 3.8 mmol) were allowed to react according to general procedure B. Crude compound was purified by flash column chromatography (SiO₂ gold 40 g; A= DCM, B= EtOH, gradient 0–10% B) to afford **94c** (611 mg, yield 75%). ¹H NMR (400 MHz, DMSO-*d*₆) δ 12.19 (s, 1H), 7.57 (dd, *J* = 8.8, 2.3 Hz, 1H), 7.53–7.47 (m, 3H), 7.42 (d, *J* = 8.8 Hz, 1H), 7.34 (dd, *J* = 10.3, 3.8 Hz, 1H), 7.27–7.19 (m, 1H), 7.02 (dd, *J* = 8.9, 5.9 Hz, 3H), 6.90 (d, *J* = 2.3 Hz, 1H), 6.80 (d, *J* = 8.7 Hz, 2H), 4.52 (td, *J* = 10.4, 2.9 Hz, 1H), 3.73 (s, 3H), 3.18 (dd, *J* = 16.4, 10.9 Hz, 1H), 2.58–2.53 (m, 1H). ¹³C NMR (101 MHz, DMSO-*d*₆) δ 166.84, 160.17, 152.10, 149.77, 149.57, 137.28, 134.76, 131.10, 129.96, 129.28, 128.71, 128.42, 128.30, 128.28, 126.41, 126.04, 124.80, 120.72, 117.58, 112.23, 58.37, 45.22, 40.19, 21.49. *t*R = 2.24 min. ESI-MS for C₂₅H₂₀ClN₃O₂: calculated 429.1, found *m/z* 430.4, 432.4 [M + H]⁺; 428.4, 430.5 [M – H][–].

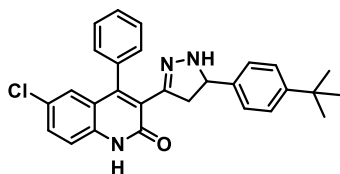
(E)-3-(3-(4-(*tert*-Butyl)phenyl)acryloyl)-6-chloro-4-phenylquinolin-2(1H)-one (95b).



Compound **95b** was synthesized via general procedure A using **71a** (543 mg, 1.80 mmol) and 4-*tert*-butylbenzaldehyde **77** (301 μ L, 1.80 mmol). Purification was performed by direct phase flash chromatography (SiO₂ gold 40 g; A= DCM, B= EtOH, gradient 0–10% B) to afford **95b** (441 mg, yield 55%). ¹H NMR (400 MHz, DMSO-*d*₆) δ 12.33 (s, 1H), 7.64 (dd, *J* = 8.8, 2.4 Hz, 1H), 7.58 (d, *J* = 8.5 Hz, 2H), 7.50–7.37 (m, 7H), 7.32 (dd, *J* = 7.7, 1.9 Hz, 2H), 6.97 (d, *J* = 2.4 Hz, 1H), 6.69 (d, *J* = 16.4 Hz, 1H), 1.26 (s, 9H). ¹³C NMR (101 MHz,

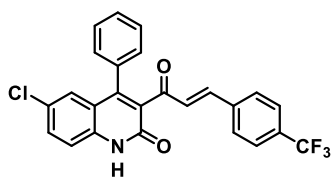
DMSO- d_6) δ 193.82, 159.40, 153.81, 146.61, 146.19, 137.50, 133.60, 132.56, 131.52, 130.89, 128.86, 128.80, 128.50, 128.43, 126.64, 126.05, 125.71, 125.56, 120.56, 117.68, 79.15, 34.62, 30.97, 30.82. Rt 2.18 min. ESI-MS for $C_{28}H_{24}ClNO_2$: calculated 441.1, found m/z 442.4, 444.4 $[M + H]^+$; 440.4, 442.4 $[M - H]^-$.

3-[5-(4-*tert*-Butylphenyl)-4,5-dihydro-1*H*-pyrazol-3-yl]-6-chloro-4-phenylquinolin-2(1*H*)-one (95c).



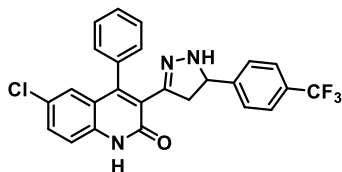
Compound **95c** was synthesized via general procedure B using **95b** (369 mg, 0.83 mmol) with hydrazine hydrate (81 μ L, 1.66 mmol). Purification was performed by direct phase flash chromatography (SiO_2 gold 24 g; A= CHX, B= EtOAc, gradient 0–90% B) to afford **95c** (351 mg, yield 93%). 1H NMR (400 MHz, DMSO- d_6) δ 12.20 (s, 1H), 7.56 (dd, $J = 8.8, 2.4$ Hz, 1H), 7.49 (dtd, $J = 9.6, 7.2, 5.3$ Hz, 3H), 7.42 (d, $J = 8.8$ Hz, 1H), 7.33 (dt, $J = 7.2, 1.7$ Hz, 1H), 7.25 (d, $J = 8.3$ Hz, 3H), 7.06 (d, $J = 3.0$ Hz, 1H), 7.02 (d, $J = 8.4$ Hz, 2H), 6.90 (d, $J = 2.3$ Hz, 1H), 4.54 (t, $J = 10.4$ Hz, 1H), 3.19 (dd, $J = 16.4, 10.9$ Hz, 1H), 2.58 (dd, $J = 16.4, 9.6$ Hz, 1H), 1.26 (s, 9H). ^{13}C NMR (101 MHz, DMSO- d_6) δ 160.54, 149.21, 148.30, 145.49, 140.31, 136.97, 135.21, 130.32, 129.19, 128.72, 128.26, 128.21, 128.14, 127.79, 127.18, 126.88, 126.33, 126.18, 125.75, 125.62, 124.92, 120.92, 117.33, 79.16, 62.69, 44.34, 34.09, 31.13, 31.05, 30.74. tR = 1.82 min. ESI-MS for $C_{28}H_{26}ClN_3O$: calculated 455.2, found m/z 456.5, 458.4, $[M + H]^+$; 454.5 456.5 $[M - H]^-$.

(*E*)-6-Chloro-4-phenyl-3-(3-(4-(trifluoromethyl)phenyl)acryloyl)quinolin-2(1*H*)-one (96b).



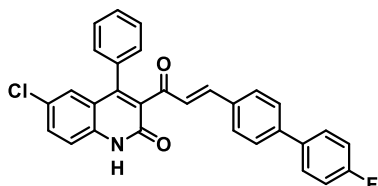
Compound **96b** was synthesized via general procedure A using **71a** (760 mg, 2.50 mmol) and 4-(trifluoromethyl)benzaldehyde **78** (341 μ L, 2.50 mmol). Purification was performed by direct phase flash chromatography (SiO_2 gold 40 g; A= DCM, B= EtOH, gradient 0–5% B) to afford **96b** (820 mg, yield 71%). 1H NMR (400 MHz, DMSO- d_6) δ 12.38 (s, 1H), 7.89 (d, $J = 8.2$ Hz, 2H), 7.74 (d, $J = 8.4$ Hz, 2H), 7.67 (dd, $J = 8.8, 2.4$ Hz, 1H), 7.62–7.57 (m, 1H), 7.53–7.40 (m, 4H), 7.36–7.31 (m, 2H), 6.99 (d, $J = 2.3$ Hz, 1H), 6.91 (d, $J = 16.5$ Hz, 1H). ^{13}C NMR (101 MHz, DMSO- d_6) δ 193.90, 159.39, 147.09, 144.03, 138.29, 137.58, 133.52, 132.23, 131.05, 130.34, 130.07, 130.02, 129.59, 129.19, 128.88, 128.48, 126.12, 125.68, 125.65, 125.62, 125.30, 122.59, 120.55, 117.74. tR = 1.65 min. ESI-MS for $C_{25}H_{15}ClF_3NO_2$: calculated 453.1, found m/z 454.4, 456.4 $[M + H]^+$; 452.4, 454.4 $[M - H]^-$.

6-Chloro-4-phenyl-3-(5-(4-(trifluoromethyl)phenyl)-4,5-dihydro-1H-pyrazol-3-yl)quinolin-2(1H)-one (96c).



Compound **96c** was synthesized via general procedure B using **96b** (752 mg, 1.70 mmol) with hydrazine hydrate (165 μ L, 3.40 mmol). Purification was performed by direct phase flash chromatography (SiO_2 gold 40 g; A= DCM, B= EtOH, gradient 0–5% B) to afford **96c** (696 mg, yield 90%). ^1H NMR (400 MHz, $\text{DMSO-}d_6$) δ 12.21 (s, 1H), 7.63–7.56 (m, 3H), 7.56–7.44 (m, 3H), 7.42 (d, J = 8.8 Hz, 1H), 7.37–7.32 (m, 1H), 7.29 (d, J = 8.5 Hz, 3H), 7.25–7.20 (m, 1H), 6.90 (d, J = 2.3 Hz, 1H), 4.75–4.64 (m, 1H), 3.39–3.25 (m, 1H), 2.63–2.54 (m, 1H). ^{13}C NMR (101 MHz, $\text{DMSO-}d_6$) δ 160.49, 148.49, 148.37, 145.45, 136.99, 135.13, 130.43, 129.25, 128.63, 128.29, 128.23, 128.20, 127.68, 127.22, 126.58, 125.79, 125.64, 125.11, 125.08, 122.95, 120.88, 117.37, 62.16, 44.50. t_R = 2.52 min. ESI-MS for $\text{C}_{25}\text{H}_{17}\text{ClF}_3\text{N}_3\text{O}$: calculated 467.1, found m/z 468.4, 469.5 $[\text{M} + \text{H}]^+$, 466.4, 468.4 $[\text{M} - \text{H}]^-$.

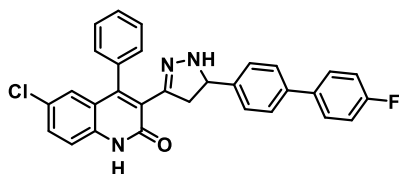
(E)-6-Chloro-3-(3-(4'-fluoro-[1,1'-biphenyl]-4-yl)acryloyl)-4-phenylquinolin-2(1H)-one (97b).



Compound **97b** was synthesized via general procedure A using **71a** (214 mg, 0.72 mmol) and 4'-fluoro-[1,1'-biphenyl]-4-carbaldehyde **79** (144 mg, 0.72 mmol). Purification was performed by direct phase flash chromatography (SiO_2 gold 24 g; A= CHCl_3 , B= EtOH, gradient 0–7% B) to afford **97b** (305 mg, yield 89%). ^1H NMR (400 MHz, $\text{DMSO-}d_6$) δ 12.35 (s, 1H), 7.82–7.62 (m, 7H), 7.57–7.40 (m, 5H), 7.36–7.26 (m, 4H), 6.98 (d, J = 2.3 Hz, 1H), 6.80 (d, J = 16.4 Hz, 1H). ^{13}C NMR (101 MHz, $\text{DMSO-}d_6$) δ 193.83, 163.40, 160.96, 159.45, 146.77, 145.64, 141.15, 137.55, 135.57, 135.54, 133.63, 133.34, 132.54, 131.52, 131.42, 130.93, 129.33, 128.90, 128.84, 128.80, 128.72, 128.46, 127.29, 126.98, 126.10, 125.60, 120.59, 117.71, 115.91, 115.70. t_R = 1.90 min. ESI-MS for $\text{C}_{30}\text{H}_{19}\text{ClFNO}_2$: calculated 479.1, found m/z 480.2, 482.2 $[\text{M} + \text{H}]^+$, 478.2, 480.5 $[\text{M} - \text{H}]^-$.

6-Chloro-3-(5-(4'-fluoro-[1,1'-biphenyl]-4-yl)-4,5-dihydro-phenylquinolin-2(1H)-one (97c).

1H-pyrazol-3-yl)-4-

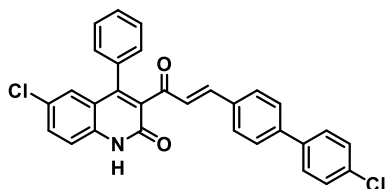


Compound **97c** was synthesized via general procedure B using **97b** (273 mg, 0.57 mmol) with hydrazine hydrate (55 μ L, 1.14 mmol). Purification was performed by direct phase flash chromatography (SiO₂ gold 24 g; A= DCM, B= EtOH, gradient

0–10% B) to afford **97c** (188 mg, yield 67%). ¹H NMR (400 MHz, DMSO-*d*₆) δ 12.18 (s, 1H), 7.71–7.64 (m, 2H), 7.60–7.46 (m, 6H), 7.42 (d, *J* = 8.8 Hz, 1H), 7.37–7.32 (m, 1H), 7.31–7.21 (m, 3H), 7.19–7.13 (m, 3H), 6.90 (d, *J* = 2.3 Hz, 1H), 4.67–4.57 (m, 1H), 3.26 (dd, *J* = 16.6, 11.1 Hz, 1H), 2.60 (dd, *J* = 16.4, 9.5 Hz, 1H). ¹³C NMR (101 MHz, DMSO-*d*₆) δ 162.98, 160.55, 160.52, 148.35, 145.48, 142.66, 137.78, 136.96, 136.44, 136.41, 135.19, 130.33, 129.22, 128.69, 128.51, 128.43, 128.25, 128.17, 127.06, 126.78, 126.48, 125.75, 125.62, 120.91, 117.32, 115.73, 115.52, 62.49, 44.43. tR = 1.72 min. ESI-MS for C₃₀H₂₁ClFN₃O: calculated 493.1, found *m/z* 494.2, 496.1 [M + H]⁺, 492.2, 494.2 [M – H][–].

(E)-6-Chloro-3-(3-(4'-chloro-[1,1'-biphenyl]-4-yl)acryloyl)-4-

phenylquinolin-2(1H)-one (98b).

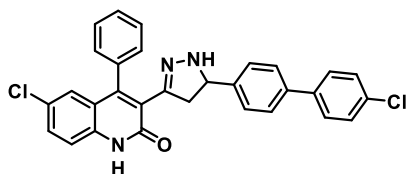


Compound **98b** was synthesized via general procedure A using **71a** (339 mg, 1.10 mmol) and 4'-chloro-[1,1'-biphenyl]-4-carbaldehyde **80** (238 mg, 1.10 mmol). Purification was performed by direct phase flash chromatography (SiO₂ gold 24

g; A= DCM, B= EtOH, gradient 0–5% B) to afford **98b** (567 mg, quantitative yield). ¹H NMR (400 MHz, DMSO-*d*₆) δ 12.35 (s, 1H), 7.78–7.68 (m, 6H), 7.65 (dd, *J* = 8.8, 2.4 Hz, 1H), 7.57–7.48 (m, 3H), 7.48–7.40 (m, 4H), 7.34 (dd, *J* = 7.8, 1.8 Hz, 2H), 6.99 (d, *J* = 2.3 Hz, 1H), 6.81 (d, *J* = 16.4 Hz, 1H). ¹³C NMR (101 MHz, DMSO-*d*₆) δ 193.80, 159.41, 146.75, 145.51, 140.78, 137.87, 137.53, 133.70, 133.61, 132.90, 132.51, 130.92, 129.34, 128.93, 128.88, 128.82, 128.45, 127.42, 126.98, 126.07, 125.58, 120.57, 117.69, 79.15. tR = 2.16 min. ESI-MS for C₃₀H₁₉Cl₂NO₂: calculated 495.1, found *m/z* 496.0, 497.9, 499.9, [M + H]⁺; 494.1, 496.0, 498.0 [M – H][–].

6-Chloro-3-(5-(4'-chloro-[1,1'-biphenyl]-4-yl)-4,5-dihydro-phenylquinolin-2(1H)-one (98c).

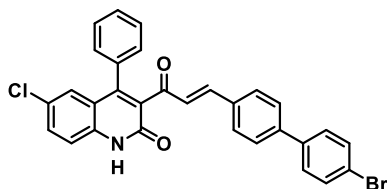
1H-pyrazol-3-yl)-4-



Compound **98c** was synthesized via general procedure B using **98b** (558 mg, 1.10 mmol) with hydrazine hydrate (107 μ L, 2.20 mmol). Purification was performed by direct phase flash chromatography (SiO_2 gold 40 g; A= DCM, B= EtOH, gradient 0–15% B) to afford **98c** (501 mg, yield 87%). ^1H NMR (400 MHz, $\text{DMSO}-d_6$) δ 12.20 (s, 1H), 7.69–7.63 (m, 2H), 7.59–7.46 (m, 8H), 7.41 (d, J = 8.7 Hz, 1H), 7.37–7.31 (m, 1H), 7.26–7.20 (m, 1H), 7.17 (d, J = 8.3 Hz, 2H), 6.90 (d, J = 2.3 Hz, 1H), 4.63 (ddd, J = 11.3, 9.5, 3.0 Hz, 1H), 3.27 (dd, J = 16.4, 11.1 Hz, 1H), 2.60 (dd, J = 16.4, 9.4 Hz, 1H). ^{13}C NMR (101 MHz, $\text{DMSO}-d_6$) δ 160.53, 148.37, 145.49, 143.11, 138.74, 137.45, 136.97, 135.20, 132.16, 130.35, 129.23, 128.82, 128.69, 128.28, 128.18, 127.14, 126.77, 126.49, 125.77, 125.63, 120.91, 117.34, 62.49, 44.45. t_R = 1.99 min. ESI-MS for $\text{C}_{30}\text{H}_{21}\text{Cl}_2\text{N}_3\text{O}$: calculated 509.1, found m/z 510.0, 511.9, 514.0 $[\text{M} + \text{H}]^+$; 508.0, 510.0, 511.9 $[\text{M} - \text{H}]^-$.

(E)-3-(3-(4'-Bromo-[1,1'-biphenyl]-4-yl)acryloyl)-6-chloro-4-

phenylquinolin-2(1H)-one (99b).



Compound **99b** was synthesized via general procedure A using **71a** (337 mg, 1.10 mmol) and 4'-bromo-[1,1'-biphenyl]-4-carbaldehyde **81** (287 mg, 1.10 mmol). Purification was performed by direct phase flash chromatography (SiO_2 gold 24 g; 0 A= DCM, B= EtOH, gradient 0–5% B) to afford **99b** (576 mg, yield 89%). ^1H NMR (400 MHz, $\text{DMSO}-d_6$) δ 12.35 (s, 1H), 7.80–7.68 (m, 4H), 7.68–7.62 (m, 5H), 7.57–7.39 (m, 5H), 7.34 (dd, J = 7.7, 1.8 Hz, 2H), 6.99 (d, J = 2.3 Hz, 1H), 6.81 (d, J = 16.4 Hz, 1H). ^{13}C NMR (101 MHz, $\text{DMSO}-d_6$) δ 193.81, 159.41, 146.76, 145.52, 140.83, 138.24, 137.53, 133.74, 133.60, 132.51, 131.85, 130.92, 129.36, 128.88, 128.82, 128.77, 128.44, 127.43, 126.94, 126.07, 125.58, 121.53, 120.57, 117.69, 79.15. t_R = 2.20 min. ESI-MS for $\text{C}_{30}\text{H}_{19}\text{BrClNO}_2$: calculated 539.0, found m/z 539.9, 541.9, 543.9 $[\text{M} + \text{H}]^+$; 538.0, 540.0, 542.0 $[\text{M} - \text{H}]^-$.

3-(5-(4'-Bromo-[1,1'-biphenyl]-4-yl)-4,5-dihydro-1H-pyrazol-3-yl)-6-chloro-4-

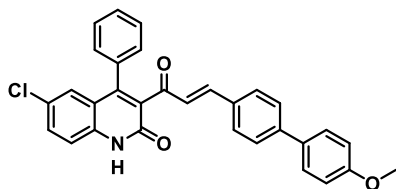
phenylquinolin-2(1H)-one (99c).



Compound **99c** was synthesized via general procedure B using **99b** (570 mg, 1.00 mmol) with hydrazine hydrate (97 μ L, 2.00 mmol). Purification was performed by direct phase flash chromatography (SiO_2 gold 24 g; A= DCM, B= EtOH, gradient

0–10% B) to afford **99c** (472 mg, yield 81%). ^1H NMR (400 MHz, $\text{DMSO-}d_6$) δ 12.20 (s, 1H), 7.68–7.46 (m, 10H), 7.41 (d, J = 8.8 Hz, 1H), 7.37–7.33 (m, 1H), 7.26–7.21 (m, 1H), 7.19–7.15 (m, 3H), 6.90 (d, J = 2.4 Hz, 1H), 4.63 (ddd, J = 11.3, 9.5, 3.1 Hz, 1H), 3.27 (dd, J = 16.4, 11.0 Hz, 1H), 2.60 (dd, J = 16.4, 9.4 Hz, 1H). ^{13}C NMR (101 MHz, $\text{DMSO-}d_6$) δ 160.53, 148.37, 145.48, 143.17, 139.11, 137.48, 136.97, 135.20, 131.74, 130.36, 129.23, 128.69, 128.63, 128.27, 128.18, 127.16, 126.77, 126.45, 125.76, 125.63, 120.91, 120.72, 117.34, 79.15, 62.49, 44.45, 40.15, 39.99, 39.94, 39.73, 39.52, 39.31, 39.10, 38.89. t_R = 2.05 min. ESI-MS for $\text{C}_{30}\text{H}_{21}\text{BrClN}_3\text{O}$: calculated 553.0, found m/z 553.9, 555.9, 557.9 [$\text{M} + \text{H}$] $^+$, 551.9, 554.0, 556.0 [$\text{M} - \text{H}$] $^-$.

(E)-6-Chloro-3-(3-(4'-methoxy-[1,1'-biphenyl]-4-yl)-acryloyl)-4-phenylquinolin-2(1H)-one (100b).

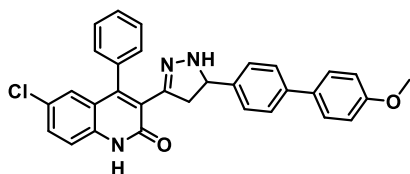


Compound **100b** was synthesized via general procedure A using **71a** (430 mg, 1.40 mmol) and 4'-methoxy-[1,1'-biphenyl]-4-carbaldehyde **82** (297 mg, 1.40 mmol). Purification was performed by direct phase flash chromatography (SiO_2 gold 24

g; A= DCM, B= EtOH, gradient 0–10% B) to afford **100b** (528 mg, yield 74%). ^1H NMR (400 MHz, $\text{DMSO-}d_6$) δ 12.35 (s, 1H), 7.75–7.62 (m, 6H), 7.55–7.40 (m, 6H), 7.33 (ddt, J = 6.7, 3.2, 1.8 Hz, 2H), 7.05–7.00 (m, 2H), 6.98 (d, J = 2.4 Hz, 1H), 6.77 (d, J = 16.4 Hz, 1H), 3.79 (s, 3H). ^{13}C NMR (101 MHz, $\text{DMSO-}d_6$) δ 193.75, 159.42, 159.38, 159.07, 146.68, 145.85, 141.92, 137.52, 133.63, 132.58, 131.32, 131.13, 130.90, 129.30, 128.88, 128.81, 128.69, 128.65, 128.43, 127.84, 126.86, 126.37, 126.22, 126.06, 125.69, 125.57, 120.58, 117.69, 114.43, 55.19, 31.34. t_R = 1.81 min. ESI-MS for $\text{C}_{31}\text{H}_{22}\text{ClNO}_3$: calculated 491.1, found m/z 492.0, 494.0 [$\text{M} + \text{H}$] $^+$; 490.0, 492.1 [$\text{M} - \text{H}$] $^-$.

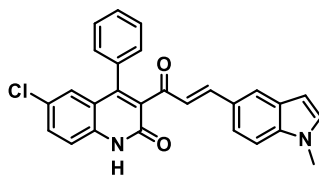
6-Chloro-3-(5-(4'-methoxy-[1,1'-biphenyl]-4-yl)-4,5-dihydro-phenylquinolin-2(1H)-one (100c).

1H-pyrazol-3-yl)-4-



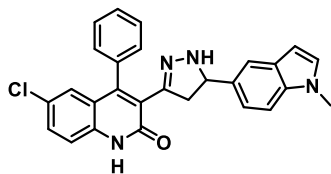
Compound **100c** was synthesized via general procedure B using **100b** (522 mg, 1.10 mmol) with hydrazine hydrate (107 μL , 2.20 mmol). Purification was performed by direct phase flash chromatography (SiO_2 gold 40 g; A= DCM, B= EtOH, gradient 0–10% B) to afford **100c** (412 mg, yield 77%). ^1H NMR (400 MHz, $\text{DMSO}-d_6$) δ 12.20 (s, 1H), 7.57 (dd, $J = 8.9, 2.4$ Hz, 3H), 7.54–7.44 (m, 5H), 7.41 (d, $J = 8.8$ Hz, 1H), 7.38– 7.31 (m, 1H), 7.24 (td, $J = 4.2, 3.7, 1.8$ Hz, 1H), 7.16–7.11 (m, 3H), 7.01 (d, $J = 8.8$ Hz, 2H), 6.90 (d, $J = 2.3$ Hz, 1H), 4.60 (ddd, $J = 11.0, 9.5, 3.1$ Hz, 1H), 3.79 (s, 3H), 3.25 (dd, $J = 16.4, 11.0$ Hz, 1H), 2.60 (dd, $J = 16.4, 9.5$ Hz, 1H). ^{13}C NMR (101 MHz, $\text{DMSO}-d_6$) δ 160.54, 158.79, 148.34, 145.49, 141.88, 138.51, 136.97, 135.21, 132.34, 130.35, 129.24, 128.71, 128.27, 128.18, 127.60, 126.99, 126.82, 126.01, 125.75, 125.63, 120.93, 117.33, 114.32, 62.58, 55.14, 44.44. $t\text{R} = 2.60$ min. ESI-MS for $\text{C}_{31}\text{H}_{24}\text{ClN}_3\text{O}_2$: calculated 505.2, found m/z 506.0, 508.0 $[\text{M} + \text{H}]^+$; 504.1, 506.1 $[\text{M} - \text{H}]^-$.

(E)-6-Chloro-3-(3-(1-methyl-1H-indol-5-yl)acryloyl)-4-phenylquinolin- 2(1H)-one (101b).



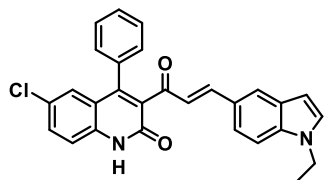
Compound **101b** was synthesized via general procedure A using **71a** (545 mg, 1.80 mmol) and 1-methyl- 1H-indole-5-carbaldehyde **83** (287 mg, 1.80 mmol). Purification was performed by direct phase flash chromatography (SiO_2 gold 24 g; A= DCM, B= EtOH, gradient 0–10% B) to afford **101b** (427 mg, yield 53%). ^1H NMR (400 MHz, $\text{DMSO}-d_6$) δ 12.31 (s, 1H), 7.86 (d, $J = 1.5$ Hz, 1H), 7.65 (dd, $J = 8.8, 2.3$ Hz, 1H), 7.56 (d, $J = 16.3$ Hz, 1H), 7.51–7.30 (m, 9H), 6.97 (d, $J = 2.3$ Hz, 1H), 6.65 (d, $J = 16.3$ Hz, 1H), 6.44 (dd, $J = 3.2, 0.7$ Hz, 1H), 3.79 (s, 3H). ^{13}C NMR (101 MHz, $\text{DMSO}-d_6$) δ 193.46, 159.48, 148.78, 146.31, 137.77, 137.46, 133.77, 132.92, 131.03, 130.76, 128.89, 128.72, 128.37, 128.15, 125.99, 125.53, 125.36, 124.31, 123.22, 121.09, 120.65, 117.63, 110.33, 101.50, 32.61. $t\text{R} = 2.45$ min. ESI-MS for $\text{C}_{27}\text{H}_{19}\text{ClN}_2\text{O}_2$: calculated 438.1, found m/z 439.2, 441.1 $[\text{M} + \text{H}]^+$; 437.3, 439.3 $[\text{M} - \text{H}]^-$.

6-Chloro-3-(5-(1-methyl-1*H*-indol-5-yl)-4,5-dihydro-1*H*-pyrazol-3-yl)-4-phenylquinolin-2(1*H*)-one (101c).



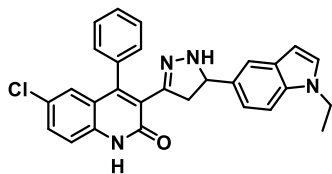
Compound **101c** was synthesized via general procedure B using **101b** (370 mg, 0.84 mmol) with hydrazine hydrate (82 μ L, 1.68 mmol). Purification was performed by direct phase flash chromatography (SiO₂ gold 24 g; A= DCM, B= EtOH, gradient 0–5% B) to afford **101c** (325 mg, yield 85%). ¹H NMR (400 MHz, DMSO-*d*₆) δ 12.20 (s, 1H), 7.57–7.46 (m, 4H), 7.41 (d, *J* = 8.8 Hz, 1H), 7.35 (dt, *J* = 7.2, 1.7 Hz, 1H), 7.31–7.21 (m, 4H), 7.02 (s, 1H), 6.91 (td, *J* = 3.9, 1.7 Hz, 2H), 6.34 (dd, *J* = 3.0, 0.7 Hz, 1H), 4.66 (t, *J* = 10.5 Hz, 1H), 3.75 (s, 3H), 3.22 (dd, *J* = 16.4, 11.0 Hz, 1H), 2.63 (dd, *J* = 16.4, 9.9 Hz, 1H). ¹³C NMR (101 MHz, DMSO-*d*₆) δ 160.60, 148.21, 145.51, 136.97, 135.70, 135.30, 133.87, 130.28, 129.72, 129.24, 128.74, 128.27, 128.17, 127.79, 127.03, 125.76, 125.62, 120.96, 120.01, 118.09, 117.32, 109.44, 100.21, 63.57, 44.92, 32.45. *t*R = 2.38 min. ESI-MS for C₂₇H₂₁ClN₄O: calculated 452.1, found *m/z* 453.2, 455.2 [M + H]⁺; 451.3, 453.3 [M – H][–].

(*E*)-6-Chloro-3-(3-(1-ethyl-1*H*-indol-5-yl)acryloyl)-4-phenylquinolin-2(1*H*)-one (102b).



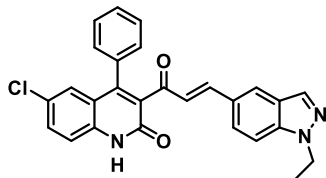
Compound **102b** was synthesized via general procedure A using **71a** (402 mg, 1.30 mmol) and 1-ethyl-1*H*-indole-5-carbaldehyde **84** (225 mg, 1.30 mmol). Purification was performed by direct phase flash chromatography (SiO₂ gold 40 g; A= DCM, B= EtOH, gradient 0–5% B) to afford **102b** (395 mg, yield 65%). ¹H NMR (400 MHz, DMSO-*d*₆) δ 12.31 (s, 1H), 7.85 (d, *J* = 1.4 Hz, 1H), 7.65 (dd, *J* = 8.8, 2.4 Hz, 1H), 7.56 (d, *J* = 16.3 Hz, 1H), 7.50–7.45 (m, 3H), 7.45–7.38 (m, 4H), 7.33 (dd, *J* = 7.7, 1.8 Hz, 2H), 6.97 (d, *J* = 2.3 Hz, 1H), 6.65 (d, *J* = 16.2 Hz, 1H), 6.45 (d, *J* = 3.1 Hz, 1H), 4.20 (q, *J* = 7.2 Hz, 2H), 1.34 (t, *J* = 7.2 Hz, 3H). ¹³C NMR (101 MHz, DMSO-*d*₆) δ 193.47, 159.48, 148.79, 146.30, 137.46, 136.80, 133.77, 132.92, 130.76, 129.42, 128.98, 128.89, 128.72, 128.66, 128.37, 128.30, 125.99, 125.53, 125.35, 124.27, 123.35, 121.02, 120.65, 117.63, 110.32, 101.75, 79.15, 15.44. *t*R = 2.56 min. ESI-MS for C₂₈H₂₁ClN₂O₂: calculated 452.1, found *m/z* 453.2, 455.2 [M + H]⁺; 451.3, 453.3 [M – H][–].

6-Chloro-3-(5-(1-ethyl-1*H*-indol-5-yl)-4,5-dihydro-1*H*-pyrazol-3-yl)-4-phenylquinolin-2(1*H*)-one (102c).



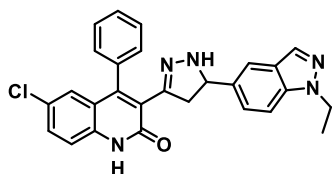
Compound **102c** was synthesized via general procedure B using **102b** (336 mg, 0.79 mmol) with hydrazine hydrate (77 μ L, 1.58 mmol). Purification was performed by direct phase flash chromatography (SiO₂ gold 24 g; A= DCM, B= EtOH, gradient 0–10% B) to afford **102c** (322 mg, yield 87%). ¹H NMR (400 MHz, DMSO-*d*₆) δ 12.18 (s, 1H), 7.60–7.48 (m, 4H), 7.41 (d, *J* = 8.8 Hz, 1H), 7.38–7.30 (m, 3H), 7.25 (dt, *J* = 6.6, 2.1 Hz, 2H), 7.00 (d, *J* = 3.2 Hz, 1H), 6.89 (dd, *J* = 9.7, 2.0 Hz, 2H), 6.34 (dd, *J* = 3.2, 0.8 Hz, 1H), 4.64 (td, *J* = 10.4, 3.2 Hz, 1H), 4.17 (q, *J* = 7.2 Hz, 2H), 3.21 (dd, *J* = 16.4, 11.0 Hz, 1H), 2.63 (dd, *J* = 16.4, 9.9 Hz, 1H), 1.33 (t, *J* = 7.2 Hz, 3H). ¹³C NMR (101 MHz, DMSO-*d*₆) δ 160.59, 148.22, 145.47, 136.97, 135.29, 134.66, 133.82, 130.30, 129.23, 128.75, 128.27, 128.18, 128.12, 127.94, 127.04, 125.74, 125.63, 120.97, 119.94, 118.22, 117.33, 109.48, 100.42, 63.56, 56.02, 44.87, 18.54, 15.49. *t*R = 2.51 min. ESI-MS for C₂₈H₂₃ClN₄O: calculated 466.2, found *m/z* 467.2, 469.2 [M + H]⁺; 465.3, 467.4 [M – H][–].

(*E*)-6-Chloro-3-(3-(1-ethyl-1*H*-indazol-5-yl)acryloyl)-4-phenylquinolin-2(1*H*)-one (103b).



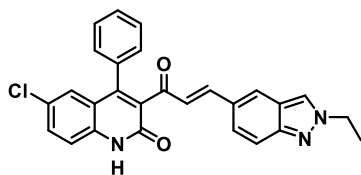
Compound **103b** was synthesized via general procedure A using **71a** (292 mg, 0.98 mmol) and 1-ethyl-1*H*-indazole-5-carbaldehyde **85** (171 mg, 0.98 mmol). Purification was performed by direct phase flash chromatography (SiO₂ gold 24 g; A= DCM, B= EtOH, gradient 0–5% B) to afford **103b** (275 mg, yield 61%). ¹H NMR (400 MHz, DMSO-*d*₆) δ 12.33 (s, 1H), 8.09 (s, 1H), 8.07 (d, *J* = 1.4 Hz, 1H), 7.72 (dd, *J* = 8.9, 1.6 Hz, 1H), 7.69–7.57 (m, 3H), 7.48 (d, *J* = 8.8 Hz, 1H), 7.46–7.36 (m, 3H), 7.34 (dd, *J* = 7.8, 1.8 Hz, 2H), 6.98 (d, *J* = 2.3 Hz, 1H), 6.74 (d, *J* = 16.3 Hz, 1H), 4.43 (q, *J* = 7.2 Hz, 2H), 1.38 (t, *J* = 7.2 Hz, 3H). ¹³C NMR (101 MHz, DMSO-*d*₆) δ 193.64, 159.45, 147.35, 146.51, 139.48, 137.50, 133.76, 133.70, 132.72, 130.84, 128.89, 128.76, 128.40, 126.97, 126.03, 125.64, 125.55, 125.18, 123.97, 123.80, 120.63, 117.66, 110.26, 43.20, 14.85. *t*R = 2.35 min. ESI-MS for C₂₇H₂₀ClN₃O₂: calculated 453.1, found *m/z* 454.4, 456.4 [M + H]⁺; 452.4, 454.4 [M – H][–].

6-Chloro-3-(5-(1-ethyl-1*H*-indazol-5-yl)-4,5-dihydro-1*H*-pyrazol-3-yl)-4-phenylquinolin-2(1*H*)-one (103c).



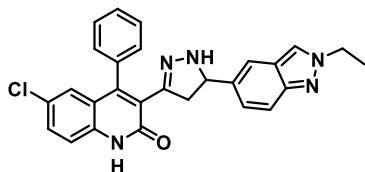
Compound **103c** was synthesized via general procedure B using **103b** (260 mg, 0.57 mmol) with hydrazine hydrate (55 μ L, 1.14 mmol). Purification was performed by direct phase flash chromatography (SiO_2 gold 24 g; A= DCM, B= EtOH, gradient 0–10% B) to afford **103c** (228 mg, yield 86%). ^1H NMR (400 MHz, $\text{DMSO-}d_6$) δ 12.21 (s, 1H), 7.97 (d, J = 0.9 Hz, 1H), 7.59–7.46 (m, 5H), 7.42 (d, J = 8.8 Hz, 2H), 7.38–7.34 (m, 1H), 7.27–7.21 (m, 1H), 7.17–7.08 (m, 2H), 6.91 (d, J = 2.4 Hz, 1H), 4.71 (ddd, J = 11.3, 9.3, 2.5 Hz, 1H), 4.41 (q, J = 7.2 Hz, 2H), 3.27 (dd, J = 16.5, 11.1 Hz, 1H), 2.62 (dd, J = 16.5, 9.4 Hz, 1H), 1.38 (t, J = 7.2 Hz, 3H). ^{13}C NMR (101 MHz, $\text{DMSO-}d_6$) δ 161.06, 148.81, 145.93, 138.63, 137.46, 136.04, 135.71, 134.85, 132.74, 130.82, 129.75, 129.17, 128.76, 128.70, 127.36, 126.93, 126.25, 126.11, 125.62, 124.49, 123.84, 121.42, 118.50, 117.82, 110.00, 109.89, 63.43, 45.22, 43.52, 15.40. t_R = 2.19 min. ESI-MS for $\text{C}_{27}\text{H}_{22}\text{ClN}_5\text{O}$: calculated 467.1, found m/z 468.5, 470.5 $[\text{M} + \text{H}]^+$, 466.5, 468.5 $[\text{M} - \text{H}]^-$.

(*E*)-6-Chloro-3-(3-(2-ethyl-2*H*-indazol-5-yl)acryloyl)-4-phenylquinolin-2(1*H*)-one (104b).



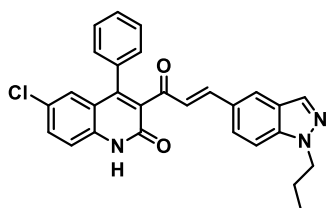
Compound **104b** was synthesized via general procedure A using **71a** (307 mg, 1.00 mmol) and 2-ethyl-2*H*-indazole-5-carbaldehyde **86** (174 mg, 1.00 mmol). Purification was performed by direct phase flash chromatography (SiO_2 gold 24 g; A= DCM, B= EtOH, gradient 0–5% B) to afford **104b** (386 mg, yield 82%). ^1H NMR (400 MHz, $\text{DMSO-}d_6$) δ 12.33 (s, 1H), 8.48 (s, 1H), 8.02 (s, 1H), 7.65 (dd, J = 8.8, 2.4 Hz, 1H), 7.61–7.51 (m, 3H), 7.51–7.38 (m, 4H), 7.34 (dd, J = 7.7, 1.9 Hz, 2H), 6.98 (d, J = 2.3 Hz, 1H), 6.68 (d, J = 16.3 Hz, 1H), 4.44 (q, J = 7.3 Hz, 2H), 1.49 (t, J = 7.2 Hz, 3H). ^{13}C NMR (101 MHz, $\text{DMSO-}d_6$) δ 193.61, 159.46, 148.47, 147.59, 146.48, 137.49, 133.71, 132.78, 130.83, 128.88, 128.76, 128.40, 127.38, 126.02, 125.55, 125.30, 125.16, 123.56, 121.42, 120.63, 117.65, 117.56, 47.87, 15.57. t_R = 2.22 min. ESI-MS for $\text{C}_{27}\text{H}_{20}\text{ClN}_3\text{O}_2$: calculated 453.1, found m/z 454.4, 456.4 $[\text{M} + \text{H}]^+$, 452.4, 454.4 $[\text{M} - \text{H}]^-$.

6-Chloro-3-(5-(2-ethyl-2*H*-indazol-5-yl)-4,5-dihydro-1*H*-pyrazol-3-yl)-4-phenylquinolin-2(1*H*)-one (104c).



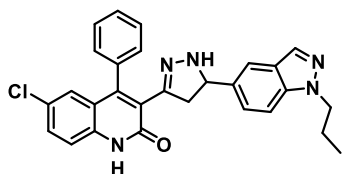
Compound **104c** was synthesized via general procedure B using **104b** (302 mg, 0.60 mmol) with hydrazine hydrate (58 μ L, 1.20 mmol). Purification was performed by direct phase flash chromatography (SiO₂ gold 24 g; A= DCM, B= EtOH, gradient 0–10% B) to afford **104c** (236 mg, yield 76%). ¹H NMR (400 MHz, DMSO-*d*₆) δ 12.19 (s, 1H), 8.27 (d, *J* = 0.9 Hz, 1H), 7.59–7.38 (m, 6H), 7.35 (td, *J* = 3.1, 1.5 Hz, 2H), 7.28–7.20 (m, 1H), 7.08 (d, *J* = 3.2 Hz, 1H), 6.98–6.86 (m, 2H), 4.65 (td, *J* = 10.3, 3.1 Hz, 1H), 4.42 (q, *J* = 7.3 Hz, 2H), 3.24 (dd, *J* = 16.5, 11.1 Hz, 1H), 2.60 (dd, *J* = 16.5, 9.6 Hz, 1H), 1.48 (t, *J* = 7.3 Hz, 3H). ¹³C NMR (101 MHz, DMSO-*d*₆) δ 160.56, 148.29, 147.50, 145.53, 136.97, 135.54, 135.22, 130.32, 129.28, 128.68, 128.27, 128.20, 126.91, 125.76, 125.62, 124.73, 122.79, 121.02, 120.94, 117.33, 117.28, 117.07, 63.27, 47.64, 44.41, 15.77. tR = 2.06 min. ESI-MS for C₂₇H₂₂ClN₅O: calculated 467.1, found *m/z* 468.5, 470.4 [M + H]⁺, 466.4, 468.5 [M – H][–].

(*E*)-6-Chloro-4-phenyl-3-(3-(1-propyl-1*H*-indazol-5-yl)-acryloyl)quinolin-2(1*H*)-one (105b).



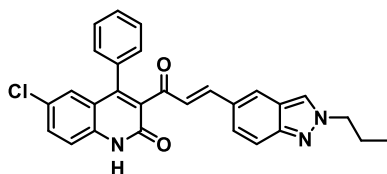
Compound **105b** was synthesized via general procedure A using **71a** (402 mg, 1.35 mmol) and 1-propyl-1*H*-indazole-5-carbaldehyde **87** (254 mg, 1.35 mmol). Purification was performed by direct phase flash chromatography (SiO₂ gold 24 g; A= DCM, B= EtOH, gradient 0–7% B) to afford **105b** (401 mg, yield 64%). ¹H NMR (400 MHz, DMSO-*d*₆) δ 12.33 (s, 1H), 8.10 (d, *J* = 0.8 Hz, 1H), 8.07 (d, *J* = 1.4 Hz, 1H), 7.72 (dd, *J* = 9.0, 1.6 Hz, 1H), 7.70–7.57 (m, 3H), 7.48 (d, *J* = 8.8 Hz, 1H), 7.44–7.38 (m, 3H), 7.34 (dd, *J* = 7.7, 1.8 Hz, 2H), 6.98 (d, *J* = 2.4 Hz, 1H), 6.74 (d, *J* = 16.3 Hz, 1H), 4.36 (t, *J* = 6.9 Hz, 2H), 1.82 (h, *J* = 7.2 Hz, 2H), 0.80 (t, *J* = 7.4 Hz, 3H). ¹³C NMR (101 MHz, DMSO-*d*₆) δ 193.66, 159.46, 147.36, 146.52, 140.12, 137.50, 133.80, 133.70, 132.74, 130.85, 128.89, 128.77, 128.41, 126.94, 126.03, 125.65, 125.55, 125.20, 123.98, 123.65, 120.64, 117.67, 110.36, 49.71, 22.82, 11.04. tR = 2.51 min. ESI-MS for C₂₈H₂₂ClN₃O₂: calculated 467.1, found *m/z* 468.2, 470.2 [M + H]⁺, 466.3, 468.3 [M – H][–].

6-Chloro-4-phenyl-3-(5-(1-propyl-1H-indazol-5-yl)-4,5-dihydro-1H-pyrazol-3-yl)quinolin-2(1H)-one (105c).



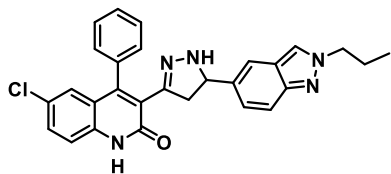
Compound **105c** was synthesized via general procedure B using **105b** (395 mg, 0.84 mmol) with hydrazine hydrate (82 μ L, 1.68 mmol). Purification was performed by direct phase flash chromatography (SiO_2 gold 24 g; A= DCM, B= EtOH, gradient 0–10% B) to afford **105c** (381 mg, yield 94%). ^1H NMR (400 MHz, $\text{DMSO-}d_6$) δ 12.19 (s, 1H), 8.00–7.91 (m, 1H), 7.59–7.45 (m, 6H), 7.42 (d, J = 8.7 Hz, 2H), 7.38–7.31 (m, 1H), 7.24 (dd, J = 6.8, 1.9 Hz, 1H), 7.12 (dd, J = 8.7, 1.6 Hz, 1H), 6.90 (d, J = 2.3 Hz, 1H), 4.70 (t, J = 10.3 Hz, 1H), 4.33 (t, J = 6.9 Hz, 2H), 3.25 (dd, J = 16.5, 11.1 Hz, 1H), 2.62 (dd, J = 16.5, 9.5 Hz, 1H), 1.88–1.77 (m, 2H), 0.81 (t, J = 7.4 Hz, 3H). ^{13}C NMR (101 MHz, $\text{DMSO-}d_6$) δ 160.54, 148.29, 145.42, 138.73, 136.96, 135.44, 135.21, 132.22, 130.31, 129.23, 128.68, 128.25, 128.22, 128.18, 126.87, 125.74, 125.60, 125.13, 123.18, 120.92, 117.98, 117.32, 109.56, 62.94, 49.59, 44.66, 22.81, 11.09. t_R = 2.34 min. ESI-MS for $\text{C}_{28}\text{H}_{24}\text{ClN}_5\text{O}$: calculated 481.2, found m/z 482.1, 484.2 $[\text{M} + \text{H}]^+$, 480.2, 482.3 $[\text{M} - \text{H}]^-$.

(E)-6-Chloro-4-phenyl-3-(3-(2-propyl-2H-indazol-5-yl)-acryloyl)quinolin-2(1H)-one (106b).



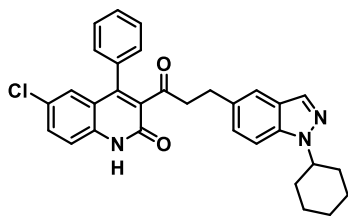
Compound **106b** was synthesized via general procedure A using **71a** (292 mg, 0.98 mmol) and 2-propyl-2H-indazole-5-carbaldehyde **88** (184 mg, 0.98 mmol). Purification was performed by direct phase flash chromatography (SiO_2 gold 24 g; A= DCM, B= EtOH, gradient 0–7% B) to afford **106b** (372 mg, yield 81%). ^1H NMR (400 MHz, $\text{DMSO-}d_6$) δ 12.33 (s, 1H), 8.47 (s, 1H), 8.04–8.00 (m, 1H), 7.65 (dd, J = 8.8, 2.3 Hz, 1H), 7.60–7.51 (m, 3H), 7.47 (d, J = 8.8 Hz, 1H), 7.44–7.38 (m, 3H), 7.36–7.32 (m, 2H), 6.97 (d, J = 2.3 Hz, 1H), 6.68 (d, J = 16.2 Hz, 1H), 4.36 (t, J = 6.9 Hz, 2H), 1.96–1.87 (m, 2H), 0.83 (t, J = 7.4 Hz, 3H). ^{13}C NMR (101 MHz, $\text{DMSO-}d_6$) δ 193.63, 159.46, 148.52, 147.59, 146.47, 137.50, 133.71, 132.79, 130.83, 128.88, 128.77, 128.41, 127.39, 126.02, 125.87, 125.55, 125.31, 123.56, 121.32, 120.63, 117.66, 117.59, 54.36, 23.22, 10.84. t_R = 2.37 min. ESI-MS for $\text{C}_{28}\text{H}_{22}\text{ClN}_3\text{O}_2$: calculated 467.1, found m/z 468.2, 470.2 $[\text{M} + \text{H}]^+$, 466.3, 468.3 $[\text{M} - \text{H}]^-$.

6-Chloro-4-phenyl-3-(5-(2-propyl-2H-indazol-5-yl)-4,5-dihydro-1H-pyrazol-3-yl)quinolin-2(1H)-one (106c).



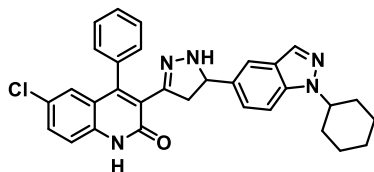
Compound **106c** was synthesized via general procedure B using **106b** (342 mg, 0.73 mmol) with hydrazine hydrate (71 μ L, 1.46 mmol). Purification was performed by direct phase flash chromatography (SiO₂ gold 24 g; A= DCM, B= EtOH, gradient 0–10% B) to afford **106c** (316 mg, yield 89%). ¹H NMR (400 MHz, DMSO-*d*₆) δ 12.19 (s, 1H), 8.27 (d, *J* = 0.9 Hz, 1H), 7.57 (dd, *J* = 8.8, 2.3 Hz, 1H), 7.55–7.44 (m, 4H), 7.41 (d, *J* = 8.8 Hz, 1H), 7.38–7.33 (m, 2H), 7.24 (dt, *J* = 6.6, 1.9 Hz, 1H), 7.08 (d, *J* = 3.2 Hz, 1H), 6.92 (dd, *J* = 8.9, 1.6 Hz, 1H), 6.90 (d, *J* = 2.4 Hz, 1H), 4.70–4.59 (m, 1H), 4.35 (t, *J* = 6.9 Hz, 2H), 3.24 (dd, *J* = 16.5, 11.1 Hz, 1H), 2.60 (dd, *J* = 16.4, 9.6 Hz, 1H), 1.96–1.87 (m, 2H), 0.82 (t, *J* = 7.4 Hz, 3H). ¹³C NMR (101 MHz, DMSO-*d*₆) δ 160.58, 148.31, 147.56, 145.50, 136.98, 135.55, 135.23, 130.37, 129.31, 128.70, 128.30, 128.28, 128.23, 126.93, 125.76, 125.64, 124.75, 123.59, 120.95, 120.89, 117.36, 117.31, 117.11, 63.26, 54.20, 44.40, 23.40, 10.89. tR = 2.23 min). ESI-MS for C₂₈H₂₄ClN₅O: calculated 481.2, found *m/z* 482.2, 484.2 [M + H]⁺, 480.3, 482.3 [M – H]⁻.

(E)-6-Chloro-3-(3-(1-cyclohexyl-1H-indazol-5-yl)acryloyl)-4-phenylquinolin-2(1H)-one (107b).



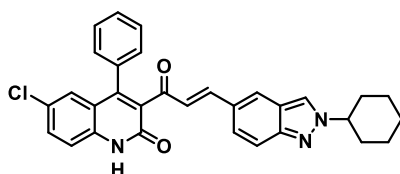
Compound **107b** was synthesized via general procedure A using **71a** (134 mg, 0.46 mmol) and 1-cyclohexyl-1H-indazole-5-carbaldehyde **89** (105 mg, 0.46 mmol). Purification was performed by direct phase flash chromatography (SiO₂ gold 24 g; A= DCM, B= EtOH, gradient 0–5% B) to afford **107b** (193 mg, yield 83%). ¹H NMR (400 MHz, DMSO-*d*₆) δ 12.33 (s, 1H), 8.08 (s, 1H), 8.06 (d, *J* = 1.4 Hz, 1H), 7.72–7.69 (m, 2H), 7.65 (dd, *J* = 8.8, 2.4 Hz, 1H), 7.60 (d, *J* = 16.3 Hz, 1H), 7.48 (d, *J* = 8.8 Hz, 1H), 7.45–7.37 (m, 3H), 7.33 (dd, *J* = 7.7, 1.8 Hz, 2H), 6.98 (d, *J* = 2.4 Hz, 1H), 6.73 (d, *J* = 16.3 Hz, 1H), 4.60 (tt, *J* = 9.6, 4.8 Hz, 1H), 1.98–1.80 (m, 6H), 1.70 (d, *J* = 13.0 Hz, 1H), 1.48 (td, *J* = 12.4, 11.1, 4.6 Hz, 2H), 1.25 (dtd, *J* = 12.9, 9.7, 3.6 Hz, 1H). ¹³C NMR (101 MHz, DMSO-*d*₆) δ 193.66, 159.47, 147.44, 146.53, 139.15, 137.51, 133.72, 133.57, 132.73, 130.86, 128.90, 128.79, 128.42, 127.00, 126.05, 125.59, 125.56, 125.00, 123.98, 123.66, 120.65, 117.68, 110.37, 56.77, 32.26, 24.98. tR = 1.94 min. ESI-MS for C₃₁H₂₆ClN₃O₂: calculated 507.2, found *m/z* 508.2, 510.2 [M + H]⁺, 506.3, 508.3 [M – H]⁻.

6-Chloro-3-(5-(1-cyclohexyl-1H-indazol-5-yl)-4,5-dihydro-1H-pyrazol-3-yl)-4-phenylquinolin-2(1H)-one (107c).



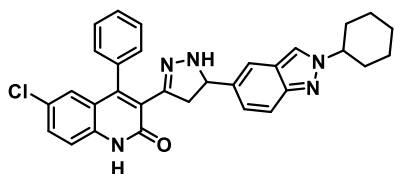
Compound **107c** was synthesized via general procedure B using **107b** (187 mg, 0.37 mmol) with hydrazine hydrate (36 μ L, 0.74 mmol). Purification was performed by direct phase flash chromatography (SiO_2 gold 24 g; A= DCM, B= EtOH, gradient 0–10% B) to afford **107c** (172 mg, yield 86%). ^1H NMR (400 MHz, $\text{DMSO-}d_6$) δ 12.20 (s, 1H), 7.95 (d, J = 0.8 Hz, 1H), 7.62–7.55 (m, 2H), 7.50 (dddd, J = 13.9, 7.1, 5.1, 4.0 Hz, 3H), 7.44–7.39 (m, 2H), 7.38–7.32 (m, 1H), 7.28–7.20 (m, 1H), 7.15–7.08 (m, 2H), 6.90 (d, J = 2.3 Hz, 1H), 4.69 (ddd, J = 11.0, 9.5, 3.2 Hz, 1H), 4.55 (tt, J = 10.0, 5.3 Hz, 1H), 3.25 (dd, J = 16.5, 11.1 Hz, 1H), 2.61 (dd, J = 16.5, 9.5 Hz, 1H), 1.88 (ddd, J = 20.4, 10.2, 3.5 Hz, 6H), 1.71 (dt, J = 13.0, 3.2 Hz, 1H), 1.51 (qd, J = 12.1, 11.7, 5.9 Hz, 2H), 1.26 (tdd, J = 12.8, 9.5, 4.4 Hz, 1H). ^{13}C NMR (101 MHz, $\text{DMSO-}d_6$) δ 160.56, 148.32, 145.45, 137.82, 36.98, 135.55, 135.24, 132.00, 130.35, 129.24, 128.70, 128.29, 128.26, 128.21, 126.89, 125.76, 125.63, 124.92, 123.21, 120.93, 118.01, 117.35, 109.60, 62.97, 56.62, 44.74, 32.30, 25.06. t_R = 2.65 min. ESI-MS for $\text{C}_{31}\text{H}_{28}\text{ClN}_5\text{O}$: calculated 521.2, found m/z 522.3, 524.3 $[\text{M} + \text{H}]^+$, 520.3, 522.4 $[\text{M} - \text{H}]^-$.

(E)-6-Chloro-3-(3-(2-cyclohexyl-2H-indazol-5-yl)acryloyl)-4-phenylquinolin-2(1H)-one (108b).



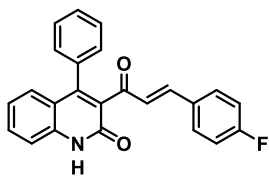
Compound **108b** was synthesized via general procedure A using **71a** (89 mg, 0.30 mmol) and 2-cyclohexyl-2H-indazole-5-carbaldehyde **90** (68 mg, 0.30 mmol). Purification was performed by direct phase flash chromatography (SiO_2 gold 12 g; A= DCM, B= EtOH, gradient 0–5% B) to afford **108b** (136 mg, yield 90%). ^1H NMR (400 MHz, $\text{DMSO-}d_6$) δ 12.33 (s, 1H), 8.49 (s, 1H), 8.00 (d, J = 1.5 Hz, 1H), 7.65 (dd, J = 8.8, 2.3 Hz, 1H), 7.59–7.52 (m, 3H), 7.47 (d, J = 8.8 Hz, 1H), 7.45–7.38 (m, 3H), 7.35–7.30 (m, 2H), 6.97 (d, J = 2.3 Hz, 1H), 6.66 (d, J = 16.3 Hz, 1H), 4.45 (tt, J = 11.3, 3.8 Hz, 1H), 2.09 (dd, J = 13.0, 4.0 Hz, 2H), 1.86 (ddt, J = 14.4, 9.8, 5.6 Hz, 4H), 1.76–1.63 (m, 1H), 1.51–1.37 (m, 2H), 1.25 (qt, J = 13.1, 3.4 Hz, 1H). ^{13}C NMR (101 MHz, $\text{DMSO-}d_6$) δ 193.63, 159.47, 148.04, 147.67, 146.47, 137.49, 133.72, 132.78, 130.84, 128.89, 128.78, 128.41, 127.34, 126.03, 125.55, 125.42, 125.24, 123.78, 123.45, 121.13, 120.65, 117.70, 61.84, 33.12, 24.85, 24.82. t_R = 2.60 min. ESI-MS for $\text{C}_{31}\text{H}_{26}\text{ClN}_3\text{O}_2$: calculated 507.2, found m/z 508.3, 510.2 $[\text{M} + \text{H}]^+$, 506.3, 508.4 $[\text{M} - \text{H}]^-$.

6-Chloro-3-(5-(2-cyclohexyl-2H-indazol-5-yl)-4,5-dihydro-1H-pyrazol-3-yl)-4-phenylquinolin-2(1H)-one (108c).



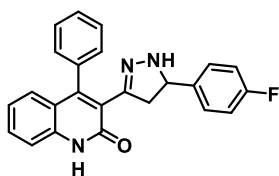
Compound **108c** was synthesized via general procedure B using **108b** (130 mg, 0.26 mmol) with hydrazine hydrate (25 μ L, 0.52 mmol). Purification was performed by direct phase flash chromatography (SiO₂ gold 24 g; A= DCM, B= EtOH, gradient 0–10% B) to afford **108c** (117 mg, yield 86%). ¹H NMR (400 MHz, DMSO-*d*₆) δ 12.19 (s, 1H), 8.28 (d, *J* = 0.9 Hz, 1H), 7.59–7.44 (m, 5H), 7.41 (d, *J* = 8.8 Hz, 1H), 7.38–7.31 (m, 2H), 7.23 (dt, *J* = 6.5, 2.0 Hz, 1H), 7.07 (d, *J* = 3.2 Hz, 1H), 6.94–6.87 (m, 2H), 4.64 (td, *J* = 9.9, 3.1 Hz, 1H), 4.43 (tt, *J* = 11.3, 3.8 Hz, 1H), 3.23 (dd, *J* = 16.5, 11.1 Hz, 1H), 2.59 (dd, *J* = 16.4, 9.6 Hz, 1H), 2.15–2.03 (m, 2H), 1.90–1.80 (m, 4H), 1.69 (dt, *J* = 12.5, 3.3 Hz, 1H), 1.44 (qt, *J* = 13.0, 3.5 Hz, 2H), 1.35–1.17 (m, 1H). ¹³C NMR (101 MHz, DMSO-*d*₆) δ 160.58, 148.32, 147.05, 145.53, 136.99, 135.52, 135.24, 130.37, 129.30, 128.70, 128.31, 128.29, 128.24, 126.93, 125.77, 125.65, 124.65, 121.38, 120.96, 120.70, 117.37, 117.34, 117.22, 63.29, 61.58, 44.46, 33.30, 24.93, 24.90. *t*R = 2.47 min. ESI-MS for C₃₁H₂₈ClN₅O: calculated 521.2, found *m/z* 522.2, 524.2 [M + H]⁺, 520.2, 522.3 [M – H][–].

(E)-3-(3-(4-Fluorophenyl)acryloyl)-4-phenylquinolin-2(1H)-one (109b).



Compound **109b** was synthesized via general procedure A using **72a** (265 mg, 1.00 mmol) and 4-fluorobenzaldehyde **73** (107 μ L, 1.00 mmol). Title compound **109b** was obtained after precipitation and filtration from the reaction crude (345 mg, yield 93%). ¹H NMR (400 MHz, DMSO-*d*₆) δ 12.30 (s, 1H), 7.73 (d, *J* = 7.2 Hz, 2H), 7.65–7.00 (m, 12H), 6.73 (d, *J* = 16.4 Hz, 1H). ¹³C NMR (101 MHz, DMSO-*d*₆) δ 194.31, 159.77, 147.76, 144.37, 134.36, 131.36, 130.92, 130.92, 128.92, 128.46, 128.23, 127.52, 126.86, 126.86, 124.54, 122.05, 119.21, 116.00, 115.92, 115.90, 115.88, 115.79. *t*R = 2.25 min. ESI-MS for C₂₄H₁₆FNO₂: calculated 369.1, found *m/z* 370.5 [M + H]⁺; 368.4 [M – H][–].

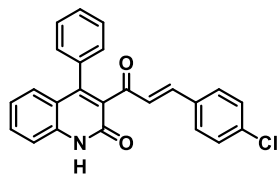
3-(5-(4-Fluorophenyl)-4,5-dihydro-1H-pyrazol-3-yl)-4-phenylquinolin-2(1H)-one (109c).



Compound **109c** was synthesized via general procedure B using **109b** (300 mg, 0.81 mmol) with hydrazine hydrate (79 μ L, 1.62 mmol). Title compound **109c** was obtained after precipitation from DCM (292 mg, yield 94%). ¹H NMR (400 MHz, DMSO-*d*₆) δ 12.11 (s, 1H), 7.54–7.44 (m, 4H), 7.40 (dd, *J* = 8.3, 1.2 Hz, 1H), 7.32 (dt, *J* = 7.4, 1.7 Hz, 1H), 7.21 (dt, *J* = 6.8, 1.9 Hz,

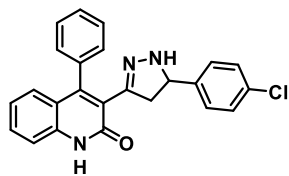
1H), 7.14–7.02 (m, 6H), 6.99 (dd, J = 8.1, 1.4 Hz, 1H), 4.58 (td, J = 10.9, 3.1 Hz, 1H), 3.23 (dd, J = 16.4, 11.0 Hz, 1H), 2.56–2.52 (m, 1H). tR = 2.13 min. ESI-MS for C₂₄H₁₈FN₃O: calculated 383.1, found m/z 384.5 [M + H]⁺, 382.5 [M – H]⁻.

(E)-3-(3-(4-Chlorophenyl)acryloyl)-4-phenylquinolin-2(1H)-one (110b)



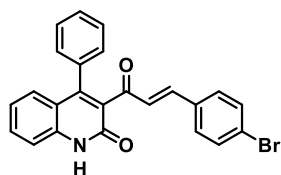
Compound **110b** was synthesized via general procedure A using **72a** (169 mg, 0.64 mmol) and 4-chlorobenzaldehyde **74** (90 mg, 0.64 mmol). Title compound **110b** was obtained after precipitation and filtration from the reaction crude (246 mg, quantitative yield). ¹H NMR (400 MHz, DMSO-*d*₆) δ 12.18 (s, 1H), 7.71 (d, J = 8.3 Hz, 2H), 7.59 (td, J = 7.6, 7.0, 1.5 Hz, 1H), 7.52–7.37 (m, 7H), 7.34–7.29 (m, 2H), 7.17 (t, J = 7.6 Hz, 1H), 7.12–7.05 (m, 1H), 6.79 (d, J = 16.4 Hz, 1H). ¹³C NMR (101 MHz, DMSO-*d*₆) δ 194.66, 160.05, 148.50, 144.66, 139.25, 135.67, 134.74, 133.75, 131.78, 131.55, 130.77, 129.39, 129.00, 128.73, 128.65, 127.42, 122.69, 119.69, 116.13. tR = 2.37 min. ESIMS for C₂₄H₁₆ClNO₂: calculated 385.1, found m/z 386.4, 388.4 [M + H]⁺; 384.4, 386.4 [M – H]⁻.

3-(5-(4-Chlorophenyl)-4,5-dihydro-1H-pyrazol-3-yl)-4-phenylquinolin-2(1H)-one (110c).



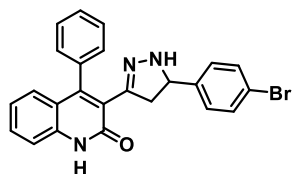
Compound **110c** was synthesized via general procedure B using **110b** (225 mg, 0.58 mmol) with hydrazine hydrate (56 μL, 1.16 mmol). Purification was performed by direct phase flash chromatography (SiO₂ gold 24 g; A= DCM, B= EtOH, gradient 1–10% B) to afford **110c** (185 mg, yield 79%). ¹H NMR (400 MHz, DMSO-*d*₆) δ 12.05 (s, 1H), 7.56–7.43 (m, 4H), 7.40 (dd, J = 8.3, 1.2 Hz, 1H), 7.35–7.26 (m, 3H), 7.21 (dt, J = 7.3, 2.0 Hz, 1H), 7.13–7.06 (m, 4H), 7.00 (dd, J = 8.2, 1.4 Hz, 1H), 4.58 (ddd, J = 10.9, 9.2, 3.2 Hz, 1H), 3.25 (dd, J = 16.5, 11.1 Hz, 1H), 2.58–2.52 (m, 1H). ¹³C NMR (101 MHz, DMSO-*d*₆) δ 161.18, 150.09, 146.43, 143.16, 138.71, 136.24, 131.79, 130.97, 129.76, 129.16, 128.82, 128.60, 128.56, 128.53, 128.36, 127.41, 125.88, 122.39, 120.04, 115.78, 62.43, 45.12. tR = 2.26 min. ESI-MS for C₂₄H₁₈ClN₃O: calculated 399.1, found m/z 400.4, 402.4 [M + H]⁺; 398.4, 400.5 [M – H]⁻.

(E)-3-(3-(4-Bromophenyl)acryloyl)-4-phenylquinolin-2(1H)-one (111b).



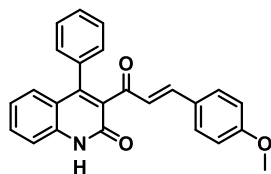
Compound **111b** was synthesized via general procedure A using **72a** (265 mg, 1.00 mmol) and 4-bromobenzaldehyde **75** (185 mg, 1.00 mmol). Title compound **111b** was obtained after precipitation and filtration from the reaction crude (396 mg, yield 92%). ¹H NMR (400 MHz, DMSO-*d*₆) δ 7.67–7.50 (m, 5H), 7.45–7.36 (m, 5H), 7.29 (dd, *J* = 7.7, 1.8 Hz, 2H), 7.15–7.02 (m, 2H), 6.79 (d, *J* = 16.4 Hz, 1H). ¹³C NMR (101 MHz, DMSO-*d*₆) δ 210.70, 133.70, 131.89, 131.23, 130.49, 129.00, 128.43, 128.25, 126.84, 124.03, 121.73, 119.29, 116.57, 99.54. tR = 2.43 min. ESI-MS for C₂₄H₁₆BrNO₂: calculated 429.0, found *m/z* 430.4, 432.4 [M + H]⁺; 428.4, 430.4 [M – H][–].

3-(5-(4-Bromophenyl)-4,5-dihydro-1H-pyrazol-3-yl)-4-phenylquinolin-2(1H)-one (111c).



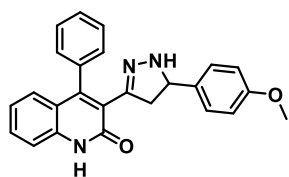
Compound **111c** was synthesized via general procedure B using **111b** (300 mg, 0.70 mmol) with hydrazine hydrate (68 μL, 1.40 mmol). Purification was performed by direct phase flash chromatography (SiO₂ gold 24 g; A= DCM, B= EtOH, gradient 0.2–3% B) to afford **111c** (213 mg, yield 69%). ¹H NMR (400 MHz, DMSO-*d*₆) δ 12.04 (s, 1H), 7.58–7.36 (m, 7H), 7.31 (dt, *J* = 7.3, 1.6 Hz, 1H), 7.20 (dt, *J* = 7.3, 2.0 Hz, 1H), 7.13–6.95 (m, 5H), 4.56 (ddd, *J* = 11.0, 9.3, 3.3 Hz, 1H), 3.30–3.14 (m, 1H), 2.57–2.51 (m, 1H). ¹³C NMR (101 MHz, DMSO-*d*₆) δ 160.71, 149.63, 145.96, 143.13, 138.24, 135.77, 131.05, 130.51, 129.28, 128.73, 128.69, 128.10, 128.06, 127.90, 126.94, 125.39, 121.92, 119.82, 119.57, 115.31, 62.01, 44.62. tR = 2.31 min. ESI-MS for C₂₄H₁₈BrN₃O: calculated 443.1, found *m/z* 444.4, 446.5 [M + H]⁺.

(E)-3-(3-(4-Methoxyphenyl)acryloyl)-4-phenylquinolin-2(1H)-one (112b).



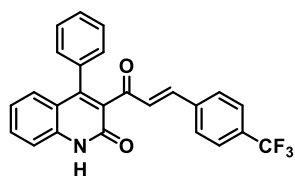
Compound **112b** was synthesized via general procedure A using **72a** (265 mg, 1.00 mmol) and *p*-anisaldehyde **76** (122 μL, 1.00 mmol). Title compound **112b** was obtained after precipitation and filtration from the reaction crude (304 mg, yield 80%). ¹H NMR (400 MHz, DMSO-*d*₆) δ 12.16 (s, 1H), 7.66–7.51 (m, 3H), 7.47–7.34 (m, 5H), 7.32–7.27 (m, 2H), 7.14 (t, *J* = 7.7 Hz, 1H), 7.06 (dd, *J* = 8.2, 1.4 Hz, 1H), 6.93 (d, *J* = 8.8 Hz, 2H), 6.60 (d, *J* = 16.3 Hz, 1H), 3.78 (s, 3H). ¹³C NMR (101 MHz, DMSO-*d*₆) δ 194.07, 161.37, 159.72, 147.51, 145.75, 138.92, 134.40, 131.59, 130.85, 130.48, 128.91, 128.41, 128.19, 126.83, 125.41, 122.04, 119.23, 115.76, 114.36, 55.33. tR = 2.19 min. ESIMS for C₂₅H₁₉NO₃: calculated 381.1, found *m/z* 382.5 [M + H]⁺, 380.5 [M – H]⁺.

3-(5-(4-Methoxyphenyl)-4,5-dihydro-1H-pyrazol-3-yl)-4-phenylquinolin-2(1H)-one (112c).



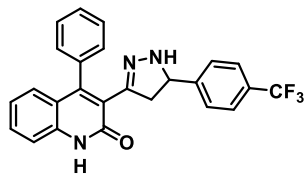
Compound **112c** was synthesized via general procedure B using **112b** (300 mg, 0.79 mmol) with hydrazine hydrate (77 μ L, 1.58 mmol). Purification was performed by direct phase flash chromatography (SiO₂ gold 24 g; A= DCM, B= EtOH, gradient 0–5% B) to afford **112c** (212 mg, yield 69%). ¹H NMR (400 MHz, DMSO-*d*₆) δ 12.02 (s, 1H), 7.54–7.43 (m, 4H), 7.39 (dd, *J* = 8.3, 1.2 Hz, 1H), 7.31 (dq, *J* = 7.6, 1.4 Hz, 1H), 7.21 (ddd, *J* = 5.3, 4.0, 2.0 Hz, 1H), 7.09 (ddd, *J* = 8.2, 7.0, 1.2 Hz, 1H), 7.00 (dt, *J* = 8.2, 2.2 Hz, 3H), 6.82–6.76 (m, 2H), 4.51 (t, *J* = 10.3 Hz, 1H), 3.72 (s, 3H), 3.16 (dd, *J* = 16.4, 10.9 Hz, 1H), 2.57–2.51 (m, 1H). ¹³C NMR (101 MHz, DMSO-*d*₆) δ 160.73, 158.22, 149.48, 146.05, 138.21, 135.81, 135.45, 130.43, 129.25, 128.74, 128.08, 128.05, 127.86, 127.59, 126.91, 125.62, 121.88, 119.59, 115.28, 113.57, 62.36, 55.02, 44.63. *t*R = 2.08 min. ESI-MS for C₂₅H₂₁N₃O₂: calculated 395.1, found *m/z* 396.5 [M + H]⁺; 394.6 [M – H][–].

(E)-4-Phenyl-3-(3-(4-(trifluoromethyl)phenyl)acryloyl)-quinolin-2(1H)-one (113b).



Compound **113b** was synthesized via general procedure A using **72a** (301 mg, 1.10 mmol) and 4- trifluoromethylbenzaldehyde **78** (150 μ L, 1.10 mmol). Title compound **113b** was obtained after precipitation and filtration from the reaction crude (414 mg, yield 87%). ¹H NMR (400 MHz, DMSO-*d*₆) δ 12.23 (s, 1H), 7.81 (dd, *J* = 62.7, 7.9 Hz, 4H), 7.67– 7.24 (m, 8H), 7.25–7.05 (m, 2H), 6.91 (d, *J* = 16.2 Hz, 1H). ¹³C NMR (101 MHz, DMSO-*d*₆) δ 194.74, 160.08, 148.71, 143.97, 139.35, 138.85, 134.71, 131.63, 130.31, 129.64, 129.40, 129.04, 128.76, 127.45, 126.14, 122.71, 119.67, 116.20. *t*R = 2.41 min. ESI-MS for C₂₅H₁₆F₃NO₂: calculated 419.1, found *m/z* 420.5 [M + H]⁺; 418.5 [M – H][–].

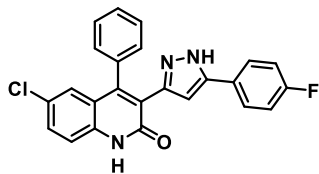
4-Phenyl-3-(5-(4-(trifluoromethyl)phenyl)-4,5-dihydro-1H-pyrazol- 3-yl)quinolin-2(1H)-one (113c).



Compound **113c** was synthesized via general procedure B using **113b** (256 mg, 0.60 mmol) with hydrazine hydrate (58 μ L, 1.20 mmol). Purification was performed by direct phase flash chromatography (SiO₂ gold 24 g; A= DCM, B= EtOH, gradient 0.8–6% B) to afford **113c** (214 mg, yield 80%). ¹H NMR (400 MHz, DMSO-*d*₆) δ 12.05 (s, 1H), 7.60 (d, *J* = 8.1 Hz, 2H), 7.55–7.37 (m, 5H), 7.32 (dd, *J* = 11.5, 7.6 Hz, 3H), 7.24–7.17 (m, 2H), 7.10 (ddd, *J* = 8.2, 7.0, 1.2 Hz, 1H), 7.00 (dd, *J* = 8.2, 1.4 Hz, 1H), 4.69 (ddd, *J* = 11.6, 9.1, 2.8 Hz, 1H), 3.33 (m, 1H),

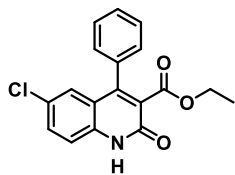
2.63–2.52 (m, 1H). ¹³C NMR (101 MHz, DMSO-*d*₆) δ 161.17, 150.18, 148.95, 146.44, 138.72, 136.22, 131.00, 129.76, 129.22, 129.13, 128.78, 128.57, 128.51, 128.37, 128.02, 127.72, 127.42, 126.14, 125.77, 125.62, 125.57, 125.53, 122.40, 120.02, 115.79, 62.59, 45.15. tR = 2.30 min. ESI-MS for C₂₅H₁₈F₃N₃O: calculated 433.1, found m/z 434.4 [M + H]⁺; 432.5 [M – H][–].

6-Chloro-3-(5-(4-fluorophenyl)-1*H*-pyrazol-3-yl)-4-phenylquinolin-2(1*H*)-one (117) (Scheme 5).



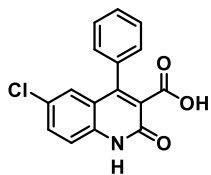
To a stirred solution of α,β ketone **91b** (600 mg, 1.49 mmol) and *t*-butyl hydrazine HCl salt (1.68 g, 5.96 mmol) in ethanol (20.0 mL) was added molecular iodine (1.5 g, 5.96 mmol). The reaction was heated to reflux under a nitrogen atmosphere overnight. The reaction was quenched with 5% Na₂S₂O₃, and the aqueous phase was extracted with ethyl acetate (3 x 20 mL). The combined organic layers were dried over anhydrous Na₂SO₄ evaporated to dryness. Purification silica gel column flash chromatography (SiO₂, A= PE, B= EtOAc, gradient 0–20% B) afforded **117** (140 mg, yield 23%). ¹H NMR (400 MHz, CDCl₃-*d*) δ 11.37 (s, 1H), 7.67 (d, J = 3.9 Hz, 2H), 7.43 (ddd, J = 37.1, 21.9, 8.0 Hz, 5H), 7.30 (s, 2H), 7.16 (s, 1H), 7.02 (t, J = 8.7 Hz, 2H), 5.14 (s, 1H).

Ethyl 6-chloro-2-oxo-4-phenyl-1,2-dihydroquinoline-3-carboxylate (118) (Scheme 6).



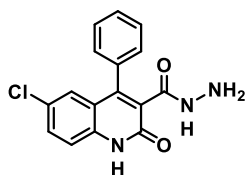
In appropriate microwavable-vessel, commercially available 2-amino-5-chlorobenzofenone **69** (2.5 g, 10.8 mmol) was dissolved in THF (10 mL), then diethylmalonate (5.74 mL, 37.8 mmol) and DBU (1.62 mL, 10.8 mmol) were added. The reaction was microwaved at 160°C for 2 hours. The solvent was removed under reduced pressure. The purification over silica gel flash chromatography (SiO₂, A= PE, B= EtOAc, gradient 0–30% B) afforded the titled compound **118** (2.2 g, yield 62%). ¹H NMR (400 MHz, DMSO-*d*₆) δ 12.42 (s, 1H), 7.65 (ddd, J = 8.8, 2.3, 1.0 Hz, 1H), 7.59 – 7.50 (m, 3H), 7.43 (dd, J = 8.8, 0.5 Hz, 1H), 7.39 – 7.29 (m, 2H), 7.01 (dd, J = 2.2, 0.7 Hz, 1H), 3.95 (tt, J = 7.0, 3.5 Hz, 2H), 0.86 (td, J = 7.0, 0.8 Hz, 3H).

6-Chloro-2-oxo-4-phenyl-1,2-dihydroquinoline-3-carboxylic acid (**119**) (Scheme 6).



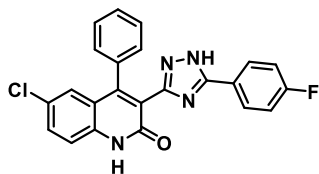
In round bottom flask, **118** (2.0 g, 6.24 mmol) was suspended in ethanol (30 mL), then LiOH 2M (12.2 mL) was added. The reaction mixture was refluxed for 2.5 h. The solvent was removed under pressure. Then H₂O was added and the aqueous phase was washed with EtOAc (3 x 15 mL). Then aqueous phase was acidified to reach pH 2 with a solution HCl 4M and the aqueous layer was extracted with (3 x 25 mL). The collected organic phases were dried over Na₂SO₄ and evaporated to dryness to afford **119** as white-yellow solid. (1.86 g, yield 99%). ¹H NMR (400 MHz, DMSO-*d*₆) δ 12.50 (s, 1H), 7.66 (dd, *J* = 8.8, 2.4 Hz, 1H), 7.61 – 7.51 (m, 3H), 7.47 (d, *J* = 8.8 Hz, 1H), 7.42 – 7.34 (m, 2H), 6.99 (d, *J* = 2.3 Hz, 1H).

6-Chloro-2-oxo-4-phenyl-1,2-dihydroquinoline-3-carbohydrazide (**120**) (Scheme 6).



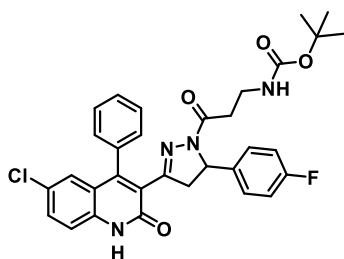
In round bottom flask, **119** (1.5g, 5.01 mmol) was suspended in MeCN (18 mL) with HOBT (813 mg, 6.01 mmol) and EDCI (1.15 g, 6.01 mmol). The mixture was stirred at rt for 3 h. A solution of hydrazine hydrate (321 μL, 6.51 mmol) in acetonitrile (9 mL) was added dropwise at 0°C to. The reaction was stirred for 1.5 h at 0°C. The reaction was quenched with H₂O (5.0 mL). Filtration and washings of the precipitate afforded the titled compound **120** as white solid (803 mg, yield 51%). ¹H NMR (400 MHz, DMSO-*d*₆) δ 12.22 (s, 1H), 9.25 (s, 1H), 7.59 (dd, *J* = 8.7, 2.2 Hz, 1H), 7.53 – 7.46 (m, 3H), 7.39 (d, *J* = 8.8 Hz, 1H), 7.32 (dd, *J* = 7.1, 2.2 Hz, 2H), 6.88 (d, *J* = 2.3 Hz, 1H), 4.09 (s, 2H).

6-Chloro-3-(5-(4-fluorophenyl)-1*H*-1,2,4-triazol-3-yl)-4-phenylquinolin-2(1*H*)-one (**122**) (Scheme 6).



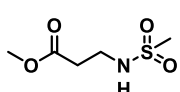
In an appropriately sized **120** (780 mg, 2.49 mmol) was dissolved in *n*-BuOH (6.0 mL), then 4-fluorobenzonitrile **121** (903 mg, 7.47 mmol) and potassium carbonate (171 mg, 1.26 mmol) were added. The reaction was microwaved at 150°C for 4 h. The solvent was removed under reduced pressure. Purification over silica gel flash chromatography (SiO₂, A= DCM, B= MeOH, gradient 1.5–2.0% B) afforded **122** as white-yellow solid (510 mg, yield 49%). ¹H NMR (400 MHz, DMSO-*d*₆) δ 12.53 (s, 1H), 7.83 (s, 2H), 7.69 (dd, *J* = 8.8, 2.1 Hz, 1H), 7.50 (d, *J* = 8.8 Hz, 1H), 7.42 (d, *J* = 6.9 Hz, 3H), 7.28 (dd, *J* = 7.7, 1.6 Hz, 4H), 7.01 (d, *J* = 2.3 Hz, 1H).

Tert-Butyl (3-(3-(6-Chloro-2-oxo-4-phenyl-1,2-dihydroquinolin-3-yl)-5-(4-fluorophenyl)-4,5-dihydro-1H-pyrazol-1-yl)-3-oxopropyl)carbamate (124) (Scheme 7).



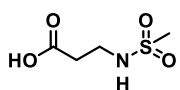
In round-bottom flask, the commercially available 3-((tert-butoxycarbonyl) amino) propanoic acid **123** (182 mg, 0.96 mmol), HOBT (156 mg, 1.16 mmol), and EDCI (222 mg, 1.16 mmol) were stirred in DCM (15 mL) at rt for 1 h. Then a solution of the **91c** (400 mg, 0.96 mmol) and Et₃N (296 μ L, 2.12 mmol) in DCM (5 mL) was added. The mixture was stirred at rt overnight. The solvent was removed under reduced pressure, the residue re dissolved with EtOAc and then washed with H₂O, NaHCO₃ 1M, and finally 10% citric acid. The organic layer was dried over Na₂SO₄ and evaporated to dryness. Purification was performed by direct phase flash chromatography (SiO₂, A= DCM, B= EtOAc, gradient 0–30% B) to afford **124** (72 mg, yield 25%). ¹H NMR (400 MHz, DMSO-*d*₆) δ 12.40 (s, 1H), 7.65 (dd, *J* = 4.0, 8.0 Hz, 1H), 7.59–7.50 (m, 4H), 7.46 (d, *J* = 8.0 Hz, 1H), 7.43–7.42 (m, 1H), 7.28 (d, *J* = 8.0 Hz, 1H), 7.04 (t, *J* = 8.0 Hz, 2H), 6.93 (d, *J* = 2.0 Hz, 1H), 6.80 (dd, *J* = 4.0, 8.0 Hz, 2H), 6.66 (t, *J* = 8.0 Hz, 1H), 5.32 (dd, *J* = 4.0, 12.0 Hz, 1H), 3.73 (dd, *J* = 12.0, 16.0 Hz, 1H), 2.99 (dd, *J* = 8.0, 12.0 Hz, 2H), 2.76 (dd, *J* = 4.0, 20.0 Hz, 1H) 2.41 (q, *J* = 8.0 Hz, 2H), 1.38 (s, 9H).

Methyl 3-(Methylsulfonamido) propanoate (127) (Scheme 10).



In a dried round-bottom flask, commercially available methyl 3-aminopropanoate **126** (745 mg, 5.34 mmol) and TEA (3.7 mL, 26.68 mmol) were stirred in anhydrous DCM (5.6 mL) prior to the addition of methane sulfonyl chloride 122 (1.65 mL, 10.67 mmol). After stirring at rt for 2 days, the reaction was quenched with NaHCO₃ sat solution and extracted three times with CHCl₃. The organic layer was dried over Na₂SO₄ and evaporated to dryness. The title compound **127** was obtained after purification over direct phase flash column chromatography (SiO₂, A= PE, B= EtOAc, gradient 0–40%) (791 mg, yield 82%). ¹H NMR (400 MHz, CDCl₃-*d*) δ 4.94 (s, 1H), 3.72 (s, 3H), m (3.42–3.37, 2H), 2.97 (s, 3H), 2.64 (t, *J* = 4 Hz, 2H). ¹³C NMR (101 MHz, Chloform-*d*) δ 172.63, 52.18, 40.60, 38.89, 34.58.

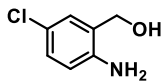
3-(Methylsulfonamido) propanoic acid (128) (Scheme 10).



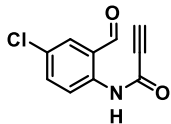
In round bottom flask, methyl 3-(methylsulfonamido) propanoate **127** (791 mg, 4.36 mmol) was stirred in MeOH/THF (1:1 v/v) prior to the addition of LiOH 2M (2.5 mL). The reaction was stirred at rt overnight. The reaction mixture was acidified with HCl_{aq}

1M (pH 2) and extracted three times with ethyl acetate. The organic layer was dried over Na_2SO_4 , filtered and evaporated to dryness to obtain the title compound **128** (600 mg, yield 82%). ^1H NMR (400 MHz, $\text{DMSO-}d_6$) δ 12.29 (s, 1H), 7.02 (t, $J = 4.0$ Hz, 1H), 7.15 (dd, $J = 7.0$, 12.6, 2H), 2.43 (t, $J = 7.2$ Hz, 2H).

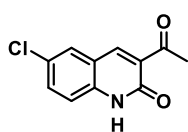
(2-amino-5-chlorophenyl) methanol (130) (Scheme 11).

 In dried round bottom flask, commercially available 2-amino-5-chloro-benzoic acid **129** (1.05 g, 6.12 mmol) was dissolved in anhydrous THF (20 mL). The solution was cooled to 0 °C and LiAlH_4 (1.1 g, 5.39 mmol) was added as powder and the reaction was stirred at rt for 2 hours. Then the reaction was quenched by water (10 mL) and 10% NaOH (18 mL) at 0°C. The mixture was stirred for 15 minutes, and then the suspension was filtered off washing with water. The aqueous phase was extracted with ethyl acetate (4 x 10 mL) and the collected organic phases were dried over Na_2SO_4 and evaporated to dryness to achieve **130** as brown-white solid (930 mg, yield 96%). ^1H NMR (400 MHz, $\text{DMSO-}d_6$) δ 7.10 (d, $J = 2.6$ Hz, 1H), 6.97 (dd, $J = 8.5$, 2.6 Hz, 1H), 6.61 (d, $J = 8.5$ Hz, 1H), 5.14 (t, $J = 5.5$ Hz, 1H), 5.05 (s, 2H), 4.34 (d, $J = 5.4$ Hz, 2H). ^{13}C NMR (101 MHz, $\text{DMSO-}d_6$) δ 145.21, 127.81, 127.24, 126.87, 119.45, 116.11, 60.43.

N-(4-chloro-2-formylphenyl) propiolamide (131) (Scheme 11).

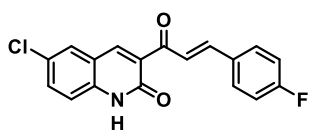
 In dried round bottom flask, 2-amino-5-chlorophenyl-methanol **130** (300 mg, 1.90 mmol) and tetrolic acid (160 mg, 1.90 mmol) were dissolved in anhydrous CH_2Cl_2 (10 mL). The mixture was cooled to 0°C, then a solution of DCC (470 mg, 2.28 mmol) in anhydrous CH_2Cl_2 (5 mL) was added dropwise. The reaction was stirred overnight at rt. The reaction mixture was filtrated on celite and the volume of filtrate was reduced under reduced pressure. A suspension of PCC (819 mg, 3.80 mmol) in CH_2Cl_2 (10 mL) was prepared apart. The mixture filtrated previously was added to the suspension of PCC and stirred for 2 h at rt. The mixture was filtered with celite and the solvent was removed under reduced pressure. The crude product was purified by flash silica gel chromatography (SiO_2 , 100% DCM) to afford **131** (295 mg, yield 70%). ^1H NMR (400 MHz, $\text{DMSO-}d_6$) δ 11.10 (s, 1H), 9.93 (s, 1H), 8.05 (d, $J = 8.8$ Hz, 1H), 7.93 (d, $J = 2.6$ Hz, 1H), 7.76 (dd, $J = 8.8$, 2.6 Hz, 1H), 2.09 (s, 3H).

3-acetyl-6-chloroquinolin-2(1H)-one (132). (Scheme 11).



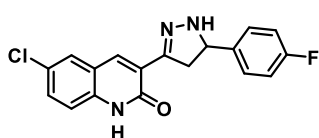
In a round bottom flask, Pd(AcO)₂ (75 mg, 0.30 mmol) and 4,4'-dimethoxy-2,2'-bipyridine (140 mg, 0.65 mmol) were dissolved in a mixture 2:1 of DCE (40 mL) and AcOH (20 mL) in presence of molecular sieves 4Å, under N₂ atmosphere. The mixture was stirred at rt. for 10 minutes. Then **131** (1.43 g, 6.45 mmol) was added and the reaction was heated to 80°C and stirred for 4 h. The purification by precipitation and filtration afforded **132** as white-yellow solid (1 g, yield 67%). ¹H NMR (400 MHz, DMSO-*d*₆) δ 12.22 (s, 3H), 8.42 (s, 3H), 8.01 (d, J = 2.3 Hz, 3H), 7.64 (dd, J = 8.9, 2.3 Hz, 3H), 7.35 (d, J = 8.9 Hz, 3H), 2.60 (s, 8H).

(E)-6-Chloro-3-(3-(4-fluorophenyl) acryloyl)quinolin-2(1H)-one (133) (Scheme 11).



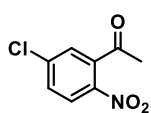
Compound **133** was synthesized via general procedure A using **132** (60 mg, 0.27 mmol) and 4-fluorobenzaldehyde **73** (43 μL, 0.41 mmol). Title compound **133** was obtained after precipitation and filtration from the reaction crude as yellow solid (88 mg). ESI-MS for C₁₈H₁₁ClFNO₂: calculated 327.0462, found m/z 326.0, 328.0 [M - H]⁻.

6-Chloro-3-(5-(4-fluorophenyl)-4,5-dihydro-1H-pyrazol-3-yl)quinolin-2(1H)-one (134). (Scheme 11).



Compound **134** was synthesized via general procedure B using **133** (1.34 g, 4.09 mmol) with hydrazine hydrate (358 μL, 7.36 mmol). Purification by precipitation and filtration afforded the titled compound **134** as yellow solid (820 mg, yield 59%). ¹H NMR (400 MHz, DMSO-*d*₆) δ 12.00 (s, 1H), 8.25 (s, 1H), 7.91 – 7.71 (m, 2H), 7.55 – 7.46 (m, 1H), 7.46 – 7.36 (m, 2H), 7.29 (d, J = 8.8 Hz, 1H), 7.17 (t, J = 8.8 Hz, 2H), 4.85 (t, J = 9.6 Hz, 1H), 3.61 (dd, J = 16.9, 10.8 Hz, 1H), 2.99 (dd, J = 17.0, 10.7 Hz, 1H).

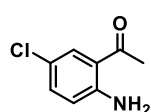
1-(5-Chloro-2-nitrophenyl) ethan-1-one (136) (Scheme 12).



In a round bottom flask, HNO₃ fuming (8.5 mL, 203.6 mmol) was stirred at -20°C, then H₂SO₄ conc. (1.3 mL, 24.3 mmol) was added slowly to prepare the nitrating mixture. Then commercially available 3-chloro acetophenone **135** (2.1 mL, 16.2 mmol) was added in portions for 15 minutes. The reaction was warmed to -10°C and stirred for 75 minutes. After the complete consumption of **135**, ice was added and the aqueous layer was

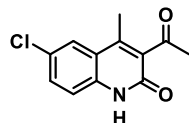
extracted with dichloromethane (3 x 10 mL). The collected organic phases were dried over Na₂SO₄ and evaporated to dryness. The crude product was purified by silica gel flash chromatography (SiO₂, A= PE, B= EtOAc, gradient 1.0–1.5 % B) to afford **136** as pure white solid (2.59 g, yield 80%). ¹H NMR (400 MHz, Chloroform-*d*) δ 8.07 (d, J = 8.8 Hz, 1H), 7.57 – 7.53 (m, 1H), 7.37 (d, J = 2.3 Hz, 1H), 2.54 (s, 3H).

1-(2-Amino-5-chlorophenyl) ethan-1-one (**137**) (Scheme 12).



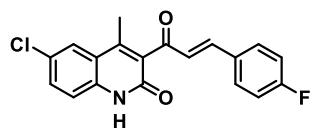
In a bottom flask, **136** (1 g, 5.01 mmol), tin powder (952 mg, 8.02 mmol) and hydrochloric acid conc. (2.4 mL) were mixed and refluxed, stirring for 5 hours. The mixture was cooled to 0 °C and NaOH in pellet was added to achieve basic pH (8.0-10.0). The aqueous phase was extracted with diethyl ether (3 x 50 mL), and then organic layer was dried over Na₂SO₄ and evaporated to dryness to obtain a brown oil. The crude product was purified by silica gel flash chromatography. **137** eluted with 100% DCM obtained as yellow pure solid (815 mg, yield 96 %). ¹H NMR (400 MHz, Chloroform-*d*) δ 7.66 (d, J = 2.4 Hz, 1H), 7.20 (dd, J = 8.8, 2.4 Hz, 1H), 6.60 (d, J = 8.8 Hz, 1H), 6.27 (s, 2H), 2.56 (s, 3H).

3-Acetyl-6-chloro-4-methylquinolin-2(1H)-one (**138**) (Scheme 12).



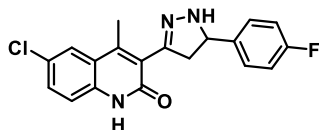
In dried appropriate microwavable-vessel, **137** (150 mg, 0.88 mmol) was dissolved in anhydrous THF (2.0 mL) in presence of molecular sieves 4 Å. Ethyl acetoacetate (169 μL, 1.33 mmol) was added. The reaction was microwaved at 140 °C for 75'. The purification was performed by precipitation and washings with diethyl ether to afford **138** as white solid (60 mg, yield 30%). ¹H NMR (400 MHz, DMSO-*d*₆) δ 12.11 (s, 1H), 7.86 (d, J = 2.3 Hz, 1H), 7.62 (dd, J = 8.8, 2.3 Hz, 1H), 7.35 (d, J = 8.8 Hz, 1H), 2.46 (s, 3H), 2.33 (s, 3H).

(*E*)-6-chloro-3-(3-(4-fluorophenyl)acryloyl)-4-methylquinolin-2(1H)-one (**139**) (Scheme 12).



Compound **139** was synthesized via general procedure A using **138** (50 mg, 0.21 mmol) and 4-fluoro benzaldehyde **73** (30 μL, 0.27 mmol). Title compound **139** was obtained after precipitation and filtration from the reaction crude as yellow solid (76 mg, yield quantitative). ¹H NMR (400 MHz, DMSO-*d*₆) δ 8.73 – 8.64 (m, 3H), 8.46 (dd, J = 8.8, 2.3 Hz, 1H), 8.33 (dd, J = 12.6, 3.7 Hz, 2H), 8.11 (t, J = 8.8 Hz, 2H), 7.89 (d, J = 16.3 Hz, 1H), 3.16 (s, 3H).

6-Chloro-3-(5-(4-fluorophenyl)-4,5-dihydro-1H-pyrazol-3-yl)-4-methylquinolin-2(1H)-one (140) (Scheme 12).

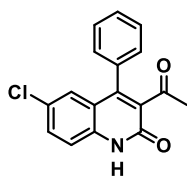


Compound **140** was synthesized via general procedure B using **139** (65 mg, 0.19 mmol) with hydrazine hydrate (16 μ L, 0.33 mmol).

Purification was performed by precipitation and washings with diethyl ether to afford **140** as white solid (25 mg, yield 37%). ^1H NMR (400 MHz, $\text{DMSO-}d_6$) δ 11.88 (s, 1H), 7.83 (d, J = 2.1 Hz, 1H), 7.57 (dd, J = 8.7, 2.1 Hz, 1H), 7.54 – 7.47 (m, 3H), 7.34 (d, J = 8.7 Hz, 1H), 7.19 (t, J = 8.9 Hz, 2H), 4.86 (td, J = 10.6, 3.3 Hz, 1H), 3.43 – 3.36 (m, 1H), 2.90 (dd, J = 16.3, 10.8 Hz, 1H).

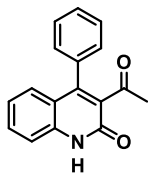
6.2.6 Synthesis of 3-acetyl-4-phenylquinolin-2(1H)-one intermediates (**71a–72a**)

3-Acetyl-6-chloro-4-phenylquinolin-2(1H)-one (71a) (Scheme 3).



2-Amino-5-chlorophenyl phenylmethanone **69** (1.460 g, 6.3 mmol) and ethyl acetoacetate (2.4 mL, 18.9 mmol) were dissolved in DMF (1.00 M) in an appropriately sized screw-capped pressure tube. The mixture was heated at 153 $^{\circ}\text{C}$ and stirred for 19 h. The solvent was removed under reduced pressure to afford **71a** (1.875 g, quantitative yield). ^1H NMR (400 MHz, $\text{DMSO-}d_6$) δ 12.38 (s, 1H), 7.64 (dd, J = 8.8, 2.4 Hz, 1H), 7.59–7.48 (m, 3H), 7.44 (d, J = 8.8 Hz, 1H), 7.39–7.28 (m, 2H), 6.95 (d, J = 2.3 Hz, 1H), 2.22 (s, 3H). $t\text{R}$ = 2.06 min. ESI-MS for $\text{C}_{17}\text{H}_{12}\text{ClNO}_2$: calculated 297.1, found m/z 298.3, 300.3 $[\text{M} + \text{H}]^+$; 296.3, 298.3 $[\text{M} - \text{H}]^-$.

3-Acetyl-4-phenylquinolin-2(1H)-one (72a) (Scheme 3).

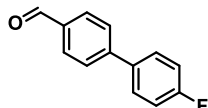


(2-Aminophenyl)phenylmethanone **70** (2.00 g, 10.1 mmol) and ethyl acetoacetate (1.9 mL, 15.2 mmol) were dissolved in DMF (1.00 M) in an appropriately sized microwaveable vessel and microwaved at 120 $^{\circ}\text{C}$ (200 W) for 1.5 h. The solvent was concentrated under reduced pressure, and the residue was diluted with DCM and washed (3 \times 100 mL) with H_2O . The organic layer was dried over Na_2SO_4 , filtered and the solvent removed under reduced pressure. **72a** was obtained after precipitation from EtOAc (1.44 g, 53% yield). ^1H NMR (400 MHz, $\text{DMSO-}d_6$) δ 12.22 (s, 1H), 7.56 (ddd, J = 8.4, 7.1, 1.5 Hz, 1H), 7.54–7.47 (m, 3H), 7.41 (dd, J = 8.4, 1.2 Hz, 1H), 7.34–7.28 (m, 2H), 7.14 (ddd, J = 8.3, 7.1, 1.2 Hz, 1H), 7.05 (dd, J = 8.2, 1.4 Hz, 1H), 2.21 (s, 3H). ^{13}C NMR (101 MHz, $\text{DMSO-}d_6$) δ 201.60, 159.26, 146.96, 138.45, 134.19, 133.29, 131.20, 128.71, 128.64, 128.46, 127.03,

122.33, 118.89, 115.64, 31.47. tR = 1.86 min (generic method). ESI-MS for C₁₇H₁₃NO₂: calculated 263.1, found m/z 264.5 [M + H]⁺; 262.4 [M - H]⁻.

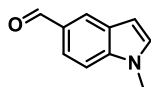
6.2.7 Synthesis of aldehydes **79**, **83**– **90**.

4'-Fluoro-[1,1'-biphenyl]-4-carbaldehyde (**79**) (Scheme 13).



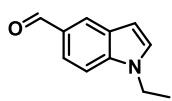
In a screw capped pressure tube commercially available 4-iodo benzaldehyde **141** (255 mg, 1.1 mmol), (4-fluorophenyl) boronic acid **142** (231 mg, 1.5 mmol) and anhydrous sodium carbonate (350 mg, 3.3 mmol) were added. The tube was deoxygenated with three cycles vacuum/Ar, then DMF (2 mL) and H₂O (400 μL) were added. The solution was stirred at rt, under Ar flux, for 15 minutes. Tetrakis (triphenylphosphine) palladium (0) (185 mg, 0.16 mmol) was thus added, the mixture was heated to 110 °C and stirred for 20 h. The crude was then diluted with DCM and washed with water (3 x 50 mL). The organic layer was dried over Na₂SO₄ and the solvent was then removed under reduced pressure. Purification over normal phase flash column chromatography (SiO₂ gold 24 g, A= Cyclohexane, B= EtOAc, gradient 0–7% B) afforded **79** (226 mg, yield 66%). ¹H NMR (400 MHz, DMSO-*d*₆) δ 10.06 (s, 1H), 8.03 – 7.97 (m, 2H), 7.94 – 7.88 (m, 2H), 7.87 – 7.81 (m, 2H), 7.40 – 7.32 (m, 2H).

1-Methyl-1*H*-indole-5-carbaldehyde (**83**) (Scheme 14).



In a screw capped pressure tube 1*H*-indole-5- carboxaldehyde **143** (333 mg, 2.3 mmol) was dissolved with 2.0 mL of anhydrous DMF then potassium carbonate (630 mg, 4.6 mmol) was added and the mixture kept under stirring for 10 minutes at rt. Methyl iodide (647 mg, d = 2.28 g/mL, 284 μL, 4.6 mmol) was then added. The reaction was thus heated to 35 °C and stirred for 18 hours. The crude mixture was diluted with DCM and washed three times with water. The organic layer was anhydridified through a phase separator and the solvent removed under reduced pressure. Purification over normal phase flash column chromatography (SiO₂ gold 24 g, A= Cyclohexane, B= EtOAc, gradient 0–7.5% B) afforded **83** (286 mg, yield 81%). ¹H NMR (400 MHz, DMSO-*d*₆) δ 9.98 (s, 1H), 8.18 (d, J = 1.5 Hz, 1H), 7.74 – 7.56 (m, 2H), 7.49 (d, J = 3.2 Hz, 1H), 6.67 (dd, J = 3.1, 0.8 Hz, 1H), 3.85 (d, J = 1.3 Hz, 3H). ESI-MS for C₁₀H₉NO: calculated 159.1, found m/z 160.1 [M+H]⁺.

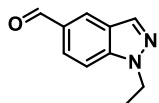
1-Ethyl-1*H*-indole-5-carbaldehyde (**84**) (Scheme 15).



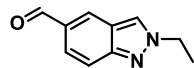
In a screw capped pressure tube 1*H*-indole-5-carboxaldehyde **143** (338 mg, 2.3 mmol) was dissolved with 2.0 mL of anhydrous DMF then potassium carbonate (638 mg, 4.6 mmol) was added and the mixture kept under stirring for 10 minutes at rt. Iodoethane (503 mg, $d = 1.94$ g/mL, 344 μ L, 4.6 mmol) was then added. The reaction was thus heated to 35 °C and stirred for 18 hours. The crude mixture was diluted with DCM and washed three times with water. The organic layer was dried through a phase separator and the solvent removed under reduced pressure. Purification over normal phase flash column chromatography (SiO₂ gold 24 g, A= Cyclohexane, B= EtOAc, gradient 0–5% B) afforded **84** (363 mg, yield 91%). ¹H NMR (400 MHz, DMSO-*d*₆) δ 9.98 (s, 1H), 8.18 (t, $J = 1.1$ Hz, 1H), 7.71 – 7.62 (m, 2H), 7.57 (d, $J = 3.2$ Hz, 1H), 6.67 (dd, $J = 3.2, 0.7$ Hz, 1H), 4.27 (q, $J = 7.2$ Hz, 2H), 1.37 (t, $J = 7.2$ Hz, 3H). ESI-MS for C₁₁H₁₁NO: calculated 173.1, found m/z 174.0 [M+H]⁺.

Ethylindazole-5-carbaldehydes (**85**, **86**) (Scheme 16).

In a screw capped pressure tube 1*H*-indazole-5-carboxaldehyde **144** (300 mg, 2.84 mmol) was dissolved with 3.0 mL of anhydrous DMF then potassium carbonate (1.13 g, 8.2 mmol) was added and the mixture kept under stirring for 10 minutes at rt. Ethyl bromide (335 mg, $d = 1.46$ g/mL, 230 μ L, 3.1 mmol) was then added. The reaction was thus heated to 40 °C and stirred for 5 hours. The crude mixture was diluted with DCM and washed with water (3 x 50 mL). The organic layer was anhydriified through a phase separator and the solvent removed under reduced pressure. Purified by normal phase flash column chromatography (SiO₂ gold 24 g, A= DCM, B= EtOH, gradient 0–50% B). Mono- and bi-dimensional ¹H- and ¹³CNMR (HMBC) analyses confirmed the structure of the title compounds named **85** (1-ethyl-1*H*-indazole-5-carbaldehyde), which showed a positive ¹H¹³C correlation between CH₂ at 4.49 ppm and a quaternary C at 141.7 ppm, and **86** (2-ethyl-2*H*-indazole-5-carbaldehyde), which showed a positive ¹H¹³C correlation between CH₂ at 4.51 ppm and the C₃ at 127.5 ppm, as shown in the reaction scheme above according to their elution order. Yields: (**85**) 179 mg, 50%; (**86**) 121 mg, 34%.



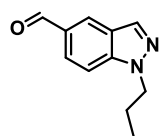
85 ¹H NMR (400 MHz, DMSO-*d*₆) δ 10.04 (s, 1H), 8.43 (t, $J = 1.1$ Hz, 1H), 8.34 (d, $J = 0.8$ Hz, 1H), 7.92 – 7.81 (m, 2H), 4.50 (q, $J = 7.2$ Hz, 2H), 1.42 (t, $J = 7.2$ Hz, 3H). ¹³C NMR (101 MHz, DMSO-*d*₆) δ 192.67, 141.43, 135.64, 130.49, 128.16, 124.80, 123.78, 110.94, 43.85, 15.32. Rt 1.56 min. ESI-MS for C₁₀H₁₀N₂O: calculated 174.1, found m/z 175.3 [M+H]⁺.



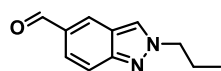
86) ^1H NMR (400 MHz, $\text{DMSO-}d_6$) δ 9.98 (s, 1H), 8.75 (s, 1H), 8.45 (d, $J = 1.2$ Hz, 1H), 7.69 (qd, $J = 9.0, 1.3$ Hz, 2H), 4.52 (q, $J = 7.3$ Hz, 2H), 1.54 (t, $J = 7.3$ Hz, 3H). ^{13}C NMR (101 MHz, $\text{DMSO-}d_6$) δ 192.69, 150.17, 130.99, 130.81, 127.49, 122.46, 121.23, 118.24, 48.63, 16.02. Rt 1.36 min. ESI-MS for $\text{C}_{10}\text{H}_{10}\text{N}_2\text{O}$: calculated 174.1, found m/z 175.3 $[\text{M}+\text{H}]^+$.

Propylindazole-5-carbaldehydes (**87**, **88**) (Scheme 17).

In a screw capped pressure tube 1*H*-indazole-5- carboxaldehyde **144** (152 mg, 1.0 mmol) was dissolved with 1.1 mL of anhydrous DMF then potassium carbonate (359 mg, 2.6 mmol) was added and the mixture kept under stirring for 30 minutes at rt. 1-Bromopropane (256 mg, $d = 1.353$ g/mL, 189 μL , 2.0 mmol) was then added. The reaction was thus stirred for 14 h at rt. The crude mixture was diluted with DCM and washed with water (3 x 50 mL). The organic layer was dried through a phase separator and the solvent removed under reduced pressure. Purified by normal phase flash column chromatography (SiO_2 gold 24 g, A= DCM, B= EtOH, gradient 0–70% B). Mono- and bi-dimensional ^1H - and ^{13}C -NMR (HMBC) analyses confirmed the structure of the title compounds named **87** (1-propyl-1*H*-indazole-5- carbaldehyde), which showed a positive $^1\text{H}^{13}\text{C}$ correlation between CH_2 at 4.42 ppm and a quaternary C at 142.0 ppm, and **88** (2-propyl-2*H*-indazole-5-carbaldehyde), which showed a positive $^1\text{H}^{13}\text{C}$ correlation between CH_2 at 4.44 ppm and the C_3 at 128.2 ppm, as shown in the reaction scheme above according to their elution order. Yields: (**87**) 99 mg, 50%; (**88**) 66 mg, 34%.



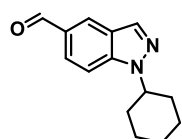
87) ^1H NMR (400 MHz, $\text{DMSO-}d_6$) δ 10.02 (s, 1H), 8.42 (d, $J = 1.2$ Hz, 1H), 8.33 (s, 1H), 7.88 – 7.80 (m, 2H), 4.42 (t, $J = 6.9$ Hz, 2H), 1.85 (h, $J = 7.2$ Hz, 2H), 0.85 – 0.77 (m, 3H). ^{13}C NMR (101 MHz, $\text{DMSO-}d_6$) δ 192.18, 141.58, 135.19, 129.99, 127.69, 124.33, 123.15, 110.55, 49.84, 22.80, 11.02. ESI-MS for $\text{C}_{11}\text{H}_{12}\text{N}_2\text{O}$: calculated 188.1, found m/z 189.1 $[\text{M}+\text{H}]^+$.



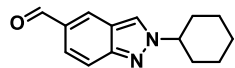
88) ^1H NMR (400 MHz, $\text{DMSO-}d_6$) δ 9.97 (s, 1H), 8.73 (s, 1H), 8.44 (d, $J = 1.4$ Hz, 1H), 7.78 – 7.62 (m, 2H), 4.43 (t, $J = 7.0$ Hz, 2H), 1.95 (h, $J = 7.2$ Hz, 2H), 0.85 (t, $J = 7.4$ Hz, 3H). ^{13}C NMR (101 MHz, $\text{DMSO-}d_6$) δ 192.21, 149.74, 130.53, 130.36, 127.71, 121.97, 120.65, 117.78, 54.60, 23.20, 10.83. Rt 1.61 min. ESI-MS for $\text{C}_{11}\text{H}_{12}\text{N}_2\text{O}$: calculated 188.1, found m/z 189 $[\text{M}+\text{H}]^+$.

Cyclohexylindazole-5-carbaldehydes (**89**, **90**) (Scheme 18).

In a screw capped pressure tube 1*H*-indazole-5-carboxaldehyde **144** (165 mg, 2.13 mmol) was dissolved with 1.0 mL of anhydrous DMF then potassium carbonate (624 mg, 4.52 mmol) was added and the mixture kept under stirring for 30 minutes at rt. Bromocyclohexane (737 mg, d = 1.335 g/mL, 552 μ L, 4.52 mmol) was then added. The reaction was thus stirred at rt for 6 days. The crude mixture was diluted with DCM and washed with water (3 x 50 mL). The organic layer was dried through a phase separator and the solvent removed under reduced pressure. Purified by normal phase flash column chromatography (SiO₂ gold 24 g, A= DCM, B= EtOH, gradient 0–50% B). Mono- and bi-dimensional ¹H- and ¹³C-NMR (HMBC) analyses confirmed the structure of the title compounds named **89** (1-cyclohexyl-1*H*-indazole-5-carbaldehyde) and **90** (2-cyclohexyl-2*H*-indazole-5-carbaldehyde) according to their elution order, as shown in the reaction scheme above. **90** showed a positive ¹H¹³C correlation between CH at 4.54 ppm and the C₃ at 126.1 ppm. Yields: (**89**) 111 mg, 21%; (**90**) 75 mg, 14%.



89 ¹H NMR (400 MHz, DMSO-*d*₆) δ 10.02 (s, 1H), 8.41 (t, *J* = 1.0 Hz, 1H), 8.32 (s, 1H), 7.91 – 7.81 (m, 2H), 4.67 (tt, *J* = 10.0, 5.0 Hz, 1H), 1.89 (ddt, *J* = 24.4, 11.6, 3.7 Hz, 6H), 1.71 (dt, *J* = 12.7, 3.3 Hz, 1H), 1.50 (dt, *J* = 16.7, 8.1, 4.4 Hz, 2H), 1.27 (qt, *J* = 12.8, 3.5 Hz, 1H). ¹³C NMR (101 MHz, DMSO-*d*₆) δ 192.18, 140.59, 134.95, 130.06, 127.69, 124.09, 123.14, 110.54, 56.92, 32.23, 24.94. Rt 2.30 min. ESI-MS for C₁₄H₁₆N₂O: calculated 228.1, found *m/z* 229.0 [M+H]⁺.



90 ¹H NMR (400 MHz, DMSO-*d*₆) δ 9.97 (s, 1H), 8.76 (d, *J* = 0.9 Hz, 1H), 8.43 (t, *J* = 1.2 Hz, 1H), 7.74 – 7.62 (m, 2H), 4.53 (tt, *J* = 11.4, 3.8 Hz, 1H), 2.18 – 2.09 (m, 2H), 1.97 – 1.81 (m, 4H), 1.78 – 1.65 (m, 1H), 1.46 (qt, *J* = 12.9, 3.5 Hz, 2H), 1.27 (qt, *J* = 12.8, 3.5 Hz, 1H). ¹³C NMR (101 MHz, DMSO-*d*₆) δ 192.23, 149.27, 130.48, 130.40, 125.65, 121.89, 120.46, 117.88, 62.06, 33.08, 24.83, 24.77. Rt 2.05 min. ESI-MS for C₁₄H₁₆N₂O: calculated 228.1, found *m/z* 228.8 [M+H]⁺.

*Separation and ELISA assay results of enantiomers **19-I** and **19-II***

The semi-preparative chiral separations of the racemic **19** by HPLC were performed on a Waters Alliance HPLC instrument consisting of a 1525 Binary HPLC Pump, Waters Fraction Collector III and a 2998 Photodiode Array Detector. The separations were run in isocratic mode on a Daicel ChiralPak AD column (250x10mmID, particle size 10 μ m) with a ChiralPak AD Semi-Prep. Guard pre-column (50x10mmID, particle size 10 μ m). The mobile phase was Heptane-2-Propanol (75:25) with a flowrate = 5mL/min.

To determine the enantiomeric excess (ee) of the enantiomers **19-I** and **19-II**, the analytical chiral separations by HPLC were run on a Waters Alliance HPLC instrument consisting of an e2695 Separation Module and a 2998 Photodiode Array Detector. The PDA range was 210-400nm. The analyses were performed in isocratic mode on a Daicel ChiralPak AD column (250x4.6mmID, particle size 10 μ m). The mobile phase was Heptane-2-Propanol (50:50) with a flow rate = 1mL/min; **19-I**: tR = 6.411min., >99.5% ee at 240nm; **19-II**: tR = 13.431min., 96.6% ee at 240nm. The ¹H NMR spectrum was identical to that of racemic **19** for each enantiomer.

Table 18. Chiral separation of **19-I** and **19-II** and ELISA assay results.

Compound	Retention time (tR)	QC (UV) @215 nm	Enantiomeric excess (ee)	EC ₅₀ ELISA (μ M)
19-I	6.411 minutes	97%	>99.5%	4 \pm 0.5
19-II	13.431 minutes	99%	96.6%	10 \pm 1

6.3 Experimental section: Part II

Material and methods

Chemicals were purchased from commercial suppliers and used without pretreatment. Solvents used for the experiments were reagent-grade and dried, if necessary, according to standard procedures. The reactions were performed under a nitrogen atmosphere unless otherwise stated. The yields were calculated for the analytically pure compounds and were not optimized. ^1H and ^{13}C -NMR spectra were measured on a Bruker Fourier 500 spectrometer (500 or 126 MHz respectively). The chemical shifts were reported in parts per million (ppm) relative to the corresponding solvent peak. The coupling constants of the splitting patterns were reported in Hz and were indicated as singlet (s), doublet (d), triplet (t), and multiplet (m). Due to the presence of isomers for acylhydrazones, some of the signals are doubled. UPLC-MS and HRMS measurements were performed using ThermoScientific systems, see supporting information.

UPLC-MS analysis in tdDCC

The periodic progress and analysis of DCC were monitored on UPLC-MS (ThermoScientific Dionex Ultimate 3000 UHPLC System coupled to a ThermoScientific Q Exactive Focus with an electrospray ion source). An Acquity Waters Column (BEH C8, 1.7 μm , 2.1 x 150 mm, Waters, Germany) equipped with a VanGuard Pre-Column (BEH C8, 1.7 μm , 5 x 2.1 mm, Waters, Germany) was used for the separation. At a flow rate of 0.25 mL/min, the gradient of H_2O (0.1% formic acid) and acetonitrile (0.1% formic acid) was held at 5% acetonitrile for 1 min and then increased to 95% over 16 min. It was held there for 1.5 min before the gradient was decreased to 5% over 0.1 min where it was held for 1.9 min. Detection was set at 210, 254, 290, and 310 nm and the mass spectrum was measured in a positive mode in the range of 100-700 m/z.

HRMS analysis for DCL1 compounds

High-resolution mass spectra were recorded with ThermoScientific system where Dionex Ultimate 3000 RSLC was coupled to a Q Exactive Focus mass spectrometer with an electrospray ion source. An Acquity UPLC $\text{\textcircled{R}}$ BEH C8, 1.7 μm , 2.1 x 150 mm, column equipped with a VanGuard Pre-Column BEH C8 1.7 μm , 5 x 2.1 mm (Waters, Germany) was used for the separation. At a flow rate of 250 $\mu\text{L}/\text{min}$, the gradient of H_2O (0.1% formic acid) and acetonitrile (0.1% formic acid) was held at 10% acetonitrile for 1 min and then increased to 95% over 4 min. It was held there for 1.2 min before the gradient was decreased to 10% over 0.3 min where it

was held for 1 min. The mass spectrum was measured in a positive mode in a range from 120-1000 m/z. The UV spectrum was recorded at 254 nm.

6.3.1 General Procedures for tdDCC experiments

General Procedure-1: DCL preparation

To a 1.5 mL Eppendorf Tube® containing HEPES buffer (pH 7.02, KCl 300 mM, glycerol 5%) was added hydrazides (300–1000 μM each, in DMSO), aldehydes (100 μM each, in DMSO), and aniline (10 mM, in DMSO) with 250 μL of end-volume. The DCL was allowed to gently mix on a rotating wheel (7 rpm) at room temperature and was frequently monitored via UPLC-MS. For analysis, 10 μL of the corresponding library was mixed with 90 μL methanol and 2 μL of NaOH (2 M), the mixture was centrifuged at 14,000 rpm for 8 min and the supernatant was used for the analysis.

General Procedure-2: Protein-templated DCL preparation

To a 1.5 mL Eppendorf Tube® containing HEPES buffer (pH 7.02, KCl 300 mM, glycerol 5%) was added hydrazides (300–1000 μM each, in DMSO), aldehydes (100 μM each, in DMSO), aniline (10 mM, in DMSO), and the protein RAD51 (17.2 μM in buffer HEPES 20 mM, pH 7.54, KCl 300 mM, glycerol 10%, EDTA 0.1 mM, DTT 2.0 mM) with 250 μL of end-volume. The DCL with the protein was allowed to gently mix on a rotating wheel (7 rpm) at room temperature and was frequently monitored via UPLC-MS and the traces were compared with the blank composition. For analysis, 10 μL of the corresponding library was mixed with 90 μL methanol and 2 μL of NaOH (2 M), the mixture was centrifuged at 14,000 rpm for 8 min and the supernatant was used for the analysis. The protein-templated DCL were run as duplicates.

General procedure-3: N-acylhydrazone synthesis

To a heat-dried Schlenk tube equipped with a magnetic stirring bar, the hydrazide (1.0 equiv.) and the corresponding aldehyde (1.0 equiv.) was dissolved/suspended in MeOH under nitrogen atmosphere. The reaction mixture was stirred at 65 °C until completion. The reaction was cooled to room temperature, then the reaction mixture was precipitated by cooling at 0 °C in an ice bath. The precipitated reaction mixture was transferred to Eppendorf Tube® and centrifuged for 2 minutes, the supernatant liquid was removed and 1 mL ice-cold MeOH was added to the

residue, which was resuspended by vigorous agitation by a vortex mixer. The cold suspension was centrifuged again for 2 min, followed by removal of supernatant liquid. This process was repeated for at least three times or till the sufficiently pure product (residue) was not isolated, which was monitored on LC-MS. The solvents were removed under reduced pressure to obtain pure acylhydrazone product in 52–87 % yields.

6.3.2 tdDCC experiments

tdDCC-1

This experiment library DCL1 consists of three aldehydes (A1–A3) and eight hydrazides (H1–H8). The DCC-experiment was carried out according to the general procedure-1 (blank) and general procedure-2 (protein-templated) in HEPES 20 mM (pH 7.02, KCl 300 mM, glycerol 5%) (Table 15).

Table 15. DCL1 composition and final concentrations.

Entry	Blank		Protein-templated (I)		Protein-templated (II)	
	Amount	Final concentration	Amount	Final concentration	Amount	Final concentration
Buffer	240.75 μ L	-	140.75 μ L	-	140.75 μ L	-
Hydrazide (100 mM)	8 x 0.75 μ L	0.3 mM	8 x 0.75 μ L	0.3 mM	8 x 0.75 μ L	0.3 mM
Aldehyde (100 mM)	3 x 0.25 μ L	0.1 mM	3 x 0.25 μ L	0.1 mM	3 x 0.25 μ L	0.1 mM
Aniline (1M)	2.5 μ L	10 mM	2.5 μ L	10 mM	2.5 μ L	10 mM
DMSO	9.25 μ L	3.7%	9.25 μ L	3.7%	9.25 μ L	3.7%
RAD51 (43 μ M)	0	-	100 μ L	17.2 μ M	100 μ L	17.2 μ M
Tot volume	250 μ L	-	250 μ L	-	250 μ L	-

The DCL1 was left shaking at room temperature and was monitored at 8 h, 24 h, 48 h, and 72 h *via* UPLC-MS.

tdDCC-2

This experiment library DCL1 consists of ten aldehydes (A1–A10) and two hydrazides (H1–H2). The DCC-experiment was carried out according to the general procedure-1 (blank) and general procedure-2 (protein-templated) in HEPES 20 mM (pH 7.02, KCl 300 mM, glycerol 5%) (Table 16).

Table 16. DCL2 composition and final concentrations.

Entry	Blank		Protein-templated (I)		Protein-templated (II)	
	Amount	Final concentration	Amount	Final concentration	Amount	Final concentration
Buffer	242.50 μ L	-	142.50 μ L	-	142.50 μ L	-

Hydrazide (100 mM)	2 x 2.50 μ L	1.0 mM	2 x 2.50 μ L	1.0 mM	2 x 2.50 μ L	1.0 mM
Aldehyde (100 mM)	10 x 0.25 μ L	0.1 mM	10 x 0.25 μ L	0.1 mM	10 x 0.25 μ L	0.1 mM
Aniline (1M)	2.5 μ L	10 mM	2.5 μ L	10 mM	2.5 μ L	10 mM
DMSO	10.0 μ L	4.0%	10.0 μ L	4.0%	10.0 μ L	4.0%
RAD51 (43 μ M)	0	-	100 μ L	17.2 μ M	100 μ L	17.2 μ M
Tot volume	250 μ L	-	250 μ L	-	250 μ L	-

The DCL2 was left shaking at room temperature and was monitored at 0 h, 2 h, 4 h, 6 h, 8 h, 10 h, and 24 h *via* UPLC-MS.

tdDCC-3

This experiment library DCL1 consists of six aldehydes (A1–A6) and three hydrazides (H1–H3). The DCC-experiment was carried out according to the general procedure-1 (blank) and general procedure-2 (protein-templated) in HEPES 20 mM (pH 7.02, KCl 300 mM, glycerol 5%) (Table 17).

Table 17. DCL3 composition and final concentrations.

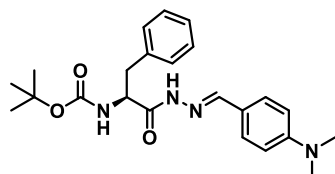
Entry	Blank		Protein-templated (I)		Protein-templated (II)	
	Amount	Final concentration	Amount	Final concentration	Amount	Final concentration
Buffer	238.25 μ L	-	138.25 μ L	-	138.25 μ L	-
Hydrazide (100 mM)	3 x 1.75 μ L	0.7 mM	3 x 1.75 μ L	0.7 mM	3 x 1.75 μ L	0.7 mM
Aldehyde (100 mM)	6 x 0.25 μ L	0.1 mM	6 x 0.25 μ L	0.1 mM	6 x 0.25 μ L	0.1 mM
Aniline (1M)	2.5 μ L	10 mM	2.5 μ L	10 mM	2.5 μ L	10 mM
DMSO	9.25 μ L	3.7%	9.25 μ L	3.7%	9.25 μ L	3.7%
RAD51 (43 μ M)	0	-	100 μ L	17.2 μ M	100 μ L	17.2 μ M
Tot volume	250 μ L	-	250 μ L	-	250 μ L	-

The DCL3 was left shaking at room temperature and was monitored at 0h, 2h, 4h, 6h, 8h, 10h, and 24h *via* UPLC-MS.

6.3.3 *N*-acylhydrazone synthesis and characterization

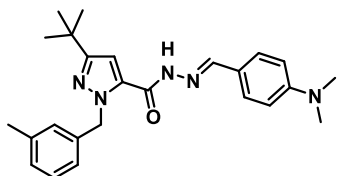
DCL1 *N*-Acylhydrazones synthetic procedures

***tert*-butyl (S) - (1- (2- (4- (dimethylamino) benzylidene) hydrazineyl) - 1 - oxo -3-phenylpropan-2-yl) carbamate (A1H3)**



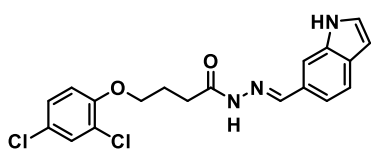
The acylhydrazone **A1H3** was synthesized according to the general procedure-3, using *N*-(*tert*-butoxycarbonyl)-L-phenylalanine acid hydrazide **H3** (46 mg, 0.165 mmol) and 4-(dimethylamino) benzaldehyde **A1** (24.6 mg, 0.165 mmol) in MeOH (1.0 mL). After purification through cold MeOH washings, **A1H3** was obtained as a mixture of *E* and *Z* isomers (*E*:*Z* = 47:53) as a white pure solid (46 mg, 70% yield). NMR spectra are reported as mixture of *E* and *Z* isomers. ¹H-NMR (500 MHz, DMSO-*d*₆) δ 11.22 (s, 1H), 11.07 (s, 1H), 8.04 (s, 1H), 7.88 (s, 1H), 7.51 (t, *J* = 8.5 Hz, 4H), 7.37 – 7.24 (m, 8H), 7.20 (m, 2H), 7.13 (d, *J* = 8.3 Hz, 1H), 6.99 (d, *J* = 8.9 Hz, 1H), 6.76 (dd, *J* = 12.9, 9.0 Hz, 4H), 5.03 (td, *J* = 10.2, 3.6 Hz, 1H), 4.19 (td, *J* = 9.5, 5.0 Hz, 1H), 2.98 (s, 6H), 2.97 (s, 6H), 2.94 (m, 2H), 2.79 (m, 2H), 1.32 (s, 9H), 1.31 (s, 9H). ¹³C-NMR (126 MHz, DMSO-*d*₆) δ 173.1, 168.2, 155.9, 155.8, 151.9, 151.8, 148.0, 144.7, 139.0, 138.5, 129.7, 129.5, 128.8, 128.5, 128.5, 128.4, 126.7, 122.0, 121.9, 112.3, 112.2, 78.5, 78.3, 55.5, 53.4, 37.8, 36.8, 28.63; HRMS (ESI) calcd for C₂₃H₃₀N₄O₃ 410.23179, found 411.23813 [M+H]⁺. UPLC-MS @254nm 98.5% purity.

3-(*tert*-butyl)-*N*'-(4-(dimethylamino)benzylidene)-1-(3-methylbenzyl)-1*H*-pyrazole-5-carbohydrazide (A1H7)



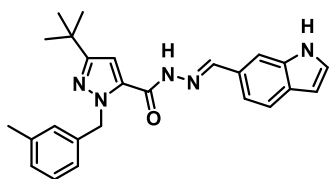
The acylhydrazone **A1H7** was synthesized according to the general procedure-3, using 3-(*tert*-butyl)-1-(3-methylbenzyl)-1*H*-pyrazole-5-carbohydrazide **H7** (62.5 mg, 0.218 mmol) and 4-(dimethylamino) benzaldehyde **A1** (32.6 mg, 0.218 mmol) in MeOH (1.0 mL). After purification through cold MeOH washings, **A1H7** was obtained as a white pure solid (59 mg, 65% yield). ¹H-NMR (500 MHz, DMSO-*d*₆) δ 11.49 (s, 1H), 8.23 (s, 1H), 7.51 (d, *J* = 8.9 Hz, 2H), 7.18 (t, *J* = 7.6 Hz, 1H), 7.05 (d, *J* = 7.5 Hz, 1H), 6.97 (s, 1H), 6.91 – 6.83 (m, 2H), 6.76 (d, *J* = 8.9 Hz, 2H), 5.66 (s, 2H), 2.98 (s, 6H), 2.25 (s, 3H), 1.29 (s, 9H); ¹³C-NMR (126 MHz, DMSO-*d*₆) δ 160.0, 155.9, 152.0, 149.2, 138.6, 137.8, 134.6, 128.9, 128.7, 128.3, 128.0, 124.4, 121.7, 112.2, 104.5, 53.9, 32.2, 30.8, 21.5; HRMS (ESI) calcd for C₂₅H₃₁N₅O 417.25286, found 418.25922 [M+H]⁺. UPLC-MS @254nm 99.5% purity.

N'-((1*H*-indol-6-yl) methylene)-4-(2,4-dichlorophenoxy)butanehydrazide (**A2H4**)



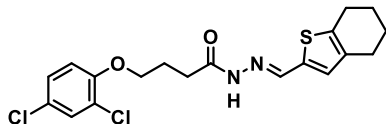
The acylhydrazone **A2H4** was synthesized according to the general procedure-3, using 4-(2,4-dichlorophenoxy)butanehydrazide **H4** (51.6 mg, 0.196 mmol) and 1*H*-indole-6-carbaldehyde **A2** (28.5 mg, 0.196 mmol) in MeOH (1.0 mL). After purification through cold MeOH washings, **A2H4** was obtained as a mixture of *E* and *Z* isomers (*E*:*Z* = 40: 60) as a white-pink pure solid (51 mg, 67% yield). NMR spectra are reported as mixture of isomers, in agreement with R.P. Jumde *et al*¹⁷⁴. ¹H-NMR (500 MHz, DMSO-*d*₆) δ 11.29 (br s, 1H), 11.27 (s, 1H), 11.25 (br s, 1H), 11.15 (s, 1H), 8.22 (s, 1H), 8.06 (s, 1H), 7.69 (s, 1H), 7.61 (s, 1H), 7.59 – 7.51 (m, 4H), 7.46 (t, J = 2.8 Hz, 1H), 7.44 (t, J = 2.7 Hz, 1H), 7.41– 7.32 (m, 4H), 7.20 (dd, J = 9.0, 2.3 Hz, 2H), 6.46 (q, J = 2.4 Hz, 2H), 4.16 (t, J = 6.4 Hz, 2H), 4.12 (t, J = 6.3 Hz, 2H), 2.85 (t, J = 7.4 Hz, 2H), 2.42 (t, J = 7.3 Hz, 2H), 2.14 – 2.00 (m, 4H). ¹³C NMR (126 MHz, DMSO-*d*₆) δ 173.9, 168.1, 153.5, 148.0, 144.9, 136.3, 136.22, 129.7, 129.5, 128.6, 127.9, 127.8, 124.8, 124.8, 122.9, 120.8, 120.7, 118.4, 117.6, 115.5, 115.47, 111.49, 111.28, 102.0, 102.0, 68.8, 30.8, 28.8, 24.8, 24.1 HRMS (ESI) calcd for C₁₉H₁₇Cl₂N₃O₂ 389.06978, found 390.07639 [M+H]⁺. UPLC-MS @254nm 98 % purity.

N'-((1*H*-indol-6-yl)methylene)-3-(*tert*-butyl)-1-(3-methylbenzyl)-1*H*-pyrazole-5-carbohydrazide (**A2H7**)



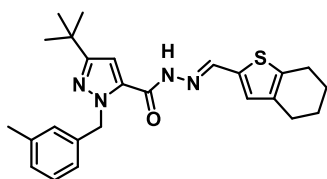
The acylhydrazone **A2H7** was synthesized according to the general procedure-3, using 3-(*tert*-butyl)-1-(3-methylbenzyl)-1*H*-pyrazole-5-carbohydrazide **H7** (73.9 mg, 0.279 mmol) and 1*H*-indole-6-carbaldehyde **A2** (37.4 mg, 0.279 mmol) in MeOH (1.0 mL). After purification through cold MeOH washings, **A2H7** was obtained as a yellow-orange pure solid (93 mg, 81% yield). ¹H-NMR (500 MHz, DMSO-*d*₆) δ 11.64 (s, 1H), 11.32 (s, 1H), 8.43 (s, 1H), 7.71 (s, 1H), 7.59 (d, J = 8.2 Hz, 1H), 7.47 (s, 1H), 7.39 (d, J = 8.3 Hz, 1H), 7.18 (t, J = 7.6 Hz, 1H), 7.05 (d, J = 7.5 Hz, 1H), 6.95 (d, J = 27.9 Hz, 2H), 6.90 (d, J = 7.6 Hz, 1H), 6.48 (d, J = 2.2 Hz, 1H), 5.68 (s, 2H), 2.25 (s, 3H), 1.30 (s, 9H); ¹³C-NMR (126 MHz, DMSO-*d*₆) δ 193.2, 160.0, 156.1, 150.2, 138.6, 137.8, 136.2, 134.5, 129.9, 128.7, 128.3, 128.1, 128.1, 127.5, 124.5, 120.8, 118.5, 111.5, 104.7, 102.0, 53.9, 32.2, 30.8, 21.5; HRMS (ESI) calcd for C₂₅H₂₇N₅O 413.22156, found 414.22830 [M+H]⁺, 412.21460 [M-H]⁻. UPLC-MS @254nm 95 % purity.

4-(2,4-dichlorophenoxy)-N'-((4,5,6,7-tetrahydrobenzo[b]thiophen-2-yl)methylene)butanehydrazide (A3H4)



The acylhydrazone **A3H4** was synthesized according to the general procedure-3, using 4-(2,4-dichlorophenoxy)butanehydrazide **H4** (91.8 mg, 0.349 mmol) and 4,5,6,7-tetrahydrobenzo[b]thiophene-2-carbaldehyde **A3** (58.0 mg, 0.349 mmol) in MeOH (1.0 mL). After purification through cold MeOH washings, **A3H4** was obtained as a mixture of *E* and *Z* isomers (*E*:*Z* = 43:57) as a yellowish pure solid (92 mg, 65% yield). NMR spectra are reported as mixture of isomers. ¹H-NMR (500 MHz, DMSO-*d*₆) δ 11.25 (s, 1H), 11.15 (s, 1H), 8.26 (s, 1H), 8.03 (s, 1H), 7.56 (t, *J* = 2.2 Hz, 2H), 7.39 – 7.30 (m, 2H), 7.18 (d, *J* = 8.8 Hz, 2H), 7.07 (s, 1H), 7.01 (s, 1H), 4.10 (dt, *J* = 12.8, 6.2 Hz, 4H), 2.70 (dt, *J* = 12.6, 6.5 Hz, 8H), 2.36 (t, *J* = 7.2 Hz, 2H), 2.01 (dd, *J* = 12.4, 6.2 Hz, 2H), 1.85 – 1.64 (m, 8H). ¹³C-NMR (126 MHz, DMSO-*d*₆) δ 173.7, 168.1, 153.4, 141.8, 138.7, 138.4, 138.1, 136.0, 135.6, 131.9, 131.1, 129.7, 128.6, 128.5, 124.8, 124.7, 122.9, 122.8, 115.5, 115.5, 68.8, 30.8, 28.6, 25.3, 25.2, 25.1, 24.7, 24.0, 23.3, 22.6; HRMS (ESI) calcd for C₁₉H₂₀Cl₂N₂O₂S, 410.06225, found 411.06716 [M+H]⁺. UPLC-MS @254nm 99 % purity.

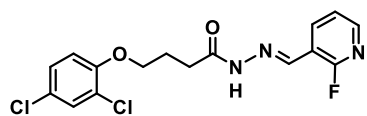
3-(*tert*-butyl)-1-(3-methylbenzyl)-N'-((4,5,6,7-tetrahydrobenzo[b]thiophen-2-yl)methylene)-1*H*-pyrazole-5-carbohydrazide (A3H7)



The acylhydrazone **A3H7** was synthesized according to the general procedure-3, using 3-(*tert*-butyl)-1-(3-methylbenzyl)-1*H*-pyrazole-5-carbohydrazide **H7** (51.9 mg, 0.180 mmol) and 4,5,6,7-tetrahydrobenzo[b]thiophene-2-carbaldehyde **A3** (30.1 mg, 0.180 mmol) in MeOH (1.0 mL). After purification through cold MeOH washings, **A3H7** was obtained as a yellow pure solid (56 mg, 72% yield). ¹H-NMR (500 MHz, DMSO-*d*₆) δ 11.64 (s, 1H), 8.46 (s, 1H), 7.17 (s, 1H), 7.13 (s, 1H), 7.05 (d, *J* = 7.5 Hz, 1H), 6.96 (s, 1H), 6.88 (s, 2H), 5.64 (s, 2H), 2.73 (t, *J* = 5.6 Hz, 2H), 2.55 (t, *J* = 5.8 Hz, 2H), 2.25 (s, 3H), 1.75 (ddd, *J* = 14.8, 9.0, 4.4 Hz, 4H), 1.28 (d, *J* = 7.3 Hz, 9H); ¹³C-NMR (126 MHz, DMSO-*d*₆) δ 160.0, 155.9, 143.7, 139.4, 138.6, 137.8, 136.2, 135.3, 134.3, 132.6, 128.7, 128.3, 128.0, 124.4, 104.7, 53.9, 32.2, 30.8, 25.2, 23.3, 22.6, 21.5; HRMS (ESI) calcd for C₂₅H₃₀N₄OS, 434.21403, found 453.22070 [M+H]⁺. UPLC-MS @254nm 98 % purity.

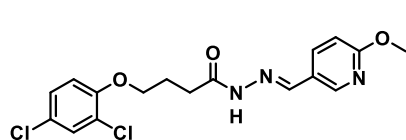
DCL2 *N*-Acylhydrazones synthetic procedures

4-(2,4-dichlorophenoxy)-*N*-((2-fluoropyridin-3-yl)methylene)butanehydrazide (H1A1)



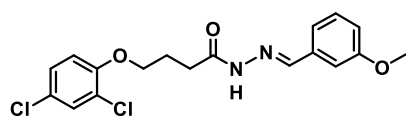
The acylhydrazone **H1A1** was synthesized according to the general procedure-3, using 4-(2,4-dichlorophenoxy)butanehydrazide **H1** (mg, mmol) and 2-fluoronicotinaldehyde **A1** (mg, mmol) in MeOH (mL). After purification through cold MeOH washings, **H1A1** was obtained as a mixture of *E* and *Z* isomers (*E*:*Z* = 30:70) as white-yellow pure solid (mg, yield). ¹H-NMR (500 MHz, DMSO-*d*₆) δ 11.54 (s, 2H), 8.30 (dt, *J* = 17.4, 6.7 Hz, 3H), 8.08 (s, 1H), 7.53 (d, *J* = 4.2 Hz, 2H), 7.48 – 7.37 (m, 2H), 7.34 (dd, *J* = 13.8, 5.6 Hz, 2H), 7.17 (dd, *J* = 8.8, 4.8 Hz, 2H), 4.12 (dd, *J* = 10.9, 4.9 Hz, 4H), 2.83 (t, *J* = 7.3 Hz, 2H), 2.43 (t, *J* = 7.3 Hz, 2H), 2.12 – 1.97 (m, 4H). ¹³C-NMR (126 MHz, DMSO-*d*₆) δ 174.0, 161.1, 152.9, 148.1, 137.2, 136.6, 134.1, 129.3, 128.2, 124.2, 122.2, 115.0, 68.3, 28.3, 23.7. ESI-MS for C₁₆H₁₄Cl₂FN₃O₂: calculated 369.04, found 370.0/372.0/374.1 [M+H]⁺, 368.1/370.1/372.1 [M+H]⁻.

4-(2,4-dichlorophenoxy)-*N*-((6-methoxypyridin-3-yl)methylene)butanehydrazide (H1A6)



The acylhydrazone **H1A6** was synthesized according to the general procedure-3, using 4-(2,4-dichlorophenoxy)butanehydrazide **H1** (mg, mmol) and 6-methoxynicotinaldehyde **A6** (mg, mmol) in MeOH (mL). After purification through cold MeOH washings, **H1A6** was obtained as a mixture of *E* and *Z* isomers (*E*:*Z* = 38:62) as a white-yellow pure solid (mg, yield). ¹H-NMR (500 MHz, DMSO-*d*₆) δ 11.40 (s, 1H), 11.29 (s, 1H), 8.37 (d, *J* = 2.0 Hz, 1H), 8.33 (d, *J* = 2.1 Hz, 1H), 8.16 (s, 1H), 8.04 (dd, *J* = 8.7, 2.2 Hz, 1H), 8.00 (dd, *J* = 8.7, 2.3 Hz, 1H), 7.95 (s, 1H), 7.56 (t, *J* = 2.8 Hz, 2H), 7.35 (td, *J* = 8.7, 2.6 Hz, 2H), 7.19 (dd, *J* = 9.0, 2.8 Hz, 2H), 6.90 (d, *J* = 8.7 Hz, 1H), 6.86 (d, *J* = 8.7 Hz, 1H), 4.12 (dt, *J* = 12.9, 6.4 Hz, 4H), 2.81 (t, *J* = 7.4 Hz), 2.41 (t, *J* = 7.3 Hz), 2.04 (p, *J* = 6.8 Hz, 4H). ¹³C-NMR (126 MHz, DMSO-*d*₆) δ 173.5, 167.6, 164.0, 152.7, 146.6, 143.0, 139.6, 135.4, 129.0, 127.9, 124.1, 122.2, 114.8, 110.9, 68.1, 53.2, 29.9, 28.2, 23.5. ESI-MS for C₁₇H₁₇Cl₂N₃O₃: calculated 381.06, found 382.0/384.0/386 [M+H]⁺, 380.1/382.1/384.1 [M+H]⁻.

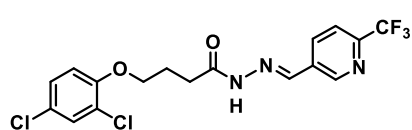
4-(2,4-dichlorophenoxy)-*N*-(3-methoxybenzylidene)butanehydrazide (H1A9)



The acylhydrazone **H1A9** was synthesized according to the general procedure-3, using 4-(2,4-dichlorophenoxy)butanehydrazide **H1** (99 mg, 0.376 mmol) and 3-methoxybenzaldehyde **A9** (45.8 μL, 0.376 mmol) in MeOH (0.76 mL). After purification through

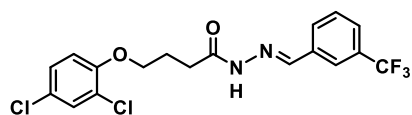
cold MeOH washings, **H1A9** was obtained as a mixture of *E* and *Z* isomers (*E:Z* = 37:63) as a white-pink pure solid (104 mg, yield 73%). NMR spectra are reported as mixture of isomers. ¹H-NMR (400 MHz, DMSO-*d*₆) δ 11.43 (s, 1H), 11.31 (s, 1H), 8.13 (s, 1H), 7.94 (s, 1H), 7.55 (dd, *J* = 4.9, 2.5 Hz, 2H), 7.39 – 7.28 (m, 4H), 7.26 – 7.14 (m, 6H), 7.01 – 6.94 (m, 2H), 4.19 – 4.06 (m, 4H), 3.78 (d, *J* = 6.4 Hz, 6H), 2.83 (t, *J* = 7.3 Hz, 2H), 2.42 (t, *J* = 7.3 Hz, 2H), 2.12 – 1.99 (m, 4H). ¹³C-NMR (101 MHz, DMSO-*d*₆) δ 174.2, 171.0, 168.4, 159.9, 153.4, 146.1, 142.8, 136.2, 136.1, 130.2, 129.6, 128.54, 128.51, 124.8, 124.7, 122.8, 120.2, 119.5, 116.4, 115.8, 115.5, 115.4, 111.9, 111.5, 68.8, 68.7, 55.58, 55.54, 30.7, 28.7, 24.7, 24.1; ESI-MS for C₁₈H₁₈Cl₂N₂O₃: calculated 380.07, found *m/z* 381.24, 383.24 [M+H]⁺. UPLC-MS @254nm 99.5% purity.

4-(2,4-dichlorophenoxy)-*N*'-((6-(trifluoromethyl)pyridin-3-yl) methylene) butanehydrazide (**H1A2**)



The acylhydrazone **H1A2** was synthesized according to the general procedure-3, using 4-(2,4-dichlorophenoxy) butanehydrazide **H1** (100 mg, 0.38 mmol) and 6-(trifluoromethyl) nicotinaldehyde **A2** (66.5 mg, 0.38 mmol) in MeOH (0.76 mL). After purification through cold MeOH washings, **H1A2** was obtained as a mixture of *E* and *Z* isomers (*E:Z* = 40:60) as a white-off pure solid (95 mg, yield 60%). NMR spectra are reported as mixture of isomers. ¹H-NMR (400 MHz, DMSO-*d*₆) δ 11.76 (s, 1H), 11.66 (s, 1H), 8.99 (s, 1H), 8.32 (dd, *J* = 23.2, 8.4 Hz, 3H), 8.08 (s, 1H), 7.96 (d, *J* = 8.2 Hz, 1H), 7.92 (d, *J* = 8.2 Hz, 1H), 7.59 – 7.51 (m, 2H), 7.35 (ddd, *J* = 11.4, 6.7, 2.6 Hz, 2H), 7.18 (dt, *J* = 8.8, 6.0 Hz, 2H), 4.12 (ddd, *J* = 18.4, 12.4, 6.3 Hz, 4H), 2.87 (t, *J* = 7.3 Hz, 2H), 2.46 (d, *J* = 7.3 Hz, 2H), 2.06 (t, *J* = 6.8 Hz, 4H). ¹³C-NMR (101 MHz, DMSO-*d*₆) δ 174.6, 171.0, 168.9, 153.3, 149.1, 148.8, 146.8, 146.5, 141.9, 138.6, 135.8, 135.4, 134.1, 133.9, 129.6, 128.5, 128.4, 126.0, 124.8, 124.7, 123.3, 122.8, 121.3, 121.2, 120.6, 115.5, 115.46, 115.41, 68.7, 68.5, 30.8, 28.8, 24.5, 24.1; ESI-MS for C₁₇H₁₄Cl₂F₃N₃O₂: calculated 419.04, found *m/z* 420.25, 422.35 [M + H]⁺. UPLC-MS @254nm 99.5% purity.

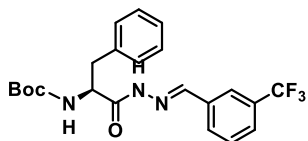
4-(2,4-dichlorophenoxy)-*N*'-(3-(trifluoromethyl)benzylidene)butanehydrazide (**H1A4**)



The acylhydrazone **H1A4** was synthesized according to the general procedure-3, using 4-(2,4-dichlorophenoxy) butanehydrazide **H1** (99 mg, 0.376 mmol) and 3-trifluoromethylbenzaldehyde **A4** (50.3 μL, 0.376 mmol) in MeOH (0.76 mL). After purification through cold MeOH washings, **H1A4** was obtained as a mixture of *E* and *Z* isomers (*E:Z* =

39:61) as a white pure solid (110 mg, yield 70%). NMR spectra are reported as mixture of isomers. ¹H-NMR (400 MHz, DMSO-*d*₆) δ 11.60 (s, 1H), 11.47 (s, 1H), 8.24 (s, 1H), 8.10 – 7.90 (m, 5H), 7.76 (t, J = 7.9 Hz, 2H), 7.66 (dt, J = 15.5, 7.8 Hz, 2H), 7.55 (dd, J = 9.2, 2.2 Hz, 2H), 7.34 (dd, J = 14.2, 5.5 Hz, 2H), 7.23 – 7.14 (m, 2H), 4.21 – 4.03 (m, 4H), 2.86 (t, J = 7.2 Hz, 2H), 2.44 (t, J = 7.2 Hz, 2H), 2.06 (dd, J = 13.4, 6.7 Hz, 4H). ¹³C-NMR (101 MHz, DMSO-*d*₆) δ 174.4, 168.7, 153.3, 144.4, 141.4, 136.0, 135.8, 131.2, 130.8, 130.38, 130.33, 130.2, 129.8, 129.66, 129.63, 128.54, 128.50, 126.3, 124.8, 124.7, 123.2, 122.8, 115.5, 115.4, 68.7, 30.7, 28.6, 24.6, 24.0; ESI-MS for C₁₈H₁₅Cl₂F₃N₂O₂: calculated 418.05, found m/z 419.25, 421.25 [M + H]⁺. UPLC-MS @254nm 99.5% purity.

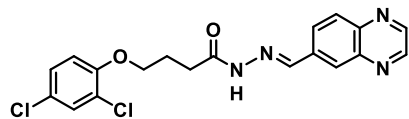
***tert*-butyl (S)-(1-oxo-3-phenyl-1-(2-(3-(trifluoromethyl)benzylidene) hydrazineyl) propan-2-yl) carbamate (H2A4)**



The acylhydrazone **H2A4** was synthesized according to the general procedure-3, using *tert*-butyl (S)-(1-hydrazineyl-1-oxo-3-phenylpropan-2-yl) carbamate **H1** (99 mg, 0.354 mmol) and 3-trifluoromethylbenzaldehyde **A2** (47.0 μL, 0.354 mmol) in MeOH (0.75 mL). After purification through cold MeOH washings, **H2A4** was obtained as a mixture of *E* and *Z* isomers (*E*:*Z* = 47:53) as a white pure solid (80 mg, yield 52%). NMR spectra are reported as mixture of isomers. ¹H-NMR (400 MHz, DMSO-*d*₆) δ 11.75 (s, 1H), 11.54 (s, 1H), 8.29 (s, 1H), 8.13 – 7.89 (m, 5H), 7.82 – 7.64 (m, 4H), 7.36 – 7.13 (m, 12H), 5.05 (s, 1H), 4.24 (s, 1H), 3.03 – 2.91 (m, 2H), 2.81 (dd, J = 26.2, 15.8 Hz, 2H), 1.31 (d, J = 3.3 Hz, 18H). ¹³C-NMR (101 MHz, DMSO-*d*₆) δ 173.8, 169.2, 155.9, 145.5, 142.0, 138.8, 138.2, 135.8, 135.7, 131.6, 131.4, 130.5, 130.4, 129.9, 129.6, 129.4, 128.5, 128.4, 126.7, 126.4, 125.8, 123.4, 122.6, 78.5, 78.4, 55.5, 53.5, 37.5, 36.8, 28.5, 20.8; ESI-MS for C₂₂H₂₄F₃N₃O₃: calculated 435.18, found m/z [M + H]⁺. UPLC-MS @254nm 96% purity.

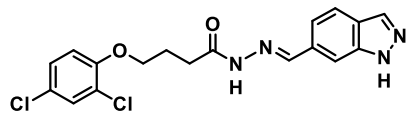
DCL3 *N*-Acylhydrazones synthetic procedures

4-(2,4-dichlorophenoxy)-*N*-(quinoxalin-6-ylmethylene)butanehydrazide (**H1A4**)



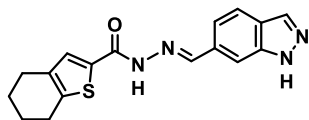
The acylhydrazone **H1A4** was synthesized according to the general procedure-3, using 4-(2,4-dichlorophenoxy)butanehydrazide **H1** (108 mg, 0.41 mmol) and quinoxaline-6-carbaldehyde **A4** (64.9 mg, 0.41 mmol) in MeOH (0.82 mL). After purification through cold MeOH washings, **H1A4** was obtained as a mixture of *E* and *Z* isomers (*E*:*Z* = 35:65) as a white-pink pure solid (122 mg, yield 74%). NMR spectra are reported as mixture of isomers. ¹H-NMR (400 MHz, DMSO-*d*₆) δ 11.70 (s, 1H), 11.56 (s, 1H), 9.00 – 8.92 (m, 4H), 8.41 (s, 1H), 8.28 (s, 1H), 8.23 (dd, *J* = 9.6, 5.8 Hz, 4H), 8.13 (d, *J* = 8.7 Hz, 1H), 8.08 (d, *J* = 9.4 Hz, 1H), 7.56 (t, *J* = 3.1 Hz, 2H), 7.40 – 7.31 (m, 2H), 7.20 (d, *J* = 8.9 Hz, 2H), 4.15 (dt, *J* = 17.9, 6.2 Hz, 4H), 2.91 (t, *J* = 7.3 Hz, 2H), 2.46 (d, *J* = 7.4 Hz, 2H), 2.15 – 2.03 (m, 4H). ¹³C-NMR (101 MHz, DMSO-*d*₆) δ 174.5, 153.4, 146.7, 146.3, 143.3, 142.9, 141.7, 136.5, 130.0, 129.6, 129.2, 128.8, 128.5, 127.0, 124.7, 122.8, 115.4, 68.7, 30.8, 28.8, 24.1; ESI-MS for C₁₉H₁₆Cl₂N₄O₂: calculated 402.07, found *m/z* 403.25, 405.25 [*M* + *H*]⁺. UPLC-MS @254nm 99.5% purity.

N'-(1*H*-indazol-6-yl)methylene)-4-(2,4-dichlorophenoxy)butanehydrazide (**H1A3**)



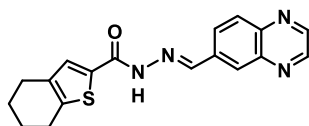
The acylhydrazone **H1A3** was synthesized according to the general procedure-3, using 4-(2,4-dichlorophenoxy)butanehydrazide **H1** (99 mg, 0.376 mmol) and 1*H*-indazole-6-carbaldehyde **A3** (55.0 mg, 0.376 mmol) in MeOH (0.75 mL). After purification through cold MeOH washings, **H1A3** was obtained as a mixture of *E* and *Z* isomers (*E*:*Z* = 36:64) as a white-off pure solid (98 mg, yield 67%). NMR spectra are reported as mixture of isomers. ¹H-NMR (400 MHz, DMSO-*d*₆) δ 13.21 (s, 1H), 13.18 (s, 1H), 11.44 (s, 1H), 11.32 (s, 1H), 8.27 (s, 1H), 8.09 (d, *J* = 4.0 Hz, 3H), 7.82 – 7.67 (m, 4H), 7.56 (d, *J* = 2.6 Hz, 2H), 7.51 (d, *J* = 8.5 Hz, 2H), 7.40 – 7.30 (m, 2H), 7.20 (d, *J* = 8.9 Hz, 2H), 4.13 (dt, *J* = 22.3, 6.4 Hz, 4H), 2.86 (t, *J* = 7.4 Hz, 2H), 2.43 (t, *J* = 7.3 Hz, 2H), 2.13 – 2.01 (m, 4H). ¹³C-NMR (101 MHz, DMSO-*d*₆) δ 173.5, 167.7, 152.7, 146.1, 143.0, 139.6, 133.4, 132.1, 132.0, 129.0, 127.8, 124.1, 124.0, 123.2, 122.0, 120.6, 118.2, 117.6, 114.89, 114.83, 109.5, 68.1, 30.17, 28.1, 24.0, 23.4; ESI-MS for C₁₈H₁₆Cl₂N₄O₂: calculated 390.07, found *m/z* 391.24, 393.34 [*M* + *H*]⁺. UPLC-MS @254nm 99.5% purity.

N'-((1*H*-indazol-6-yl)methylene)-4,5,6,7-tetrahydrobenzo[*b*]thiophene-2-carbohydrazide (H3A3)



The acylhydrazone **H3A3** was synthesized according to the general procedure-3, using 4,5,6,7-tetrahydrobenzo[*b*]thiophene-2-carbohydrazide **H3** (93 mg, 0.473 mmol) and 1*H*-indazole-6-carbaldehyde **A3** (69.3 mg, 0.473 mmol) in MeOH (0.95 mL). After purification through cold MeOH washings, **H3A3** was obtained as a mixture of *E* and *Z* isomers (*E*:*Z* = 50:50) as a white-off pure solid (131 mg, yield 86%). NMR spectra are reported as mixture of isomers. ¹H-NMR (400 MHz, DMSO-*d*₆) δ 13.224 (s, 2H), 11.74 (s, 1H), 11.67 (s, 1H), 8.48 (s, 1H), 8.18 (s, 1H), 8.08 (s, 2H), 7.77 (d, *J* = 11.4 Hz, 4H), 7.61 (t, *J* = 31.9 Hz, 4H), 2.74 (s, 4H), 2.58 (s, 4H), 1.84 – 1.62 (m, 8H). ¹³C-NMR (101 MHz, DMSO-*d*₆) δ 161.8, 158.2, 147.9, 144.8, 142.1, 140.3, 135.7, 134.1, 132.6, 129.9, 124.0, 121.4, 118.8, 110.2, 25.0, 23.2, 22.6; ESI-MS for C₁₇H₁₆N₄OS: calculated 324.10, found *m/z* 325.23 [*M* + *H*]⁺. UPLC-MS @254nm 99.5% purity.

N'-((quinoxalin-6-yl)methylene)-4,5,6,7-tetrahydrobenzo[*b*]thiophene-2-carbohydrazide (H3A4)



The acylhydrazone **H3A4** was synthesized according to the general procedure-3, using 4,5,6,7-tetrahydrobenzo[*b*]thiophene-2-carbohydrazide **H3** (99 mg, 0.504 mmol) and quinoxaline-6-carbaldehyde **A4** (79.7 mg, 0.504 mmol) in MeOH (1.0 mL). After purification through cold MeOH washings, **H3A4** was obtained as a mixture of *E* and *Z* isomers (*E*:*Z* = 50:50) as a white-yellowish pure solid (147 mg, yield 87%). NMR spectra are reported as mixture of isomers. ¹H-NMR (400 MHz, DMSO-*d*₆) δ 11.97 (s, 2H), 8.98 (dd, *J* = 12.2, 1.7 Hz, 4H), 8.64 (s, 1H), 8.31 (s, 5H), 8.18 (s, 2H), 7.71 (d, *J* = 29.6 Hz, 2H), 2.80 (s, 4H), 2.63 (t, *J* = 5.4 Hz, 4H), 1.87 – 1.68 (m, 8H). ¹³C-NMR (101 MHz, DMSO-*d*₆) δ 146.8, 146.4, 143.4, 142.9, 136.4, 130.8, 130.3, 129.3, 127.4, 25.0, 23.2, 22.6; ESI-MS for C₁₈H₁₆N₄OS: calculated 336.10, found *m/z* 337.23 [*M* + *H*]⁺. UPLC-MS @254nm 99.5% purity.

Appendix

Biochemical ELISA assay procedure

Competitive ELISA screening assay using biotinylated BRC4 peptide to disrupt the BRC4–RAD51 interaction was performed by modifying the method described by Rajendra *et al.*¹²¹ BRC4-biotinylated peptide (N-term biotin-KEPTLLGFHTASGKKVKI AKESLDKVKNLDFEKEQ from Life Technologies) was used to coat 384-well plates (Nunc). After washing with PBS containing 0.05% Tween-20 (PBST) and blocking with the solution BSA 1% /PBST, overnight hybridization with human RAD51 protein (NP_002866 Creative Biomart, NY) was performed. Test compounds were added in dose response from 0.01 to 100 μ M in triplicate with constant DMSO 1%. Antibody raised against RAD51 (Millipore) and HRP-secondary antibody staining to develop the 3,3',5,5'- tetramethyl benzidine signal (Sigma) quenched with 1 M HCl was used as the assay readout. Colorimetric measure was read on a Victor5 (PerkinElmer) plate reader. BRC4 and Rad51 were included in the assay as positive control. Results were analyzed by using Graph Pad software. The experiments were performed by Francesca De Franco PhD, TES Pharma s.r.l.

Protocol for the Expression and Purification of His-hRAD51

hRAD51 was expressed in *E. coli* Rosetta2(DE3)pLysS cells. A saturated overnight culture of Rosetta2(DE3) pLysS/pET15b-HishRAD51 was diluted (1:1000) into a fresh TB-5052 auto induction medium containing ampicillin (100 μ g/mL). The flasks were shaken at 200 rpm at 20 °C for 72 h. The pellet was subsequently re-suspended in an appropriate volume of buffer A (20 mM Tris-HCl (pH 8.00), 500 mM NaCl, 10 mM imidazole, 5 mM DTT, 10% (v/v) glycerol) supplemented with protease inhibitor cocktail (SIGMAFAST protease inhibitor cocktail tablets, EDTA-50 free). The cell suspension was lysed on ice trough sonication (24 rounds of 30 in.; amplitude 85%; Tip MS72; Bandelin Sonoplus HD2070 sonicator). The disrupted cell suspension was centrifuged for 1 h at 13 000 rpm. The supernatant fraction was filtered with a 0.45 μ m (MiniSart syringe filter 0.45 μ m) membrane to remove residual particulates before chromatography. The supernatant was applied onto a His-Trap column (His-TrapTM FF 5 mL, GE Healthcare) equilibrated with buffer A. A wash step was performed using 10% of buffer B (20 mM Tris-HCl (pH 8.00), 500 mM NaCl, 500 mM imidazole, 10% (v/v) glycerol). The protein was then eluted with a linear gradient from 10% to 100% of buffer B over 10 column volumes. Fractions (0.5 mL) were collected and analyzed by SDS–PAGE. Collected fractions

corresponding to the recombinant protein were dialyzed overnight at 4 °C against buffer C (50 mM Tris-HCl (pH 8.00), 200 mM KCl, 0.25 mM EDTA, 2 mM DTT, 10% (v/v) glycerol). Dialyzed protein was loaded onto an anion exchange column (ResQ, GE Healthcare) equilibrated in buffer C. The elution was performed with a linear gradient of buffer B (50 mM Tris-HCl (pH 8.00), 1 M KCl, 0.25 mM EDTA, 2 mM DTT, 10% (v/v) glycerol). Fractions (0.5 mL) were collected and analyzed by SDS-PAGE. Fractions containing HishRAD51 were pooled and dialyzed against the storage buffer (20 mM Hepes (pH 8.00), 250 mM KCl, 0.1 mM EDTA, 2 mM DTT, 10% (v/v) glycerol). The protein yield was determined from the optical absorption at 280 nm (extinction coefficient $14\ 900\ \text{M}^{-1}\ \text{cm}^{-1}$) of the final sample. This protocol was optimized and performed by Fabrizio Schipani PhD and Stefania Giroto PhD from Computational and Chemical Biology (CCB), Italian Institute of Technology IIT.

Microscale Thermophoresis

The recombinant protein hRAD51 was labeled with the Monolith His-Tag labeling kit RED-tris-NTA 2nd Generation kit (NanoTemper Technologies). MST measurements were simultaneously performed on 16 capillaries containing a constant concentration (25 nM) of labeled RED-tris-NTA 2nd Generation His-hRAD51 protein and 16 different concentrations of 35d in order to determine a concentration-dependent MST binding curve. The highest 35d concentration tested was 40 μM . Measurements were carried out in MST buffer (20 mM Hepes (pH 8.00), 250 mM KCl, 0.1 mM EDTA, 5% (v/v) glycerol, 5% DMSO). The experiments were performed by Fabrizio Schipani PhD and Stefania Giroto PhD from Computational and Chemical Biology (CCB), Italian Institute of Technology IIT.

Homologous Recombination Assay

Homologous recombination (HR) was assessed by using a commercially available assay (Norgen). This assay is based on cell transfection with two plasmids that, upon cell entry, recombine. The efficiency of HR can be assessed by real-time PCR, using primer mixtures included in the assay kit. Different primer mixtures allow one to discriminate between the original plasmid backbones and their recombination product. BxPC3 cells (2×10^5 per well) were seeded in a 24-well plate and allowed to adhere overnight. Co-transfection with the two plasmids was performed in Lipofectamine 2000 (Invitrogen) according to the manufacturer's instructions. During transfection (5 h), cells were exposed to different doses of RAD51-BRCA2

disruptors, dissolved in RPMI in the presence of 0.6% DMSO. After washing with PBS, cells were harvested, and DNA was isolated using Illustra Tissue and Cell Genomic Prep Mini Spin kit (GE Healthcare). Sample concentration was measured using an ONDA Nano Genius photometer. The efficiency of HR was assessed by real-time PCR, using 25 ng of template, the primer mixtures included in the assay kit and following the protocol indicated by the manufacturer. Data analysis was based on the $\Delta\Delta C_t$ method: [recombination product/backbone plasmids] treated versus [recombination product/backbone plasmids] control. The experiments were performed by Marcella Manerba PhD (Computational and Chemical Biology, IIT) in the group of Professor Giuseppina Di Stefano, University of Bologna.

Immunofluorescence

Immunofluorescence was used for studying RAD51 nuclear translocation and for evaluating DNA damage through the detection of γ H2AX nuclear foci. To visualize RAD51 in cell nuclei, BxPC-3 cells were seeded on glass coverslips placed in a 6- well culture plate (2×10^5 cells/well) and allowed to adhere overnight. Cultures were then preincubated with 20 μ M 35d for 1 h and subsequently exposed to 50 μ M cisplatin for an additional 1.5 h. Medium was removed, and cells were maintained in the presence of 20 μ M 35d for 4 h. After this time, cultures growing on coverslips were fixed in PBS containing 1% formalin for 20 min, permeabilized in 70% ethanol, air-dried, and washed twice with PBS. Samples were incubated in 10% bovine serum albumin (BSA) in PBS for 30 min at 37 °C and subsequently exposed to an anti-RAD51 mouse monoclonal antibody (Santa Cruz Biotechnology, 1:1000 in 5% BSA/PBS) overnight at 4 °C. After washing, coverslips were incubated with an anti-mouse FITC-conjugated secondary antibody (1:1000 in 1% BSA/PBS) for 1 h at 37 °C, washed, air-dried, and mounted with a solution of DAPI (2 μ g/mL) and DABCO. To evaluate DNA damage through γ H2AX nuclear foci, BxPC3 and Capan1 cells were seeded on glass coverslips in 6-well tissue culture plate (2×10^5 cells/well) and allowed to adhere overnight. After 48 h treatment with olaparib (10 μ M) or 35d (20 μ M) given alone or in combination, cultures growing on coverslips were fixed and treated as described above. For this experiment, the used antibodies were a rabbit polyclonal anti- γ H2AX (Abcam, 1:1000 in 5% BSA/PBS) and a secondary anti-rabbit rhodamine-labeled (Novus Biologicals, 1:1000 in 1% BSA/PBS). For both experiments, images were acquired using a Nikon fluorescent microscope equipped with filters for FITC, TRITC, and DAPI. The percentage of cells bearing nuclear foci was estimated by two independent observers, by analyzing 100–250 cells for each treatment sample. The experiments were performed by

Marcella Manerba PhD (Computational and Chemical Biology, IIT) in the group of Professor Giuseppina Di Stefano, University of Bologna.

Cell Viability Assay

Cell viability was assessed with the CellTiter-Glo luminescent cell viability assay from Promega. For this experiment, 1×10^4 cells in 200 μ L of culture medium were seeded into each well of a 96-multiwell white body plate and allowed to adhere overnight. After 72 h incubation in the presence of olaparib (10 μ M) and the RAD51-BRCA2 disruptors alone or in combination, the plate was allowed to equilibrate at room temperature for 30 min and the CellTiter-Glo reactive was directly added to each well. The plate was kept on a shaker for 10 min to induce cell lysis, and its luminescence was measured with a Fluoroskan Ascent FL reader (Labsystems). Cytotoxicity Assay. The experiments were performed by Marcella Manerba PhD (Computational and Chemical Biology, IIT), Andrea Balboni PhD Student, (FaBIT, University of Bologna, Computational and Chemical Biology, IIT) in the group of Professor Giuseppina Di Stefano, University of Bologna.

Cell Culture and Treatments

BxPC-3 and Capan-1 cells were grown in RPMI 1640 supplemented with 10% FBS, 100 U/mL penicillin/streptomycin, 2 mM glutamine. All media and supplements were from Sigma-Aldrich. Non-neoplastic, immortalized cells from human kidney (HK-2, ATCC CRL2190) were grown in DMEM:F12 medium containing 40 ng/mL dexamethasone and supplemented as described above. All cultures were routinely tested for Mycoplasma contamination. Treatments (olaparib and BRCA2-RAD51 disruptors) were administered in culture medium supplemented with 0.6% DMSO. The same amount of DMSO was added to the control, untreated cultures.

Abbreviations and acronyms

ADP	Adenosine diphosphate
ATM	Ataxia Telangiectasia Mutated
ATP	Adenosine triphosphate
ATR	ATM-related kinase
BER	Base excision repair
BRCA1/2	Breast cancer type 1/2 susceptibility protein
CDK	Cyclin-dependent kinase
CI	Combination index
CTD	C-terminal domain
DAPI	4',6-Diamidino-2-phenylindole
DBD	DNA binding domain
DBU	1,8-Diazabicyclo[5.4.0]undec-7-ene
DCL	Dynamic combinatorial library
DCM	Dichloromethane
DDR	DNA Damage Response
DIDS	4,4'-Diisothiocyano-2,2'-stilbenedisulfonic acid
DIPEA	N,N-Diisopropylethylamine
DMF	Dimethylformamide
DMSO	Dimethyl sulfoxide
DNA	Deoxyribonucleic acid
DSB	Double strand break
dsDNA	Double strand DNA
DSF	Differential scanning fluorimetry

DTT	1,4-Dithiothreitol
EDC	1-Ethyl-3-(3-dimethylaminopropyl)carbodiimide
EDTA	Ethylenediaminetetraacetic acid
EGFR	Epidermal growth factor receptor
EJ	End joining
EtOAc	Ethyl acetate
EtOH	Ethanol
FGFR1	Fibroblast growth factor receptor 1
HATU	1-[Bis(dimethylamino)methylene]-1H-1,2,3-triazolo[4,5-b]pyridinium 3-oxid hexafluorophosphate
HBOC	Hereditary breast ovarian cancer
hDNA	Heteroduplex DNA
HIPS	Helmholtz Institute for Pharmaceutical Research Saarland
HOBT	1-Hydroxybenzotriazole hydrate
HOS	Human osteosarcoma
HPLC	High performance liquid chromatography
HR	Homologous recombination
HRMS	High resolution mass spectrometry
ICL	Interlink cross link
MeCN	Acetonitrile
MeOH	Methanol
MET	Mesenchymal epithelial transition
MS	Molecular sieves
MSL	Mesenchymal stem-like
MST	Microscale thermophoresis

mTOR	Mammalian target of rapamycin
NAH	<i>N</i> -acylhydrazone
NHEJ	Non homologous end joining
NSCLC	Non small cell lung cancer
NTD	N-terminal domain
PAINS	Pan-assay interference compounds
PALB2	Partner and localizer of BRCA2
PARP	Poly (ADP-ribose) polymerase
PARPi	PARP inhibitor
PE	Petroleum ether
PI3K	Phosphoinositide 3-kinase
PIKK	Phosphatidylinositol 3-kinase-related kinase
PPI	Protein-protein interaction
RMS	Rhabdomyosarcoma
RPA	Replication protein A
RPS6	Phosphor ribosomal protein 6
RTK	Receptor tyrosine kinase
SAR	Structure-activity relationship
SL	Synthetic lethality
SN	Streptonigrin
SPR	Surface plasmon resonance
SSB	Single strand break
ssDNA	Single strand DNA
STAT3	Signal transducer and activator of transcription 3
tdDCC	Target directed dynamic combinatorial chemistry

TEA	Triethylamine
THF	Tetrahydrofuran
TKI	Tyrosine kinase inhibitor
TNBC	Triple-negative breast cancer
TSA	Thermal shift assay
VS	Virtual screening

References

- 1 <https://gco.iarc.fr/today/home>. CANCER TODAY Data visualization tools for exploring the global cancer burden in 2018.
- 2 Greaves, M. & Maley, C. C. Clonal evolution in cancer. *Nature* **481**, 306-313, doi:10.1038/nature10762 (2012).
- 3 Manchester, K. L. Theodor Boveri and the origin of malignant tumours. *Trends Cell Biol* **5**, 384-387, doi:10.1016/s0962-8924(00)89080-7 (1995).
- 4 Lord, C. J. & Ashworth, A. The DNA damage response and cancer therapy. *Nature* **481**, 287-294, doi:10.1038/nature10760 (2012).
- 5 Gillies R.J., V. D., Gatenby R.A. Evolutionary Dynamics Unifies Carcinogenesis and Cancer Therapy. *Nat Rev Cancer* **12**, 487–493, doi:doi:10.1038/nrc3298 (2014).
- 6 Zhao, S. *et al.* Detailed modeling of positive selection improves detection of cancer driver genes. *Nat Commun* **10**, 3399, doi:10.1038/s41467-019-11284-9 (2019).
- 7 Vogelstein, B. *et al.* Cancer genome landscapes. *Science* **339**, 1546-1558, doi:10.1126/science.1235122 (2013).
- 8 Pylayeva-Gupta, Y., Grabocka, E. & Bar-Sagi, D. RAS oncogenes: weaving a tumorigenic web. *Nat Rev Cancer* **11**, 761-774, doi:10.1038/nrc3106 (2011).
- 9 Chen, H., Liu, H. & Qing, G. Targeting oncogenic Myc as a strategy for cancer treatment. *Signal Transduct Target Ther* **3**, 5, doi:10.1038/s41392-018-0008-7 (2018).
- 10 Teng, L. S., Zheng, Y. & Wang, H. H. BRCA1/2 associated hereditary breast cancer. *J Zhejiang Univ Sci B* **9**, 85-89, doi:10.1631/jzus.B0710617 (2008).
- 11 Mantovani, F., Collavin, L. & Del Sal, G. Mutant p53 as a guardian of the cancer cell. *Cell Death Differ* **26**, 199-212, doi:10.1038/s41418-018-0246-9 (2019).
- 12 Velez-Cruz, R. *et al.* RB localizes to DNA double-strand breaks and promotes DNA end resection and homologous recombination through the recruitment of BRG1. *Genes Dev* **30**, 2500-2512, doi:10.1101/gad.288282.116 (2016).
- 13 McGranahan, N. & Swanton, C. Biological and therapeutic impact of intratumor heterogeneity in cancer evolution. *Cancer Cell* **27**, 15-26, doi:10.1016/j.ccell.2014.12.001 (2015).

- 14 Gottesman, M. M., Lavi, O., Hall, M. D. & Gillet, J. P. Toward a Better Understanding of the Complexity of Cancer Drug Resistance. *Annu Rev Pharmacol Toxicol* **56**, 85-102, doi:10.1146/annurev-pharmtox-010715-103111 (2016).
- 15 Nowell, P. C. The clonal evolution of tumor cell populations. *Science* **194**, 23-28, doi:10.1126/science.959840 (1976).
- 16 Turajlic, S., Sottoriva, A., Graham, T. & Swanton, C. Resolving genetic heterogeneity in cancer. *Nat Rev Genet* **20**, 404-416, doi:10.1038/s41576-019-0114-6 (2019).
- 17 Reya, T., Morrison, S. J., Clarke, M. F. & Weissman, I. L. Stem cells, cancer, and cancer stem cells. *Nature* **414**, 105-111, doi:10.1038/35102167 (2001).
- 18 Lavi, O., Greene, J. M., Levy, D. & Gottesman, M. M. The role of cell density and intratumoral heterogeneity in multidrug resistance. *Cancer Res* **73**, 7168-7175, doi:10.1158/0008-5472.CAN-13-1768 (2013).
- 19 Schmitt, M. W., Loeb, L. A. & Salk, J. J. The influence of subclonal resistance mutations on targeted cancer therapy. *Nat Rev Clin Oncol* **13**, 335-347, doi:10.1038/nrclinonc.2015.175 (2016).
- 20 Bayat Mokhtari, R. *et al.* Combination therapy in combating cancer. *Oncotarget* **8**, 38022-38043, doi:10.18632/oncotarget.16723 (2017).
- 21 Wang, T., Narayanaswamy, R., Ren, H. & Torchilin, V. P. Combination therapy targeting both cancer stem-like cells and bulk tumor cells for improved efficacy of breast cancer treatment. *Cancer Biol Ther* **17**, 698-707, doi:10.1080/15384047.2016.1190488 (2016).
- 22 Chou, T. C. Theoretical basis, experimental design, and computerized simulation of synergism and antagonism in drug combination studies. *Pharmacol Rev* **58**, 621-681, doi:10.1124/pr.58.3.10 (2006).
- 23 Palmer, A. C. & Sorger, P. K. Combination Cancer Therapy Can Confer Benefit via Patient-to-Patient Variability without Drug Additivity or Synergy. *Cell* **171**, 1678-1691 e1613, doi:10.1016/j.cell.2017.11.009 (2017).
- 24 Zagidullin, B. *et al.* DrugComb: an integrative cancer drug combination data portal. *Nucleic Acids Res* **47**, W43-W51, doi:10.1093/nar/gkz337 (2019).
- 25 Greco, W. R., Bravo, G. & Parsons, J. C. The search for synergy: a critical review from a response surface perspective. *Pharmacol Rev* **47**, 331-385 (1995).

- 26 Saputra, E. C., Huang, L., Chen, Y. & Tucker-Kellogg, L. Combination Therapy and the Evolution of Resistance: The Theoretical Merits of Synergism and Antagonism in Cancer. *Cancer Res* **78**, 2419-2431, doi:10.1158/0008-5472.CAN-17-1201 (2018).
- 27 Bozic, I. *et al.* Evolutionary dynamics of cancer in response to targeted combination therapy. *Elife* **2**, e00747, doi:10.7554/eLife.00747 (2013).
- 28 Dobzhansky, T. Genetics of natural populations; recombination and variability in populations of *Drosophila pseudoobscura*. *Genetics* **31**, 269-290 (1946).
- 29 Lucchesi, J. C. Synthetic lethality and semi-lethality among functionally related mutants of *Drosophila melanogaster*. *Genetics* **59**, 37-44 (1968).
- 30 Kaiser, C. A. & Schekman, R. Distinct sets of SEC genes govern transport vesicle formation and fusion early in the secretory pathway. *Cell* **61**, 723-733, doi:10.1016/0092-8674(90)90483-u (1990).
- 31 Hennessy, K. M., Lee, A., Chen, E. & Botstein, D. A group of interacting yeast DNA replication genes. *Genes Dev* **5**, 958-969, doi:10.1101/gad.5.6.958 (1991).
- 32 Bender, A. & Pringle, J. R. Use of a screen for synthetic lethal and multicopy suppressor mutants to identify two new genes involved in morphogenesis in *Saccharomyces cerevisiae*. *Mol Cell Biol* **11**, 1295-1305, doi:10.1128/mcb.11.3.1295 (1991).
- 33 Chan, D. A. & Giaccia, A. J. Harnessing synthetic lethal interactions in anticancer drug discovery. *Nat Rev Drug Discov* **10**, 351-364, doi:10.1038/nrd3374 (2011).
- 34 Kaelin, W. G., Jr. The concept of synthetic lethality in the context of anticancer therapy. *Nat Rev Cancer* **5**, 689-698, doi:10.1038/nrc1691 (2005).
- 35 Beijersbergen, R. L., Wessels, L. F. A. & Bernards, R. Synthetic Lethality in Cancer Therapeutics. *Annu Rev Canc Biol* **1**, 141-161, doi:10.1146/annurev-cancerbio-042016-073434 (2017).
- 36 O'Neil, N. J., Bailey, M. L. & Hieter, P. Synthetic lethality and cancer. *Nat Rev Genet* **18**, 613-623, doi:10.1038/nrg.2017.47 (2017).
- 37 Parameswaran, S. *et al.* A Road Map to Personalizing Targeted Cancer Therapies Using Synthetic Lethality. *Trends Cancer* **5**, 11-29, doi:10.1016/j.trecan.2018.11.001 (2019).
- 38 Chen, E. S. Targeting epigenetics using synthetic lethality in precision medicine. *Cell Mol Life Sci* **75**, 3381-3392, doi:10.1007/s00018-018-2866-0 (2018).

- 39 Pauli, C. *et al.* Personalized In Vitro and In Vivo Cancer Models to Guide Precision Medicine. *Cancer Discov* **7**, 462-477, doi:10.1158/2159-8290.CD-16-1154 (2017).
- 40 Shin, S. H., Bode, A. M. & Dong, Z. Precision medicine: the foundation of future cancer therapeutics. *NPJ Precis Oncol* **1**, 12, doi:10.1038/s41698-017-0016-z (2017).
- 41 Zhou, Z. & Wei, W. PrePAIRing Cas9s for screening success. *Nat Biotechnol* **36**, 147-148, doi:10.1038/nbt.4075 (2018).
- 42 Oliver, D. *et al.* Identification of novel cancer therapeutic targets using a designed and pooled shRNA library screen. *Sci Rep* **7**, 43023, doi:10.1038/srep43023 (2017).
- 43 Najm, F. J. *et al.* Orthologous CRISPR-Cas9 enzymes for combinatorial genetic screens. *Nat Biotechnol* **36**, 179-189, doi:10.1038/nbt.4048 (2018).
- 44 Zimmermann, M. *et al.* CRISPR screens identify genomic ribonucleotides as a source of PARP-trapping lesions. *Nature* **559**, 285-289, doi:10.1038/s41586-018-0291-z (2018).
- 45 Cluse, L. A. *et al.* A Comprehensive Protocol Resource for Performing Pooled shRNA and CRISPR Screens. *Methods Mol Biol* **1725**, 201-227, doi:10.1007/978-1-4939-7568-6_17 (2018).
- 46 Han, K. *et al.* Synergistic drug combinations for cancer identified in a CRISPR screen for pairwise genetic interactions. *Nat Biotechnol* **35**, 463-474, doi:10.1038/nbt.3834 (2017).
- 47 Sinha, S. *et al.* Systematic discovery of mutation-specific synthetic lethals by mining pan-cancer human primary tumor data. *Nat Commun* **8**, 15580, doi:10.1038/ncomms15580 (2017).
- 48 Guo, J., Liu, H. & Zheng, J. SynLethDB: synthetic lethality database toward discovery of selective and sensitive anticancer drug targets. *Nucleic Acids Res* **44**, D1011-1017, doi:10.1093/nar/gkv1108 (2016).
- 49 Liu, C. *et al.* Individualized genetic network analysis reveals new therapeutic vulnerabilities in 6,700 cancer genomes. *PLoS Comput Biol* **16**, e1007701, doi:10.1371/journal.pcbi.1007701 (2020).
- 50 Heinzl, A. *et al.* Synthetic lethality guiding selection of drug combinations in ovarian cancer. *PLoS One* **14**, e0210859, doi:10.1371/journal.pone.0210859 (2019).
- 51 Lord, C. J. & Ashworth, A. PARP inhibitors: Synthetic lethality in the clinic. *Science* **355**, 1152-1158, doi:10.1126/science.aam7344 (2017).
- 52 Ashworth, A. & Lord, C. J. Synthetic lethal therapies for cancer: what's next after PARP inhibitors? *Nat Rev Clin Oncol* **15**, 564-576, doi:10.1038/s41571-018-0055-6 (2018).

- 53 Lord, C. J., Tutt, A. N. & Ashworth, A. Synthetic lethality and cancer therapy: lessons learned from the development of PARP inhibitors. *Annu Rev Med* **66**, 455-470, doi:10.1146/annurev-med-050913-022545 (2015).
- 54 Bryant, H. E. *et al.* Specific killing of BRCA2-deficient tumours with inhibitors of poly(ADP-ribose) polymerase. *Nature* **434**, 913-917, doi:10.1038/nature03443 (2005).
- 55 Roderick L. Beijersbergen, L. F. A. W., Rene Bernards Synthetic Lethality in Cancer Therapeutics. *Annu. Rev. Cancer Biol.* **1**, 141-161, doi:10.1146/annurev-cancerbio-042016-073434 (2017).
- 56 Farmer, H. *et al.* Targeting the DNA repair defect in BRCA mutant cells as a therapeutic strategy. *Nature* **434**, 917-921, doi:10.1038/nature03445 (2005).
- 57 Xu, G. *et al.* REV7 counteracts DNA double-strand break resection and affects PARP inhibition. *Nature* **521**, 541-544, doi:10.1038/nature14328 (2015).
- 58 Jaspers, J. E. *et al.* Loss of 53BP1 causes PARP inhibitor resistance in Brca1-mutated mouse mammary tumors. *Cancer Discov* **3**, 68-81, doi:10.1158/2159-8290.CD-12-0049 (2013).
- 59 Pettitt, S. J. *et al.* A genetic screen using the PiggyBac transposon in haploid cells identifies Parp1 as a mediator of olaparib toxicity. *PLoS One* **8**, e61520, doi:10.1371/journal.pone.0061520 (2013).
- 60 Yi, Y. W. *et al.* Dual inhibition of EGFR and MET induces synthetic lethality in triple-negative breast cancer cells through downregulation of ribosomal protein S6. *Int J Oncol* **47**, 122-132, doi:10.3892/ijo.2015.2982 (2015).
- 61 Eccles, S. A. The epidermal growth factor receptor/Erb-B/HER family in normal and malignant breast biology. *Int J Dev Biol* **55**, 685-696, doi:10.1387/ijdb.113396se (2011).
- 62 Yarden, Y. & Pines, G. The ERBB network: at last, cancer therapy meets systems biology. *Nat Rev Cancer* **12**, 553-563, doi:10.1038/nrc3309 (2012).
- 63 Anderson, N. G., Ahmad, T., Chan, K., Dobson, R. & Bundred, N. J. ZD1839 (Iressa), a novel epidermal growth factor receptor (EGFR) tyrosine kinase inhibitor, potently inhibits the growth of EGFR-positive cancer cell lines with or without erbB2 overexpression. *Int J Cancer* **94**, 774-782, doi:10.1002/ijc.1557 (2001).

- 64 Ciardiello, F. *et al.* Antitumor effect and potentiation of cytotoxic drugs activity in human cancer cells by ZD-1839 (Iressa), an epidermal growth factor receptor-selective tyrosine kinase inhibitor. *Clin Cancer Res* **6**, 2053-2063 (2000).
- 65 Wakeling, A. E. *et al.* ZD1839 (Iressa): an orally active inhibitor of epidermal growth factor signaling with potential for cancer therapy. *Cancer Res* **62**, 5749-5754 (2002).
- 66 Meyuhas, O. Physiological roles of ribosomal protein S6: one of its kind. *Int Rev Cell Mol Biol* **268**, 1-37, doi:10.1016/S1937-6448(08)00801-0 (2008).
- 67 Chen, B. *et al.* Hyperphosphorylation of ribosomal protein S6 predicts unfavorable clinical survival in non-small cell lung cancer. *J Exp Clin Cancer Res* **34**, 126, doi:10.1186/s13046-015-0239-1 (2015).
- 68 Gambardella, V. *et al.* NRF2 through RPS6 Activation Is Related to Anti-HER2 Drug Resistance in HER2-Amplified Gastric Cancer. *Clin Cancer Res* **25**, 1639-1649, doi:10.1158/1078-0432.CCR-18-2421 (2019).
- 69 Knoll, M. *et al.* The ribosomal protein S6 in renal cell carcinoma: functional relevance and potential as biomarker. *Oncotarget* **7**, 418-432, doi:10.18632/oncotarget.6225 (2016).
- 70 Eiring, A. M. *et al.* Combined STAT3 and BCR-ABL1 inhibition induces synthetic lethality in therapy-resistant chronic myeloid leukemia. *Leukemia* **29**, 586-597, doi:10.1038/leu.2014.245 (2015).
- 71 Druker, B. J. *et al.* Five-year follow-up of patients receiving imatinib for chronic myeloid leukemia. *N Engl J Med* **355**, 2408-2417, doi:10.1056/NEJMoa062867 (2006).
- 72 Gorre, M. E. *et al.* Clinical resistance to STI-571 cancer therapy caused by BCR-ABL gene mutation or amplification. *Science* **293**, 876-880, doi:10.1126/science.1062538 (2001).
- 73 Patel, A. B., O'Hare, T. & Deininger, M. W. Mechanisms of Resistance to ABL Kinase Inhibition in Chronic Myeloid Leukemia and the Development of Next Generation ABL Kinase Inhibitors. *Hematol Oncol Clin North Am* **31**, 589-612, doi:10.1016/j.hoc.2017.04.007 (2017).
- 74 Chandrasekhar, C., Kumar, P. S. & Sarma, P. Novel mutations in the kinase domain of BCR-ABL gene causing imatinib resistance in chronic myeloid leukemia patients. *Sci Rep* **9**, 2412, doi:10.1038/s41598-019-38672-x (2019).
- 75 Fletcher, S. *et al.* Disruption of transcriptionally active Stat3 dimers with non-phosphorylated, salicylic acid-based small molecules: potent in vitro and tumor cell activities. *Chembiochem* **10**, 1959-1964, doi:10.1002/cbic.200900172 (2009).

- 76 Lai, S. W. *et al.* Targeted PARP Inhibition Combined with FGFR1 Blockade is Synthetically Lethal to Malignant Cells in Patients with Pancreatic Cancer. *Cells* **9**, doi:10.3390/cells9040911 (2020).
- 77 Cleo JC Connolly, J. M. H., Mel C. Schroeder, Mark Barvian, Gina H. Lu, Robert L. Panek, & Aneesa Amar, C. S., Alan J. Kraker, David W. Fry, c Wayne D. Klohs, and Annette M. Doherty DISCOVERY AND STRUCTURE-ACTIVITY STUDIES OF A NOVEL SERIES OF PYRIDO[2,3-d]PYRIMIDINE TYROSINE KINASE INHIBITORS *Bioorganic & Medicinal Chemistry Letters* **7**, 2415-2420 (1997).
- 78 Mohammadi, M. *et al.* Crystal structure of an angiogenesis inhibitor bound to the FGF receptor tyrosine kinase domain. *EMBO J* **17**, 5896-5904, doi:10.1093/emboj/17.20.5896 (1998).
- 79 Lai, S. W. *et al.* Correction to: The therapeutic targeting of the FGFR1/Src/NF-kappaB signaling axis inhibits pancreatic ductal adenocarcinoma stemness and oncogenicity. *Clin Exp Metastasis* **36**, 67, doi:10.1007/s10585-018-9949-z (2019).
- 80 Graab, U., Hahn, H. & Fulda, S. Identification of a novel synthetic lethality of combined inhibition of hedgehog and PI3K signaling in rhabdomyosarcoma. *Oncotarget* **6**, 8722-8735, doi:10.18632/oncotarget.2726 (2015).
- 81 Zibat, A. *et al.* Activation of the hedgehog pathway confers a poor prognosis in embryonal and fusion gene-negative alveolar rhabdomyosarcoma. *Oncogene* **29**, 6323-6330, doi:10.1038/onc.2010.368 (2010).
- 82 Lauth, M., Bergstrom, A., Shimokawa, T. & Toftgard, R. Inhibition of GLI-mediated transcription and tumor cell growth by small-molecule antagonists. *Proc Natl Acad Sci U S A* **104**, 8455-8460, doi:10.1073/pnas.0609699104 (2007).
- 83 Zhang, R., Wu, J., Ferrandon, S., Glowacki, K. J. & Houghton, J. A. Targeting GLI by GANT61 involves mechanisms dependent on inhibition of both transcription and DNA licensing. *Oncotarget* **7**, 80190-80207, doi:10.18632/oncotarget.13376 (2016).
- 84 Park, S. *et al.* PI-103, a dual inhibitor of Class IA phosphatidylinositide 3-kinase and mTOR, has antileukemic activity in AML. *Leukemia* **22**, 1698-1706, doi:10.1038/leu.2008.144 (2008).
- 85 Gao, S. & Lai, L. Synthetic lethality in drug development: the dawn is coming. *Future Med Chem* **10**, 2129-2132, doi:10.4155/fmc-2018-0227 (2018).
- 86 Vyse, S., Howitt, A. & Huang, P. H. Exploiting Synthetic Lethality and Network Biology to Overcome EGFR Inhibitor Resistance in Lung Cancer. *J Mol Biol* **429**, 1767-1786, doi:10.1016/j.jmb.2017.04.018 (2017).

- 87 Whitmore, A. V. & Wray, J. Networks for better drug discovery: making optimal use of existing chemical space. *Future Med Chem*, doi:10.4155/fmc-2018-0265 (2018).
- 88 Jerby-Arnon, L. *et al.* Predicting cancer-specific vulnerability via data-driven detection of synthetic lethality. *Cell* **158**, 1199-1209, doi:10.1016/j.cell.2014.07.027 (2014).
- 89 Preuer, K. *et al.* DeepSynergy: predicting anti-cancer drug synergy with Deep Learning. *Bioinformatics* **34**, 1538-1546, doi:10.1093/bioinformatics/btx806 (2018).
- 90 Sun, Y., McCorvie, T. J., Yates, L. A. & Zhang, X. Structural basis of homologous recombination. *Cell Mol Life Sci* **77**, 3-18, doi:10.1007/s00018-019-03365-1 (2020).
- 91 Kostyrko, K., Bosshard, S., Urban, Z. & Mermod, N. A role for homologous recombination proteins in cell cycle regulation. *Cell Cycle* **14**, 2853-2861, doi:10.1080/15384101.2015.1049784 (2015).
- 92 Li, X. & Heyer, W. D. Homologous recombination in DNA repair and DNA damage tolerance. *Cell Res* **18**, 99-113, doi:10.1038/cr.2008.1 (2008).
- 93 Nogueira, A., Fernandes, M., Catarino, R. & Medeiros, R. RAD52 Functions in Homologous Recombination and Its Importance on Genomic Integrity Maintenance and Cancer Therapy. *Cancers (Basel)* **11**, doi:10.3390/cancers11111622 (2019).
- 94 Lamarche, B. J., Orazio, N. I. & Weitzman, M. D. The MRN complex in double-strand break repair and telomere maintenance. *FEBS Lett* **584**, 3682-3695, doi:10.1016/j.febslet.2010.07.029 (2010).
- 95 de Jager, M. *et al.* Human Rad50/Mre11 is a flexible complex that can tether DNA ends. *Mol Cell* **8**, 1129-1135, doi:10.1016/s1097-2765(01)00381-1 (2001).
- 96 Kashammer, L. *et al.* Mechanism of DNA End Sensing and Processing by the Mre11-Rad50 Complex. *Mol Cell* **76**, 382-394 e386, doi:10.1016/j.molcel.2019.07.035 (2019).
- 97 Nimonkar, A. V., Ozsoy, A. Z., Genschel, J., Modrich, P. & Kowalczykowski, S. C. Human exonuclease 1 and BLM helicase interact to resect DNA and initiate DNA repair. *Proc Natl Acad Sci U S A* **105**, 16906-16911, doi:10.1073/pnas.0809380105 (2008).
- 98 Myler, L. R. *et al.* Single-Molecule Imaging Reveals How Mre11-Rad50-Nbs1 Initiates DNA Break Repair. *Mol Cell* **67**, 891-898 e894, doi:10.1016/j.molcel.2017.08.002 (2017).
- 99 Burma, S., Chen, B. P., Murphy, M., Kurimasa, A. & Chen, D. J. ATM phosphorylates histone H2AX in response to DNA double-strand breaks. *J Biol Chem* **276**, 42462-42467, doi:10.1074/jbc.C100466200 (2001).

- 100 Smith, J., Tho, L. M., Xu, N. & Gillespie, D. A. The ATM-Chk2 and ATR-Chk1 pathways in DNA damage signaling and cancer. *Adv Cancer Res* **108**, 73-112, doi:10.1016/B978-0-12-380888-2.00003-0 (2010).
- 101 Ball, H. L., Myers, J. S. & Cortez, D. ATRIP binding to replication protein A-single-stranded DNA promotes ATR-ATRIP localization but is dispensable for Chk1 phosphorylation. *Mol Biol Cell* **16**, 2372-2381, doi:10.1091/mbc.e04-11-1006 (2005).
- 102 Bass, T. E. *et al.* ETAA1 acts at stalled replication forks to maintain genome integrity. *Nat Cell Biol* **18**, 1185-1195, doi:10.1038/ncb3415 (2016).
- 103 Mordes, D. A., Glick, G. G., Zhao, R. & Cortez, D. TopBP1 activates ATR through ATRIP and a PIKK regulatory domain. *Genes Dev* **22**, 1478-1489, doi:10.1101/gad.1666208 (2008).
- 104 Ball, H. L. & Cortez, D. ATRIP oligomerization is required for ATR-dependent checkpoint signaling. *J Biol Chem* **280**, 31390-31396, doi:10.1074/jbc.M504961200 (2005).
- 105 Sakaguchi, K., Ishibashi, T., Uchiyama, Y. & Iwabata, K. The multi-replication protein A (RPA) system--a new perspective. *FEBS J* **276**, 943-963, doi:10.1111/j.1742-4658.2008.06841.x (2009).
- 106 Ma, C. J., Gibb, B., Kwon, Y., Sung, P. & Greene, E. C. Protein dynamics of human RPA and RAD51 on ssDNA during assembly and disassembly of the RAD51 filament. *Nucleic Acids Res* **45**, 749-761, doi:10.1093/nar/gkw1125 (2017).
- 107 Jensen, R. B., Carreira, A. & Kowalczykowski, S. C. Purified human BRCA2 stimulates RAD51-mediated recombination. *Nature* **467**, 678-683, doi:10.1038/nature09399 (2010).
- 108 Roy, R., Chun, J. & Powell, S. N. BRCA1 and BRCA2: different roles in a common pathway of genome protection. *Nat Rev Cancer* **12**, 68-78, doi:10.1038/nrc3181 (2011).
- 109 Yokoyama, H. *et al.* Preferential binding to branched DNA strands and strand-annealing activity of the human Rad51B, Rad51C, Rad51D and Xrcc2 protein complex. *Nucleic Acids Res* **32**, 2556-2565, doi:10.1093/nar/gkh578 (2004).
- 110 Liu, J. *et al.* Rad51 paralogues Rad55-Rad57 balance the antirecombinase Srs2 in Rad51 filament formation. *Nature* **479**, 245-248, doi:10.1038/nature10522 (2011).
- 111 Masson, J. Y. *et al.* Identification and purification of two distinct complexes containing the five RAD51 paralogs. *Genes Dev* **15**, 3296-3307, doi:10.1101/gad.947001 (2001).

- 112 Schild, D., Lio, Y. C., Collins, D. W., Tsomondo, T. & Chen, D. J. Evidence for simultaneous protein interactions between human Rad51 paralogs. *J Biol Chem* **275**, 16443-16449, doi:10.1074/jbc.M001473200 (2000).
- 113 Carreira, A. & Kowalczykowski, S. C. Two classes of BRC repeats in BRCA2 promote RAD51 nucleoprotein filament function by distinct mechanisms. *Proc Natl Acad Sci U S A* **108**, 10448-10453, doi:10.1073/pnas.1106971108 (2011).
- 114 Pellegrini, L. *et al.* Insights into DNA recombination from the structure of a RAD51-BRCA2 complex. *Nature* **420**, 287-293, doi:10.1038/nature01230 (2002).
- 115 Oliver, A. W., Swift, S., Lord, C. J., Ashworth, A. & Pearl, L. H. Structural basis for recruitment of BRCA2 by PALB2. **10**, 990-996, doi:10.1038/embor.2009.126 (2009).
- 116 Yang, H. *et al.* BRCA2 function in DNA binding and recombination from a BRCA2-DSS1-ssDNA structure. *Science* **297**, 1837-1848, doi:10.1126/science.297.5588.1837 (2002).
- 117 Xu, J. *et al.* Cryo-EM structures of human RAD51 recombinase filaments during catalysis of DNA-strand exchange. *Nat Struct Mol Biol* **24**, 40-46, doi:10.1038/nsmb.3336 (2017).
- 118 Tomblin, G. & Fishel, R. Biochemical characterization of the human RAD51 protein. I. ATP hydrolysis. *J Biol Chem* **277**, 14417-14425, doi:10.1074/jbc.M109915200 (2002).
- 119 Brouwer, I. *et al.* Two distinct conformational states define the interaction of human RAD51-ATP with single-stranded DNA. *EMBO J* **37**, doi:10.15252/embj.201798162 (2018).
- 120 Carreira, A. *et al.* The BRC repeats of BRCA2 modulate the DNA-binding selectivity of RAD51. *Cell* **136**, 1032-1043, doi:10.1016/j.cell.2009.02.019 (2009).
- 121 Rajendra, E. & Venkitaraman, A. R. Two modules in the BRC repeats of BRCA2 mediate structural and functional interactions with the RAD51 recombinase. *Nucleic Acids Res* **38**, 82-96, doi:10.1093/nar/gkp873 (2010).
- 122 Hengel, S. R., Spies, M. A. & Spies, M. Small-Molecule Inhibitors Targeting DNA Repair and DNA Repair Deficiency in Research and Cancer Therapy. *Cell Chem Biol* **24**, 1101-1119, doi:10.1016/j.chembiol.2017.08.027 (2017).
- 123 Abbotts, R. & Wilson, D. M., 3rd. Coordination of DNA single strand break repair. *Free Radic Biol Med* **107**, 228-244, doi:10.1016/j.freeradbiomed.2016.11.039 (2017).
- 124 Malyuchenko, N. V., Kotova, E. Y., Kulaeva, O. I., Kirpichnikov, M. P. & Studitskiy, V. M. PARP1 Inhibitors: antitumor drug design. *Acta Naturae* **7**, 27-37 (2015).

125 <https://www.fda.gov/drugs/fda-grants-accelerated-approval-rucaparib-brca-mutated-metastatic-castration-resistant-prostate>. (15/05/2020).

126 <https://www.fda.gov/drugs/drug-approvals-and-databases/fda-approves-olaparib-plus-bevacizumab-maintenance-treatment-ovarian-fallopian-tube-or-primary>. (05/11/2020).

127 <https://www.fda.gov/drugs/drug-approvals-and-databases/fda-approves-niraparib-first-line-maintenance-advanced-ovarian-cancer>. (29.04.2020).

128 <https://www.fda.gov/drugs/drug-approvals-and-databases/fda-approves-talazoparib-gbrcam-her2-negative-locally-advanced-or-metastatic-breast-cancer#:~:text=On%20October%2016%2C%202018%2C%20the,advanced%20or%20metastatic%20breast%20cancer>. (12.12.2018).

129 Murata, S. *et al.* Predictors and Modulators of Synthetic Lethality: An Update on PARP Inhibitors and Personalized Medicine. *Biomed Res Int* **2016**, 2346585, doi:10.1155/2016/2346585 (2016).

130 Purnell, M. R. & Whish, W. J. Novel inhibitors of poly(ADP-ribose) synthetase. *Biochem J* **185**, 775-777, doi:10.1042/bj1850775 (1980).

131 Wahlberg, E. *et al.* Family-wide chemical profiling and structural analysis of PARP and tankyrase inhibitors. *Nat Biotechnol* **30**, 283-288, doi:10.1038/nbt.2121 (2012).

132 Thorsell, A. G. *et al.* Structural Basis for Potency and Promiscuity in Poly(ADP-ribose) Polymerase (PARP) and Tankyrase Inhibitors. *J Med Chem* **60**, 1262-1271, doi:10.1021/acs.jmedchem.6b00990 (2017).

133 Axelle Renodon-Cornière, P. W., Magali Le Breton, Fabrice Fleury. New Potential Therapeutic Approaches by Targeting Rad51-Dependent Homologous Recombination. *New Research Directions in DNA Repair*, 467-, doi:10.5772/53973 (2013).

134 Klein, H. L. The consequences of Rad51 overexpression for normal and tumor cells. *DNA Repair (Amst)* **7**, 686-693, doi:10.1016/j.dnarep.2007.12.008 (2008).

135 Schild, D. & Wiese, C. Overexpression of RAD51 suppresses recombination defects: a possible mechanism to reverse genomic instability. *Nucleic Acids Res* **38**, 1061-1070, doi:10.1093/nar/gkp1063 (2010).

136 Ishida, T. *et al.* DIDS, a chemical compound that inhibits RAD51-mediated homologous pairing and strand exchange. *Nucleic Acids Res* **37**, 3367-3376, doi:10.1093/nar/gkp200 (2009).

137 Takaku, M. *et al.* Halenaquinone, a chemical compound that specifically inhibits the secondary DNA binding of RAD51. *Genes Cells* **16**, 427-436, doi:10.1111/j.1365-2443.2011.01494.x (2011).

138 Huang, F. *et al.* Identification of specific inhibitors of human RAD51 recombinase using high-throughput screening. *ACS Chem Biol* **6**, 628-635, doi:10.1021/cb100428c (2011).

139 Huang, F., Mazina, O. M., Zentner, I. J., Cocklin, S. & Mazin, A. V. Inhibition of homologous recombination in human cells by targeting RAD51 recombinase. *J Med Chem* **55**, 3011-3020, doi:10.1021/jm201173g (2012).

140 Huang, F. & Mazin, A. V. A small molecule inhibitor of human RAD51 potentiates breast cancer cell killing by therapeutic agents in mouse xenografts. *PLoS One* **9**, e100993, doi:10.1371/journal.pone.0100993 (2014).

141 Alagpulinsa, D. A., Ayyadevara, S. & Shmookler Reis, R. J. A Small-Molecule Inhibitor of RAD51 Reduces Homologous Recombination and Sensitizes Multiple Myeloma Cells to Doxorubicin. *Front Oncol* **4**, 289, doi:10.3389/fonc.2014.00289 (2014).

142 Normand, A., Riviere, E. & Renodon-Corniere, A. Identification and characterization of human Rad51 inhibitors by screening of an existing drug library. *Biochem Pharmacol* **91**, 293-300, doi:10.1016/j.bcp.2014.07.033 (2014).

143 Budke, B. *et al.* RI-1: a chemical inhibitor of RAD51 that disrupts homologous recombination in human cells. *Nucleic Acids Res* **40**, 7347-7357, doi:10.1093/nar/gks353 (2012).

144 Budke, B. *et al.* An optimized RAD51 inhibitor that disrupts homologous recombination without requiring Michael acceptor reactivity. *J Med Chem* **56**, 254-263, doi:10.1021/jm301565b (2013).

145 Budke, B., Lv, W., Kozikowski, A. P. & Connell, P. P. Recent Developments Using Small Molecules to Target RAD51: How to Best Modulate RAD51 for Anticancer Therapy? *ChemMedChem* **11**, 2468-2473, doi:10.1002/cmde.201600426 (2016).

146 Du, L. Q. *et al.* Methotrexate-mediated inhibition of RAD51 expression and homologous recombination in cancer cells. *J Cancer Res Clin Oncol* **138**, 811-818, doi:10.1007/s00432-011-1132-8 (2012).

147 Adimoolam, S. *et al.* HDAC inhibitor PCI-24781 decreases RAD51 expression and inhibits homologous recombination. *Proc Natl Acad Sci U S A* **104**, 19482-19487, doi:10.1073/pnas.0707828104 (2007).

- 148 Lu, C. H. *et al.* Prodigiosin-induced cytotoxicity involves RAD51 down-regulation through the JNK and p38 MAPK pathways in human breast carcinoma cell lines. *Toxicol Lett* **212**, 83-89, doi:10.1016/j.toxlet.2012.05.002 (2012).
- 149 Zhu, J. *et al.* A novel small molecule RAD51 inactivator overcomes imatinib-resistance in chronic myeloid leukaemia. *EMBO Mol Med* **5**, 353-365, doi:10.1002/emmm.201201760 (2013).
- 150 Scott, D. E. *et al.* A small-molecule inhibitor of the BRCA2-RAD51 interaction modulates RAD51 assembly and potentiates DNA damage-induced cell death. *bioRxiv*, 2020.2007.2015.200709, doi:10.1101/2020.07.15.200709 (2020).
- 151 Huang, F. *et al.* Targeting BRCA1- and BRCA2-deficient cells with RAD52 small molecule inhibitors. *Nucleic Acids Res* **44**, 4189-4199, doi:10.1093/nar/gkw087 (2016).
- 152 Lok, B. H., Carley, A. C., Tchang, B. & Powell, S. N. RAD52 inactivation is synthetically lethal with deficiencies in BRCA1 and PALB2 in addition to BRCA2 through RAD51-mediated homologous recombination. *Oncogene* **32**, 3552-3558, doi:10.1038/onc.2012.391 (2013).
- 153 Hengel, S. R. *et al.* Small-molecule inhibitors identify the RAD52-ssDNA interaction as critical for recovery from replication stress and for survival of BRCA2 deficient cells. *Elife* **5**, doi:10.7554/eLife.14740 (2016).
- 154 Chandramouly, G. *et al.* Small-Molecule Disruption of RAD52 Rings as a Mechanism for Precision Medicine in BRCA-Deficient Cancers. *Chem Biol* **22**, 1491-1504, doi:10.1016/j.chembiol.2015.10.003 (2015).
- 155 Kagawa, W. *et al.* Crystal structure of the homologous-pairing domain from the human Rad52 recombinase in the undecameric form. *Mol Cell* **10**, 359-371, doi:10.1016/s1097-2765(02)00587-7 (2002).
- 156 Sullivan, K. *et al.* Identification of a Small Molecule Inhibitor of RAD52 by Structure-Based Selection. *PLoS One* **11**, e0147230, doi:10.1371/journal.pone.0147230 (2016).
- 157 Deakyne, J. S. *et al.* Analysis of the activities of RAD54, a SWI2/SNF2 protein, using a specific small-molecule inhibitor. *J Biol Chem* **288**, 31567-31580, doi:10.1074/jbc.M113.502195 (2013).
- 158 Mazin, A. V., Mazina, O. M., Bugreev, D. V. & Rossi, M. J. Rad54, the motor of homologous recombination. *DNA Repair (Amst)* **9**, 286-302, doi:10.1016/j.dnarep.2009.12.006 (2010).

- 159 Wolner, B. & Peterson, C. L. ATP-dependent and ATP-independent roles for the Rad54 chromatin remodeling enzyme during recombinational repair of a DNA double strand break. *J Biol Chem* **280**, 10855-10860, doi:10.1074/jbc.M414388200 (2005).
- 160 Loyola, A. C. *et al.* Streptonigrin at low concentration promotes heterochromatin formation. *Sci Rep* **10**, 3478, doi:10.1038/s41598-020-60469-6 (2020).
- 161 Ehmsen, K. T. *et al.* Small molecule inhibitors of a human recombination-associated ATPase, RAD54. *bioRxiv*, 614586, doi:10.1101/614586 (2019).
- 162 Bagnolini, G. *et al.* Synthetic Lethality in Pancreatic Cancer: Discovery of a New RAD51-BRCA2 Small Molecule Disruptor That Inhibits Homologous Recombination and Synergizes with Olaparib. *J Med Chem* **63**, 2588-2619, doi:10.1021/acs.jmedchem.9b01526 (2020).
- 163 Golan, T. *et al.* Maintenance Olaparib for Germline BRCA-Mutated Metastatic Pancreatic Cancer. *N Engl J Med* **381**, 317-327, doi:10.1056/NEJMoa1903387 (2019).
- 164 Roberti, M. *et al.* Rad51/BRCA2 disruptors inhibit homologous recombination and synergize with olaparib in pancreatic cancer cells. *Eur J Med Chem* **165**, 80-92, doi:10.1016/j.ejmech.2019.01.008 (2019).
- 165 Ivanov, A. A., Khuri, F. R. & Fu, H. Targeting protein-protein interactions as an anticancer strategy. *Trends Pharmacol Sci* **34**, 393-400, doi:10.1016/j.tips.2013.04.007 (2013).
- 166 Moreira, I. S., Fernandes, P. A. & Ramos, M. J. Hot spots--a review of the protein-protein interface determinant amino-acid residues. *Proteins* **68**, 803-812, doi:10.1002/prot.21396 (2007).
- 167 Perot, S., Sperandio, O., Miteva, M. A., Camproux, A. C. & Villoutreix, B. O. Druggable pockets and binding site centric chemical space: a paradigm shift in drug discovery. *Drug Discov Today* **15**, 656-667, doi:10.1016/j.drudis.2010.05.015 (2010).
- 168 Falchi, F. *et al.* Synthetic Lethality Triggered by Combining Olaparib with BRCA2-Rad51 Disruptors. *ACS Chem Biol* **12**, 2491-2497, doi:10.1021/acscchembio.7b00707 (2017).
- 169 Sankaran, M., Uvarani, C., Chandraprakash, K., Umamaheswari, M. & Mohan, P. S. An Expedient Approach for the Synthesis of Bioactive Pyrazole, Isoxazole and Benzodiazepine-Substituted Quinolin-2(1H)-one Derivatives. *Journal of Heterocyclic Chemistry* **52**, 1082-1092, doi:10.1002/jhet.2192 (2015).

170 Acker, T. M. *et al.* Structure-activity relationships and pharmacophore model of a noncompetitive pyrazoline containing class of GluN2C/GluN2D selective antagonists. *J Med Chem* **56**, 6434-6456, doi:10.1021/jm400652r (2013).

171 Frei, P., Hevey, R. & Ernst, B. Dynamic Combinatorial Chemistry: A New Methodology Comes of Age. *Chemistry* **25**, 60-73, doi:10.1002/chem.201803365 (2019).

172 Huc, I. & Lehn, J. M. Virtual combinatorial libraries: dynamic generation of molecular and supramolecular diversity by self-assembly. *Proc Natl Acad Sci U S A* **94**, 2106-2110, doi:10.1073/pnas.94.6.2106 (1997).

173 Huang, R. & Leung, I. K. Protein-Directed Dynamic Combinatorial Chemistry: A Guide to Protein Ligand and Inhibitor Discovery. *Molecules* **21**, doi:10.3390/molecules21070910 (2016).

174 Jumde, R. P. G., Melissa; Gierse, Robin M.; Alhayek, Alaa; Zhu, Di; Hamed, Zhoor; et al. . Hit-Optimization Using Target-Directed Dynamic Combinatorial Chemistry: Development of Inhibitors of the Anti-Infective Target 1-Deoxy-D-Xylulose-5-Phosphate Synthase. *ChemRxiv. Preprint.* , doi:<https://doi.org/10.26434/chemrxiv.12681761.v1> (2020).

175 Hartman, A. M., Gierse, R. M. & Hirsch, A. K. H. Protein-Templated Dynamic Combinatorial Chemistry: Brief Overview and Experimental Protocol. *European J Org Chem* **2019**, 3581-3590, doi:10.1002/ejoc.201900327 (2019).

176 Dirksen, A., Dirksen, S., Hackeng, T. M. & Dawson, P. E. Nucleophilic catalysis of hydrazone formation and transimination: implications for dynamic covalent chemistry. *J Am Chem Soc* **128**, 15602-15603, doi:10.1021/ja067189k (2006).

177 Hewitt, S. H. & Wilson, A. J. Generation of Dynamic Combinatorial Libraries Using Hydrazone-Functionalized Surface Mimetics. *European J Org Chem* **2018**, 1872-1879, doi:10.1002/ejoc.201800022 (2018).

178 Crisalli, P. & Kool, E. T. Water-soluble organocatalysts for hydrazone and oxime formation. *J Org Chem* **78**, 1184-1189, doi:10.1021/jo302746p (2013).

179 Crisalli, P. & Kool, E. T. Importance of ortho proton donors in catalysis of hydrazone formation. *Org Lett* **15**, 1646-1649, doi:10.1021/ol400427x (2013).

180 Thota, S. *et al.* N-Acylhydrazones as drugs. *Bioorg Med Chem Lett* **28**, 2797-2806, doi:10.1016/j.bmcl.2018.07.015 (2018).

- 181 Himmel, D. M. *et al.* HIV-1 reverse transcriptase structure with RNase H inhibitor dihydroxy benzoyl naphthyl hydrazone bound at a novel site. *ACS Chem Biol* **1**, 702-712, doi:10.1021/cb600303y (2006).
- 182 Kovaleva, K. S. *et al.* Synthesis of d-(+)-camphor-based N-acylhydrazones and their antiviral activity. *Medchemcomm* **9**, 2072-2082, doi:10.1039/c8md00442k (2018).
- 183 Yang, Z. B., Li, P. & He, Y. J. Design, Synthesis, and Bioactivity Evaluation of Novel Isoxazole-Amide Derivatives Containing an Acylhydrazone Moiety as New Active Antiviral Agents. *Molecules* **24**, doi:10.3390/molecules24203766 (2019).
- 184 He, L. *et al.* Discovering potent inhibitors against the beta-hydroxyacyl-acyl carrier protein dehydratase (FabZ) of *Helicobacter pylori*: structure-based design, synthesis, bioassay, and crystal structure determination. *J Med Chem* **52**, 2465-2481, doi:10.1021/jm8015602 (2009).
- 185 Wu, J. *et al.* Discovery and mechanism study of SIRT1 activators that promote the deacetylation of fluorophore-labeled substrate. *J Med Chem* **56**, 761-780, doi:10.1021/jm301032j (2013).
- 186 Putt, K. S. *et al.* Small-molecule activation of procaspase-3 to caspase-3 as a personalized anticancer strategy. *Nat Chem Biol* **2**, 543-550, doi:10.1038/nchembio814 (2006).
- 187 Meira, C. S. *et al.* Structural design, synthesis and substituent effect of hydrazone-N-acylhydrazones reveal potent immunomodulatory agents. *Bioorg Med Chem* **26**, 1971-1985, doi:10.1016/j.bmc.2018.02.047 (2018).
- 188 Maia Rdo, C., Tesch, R. & Fraga, C. A. Acylhydrazone derivatives: a patent review. *Expert Opin Ther Pat* **24**, 1161-1170, doi:10.1517/13543776.2014.959491 (2014).
- 189 Baell, J. B., Ferrins, L., Falk, H. & Nikolakopoulos, G. PAINS: Relevance to Tool Compound Discovery and Fragment-Based Screening. *Australian Journal of Chemistry* **66**, 1483-1494, doi:<https://doi.org/10.1071/CH13551> (2013).
- 190 van Dijken, D. J., Kovaricek, P., Ihrig, S. P. & Hecht, S. Acylhydrazones as Widely Tunable Photoswitches. *J Am Chem Soc* **137**, 14982-14991, doi:10.1021/jacs.5b09519 (2015).
- 191 Jumde, V. R. *et al.* Design and Synthesis of Bioisosteres of Acylhydrazones as Stable Inhibitors of the Aspartic Protease Endothiapepsin. *ChemMedChem* **13**, 2266-2270, doi:10.1002/cmdc.201800446 (2018).

Acknowledgements

I would like to show all my gratitude to my supervisor, Prof. Andrea Cavalli, for the invaluable opportunity to join his inspiring research group and grow as PhD student. My gratitude extends to the Italian Institute of Technology (IIT) for the funding opportunity to carry out my PhD studies at the Department of Pharmacy and Biotechnology (FaBiT) of the University of Bologna.

I wish to express my deepest gratitude to Prof. Marinella Roberti for her supervision and guidance, scientific mentorship, invaluable human support and patience during my PhD studies. Her enthusiasm and experience have inspired and encouraged me in all the time of my academic research and daily life. Her contribution to my PhD path is whole-heartedly appreciated.

I would like to pay my special regards to all the members of the research group I have had the pleasure to join. In particular I wish to thank Jose Antonio Ortega, Domenico Milano, Andrea Balboni, Marcella Manerba, Fabrizio Schipani and Dario Gioia, whose work, expertise, guide and advices have deeply contributed to my training as PhD student.

I wish to thank heartedly my labmate Irene Brusa whose daily support, kind help and true friendship made me appreciate and enjoy all the time spent together in lab daily work and more.

My special thank extends to all my colleagues of the FaBiT Department for the cherished time spent together and all the shared moments that made me feel part of a great team of young scientist and friends.

I wish to show my deep gratitude to Prof. A. K. H. Hirsch who kindly welcomed me as visiting PhD student to join her research group at HIPS.

I would like to kindly thank all the engaged and delightful scientists I had the pleasure to meet and work with at HIPS. Their assistance and support have been indispensable milestones in the realization of my experience as visiting PhD student. In particular I wish to recognize Ravindra Jumde's precious assistance and scientific collaboration, which guided me during my experience at HIPS.

I am deeply grateful to all the brilliant and awesome people who made my staying in Saarbrücken an amazing and unforgettable experience, with a special thought to friends, Eleonora, Anna, Jelena, Cansu, Alaa and Yingwen.

I wish to recognize Elisa Giacomini's treasured contribution to my choice to pursue PhD path thank to her passion, enthusiasm and integrity.

I wish to acknowledge the unwavering support and great love I constantly received from my parents, extraordinary people who never failed to believe in me. I will never be able to thank them enough for what they did for me.

I thank heartedly all my friends, who have stayed with me and supported me through all this, thank you for the huge support and patience. I would never be able to complete this professional and personal journey without you, guys!

Financial support

This work was supported by the Associazione Italiana per la Ricerca sul Cancro AIRC (Progetto IG 2018, id 21386), the Italian Institute of Technology (IIT), and the University of Bologna.